NASA
Reference
Publication
1268

September 1991

Development of the Burst and Transient Source Experiment (BATSE)

J. M. Horack

NASA

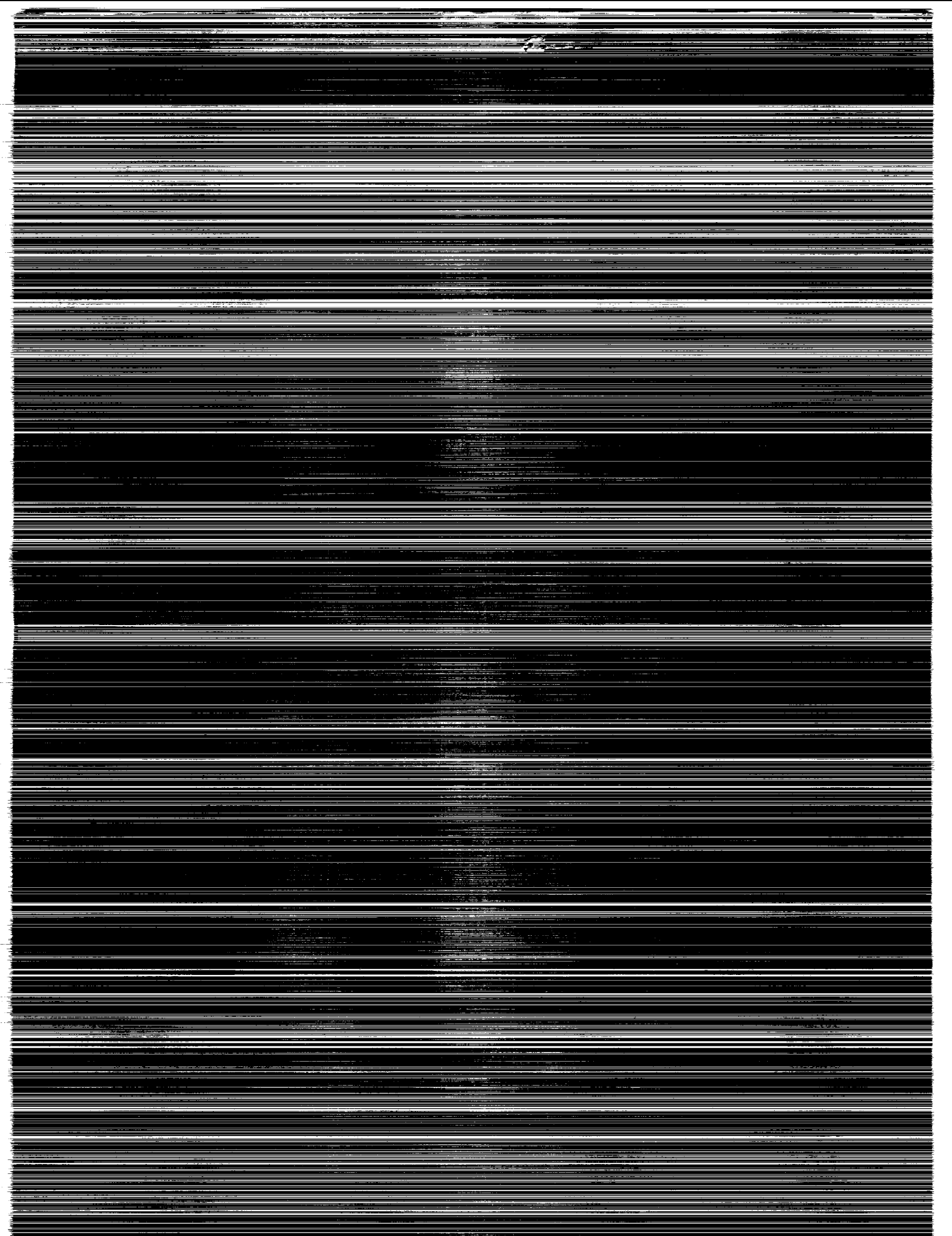

NASA Reference Publication 1268

1991

Development of the Burst and Transient Source Experiment (BATSE)

J. M. Horack
George C. Marshall Space Flight Center
Marshall Space Flight Center, Alabama

NASA
National Aeronautics and Space Administration
Office of Management
Scientific and Technical Information Program

TABLE OF CONTENTS

ii blank

Page

Page

Page

Page

Page

Page

Page

LIST OF ILLUSTRATIONS

LIST OF ILLUSTRATIONS (Continued)

LIST OF ILLUSTRATIONS (Concluded)

LIST OF TABLES

LIST OF TABLES (Continued)

LIST OF TABLES (Continued)

LIST OF TABLES (Continued)

LIST OF TABLES (Concluded)

NASA REFERENCE PUBLICATION

DEVELOPMENT OF THE BURST AND TRANSIENT SOURCE EXPERIMENT

I. INTRODUCTION

A. Overview

The Gamma Ray Observatory (GRO) is the second in NASA's series of "Great Observatories" designed to explore the universe over many wavelengths with unprecedented sensitivity from low Earth orbit. Scheduled for launch in April of 1991 aboard the space shuttle Atlantis, GRO will operate at an altitude of 450 km with an orbital inclination of 28.5°.

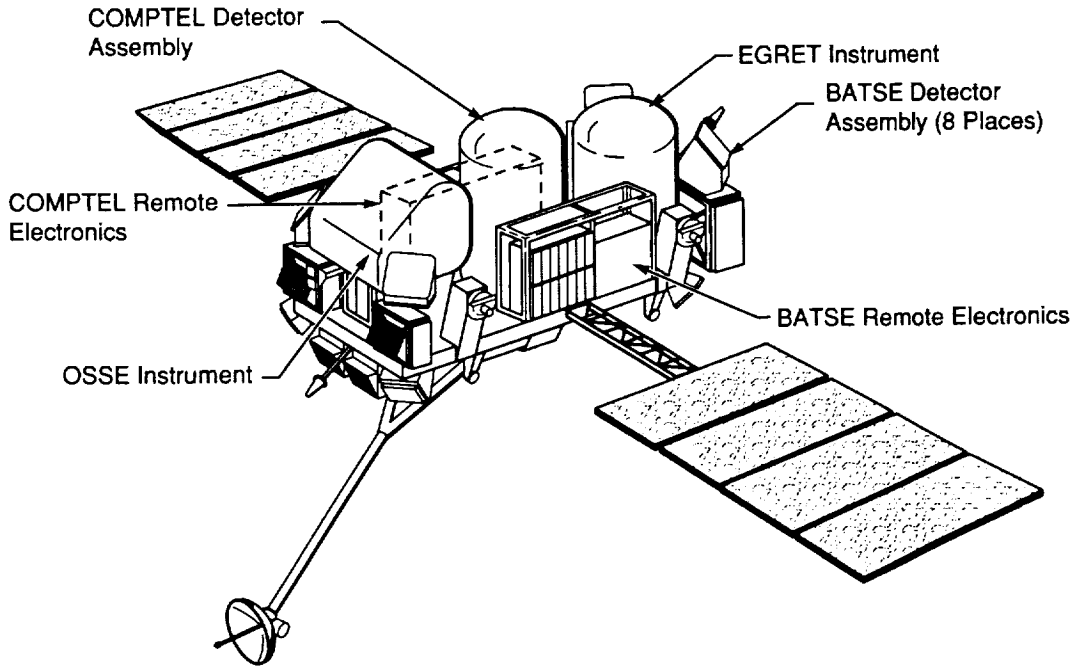

Figure 1.1. Gamma Ray Observatory and BATSE Detector Module.

The GRO weighs 17 tons, and contains four scientific instruments:

- Oriented Scintillation Spectrometer Experiment (OSSE)
- Compton Telescope (COMPTEL)
- Energetic Gamma Ray Experiment Telescope (EGRET)
- Burst and Transient Source Experiment (BATSE)

The BATSE flight hardware consists of eight identical detector modules, mounted on the corners of the spacecraft (see Figure 1.1), and associated electronics. Each of the detector modules consist of a large area detector (LAD), a spectroscopy detector (SD), a charged particle detector (CPD), and associated electronics. The modules are numbered according to their positions on the GRO. This numbering scheme is given in Table 1.1. BATSE provides monitoring of the entire sky, continuously on-watch for gamma ray bursts and other transient phenomena. When a gamma ray burst is detected by BATSE, a signal is sent to the other three instruments, notifying them of the event. BATSE will detect and analyze hundreds of gamma ray bursts per year, with unprecedented combinations of temporal and spectral sensitivity. This improved sensitivity will allow the BATSE instrument to observe gamma ray bursts 10 times fainter than any detected before.

Table 1.1. BATSE Detector Module Numbering

Detector	GRO (X, Y, Z) Coordinates
B0	+, +, +
B1	+, +, -
B2	+, -, +
B3	+, -, -
B4	-, +, +
B5	-, +, -
B6	-, -, +
B7	-, -, -

In August of 1977, an Announcement of Opportunity for the GRO was made by NASA. In the following 13 years, many milestones were reached in transforming BATSE from a proposal into a flight experiment. The major milestones reached during this time period are outlined in Table 1.2.

Table 1.2. Milestones of the BATSE-GRO Project - 1977-1991

Event/Milestone	Date
Announcement of Opportunity for GRO	August 1977
Proposal Submitted - "A Transient Event Monitor for the GRO," G. Fishman, PI; C. Meegan, T. Parnell, Co-I's (Proposed 12 detectors, with 2-6 detector arrays)	February 1978
Proposal Accepted by NASA Headquarters (6 detectors, 1-6 detector array)	August 1978
Name changed to Burst and Transient Source Experiment (BATSE) with 8 detectors in separate modules proposed and accepted	1979
Concept Design Review	November 1980
TRW selected as GRO Mission Contractor	1981
GRO receives new-start from Congress	1980

Table 1.2. Milestones of the BATSE-GRO Project - 1977-1991 (Cont.)

Event/Milestone	Date
GRSE Experiment removed from GRO	1981
BATSE Program Requirements Review	1981
R. Wilson becomes BATSE Co-I	1982
BATSE developmental balloon flight	May 1982
BATSE design and performance specification	April 1984
Spectroscopy detector modification to BATSE proposed	January 1983
ATSE Preliminary Design Review	March 1983
Spectroscopy modification to BATSE accepted; J. Matteson, B. Teegarden, and T. Cline become BATSE Co-I's	1983
Spectroscopy detector PDR	October 1983
Critical Design Review	June 1984
W. Paciesas becomes BATSE Co-I	1985
GRO designated a Great Observatory, extended mission and comprehensive guest investigator program planned	1986
Fabrication of flight components	1985 - 1987
MSFC assembly and test program	1986 - 1988
Detector module assembly and testing	1986 - 1988
Pre-Environmental Review	March 1987
BATSE system thermal-vacuum testing	August - September 1988
Calibration Review I	July 1988
Pre-Ship Review	September 1988
BATSE shipped to TRW	October 1988
GRO instrument integration and testing Redondo Beach, California	November 1988 - November 1989
GRO thermal vacuum testing	July - August 1989
GRO shipped to KSC	February 1990
GRO test program at KSC	February 1990 - March 1991
BATSE Calibration Review II	July 1990
Phase I guest investigators selected	August 1990
Launch of GRO aboard space shuttle Atlantis, mission STS-37	April 1991

The milestones shown in Table 1.2 could not have been met without the hard work and dedication of countless personnel during the development, fabrication, and test phases of the BATSE program. The persons listed in Table 1.3 contributed significantly to the design, development, and testing of BATSE. A much larger list of personnel participated in the development of the experiment; however, in the interest of conciseness, this list is necessarily limited to those persons who were major contributors to the program. Table 1.4 lists the primary component fabricators and contractors for BATSE.

Table 1.3. BATSE Development Personnel

Byron Schrick	BATSE Program Manager
Dennis Ellsworth	BATSE Chief Engineer
Laboratory Lead Engineers:	
Robert Austin	Space Science Laboratory
Frayne Smith	EB Laboratory (electronics)
David McGaha	Test Laboratory
Joe Smith	EP Laboratory (structures)
Principal BATSE Designers:	
Robert Austin	Analog electronics design
Richard Rehage	Digital electronics design
Charles Meegan	Flight software
Bob Wilson	Flight software test design
Richard Acker	Power supply design
Mark Chapman (UCSD)	Detector and PMT housing design
Ed Stephan (UCSD)	Detector and PMT housing design
Joe Smith	Mechanical design
Ken Anthony	Thermal protection system design
Dave Clark	Thermal analysis
David Christian	Dynamics analysis
Henry Lee	Stress analysis
Robert Rowe	GSE software
Al English	GSE hardware

Table 1.4. Primary Component Fabricators and Contractors for BATSE

Bicron Corporation	Detector crystals, detector encapsulation, plastic scintillators
Thorn EMI Limited	Photomultiplier tubes
Omni Technology, Inc.	Electronics parts screening
University of California, San Diego	Detector housings, PMT assemblies
Whitesburg Electronics	Electronics fabrication
Beowulf Corporation	Electronics fabrication
Twin-Tech, Inc.	Electronics fabrication
Ver-Val, Inc.	Mechanical fabrication

B. Purpose and Scope

The purpose of this manual is to provide the reader with a detailed view of BATSE's history, with an emphasis placed on hardware development, calibration, and testing. The manual provides detailed descriptions of BATSE flight hardware, complete with drawings. BATSE's extensive test and calibration program is presented; however, the reader is referred to the BATSE Calibration and Performance Summary for a detailed look into the BATSE science calibrations. In this manual, emphasis is placed on qualification, performance, and environmental test results. Several appendices are included for further reference. This document provides a means by which the BATSE user can become more familiar with the details of the BATSE instrument, not only the data which it produces.

As discussed previously, the history of BATSE dates from the late 1970's; however, the information presented here begins with the development of the BATSE flight hardware. It concludes with the final tests and calibrations performed prior to launch of the satellite. Major components of the BATSE instrument are presented, followed by a presentation of component, subsystem, and finally experiment-level test results. A complete list of drawings and released documents is provided as one of an extensive list of appendices.

II. BATSE HARDWARE DESCRIPTION

A. BATSE Large Area Detector

The large area detector (LAD) is the principal gamma ray detector on the BATSE module. Consisting of a NaI(Tl) crystal 50.8 cm in diameter and 1.27 cm in thickness, the LAD is uncollimated and views the entire forward hemisphere. The NaI crystal is hermetically sealed inside its housing and mated to a light collection cone. The scintillation photons from the LAD are collected by three 12.7-cm PMTs at the back of the cone.

The LAD assembly is mounted on the upper half of the detector module (see Figure 2.1). The orientation is such that the normal to the LAD and the normal to the front baseplate of the detector module lie in the local vertical plane. When the detector module is upright, the LAD normal makes a 54.736° ($\arctan\sqrt{2}$) angle with the local vertical. This angle is required so that when the modules are placed into the flight configuration on the GRO, the planes of the LADs intersect to form the faces of a regular-right octahedron. This is done so that gamma ray bursts will be seen by four detectors simultaneously. The location of a detected burst can be determined by comparison of counting rates on the LADs, which depend to first order on the differences in projected areas of the illuminated detectors.

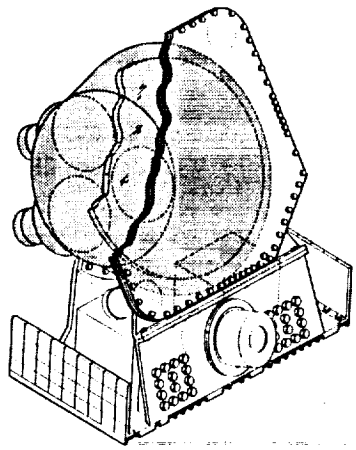

Figure 2.1. BATSE Detector Module and LAD Assembly.

Bicron Corporation of Newbury, Ohio was the principal contractor for the fabrication of the LAD assembly, and the detectors were manufactured according to MSFC-PROC-1495. The NaI crystals were grown in a large boule and machined to their proper size. Fabrication of the LAD housing was performed at UCSD. Figure 2.2 shows a cross-sectional view of the LAD and its housing.

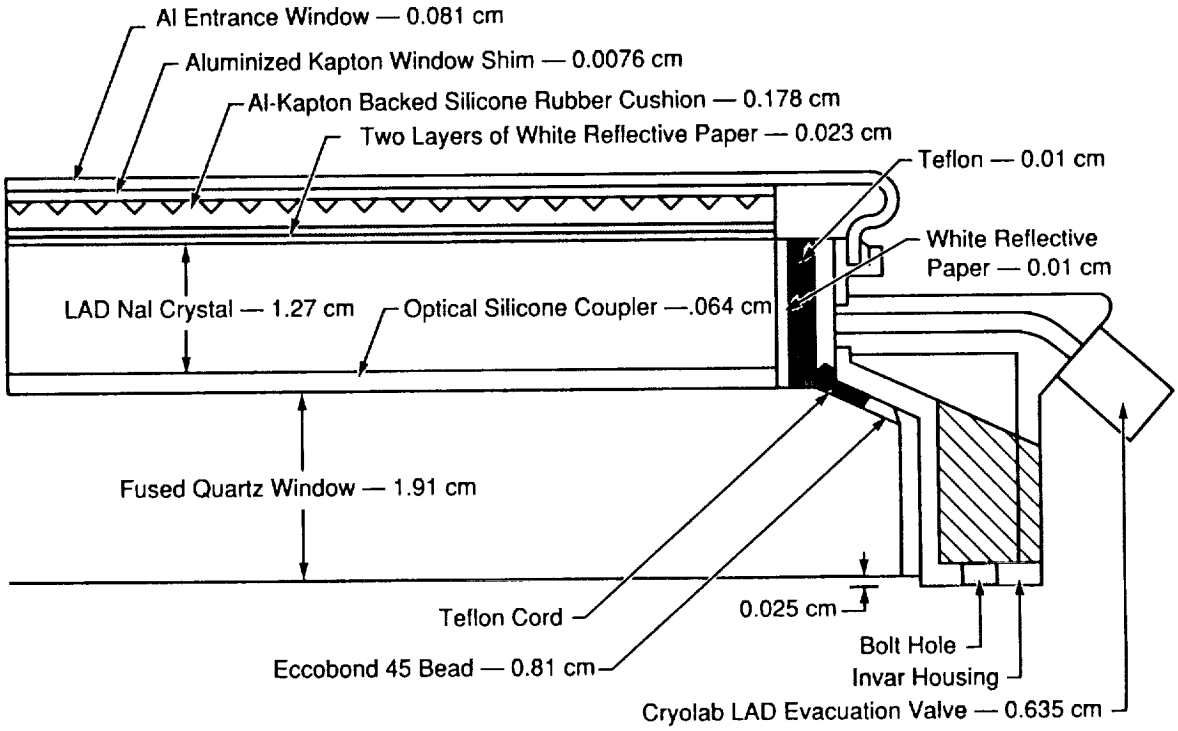

Figure 2.2. BATSE Large Area Detector Assembly (Cross-Section).

Detected gamma rays enter the LAD through an 0.081-cm aluminum entrance window. This window allows for the entrance of high energy photons, while attenuating lower energy x-rays which pass through the charged particle detector in front of the LAD. Directly behind the entrance window is an aluminized kapton window shim and a silicone rubber cushion backed with aluminized kapton. This layer is approximately 0.18 cm thick; however, it varies slightly from detector to detector. Two layers of white reflective paper are located at the next layer of the LAD. These layers, 0.023 cm thick, reflect scintillation photons back toward the exit window of the LAD. The NaI crystal is the next layer. Optical photons generated in the interaction between the gamma ray and the NaI then pass through the fused quartz optical window and its optical coupling into the light collection cone. The window has a thickness of 1.9 cm, and the optical coupling is approximately 0.03 of this value.

This assembly is hermetically sealed inside a circular Invar housing. The housing serves as the mechanical mount for the LAD assembly and the point at which the assembly fastens to the light collection cone. A ring of teflon, and white reflective paper, each 0.01 cm thick, line the inner perimeter of the Invar ring next to the NaI. A teflon cord and an 0.81-cm bead of Eccobond 45 are seated at the boundary of the NaI crystal, the quartz window, and the Invar flange. This entire region is kept evacuated to a pressure of 30 milliTorr or less. This prevents hydration of the NaI crystal, and deformation of the assembly in the vacuum of space. The procedure of evacuation and pressure checking is discussed in section II.A.1 of this manual. Table 2.1 details the LAD assembly specifications.

The LAD assembly mounts to the light collection cone with a series of bolts fastened through the Invar flange. The assembly is mounted so that the fused quartz window is interior to the collection cone. The interior walls of the cone are painted with a highly reflective BaSO4 white paint to prevent absorption of the light generated in the NaI detector. In addition, the cone provides passive shielding of the LAD in the rear hemisphere by means of lead and tin layers. The lead layer, exterior to the tin, is 0.08 cm thick. The tin layer absorbs approximately 90% of the k-shell x-rays generated in the lead and has a thickness of 0.05 cm. This shielding arrangement is very effective for absorbing gamma rays entering the back of the detector up to an energy of 300-400 keV.

Table 2.1. BATSE Large Area Detector Specifications

LAD Component	Thickness (cm)
Aluminum window	0.081
Al-Kapton shim	0.0076
Silicone rubber pad	0.178
White reflective paper	0.023
Minimum total attenuation length in front of NaI crystal	0.2896
NaI (Tl) LAD crystal	1.27
Silicone optical coupler	0.064
Fused silicon quartz window	1.91
Light cone passive shield	
Lead	0.76
Tin	0.51

B. BATSE Spectroscopy Detector

The second gamma ray detector on the BATSE module is the spectroscopy detector (SD). Although smaller in area than the LAD, and thus less sensitive to temporal fluctuations, the SD provides superior energy resolution to the LAD, in addition to coverage in energy regions both higher and lower than that of the LAD. These detector units were fabricated at UCSD and delivered to MSFC. The SD is mounted on the detector module below the LAD, and is also uncollimated. The SD consists of a cylindrical crystal of NaI(Tl) 12.7 cm in diameter and 7.6 cm in thickness. This NaI crystal is mounted to a 12.7-cm PMT through direct optical coupling. The NaI crystal is encased in an aluminum can, approximately 0.2 cm thick. The aluminum housing provides shielding against low energy x-rays. Gamma rays enter the SD through an 0.068 cm thick, 8.3 cm diameter beryllium window. This thin window covers 53.52 cm^2 and allows for effective observations to energies of 15 keV with the SD. Figure 2.3 details the SD construction.

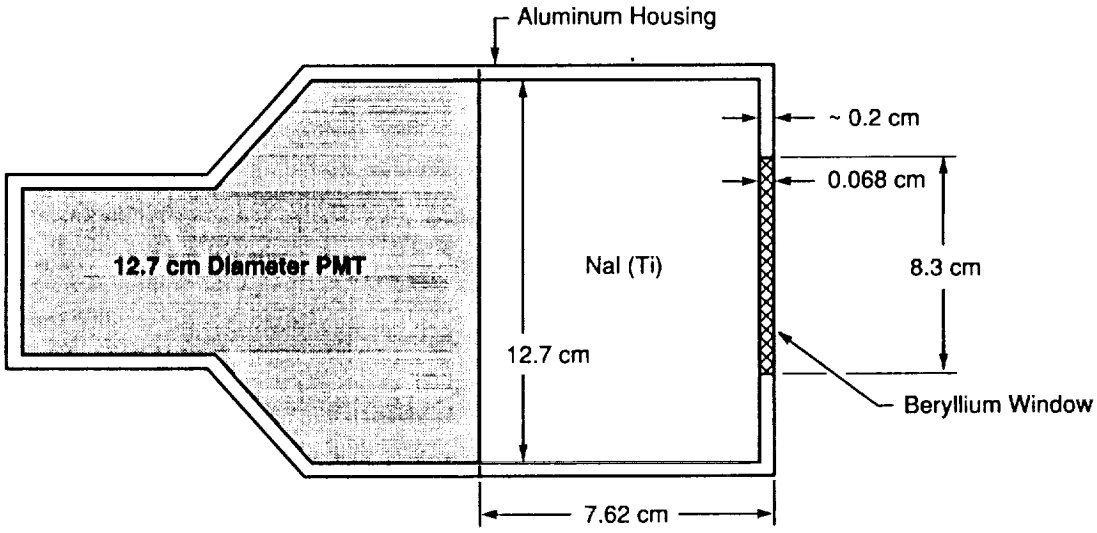

Figure 2.3. BATSE Spectroscopy Detector Assembly.

The SD is installed on the BATSE detector module below the large area detector. The axes of symmetry of the two detectors form the local vertical plane when the detector module is upright. However, the SD axis is offset approximately 18.5° in pitch below that of the large area detector due to constraints on the mechanical envelope. Both the cylinder-wall portion and the Be-window end of the SD are exposed to incoming radiation when the detector is installed onto the module. The PMT used to collect the scintillation light is identical to the ones used on the LAD light collection cone. Figure 2.4 illustrates the SD installation on the BATSE detector module.

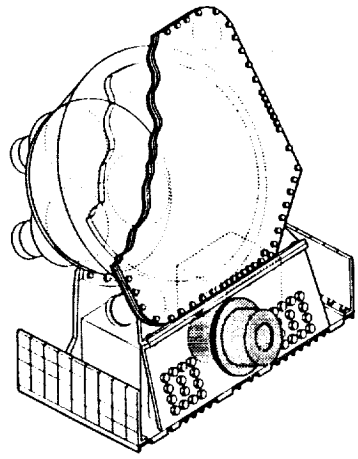

Figure 2.4. BATSE SD and Detector Module.

C. BATSE Charged Particle Detector

The charged particle detector (CPD) provides the BATSE LAD with active shielding from incident charged particles. Events which are registered in both the CPD and the LAD are rejected through electronic anti-coincidence circuitry in the detector's electronics. The CPD and LAD can also be operated in a coincidence mode. Manufactured in Building 4705 at MSFC, the CPD is an octagonal piece of plastic scintillator, 55.9 cm in diameter. The plastic scintillator is wrapped in a layer of aluminum foil and then sandwiched between two layers of aluminum honeycomb. The honeycomb provides protection of the CPD from damage, while minimizing the mass attenuation in front of the detector. The entire assembly is then covered with a face sheet of aluminum. The assembly is vented on ascent during launch through two square pieces of sintered bronze, 2.54 cm on a side. The addition of these pieces came after damage was done to the CPD during thermal vacuum testing, which demonstrated that the original CPD design was not sufficiently vented. Figure 2.5 shows the assembly of the charge particle detector.

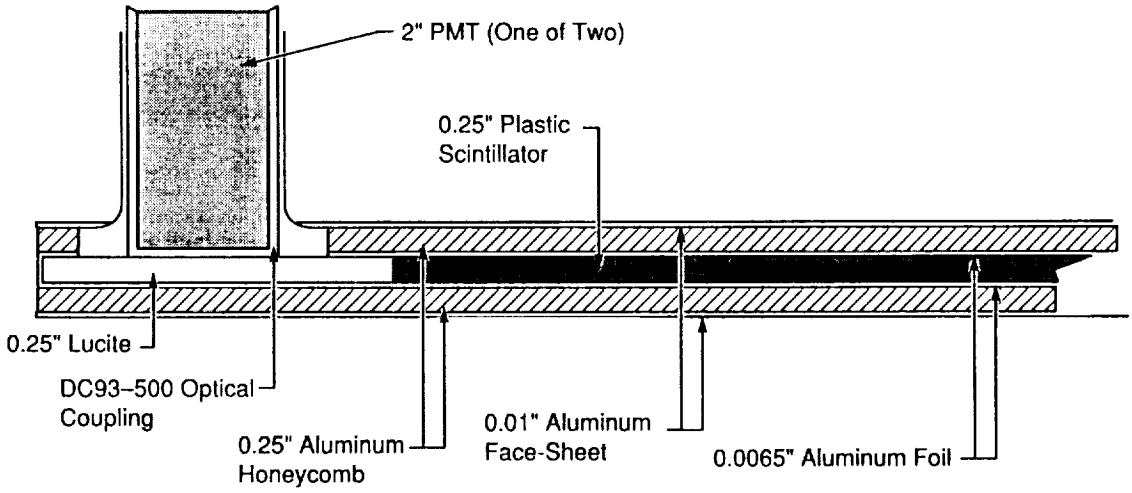

Figure 2.5. BATSE Charged Particle Detector.

Two triangular pieces of lucite are mounted on corners of the CPD. These pieces are optically coupled to the plastic scintillator. Light generated inside the plastic scintillator through interactions with charged particles is collected on these corners by two 5.08 cm diameter PMTs. These phototubes are optically coupled to the lucite using Dow-Corning DC-93-500 optical coupling material. The signals from the two PMTs are joined at the detector electronics unit into one signal. High voltage for the two PMTs is provided by a common commandable supply. Energy information is not available from the CPDs, as they are not connected to pulse-height analysis circuitry. They simply identify when a charged-particle event has occurred through use of a single discriminator.

The CPD is installed onto the detector module directly in front of the large area detector. Figure 2.6 shows the location of the CPD on the module. The perpendicular distance from the front of the CPD to the front of the LAD is 3.81 cm.

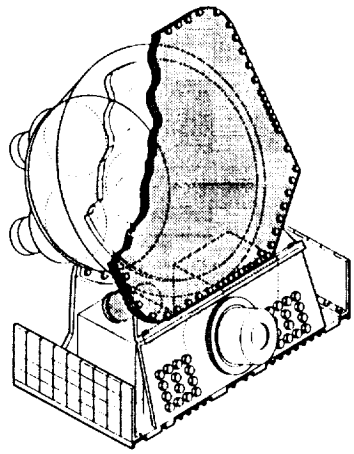

Figure 2.6. BATSE CPD on the Detector Module.

D. BATSE Photomultiplier Tubes

The BATSE photomultiplier tubes were procured from EMI Ltd. of Great Britain. All flight PMTs were constructed with Bi-alkali photocathodes and beryllium-copper dynodes. Initial specifications called for the installation of cesium-antimony dynodes; however, fabrication with these dynodes could not be done without contamination from electrically conductive particles inside the tube. The first shipment of flight PMTs arrived at NASA Marshall Space Flight Center in November of 1984. After arrival, each of the candidate PMTs were processed through a detailed testing and inspection procedure, under the direction of Bob Wilson.

A visual inspection was performed on each of the PMTs. This inspection determined the number and size of any loose particles which might have been present in the PMT, identified any scratches or defects in the PMT optical window, and examined the photocathode for any immediately observable flaws or non-uniformities. Following the visual inspection, a series of tests were executed to determine the performance of these PMTs. Because the tubes were environmentally tested before arrival at MSFC, these tests were not repeated. The tests done at MSFC included a gain scan, a measurement of the PMT linearity, determination of the noise spectrum at several gain settings, transient/fatigue measurements, SAA exposure gain recovery measurements, magnetic field sensitivity determinations, and measurements of the stability of the gain. Each of these tests and their results are discussed in detail in a later section of this document.

The PMTs used for the BATSE large area detectors and the spectroscopy detectors are all 12.7 cm (5 inch) diameter tubes, EMI model D302NA. These phototubes have a minimum quantum efficiency of 26% at 410 nM, and an energy resolution of better than 8% at 662 keV. Each of these nine-stage tubes contain their own potted hard-pin base, which is spot-welded to a PC board containing the voltage-divider string. Figure 2.7 shows the configuration of the base electronics for each of the 12.7-cm PMTs on the instrument.

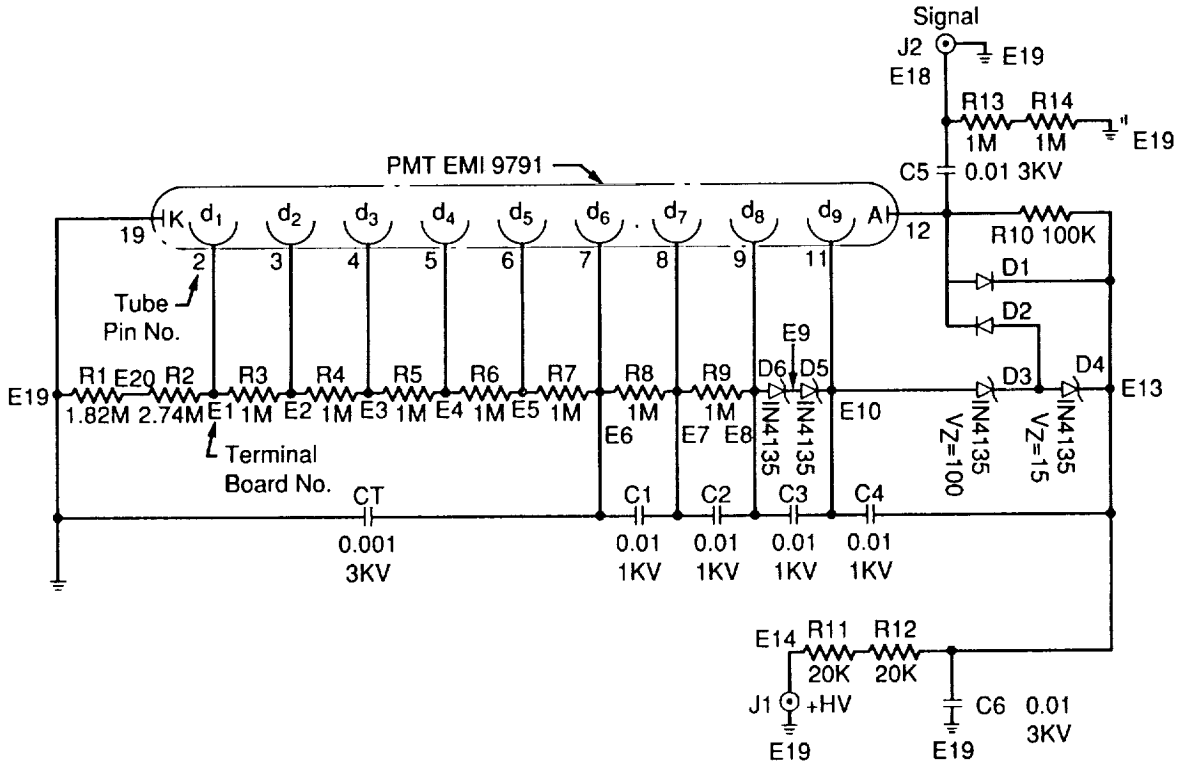

Figure 2.7. BATSE Nine-Stage, 12.7-cm PMT Potted Tube-Base Assembly.

Each of the BATSE charged particle detectors employs two 5.08 cm diameter PMTs. These are ten-stage photomultiplier tubes, EMI model number 9956. The CPD tubes have a minimum quantum efficiency of 24% at 440 nM and an energy resolution of 10.5% at 122 keV. As with the larger tubes, these PMTs each have their own potted base assembly. Figure 2.8 details the potted assembly for the 5.08-cm PMTs on the instrument.

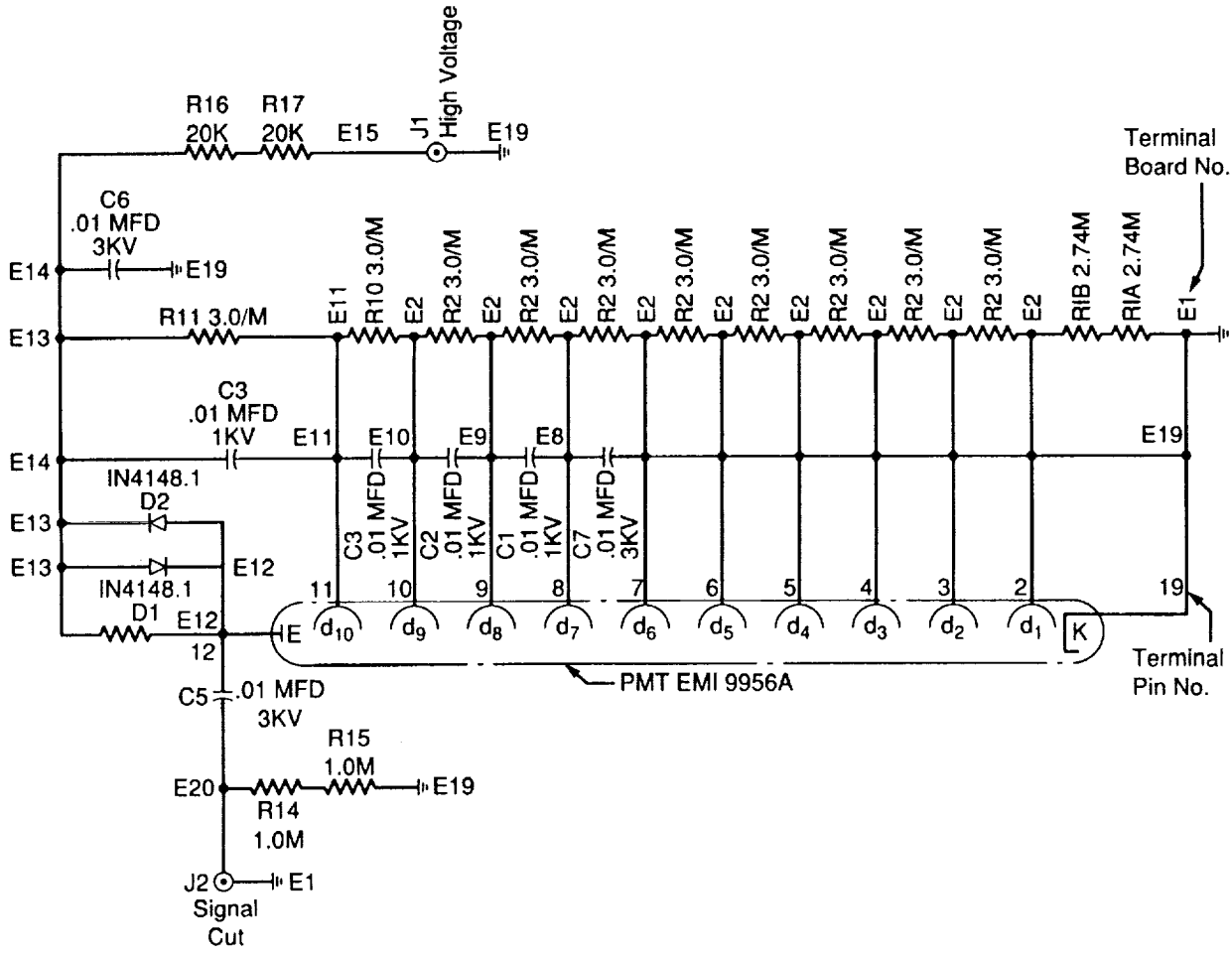

Figure 2.8. BATSE Ten-Stage, 5.08-cm PMT Potted Tube-Base Assembly.

E. BATSE Detector Electronics Unit and HVPU

Each of the BATSE detector modules contains its own detector electronics unit (DEU), which is located under the LAD light collection cone. The electronics contained in the DEU perform several functions which are detailed in the following table.

Table 2.2. Detector Electronics Unit Functions

- Power isolation and regulation for HVPU and DEU
- Command decoding and execution for HVPU and DEU
- Digitization of detector science signals
- Detector discriminator control
- Generation of LED drive signals
- Buffering of all digital input and output signals
- Routing of analog HKG signals to CEU

The functions shown in the table above are implemented on five printed circuit boards each 17.2 cm x 10.6 cm. These boards are housed in the DEU aluminum enclosure which measures 17.6 cm x 15.2 cm x 15.2 cm. The housing is divided internally into two sections. The first and smaller compartment contains the power supply board. Bypassing feed-throughs route output power from the power supply board into the second compartment that contains the four remaining boards. Each of the boards in the DEU are discussed in the following sections.

1. Power Supply Board

The power supply board receives regulated +15 Vdc from the BATSE power module (BPM) and converts it into +15, -15, +6, -6, -3, and +5 volts. Active regulation is provided for the latter four voltage outputs. The DEU uses each of these voltage outputs in a variety of functions. In addition, the high voltage power unit (HVPU) uses the +5 and +15 volt outputs to generate and control the high voltage for the PMTs.

2. Housekeeping and Command Board

The housekeeping and command board receives the serial command signals from the CEU and subsequently decodes and executes or forwards these commands as appropriate. The following commands are executed within the DEU:

- LAD and SD discriminator settings
- Housekeeping multiplexer channel values
- LAD coincidence/anti-coincidence mode settings
- LED amplitude settings

Commands for the setting of PMT high voltages are forwarded to the HVPU for execution. The housekeeping and command board also contains the differential receivers for serial commands.

3. Interface and LED Driver Board

All digital signals that pass between the DEU and the CEU are handled with differential drivers and receivers. These drivers and receivers (with the exception of the serial command receivers) are located on this board. The interface and LED driver board also contains the digital-to-analog converter for the SD discriminator threshold, the analog-to-digital converter and driver for the LED amplitude, and the level converters for the telemetered negative supply voltages.

4. Spectroscopy MQT Board

The SD MQT board receives the signal from the spectroscopy 12.7-cm PMT and passes it through a charge-sensitive amplifier/baseline restorer (CSA/BLR). From the output of this CSA/BLR, the signal branches to a four-channel fast discriminator section and to the high resolution charge-to-time (MQT) converter. The fast discriminator section of the circuit generates the SFAST data, while the MQT generates SHER data from the PMT signals. The output of both of these sections is in digital form and is passed to the CEU with the use of differential drivers. The energy thresholds of the discriminators and resolution of the SHER data are covered elsewhere in this document. The output of the four SFAST discriminators is integral.

5. Large Area Detector MQT Board

This board receives the summed signal from the three LAD 12.7-cm PMTs and passes it through a CSA/BLR similar to what exists on the SD MQT board. From this CSA/BLR, the signal branches to a four-channel fast discriminator section, and to the high resolution charge-to-time converter (MQT). The fast discriminator section produces the FAST discriminator data, while the MQT generates the LAD high energy resolution (HER) data type. These outputs are sent to the CEU through the use of differential driver circuits. Other data types are also generated downstream from these signals in the CEU and are discussed fully in section II.F.3. The output of the first three FAST discriminators is differential, and the fourth is integral above its threshold.

The LAD MQT board also receives the signals from the charged particle detector PMTs and compares the amplitude of the voltage pulse to a level expected from a charged-particle event. For those signals which exceed this threshold, a count in the PLASTIC data is generated. The capability exists to require that these events be either absent or present simultaneously with a LAD-generated signal to produce a gamma ray count in the HER data. This coincidence/ anti-coincidence feature serves to reduce the background level and to calibrate the LAD with charged particles. The mode of operation is selected individually for each module with serial commands.

6. BATSE High Voltage Power Unit

The second electronics box located on the BATSE detector module is the high voltage power unit (HVPU). The HVPU contains five separate commandable high voltage power supplies. These supplies accept the +15 and +5 volt outputs from the DEU and produce high voltage in the range of 1000 to 2000 volts. The output voltage for each of the five supplies is programmable in steps of approximately 4 volts across this range. Each supply can be programmed off and is current-limited at 200 μA. The supplies also produce analog voltages for telemetry corresponding to the value of voltage and current which it is supplying. The three LAD 12.7-cm PMTs and the SD 12.7-cm PMT have their own individual +HV supply. The two 5.08-cm PMTs on the charged particle detector share a single supply. The HVPU is housed in an aluminum enclosure measuring 15.2 cm x 12.7 cm x 22.3 cm. The enclosure is installed on the detector module underneath the LAD light collection cone, opposite the detector electronics unit.

F. BATSE Central Electronics Unit

The BATSE central electronics unit (CEU) is the digital processing system for the experiment. The CEU was designed and built at MSFC. No single point failure in the CEU will cause the loss of BATSE, or more than half of the science data. As the interface between the GRO and BATSE, the CEU receives serial commands, the telemetry master frame reset signal, and clock data. The CEU transmits packetized serial telemetry data and hard-wired engineering data back to the spacecraft. It also provides the other three experiments with the burst trigger signal and notifies COMPTEL of a solar flare through the GRO's onboard computer. As the internal interface between BATSE components, the CEU accepts pre-processed detector data from the detector modules and controls the acquisition of engineering data from the experiment. Furthermore, the CEU controls the settings of the high voltage power supplies and the calibration LED. A complete listing of CEU boards and functions is provided in Appendix C.

Internal to the CEU are several discrete functions. Each function is somewhat independent of the others; however, significant interfacing among functions is accomplished. These functions are discussed individually in the following paragraphs.

1. CEU Control Function

The CEU control function (CCF) is a programmable, microprocessor-based function that interfaces to the GRO and the other CEU functions. It provides all of the hardware controls necessary to initialize, monitor, and acquire data from the science data function (SDF), the power control function (PCF), the BATSE status function (BSF), and the analog data function (ADF). The CCF can also command the detector modules via DEUs.

The CCF function is controlled by two redundant CCF boards present in the CEU. During normal operations, both CCF boards are powered, but only one is in control. Either CCF is capable of controlling all CEU functions. Each board contains its own Texas Instruments SBP-9900A microprocessor chip and supporting logic elements. Among these support elements,

a CPU clock generator develops the 1.365 MHz non-symmetrical clock required by the microprocessor. A 500 mA current source is present to power the SBP-9900A. CPU interrupts are detected and priority encoded by an interrupt encoder. An input/output device selector decodes the CPU control lines and address bus to control the CEU input/output devices. A discrete command decoder generates pulse commands to control various CEU devices. A status input multiplexer inputs discrete status signals for the software program test and status words for housekeeping data. Finally, a watch-dog timer, if enabled, will time out and reload the flight software within 2.048 seconds if not reset by the flight software in operation.

Cross-strapping from the CCF function to the remote interface unit (RIU) is employed. Isolation is maintained between the CCF functions by using separate RIU serial commands, timing, and data channels. GRO discrete commands to the power control function are used to select which of the CCF boards will control operations. The CCF's tasks are outlined in Table 2.3. The major elements of the CCF are shown in Table 2.4.

Table 2.3. BATSE CCF Function Tasks

- Process serial commands from the GRO
- Format and output serial packetized telemetry to the GRO
- Initialize and acquire data from the SDF and ADF functional elements
- Alert the other GRO instruments of a gamma ray burst
- Alert COMPTEL of a solar flare via the GRO onboard computer
- Command and calibrate the detector modules via the DEUs

Table 2.4. BATSE CCF Elements

- GRO interface
- CPU (described above)
- CPU memory
- Serial input/output controller
- HER burst memory for the LAD

The GRO interface is interconnected to both RIUs and time transfer units (TTUs). These elements are mounted onto the BATSE electronics panel next to the CEU and BPM. There are three serial digital command channels into the CEU, one for BATSE serial commands using CCF-A, another for CCF-B, and the third for the universal time code updates. The BATSE serial command channel is selected by the setting of a bit in the serial command. Eight discrete command channels provide control of CCF-A, CCF-B, and the watch-dog timers. A serial telemetry channel exists for the output of BATSE packetized data.The master frame reset timing signal starts a BATSE data packet transfer every 2.048 seconds. A 1.024 kHz clock channel provides most of the CEU internal timing, and a 1 Hz clock from the TTU synchronizes the CEU time counters and the UTC updates.

The CPU memory consists of 4K words of read only memory (ROM), 4K words of random access memory (RAM), and 8K words of RAM along with a program ROM to RAM loader. The flight software is executed from RAM, and must be down loaded from ROM prior to execution. This occurs automatically when power is applied to the CEU. The load controller can be commanded from the ground via the GRO interface, or automatically in response to a watch-dog time out due to a malfunction. The additional RAM is provided for software tables, program work space, and storage of temporary data.

The serial input/output controller (SIO) enables the CCF to transfer commands and data. The serial interfaces are implemented with differential drivers and receivers which provide good noise rejection and isolation from functions which are powered off. The CPU controls the SIO from its parallel control and data bus. The system speed is maintained by performing serial transfers between CPU parallel transfers.

The HER burst memory is loaded with the LAD HER data during a gamma ray burst. The CCF acquires the HER data from the SDF and stores it until the memory is full. After the burst, the data are transmitted in the BATSE packet.

2. Power Control Function (PCF)

The PCF allows power for CEU functional elements to be individually switched using RIU discrete commands. A schematic of the PCF is given in Figure 2.9.

The PCF is implemented using magnetically latched relays that can be set or reset by RIU discrete commands. To satisfy the CEU single point failure criteria, two relays are used to power each CEU function. To enable a single RIU discrete command to control a magnetic latching relay (two control coils), the PCF directs the corresponding 28 Vdc pulse to the desired set or reset relay coil. To provide the required redundancy, separate relay control buses are used for the primary and redundant relays.

The relay set/reset control circuit develops the following 28 Vdc relay control buses:

- Primary relay control bus-I and backup relay control bus-I for control using RIU discrete command channels 2-62 (even only).

- Primary relay control bus-II and backup relay control bus-II for control using RIU discrete command channels 1-47 (odd only).

The relay control buses are also used to control the detector module power control relays and to switch the output of the redundant power supplies in the BPM.

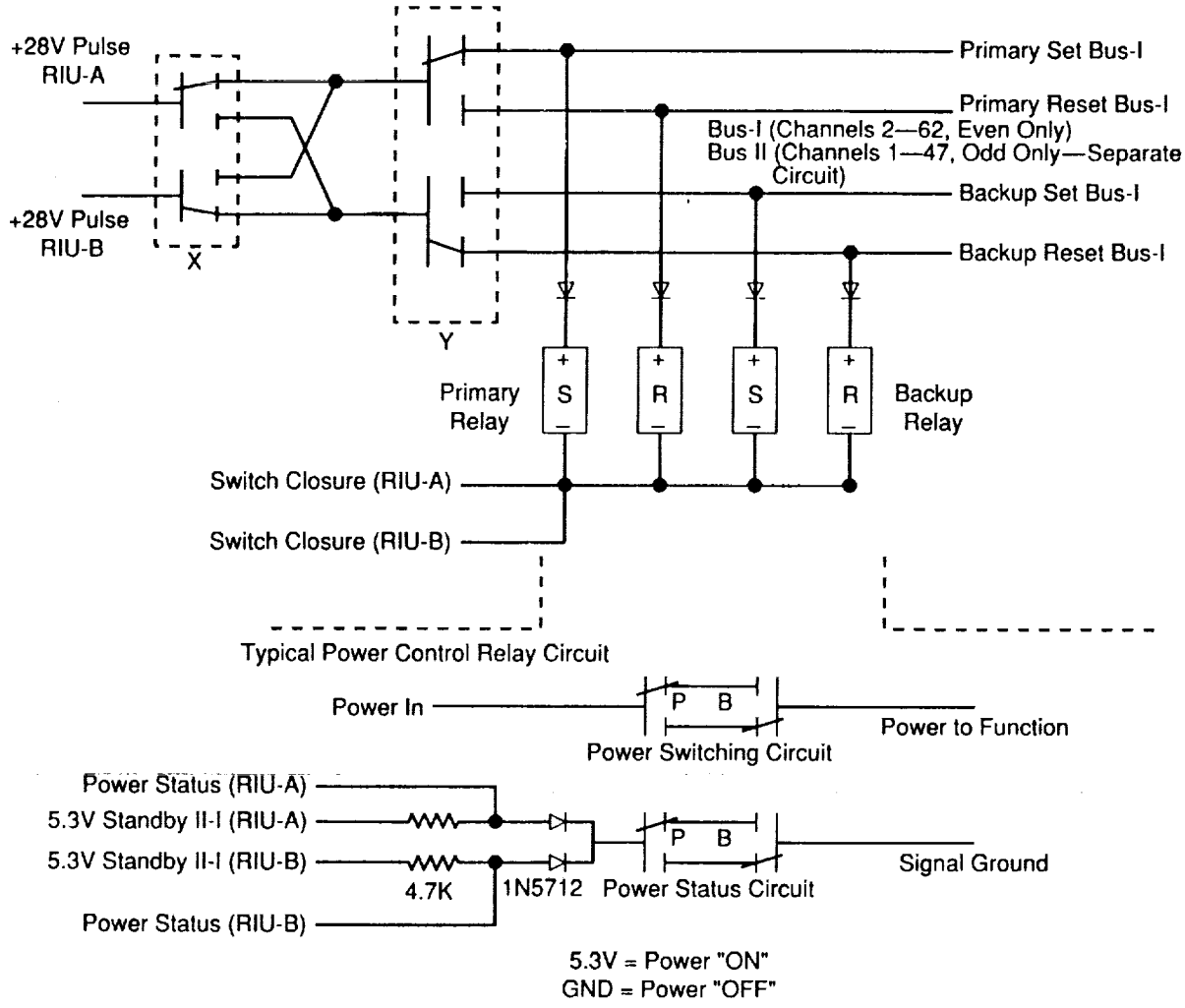

Figure 2.9. BATSE Power Control Function Schematic.

The relay set/reset control circuit is composed of relay circuits X and Y. The function of circuit X is to direct the RIU 28 Vdc command pulse from either RIU to the primary or backup relays. The function of relay control circuit Y is to further direct the command pulse to the relay's set or reset coil. The circuits operate in the following manner:

- Relay circuit X in the set state enables RIU-A to control the primary relays and RIU-B to control the backup relays. This arrangement allows relay circuit X to fail in either state without losing control of the PCF relay circuits. This circuit also maintains the required RIU isolation without the use of diodes.

- Relay circuit Y in the set state enables either RIU, by switching X, to set any primary relay and reset any backup relay. This arrangement allows relay circuit Y to fail in either state and still any CEU function can be powered off by either RIU if X functions, or by the use of both RIUs if both X and Y fail.

3. Science Data Function

The science data function (SDF) acquires, accumulates, and pre-processes BATSE science data from the eight detector modules. The DEUs pre-processes and conditions the data signals produced by the LADs, SDs, and CPDs, providing a compatible interface to the SDF.

Table 2.5. BATSE Science Data Types

Name	Detectors	Energy Channels	Time Resolution	Uses
Continuous (CONT)	Separate	16	2 sec	Transient detection, strong source monitor, weak burst detection, long-period pulsars
HER and HERB**	Separate	128	> 0.128 sec (programmable)	Detector energy calibration, burst spectral lines, burst locations
Pulsar (PSR-A) and (PSR-B)	Combined	16	4 - 16 secs per readout 64 phase bins (programmable)	Profiles of known pulsars, low duty cycle-high time resolution data
Discriminator (DISC)	Separate	4	0.064 sec-burst 1 sec-continuous	Onboard burst detection, burst precursors
NaI	Separate	1	1 sec	Total LAD NaI Ct. rate
Plastic	Separate	1	1 sec	CPD count rate
Time to spill (TTS)	Combined	4	~1 μsec, rate dependent	Burst temporal structures
Medium energy resolution (MER)	Combined	16	0.016 - 0.064 sec (programmable)	Burst spectral evolution
Time tagged event (TTE)	Separate	4	2 μsec	Burst risetime, burst temporal structures, periodicities and locations of short bursts
SD HER (SHER) and SHERB**	Separate	256	> 0.128 sec (programmable)	Burst spectroscopy, background and calibration data
Spectroscopy discriminators (SDISC)	Separate	4	0.064 sec-burst 2 sec-continuous	Dead time corrections, state of health, high energy counts
Spectroscopy time tagged event (STTE)	Separate	256	128 μsec	Spectral fine time resolution

**The HERB and SHERB data are generated only from a triggered gamma ray burst and have programmable time resolutions greater than 0.128 seconds. The HER and SHER data are standard data types and are programmable in intervals larger than 49 seconds. Nominally these data types have a time resolution of 300 seconds.

In the SDF are several major elements, each contributing to the development of the science data types shown above. Each of these elements will be discussed in the following paragraphs. These elements are:

- Discriminator, continuous, and high energy resolution (DCH)
- Medium energy resolution/pulsar (MER/PSR)
- Time to spill (TTS)
- Time tagged event (TTE)
- Spectroscopy discriminator and high energy resolution (SDH)
- Spectroscopy time tagged event (STTE)
- Spectroscopy high energy resolution burst (SHERB)

The DCH provides the interface for the eight science data signals generated from the LAD in the DEU of each detector module. The eight DCH boards in the CEU are independently connected to the DEUs such that no single failure will affect the operation of the others. The DCH also provides the interface for the active CCF to send serial commands and LED calibration control pulses to the modules' calibration assemblies. This board processes seven of the eight detector science data signals into five separate data types: discriminator (DISC), continuous (CONT), high energy resolution (HER), burst discriminator (DISCB), and burst HER (HERB). The eighth signal, a sum of FAST1 - FAST4, is not processed into telemetry (FASTn = discriminator channel #n, n = 1-4). DCH also generates discrete signals to be used by the MER/PSR function.

The DISC data type is produced by counting for each detector module the number of FAST1, FAST2, FAST3, FAST4, NaI, and PLASTIC data signal pulses that occur during a fixed period of time. These pulses represent threshold energy levels and event rates on the CPD and LAD. The four FAST signals and a FASTID signal are provided to the TTS and TTE functions for use when a burst occurs.

The CONT and HER data types are produced from the LAD MQT signal, which is developed by a charge-to-time converter in the DEU (see section II.E). The width of this signal is a measure of the detected energy loss in the NaI crystal. The MQT pulse width from the DEU is digitized by the SDH board into 384 linear channels. These are subsequently compressed into 128 channels as follows. For the first 65 bins, there is a one-to-one correspondence between channel width from the DEU and bin width in the data. After channel 65, the following 32 bins are two DEU channels wide. Thus the gain of the detector has been compressed by a factor of 2 in this region. Starting at channel 96, the compression changes to eight DEU channels per energy bin. This quasi-logarithmic compression of the data saves telemetry space with limited loss of information, because at high energies (where the compression takes place), the resolution of the detector is larger than one DEU energy channel. During nominal LAD operations, the gain of the PMTs is set so that one DEU channel corresponds to 5 keV of energy. HER data are developed by counting the number of times each of the possible 128 energy bins is detected over a fixed time period. For each MQT signal, one of the energy bin counters is incremented. The CONT data type is developed by using a programmable look-up table to map the digitized MQT

signal into one of 16 energy channels, and then accumulating the number of events for each channel that occur over a fixed time period. The look-up table can be changed by commands from the ground.

The DISCSC and HERB data types are developed only during a burst in the same manner that DISC and HER are developed during non-burst periods.

The MER/PSR function is provided with discrete signals from the DCH (or SDH in the case of SD data) which are discrete pulses representing one of the 16 energy channels discussed above. MER data are obtained only during a burst by counting the number of logically summed pulses from software-selected LADs occurring in each of these 16 energy channels during a specified time period. PSR tasks operate when the MER task is not active (no burst), and counts the same pulses in a different manner. A specified time period is divided into equal sub-time periods called phase bins. A scan number is specified to be used during the PSR task as well. A profile is developed for the specified number of scans through these phase bins. Each of the 16 energy channels has its own separate profile. The user has complete control over which detector(s), including LAD or SD, to select for the PSR task. However, only the SDs selected for the pulsar task will appear in STTE pre-burst data if and when a burst is detected.

The TTS functional element measures the time required for a specified number of FAST discriminator pulses to occur, and only acquires data during a burst. As in the MER/PSR function, only signals from selected detectors are used for measurements. All of the like signals (FASTn) from selected detectors are logically summed to provide four signals from which the measurements are made.

The TTE function records the time of a detected gamma ray event. The four FAST signals and the FASTID signal from each LAD are used to produce this data type. Along with the time, the event ID (which FAST signal), and the detector ID (which of the LADs) are recorded. The TTE operates prior to a burst in a pre-burst mode. In this mode, all LADs contribute to the tagged events, and the memory rotates to keep only "fresh" data in the memory. At the time of burst detection, the TTE is commanded to burst mode. In this mode, only selected detectors are enabled to contribute to the data type, and continues until three-fourths of the memory is filled. In this way, the remaining one-fourth of the memory contains data prior to the burst. Figure 2.10 details the generation of LAD data types.

The spectroscopy discriminator and high energy resolution (SDH) function provides the interface for the five data signals generated by the SD MQT board in the DEU of each DM. Like the DCH function, the eight SDH boards are independently connected to the DEUs such that a failure in one will not affect the operation of the other seven. The primary function of the SDH is to process the five science data signals into two separate data types, SDISC and SHER. SDISC data are produced by counting the number of SFAST1, SFAST2, SFAST3, and SFAST4 data pulses received over a fixed time period. This is identical to what was described for the DCH function. The pulses represent threshold levels of energy incident on the SD NaI detector. SHER data are produced by processing the SD MQT signal. This signal is equivalent to the

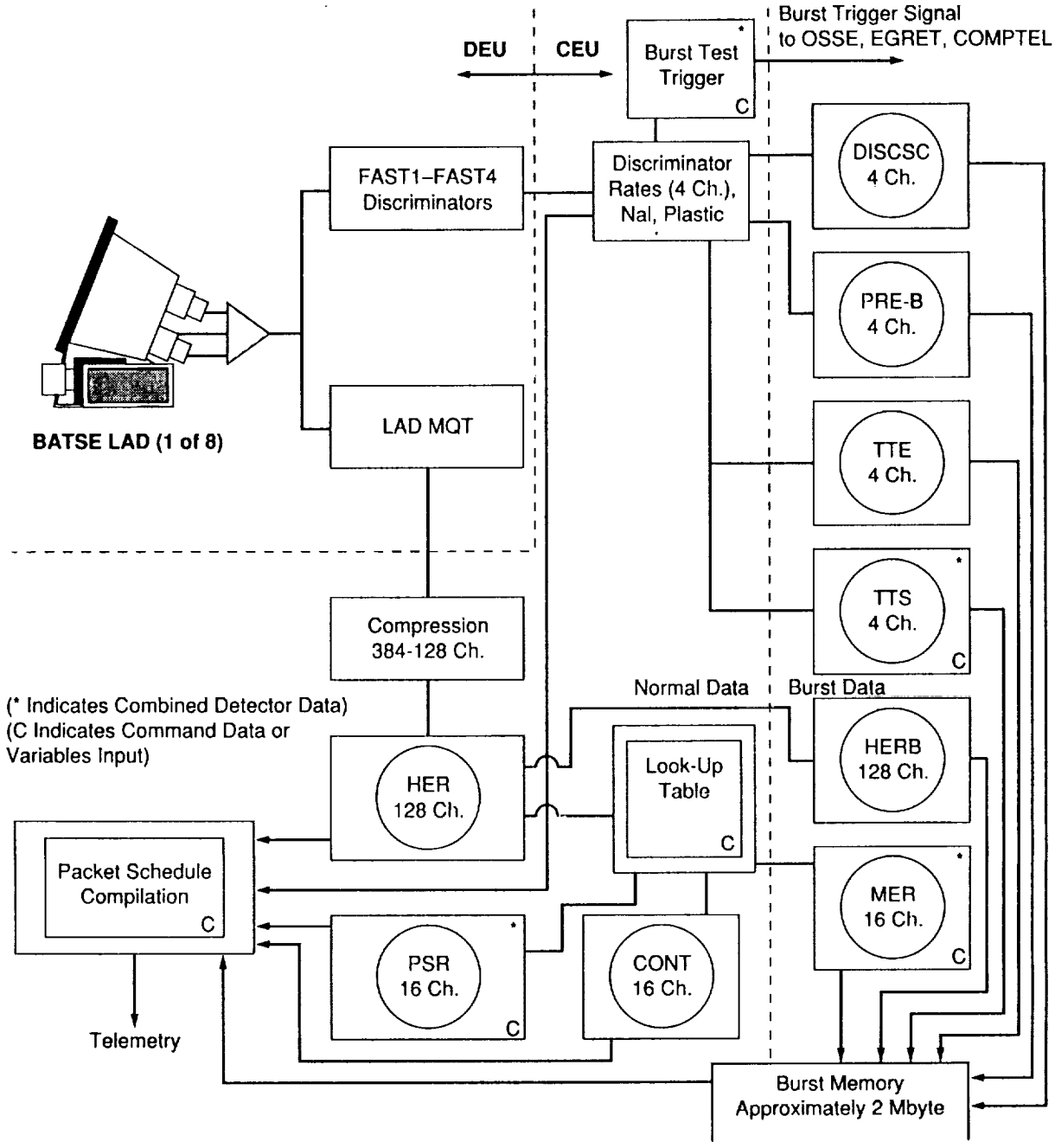

Figure 2.10. Large Area Detector Data Flow Diagram.

LAD MQT signal, but here is digitized into one of 256 increments (energy channels), compressed from 2752 linear channels. The gain-compression scheme is similar for the SD; however, each compression region is 64 channels wide. The first region of 64 channels has no compression of the SD MQT pulse. The second region is compressed by a factor of 2, with the next two regions being compressed by factors of 8 and 32, respectively. The SHER data type is developed directly from the digitized signal using the same process as the HER data type. This digitized signal is also used to develop the STTE data type and, indirectly, to develop the spectroscopy pulsar (PSR) data type. A look-up table is used to map the 256 energy channels into 16 energy channels used for the SD PSR data type and to define a low-level discriminator setting which controls the STTE data type. This look-up table is programmable by ground commands.

STTE events are derived from flight-software-selected SDs during a burst. The data are developed from the digitized SD MQT signal. The SDH function of each detector module generates a signal when that module is selected and the data value exceeds the low-level discriminator setting. The discriminator event signals are then processed by the STTE on a first-come, first-served basis. Other detectors are ignored until that particular signal is finished. The STTE tags the event data with the identity of the detector and the time of the event. Only SDs on modules whose LADs exceed burst threshold will be used by the software.

The SHERB functional element accumulates a large amount of the SHER data during a burst. The data accumulated come from the four SDs on modules whose LADs show the highest rates above background, and consists of the 256 energy channels from each selected detector. Figure 2.11 details the generation of spectroscopy data types. Storage of the SHERB spectra is under flight-software control.

4. Analog Data Function

The analog data function (ADF) performs analog-to-digital conversion of the BATSE housekeeping measurements and controls the LED calibration assembly. When a burst occurs, circuitry on the ADF board generates the burst trigger signal for the other three instruments on the GRO. Two independent ADF boards (ADF-A and ADF-B) reside in the CEU. Either ADF can be operated in conjunction with either CCF. During normal operations, only one of the ADF boards is powered. The ADF can be divided into three sub-functions: analog data conversion (ADC), detector calibration control (DCC), and the burst trigger signal (BTS).

The ADC functional element performs the task of converting the analog housekeeping measurements from each detector module, the CEU, and BPM into 12-bit digital words. It is composed of a 16-channel multiplexer that gates the analog input to be converted; a 12-bit analog-to-digital converter; and a controller that selects the analog input, starts the conversion, and alerts the CCF when complete. Each conversion is commanded by the CCF. The analog input selection is sequential and is automatically stepped after a conversion is completed by the controller.

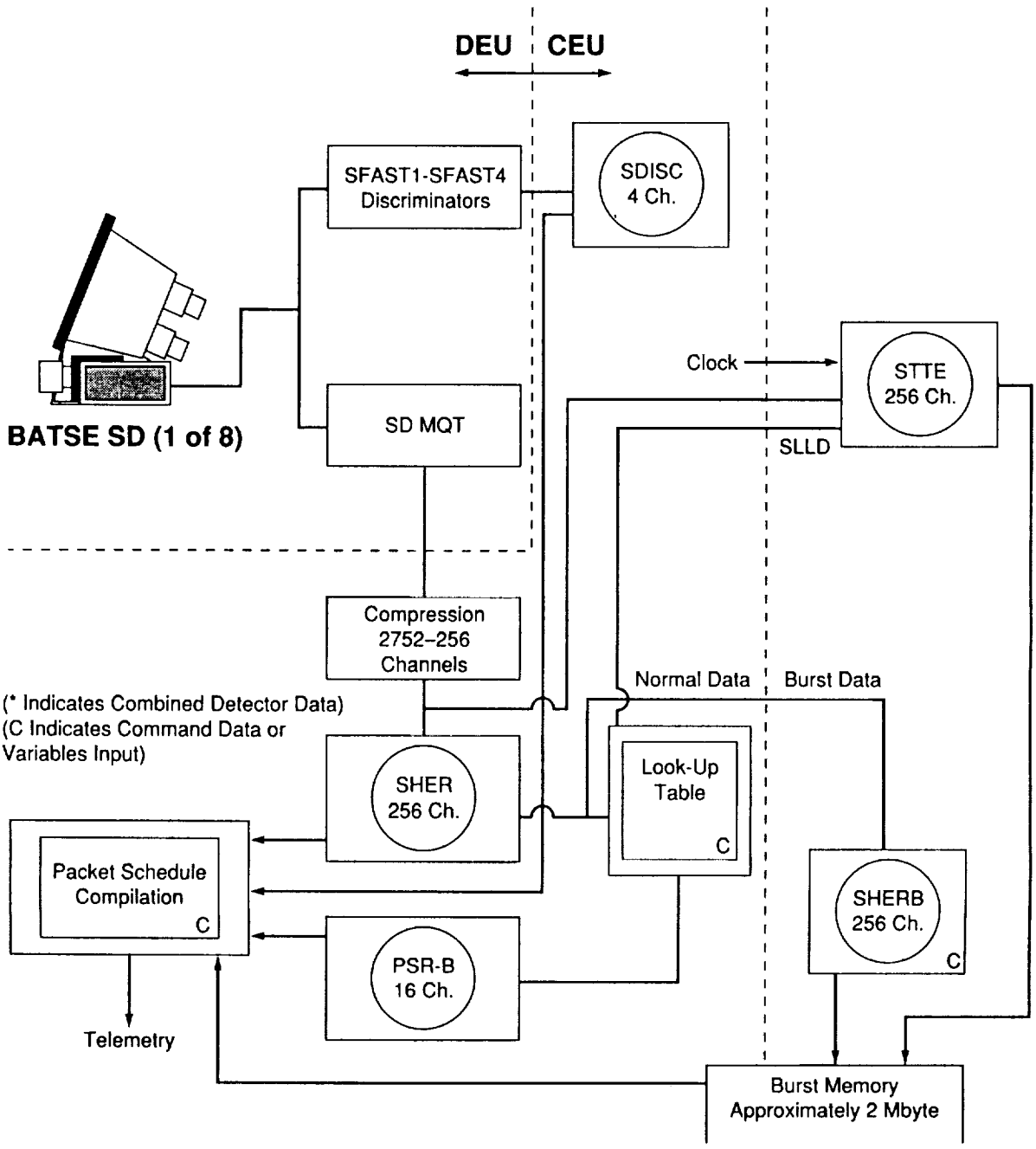

Figure 2.11. Spectroscopy Detector Data Flow Diagram.

The DCC provides the timed digital component of the signal required to calibrate the LADs. The magnitude component of the calibration signal is provided by the DEU in each detector module. The DCC signal establishes the calibration signal time period and the DEUs with the magnitude prior to starting detector calibration. The flight software controls the calibration with start and stop commands to the DCC. The DCC signal is routed to the DEUs via the DCH functional element.

The BTS is digital (on/off) and controlled by the CCF. It provides separate interface signal drivers for each of the other three instruments under flight-software control when a burst occurs.

5. BATSE Status Function (BSF)

The BSF conditions BPM and detector module signals prior to transmission to the RIU. To satisfy the single point failure requirement, the circuits on the board are redundant and independent. When the flight software determines that a solar flare has been detected, the BSF generates a bi-level telemetry signal for the GRO onboard computer. The OBC then recognizes this signal and notifies the COMPTEL instrument according to a predetermined sequence of commands stored in memory. Also in the event of a solar flare, the BATSE burst trigger signal (BTS) is given a longer duration. OSSE decodes the length of the BATSE BTS to determine if there is a solar flare event. The duration of the BTS is programmable in units of 64 milliseconds through a parameter in the flight software. Coordination between the BATSE and OSSE experiments determines all relevant solar flare parameters, including the duration of the BTS.

G. BATSE Power Module

The BATSE power module (BPM) is located with the CEU on the BATSE electronics panel. The BPM has several functions. It interfaces with the GRO to receive instrument and heater power. Instrument power is then converted and conditioned for use by the detector modules and the CEU. The BPM monitors the detector module temperatures and provides on/off control of thermal control and make-up heaters. STS heater power is distributed to the detector modules through the BPM. An interface connector is provided at the BPM for the testing and control of the STS heaters while the instrument is on the ground. The BPM accepts control commands from the CEU to switch power supply outputs and on/off control of power for each of the detector modules. Status data for relays, temperatures, heaters, and currents are provided to the CEU by the BPM.

Redundant power supplies (SLCCs) are provided in the BPM. These interface to the GRO and receive redundant +28 Vdc instrument input power. To maintain isolation between the GRO input power sources, no cross-strapping is utilized. Therefore, primary input power interfaces to SLCC-A, and backup input power interfaces to SLCC-B. The failure of a SLCC or its input power source will require switching to the other SLCC and input power source.

Each of the SLCCs contains a module to convert the input power to +15 Vdc, required for the detector modules, and a module to convert the input power to +5 Vdc, which is required by the CEU. Cross-strapping is not provided on the SLCC outputs. Redundant power switching relays are utilized to effect transfer of output power to the appropriate SLCC. The transfer is accomplished using ground commands which are implemented through the CEU.

The +5 Vdc output of the SLCC is current-limited to prevent damage to internal components in the event of a failure. A feedback loop is also utilized for the +5 Vdc output power to assure that the voltage is maintained at the interface to the CEU. Over-voltage cut-off circuitry is provided to prevent voltage transients from damaging the SLCC. The current from the +15 Vdc and +5 Vdc outputs is monitored as part of the housekeeping data to aid in the detection of anomalies.

Redundant relays are provided in the BPM for on/off control of the +15 Vdc power for the detector modules. Power can be controlled on an individual basis using ground commands implemented through the CEU to the BPM. Heater power to operate the STS heaters is provided by the GRO. The BPM accepts this simplex power input and distributes it to the modules. Circuitry in the BPM provides STS heater thermostat status to the CEU for transmission to the RIU. A tri-state output is provided to indicate three possible states of power: STS power off, STS power on with thermostat open, and STS power on with thermostat closed. STS heater status is only readable through RIU-A.

Two types of detector module heater control power are provided to the BPM by the GRO. Each type has a primary and redundant input. The first is called thermal control (T/C) heater power. The BPM uses this power and a temperature sensor on the module to open or close an electronic thermostat to control the heaters on the module. The status of the thermostat is provided to the CEU for transmission to the RIU. The second type is called make-up (M/U) heater power. The circuitry for this type is identical to that of the T/C heater system; however, the set-point value of the thermostat is lower than that of the T/C system. This prevents both heaters from turning on at the same time for normal operations. Cross-strapping of heater power is not used, so that a failure of a primary T/C heater circuit will require the GRO to switch to the redundant T/C heater power. Detector module heater power is not individually controllable. All modules are either enabled or disabled. In addition, primary heater status can only be read through RIU-A, while backup heater status is only readable through RIU-B.

H. BATSE Cables

Because of the locations of the eight detector modules on the spacecraft, extensive cabling is required to connect them into the CEU and the BPM, located on the BATSE electronics panel. Each of the detector modules has two connections, one which interfaces to the CEU and the other to the BPM. All data, telemetry, power and other communication is carried over these cables. Figure 2.12 details the BATSE interconnections on the GRO. Each interconnect cable is shown with a drawing number next to it. The Interface Control Document J-numbers are also provided.

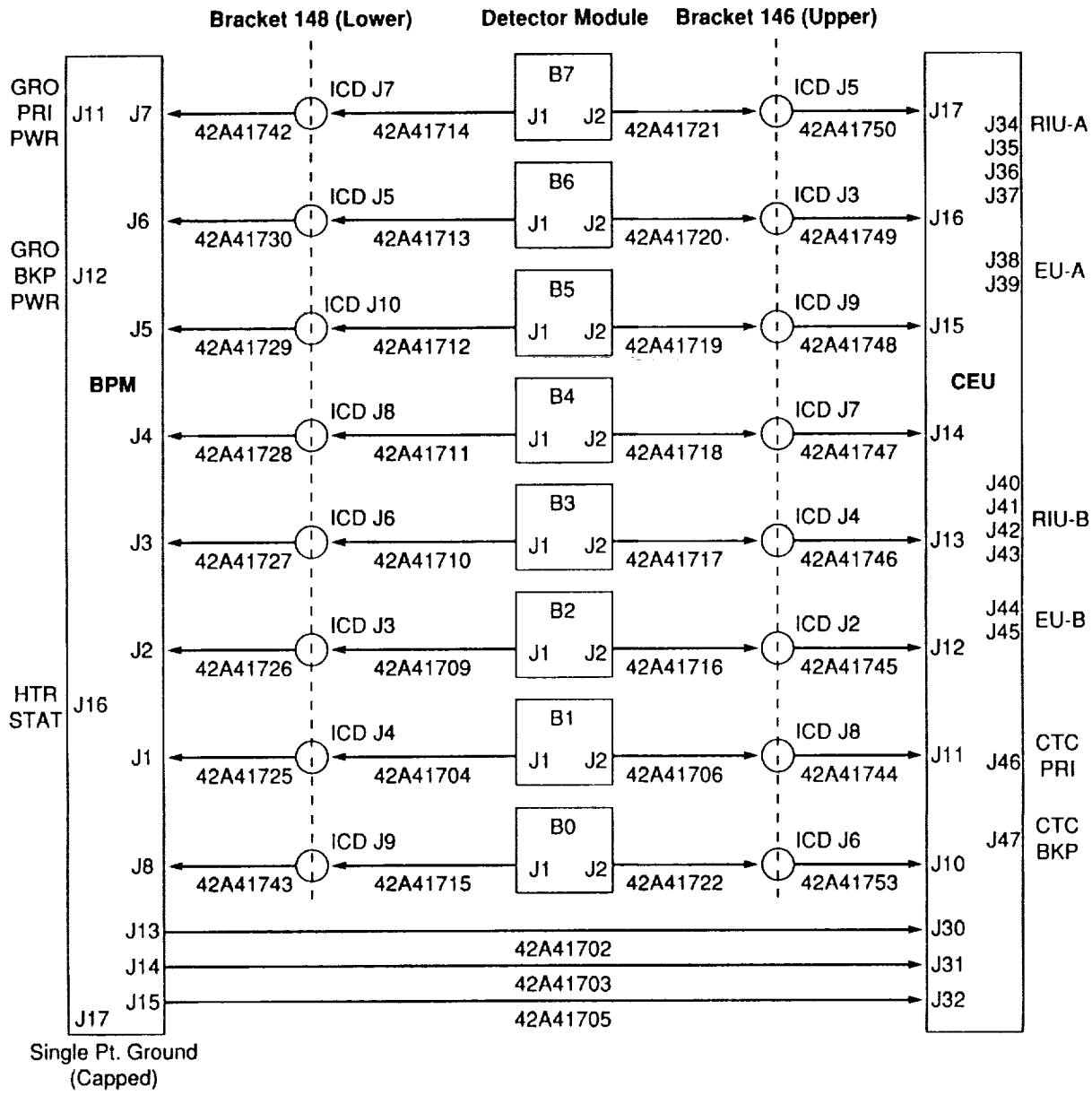

Figure 2.12. BATSE Cable Interconnect Schematic.

Connections from the detector module to the BPM and the CEU are done with two cables. The first set of cables runs from the module itself to one of two brackets mounted on the BATSE electronics panel. These are the 146 and 148 brackets. From the brackets, the connections are made to the proper receptacles on the BPM or the CEU. Because the BATSE electronics panel is hinged, it can be opened like a door. The placement of the 146 and 148 brackets allowed BATSE to test the instrument on the ground with the panel open through the employment of 16 extender cables. Without the extender cables, the flight cables are too short to be mated with the door open.

I. BATSE Thermal Control System

The thermal control of the BATSE electronics panel is the responsibility of the GRO. The GRO controls the mounting surface interface temperature and the radiant environment of the panel on which the boxes are mounted. Primary heat transfer is accomplished through conduction to the baseplates of the CEU and BPM. In addition, each are coated with a high-emissivity paint to aid in radiative heat transfer.

The detector module thermal control is accomplished through the use of heaters, passive radiators, and a multi-layer insulation (MLI) blanket. The goal of the thermal control system is to keep the rate of change in temperature of the NaI detectors (both SD and LAD) to less than 5 °C per hour. In addition, the temperature is to remain in the range of 0-30 °C.

Prior to deployment of the GRO, the thermal control of the detector modules is maintained by the STS heaters. Detectors mounted on the +Z side of the spacecraft have 15-watt heaters attached to the baseplate of the module. Detectors on the -Z side have 10-watt heaters. These heaters are under thermostat control and turn on at approximately °0 C. The turn-off temperature is approximately 8 °C, with a backup thermostat set near 14 °C. For exact turn-on and turn-off temperatures, consult the test and calibration section of this manual.

After deployment, the detector module relies on four separate heater circuits and the exposed mirrored radiator for control. Two of the heater circuits are primary, and two are redundant. The primary T/C heater circuit consists of two heaters, an 8-watt heater on the rear of the light collection cone and a 7-watt heater on the front of the LAD cone. A control sensor is mounted on the front of the cone, near the LAD's NaI crystal, and transmits an output to the control circuitry in the BPM. A thermostat there will allow these heaters to operate in the region of 4-5 °C. Over-temperature protection thermostats, identical to those used in the STS, are employed here. The primary M/U heater circuits are identical to the T/C circuits, with the exception that the operating range is lower, 0-1 °C.

During flight, both heater circuits are powered on; however, the difference in operating range prevents the M/U heaters from coming on unless there is a failure in the primary heater circuit. For each of these heater circuits, there is a redundant circuit.

The BATSE detector module is entirely enclosed inside an MLI blanket. Consisting of a tray (underneath the module) and an upper section, the blanket is coated with a highly reflective zinc-oxide based S13GLO white paint, except for the region directly in front of the BATSE LAD and SD. This region is covered with aluminized Teflon, 0.013 cm thick. Each of the aluminized teflon sections is applied to the blanket with adhesive and secured with lacing. The MLI blanket is grounded to the detector module structure in eight locations through the use of grounding straps bolted into the module housing. The MLI blanket has a cut-out for exposure of the mirrored radiator.

Each BATSE detector module was fabricated with two identical mirrored radiators, one on each side of the module, attached at the baseplate. However, at installation of the blanket, only the radiator facing nearest the -X direction (away from the Sun) was left exposed. The exposed radiator consists of 77.4 cm^2 of second-surface mirrors.

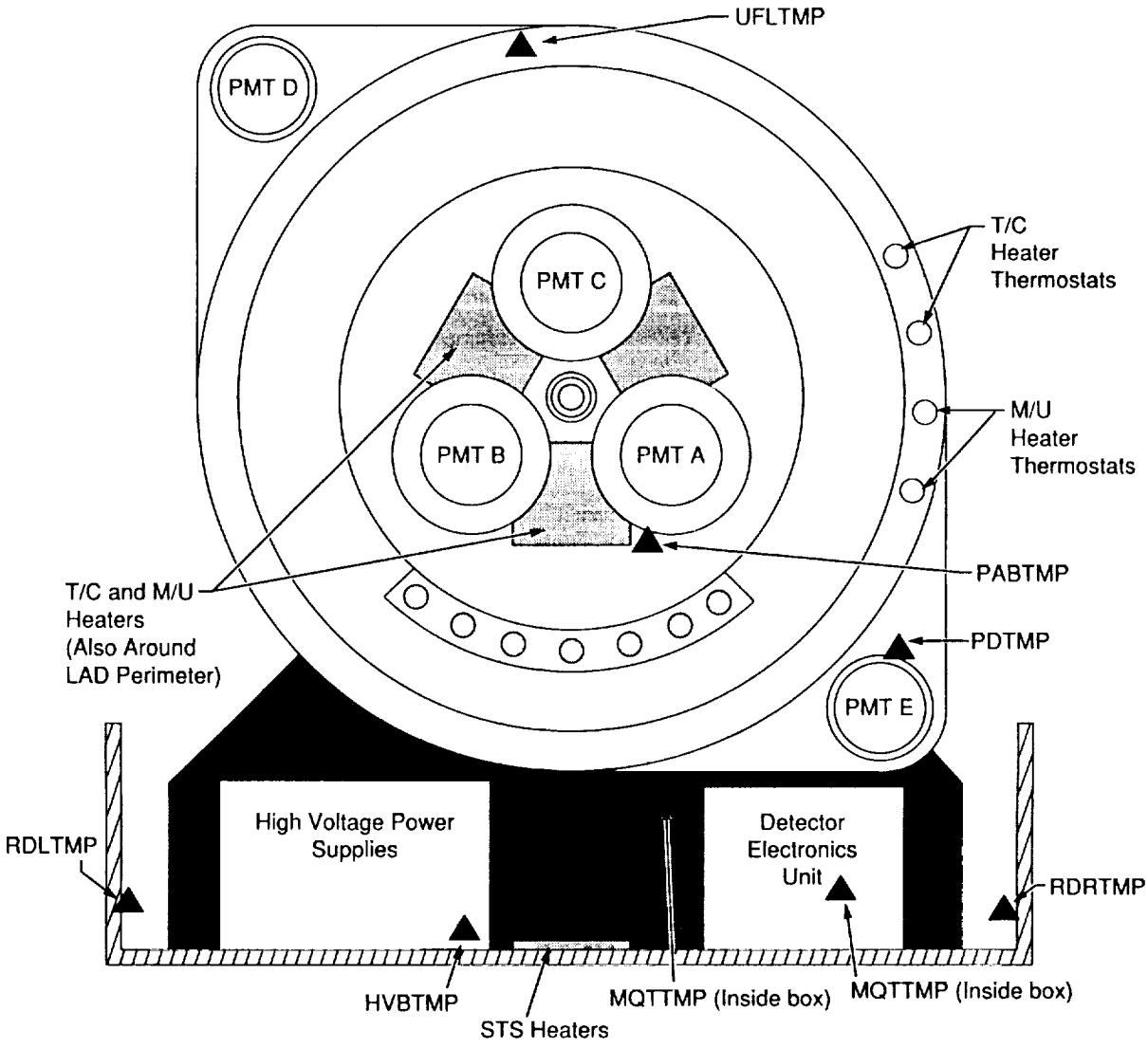

Figure 2.13. Detector Module Heater, Thermostat, and Temperature Sensor Locations.

III. BATSE TEST AND CALIBRATION PROGRAM

A. Component Level Testing

1. BATSE Large Area Detector

After assembly at the Bicron Corporation in Ohio, the BATSE LAD crystals were shipped to MSFC by overnight air-freight. Upon arrival, the detector was submitted to a thorough quality inspection in Building 4705. The first LAD used for installation onto a flight-qualified module (LAD #6 onto B1) arrived at MSFC on September 28, 1987. After passing the quality inspection, each detector began its trip through the testing and calibration program. These tests included a performance test, vacuum check, vibration testing, performance re-test, thermal balance/cycle tests, a vacuum retest, a third performance test, and a helium leak-test. If the unit successfully completed this program, it was sent for installation onto a detector module. Figure 3.1 depicts the flow of the test program.

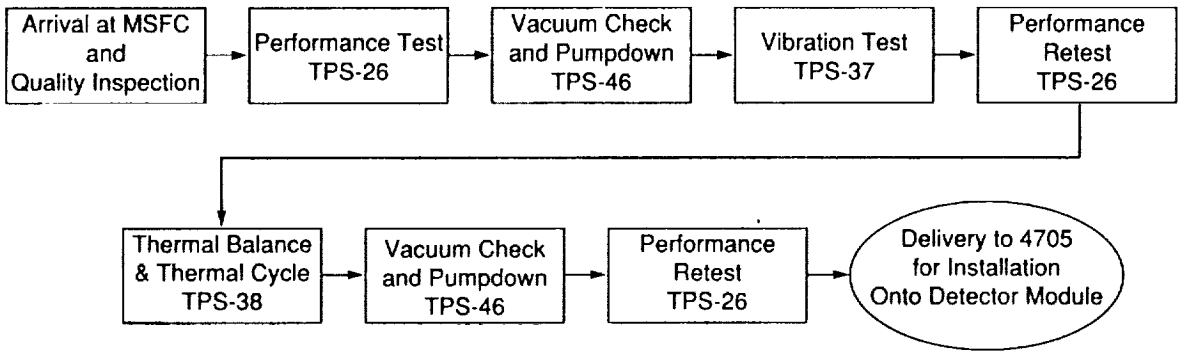

Figure 3.1. BATSE LAD Test Flow Diagram.

On average, the LAD was routed through the test program in 4 to 6 weeks. This flow is the nominal path for the LAD; however, with many LADs going through the same system, deviations from the sequence were experienced. To conserve manpower, several of the LADs had the performance test between the vibration and thermal tests omitted. LADs which did not meet performance specifications required re-testing or other special tests. This constituted a deviation from the flow described above. At any given time, six or eight LADs could be at some stage of the test flow, each in a different building requiring different tests to be performed.

In the following pages, each of these tests will be discussed in detail. Test procedures, spectra, and detailed log books are on file in the BATSE library and are available for inspection. They will not be reproduced here. Results of the testing, however, will be presented. Detectors which experienced anomalies and retests will also be discussed.

a. LAD Performance Test—TPS-26

BATSE-ES-62-TPS-26 is the LAD performance test. This procedure was used as the initial acceptance test and as a test of the detector performance. The primary goal of this test was to measure the photopeak resolution of the detector over a wide range of incident energies. The measured value was then compared against a set of criteria values to determine if the detector passed or not.

For the test, the LAD was placed inside a dark box with the entrance window face-down onto a foam rubber pad. A light collection cone was then lowered onto the LAD and mated with three pins to the Invar flange. The same cone was used for all of the LADs, and the seating of the cone with pins ensured the same fit every time. Three, 12.7 cm diameter PMTs were installed on the top of the cone. Each of the PMTs had its own +HV supply, which could be regulated to fix the proper gain on each tube. The signal from each tube was joined and fed to a Tennelec TC 203 linear amplifier. The amplifier output was then routed to an ND-580 ADC which interfaced to the ND-76 pulse height analyzer. Spectra were accumulated and analyzed on the ND-76. After analysis, the spectra were stored onto RX-50 compatible floppy-disks. Figure 3.2 shows this test setup.

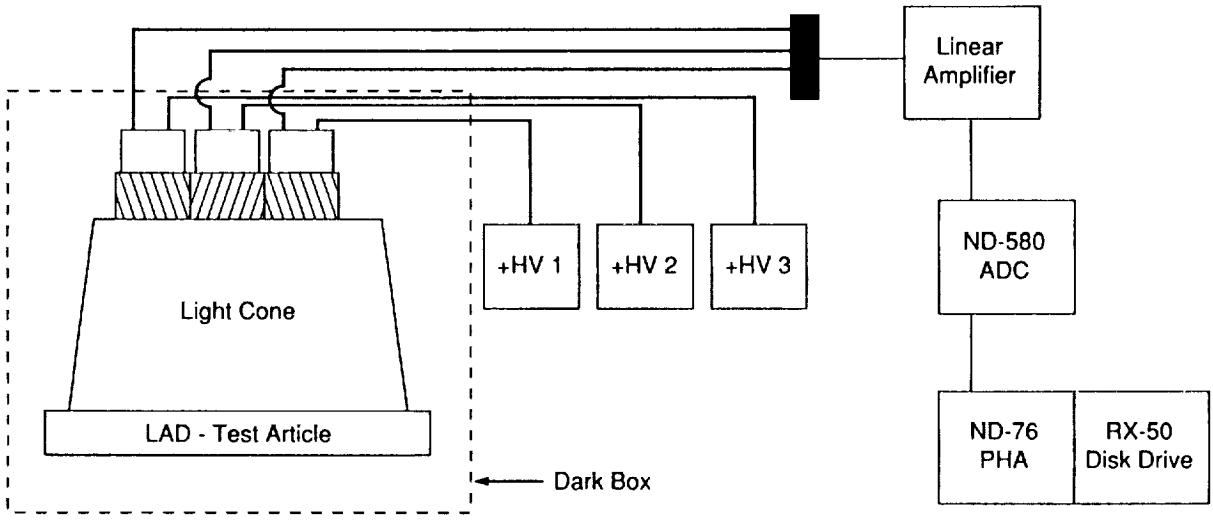

Figure 3.2. TPS-26 Setup Diagram.

After the completion of the configuration, the three PMTs were balanced according to the procedure using a Cd 109 source. The gain was continually monitored throughout the test so that drift of the PMTs would not contribute to a degradation in measured resolution. Cd 109, Am 241, Na 22, Cs 137, and Mn 54 sources were used during this test and allowed measurements in the range from 23 keV to 835 keV. Each isotope was placed on the LAD axis of symmetry at a distance of 50.8 cm below the LAD. This location was outside the dark box. Background

spectra were taken at several points during the test and monitored for any changes. Each of the isotopes was used to collect a 300-second integration. After the appropriate background spectra was measured, the FWHM resolution of the photopeaks was calculated. The LAD was required to have a resolution not in excess of 29.5% at 88 keV. If this value was exceeded, the LAD failed. Results from the initial performance test of all nine LADs installed on flight modules are presented below:

Table 3.1. TPS-26 Initial Test Results (All Nine Module LADs)

		FWHM Resolution % (energy in keV)							
LAD#	B#	23	32	60	88	511	662	835	Test Date
8	P-F	39.8	39.5	28.6	23.9	19.7	17.6	16.0	11-6-87
13	B0	37.9	36.3	28.8	22.6	18.0	16.5	15.7	2-3-88
6	B1	41.6	40.9	30.0	25.5	21.8	21.8	19.3	9-29-87
7	B2	38.3	37.0	29.8	24.6	17.7	16.2	15.0	12-14-87
10	B3	44.4	41.4	30.6	23.5	18.9	16.6	14.6	12-11-87
11	B4	55.4	39.1	34.2	25.6	17.2	15.8	11.2	1-27-88
12	B5	52.2	44.5	35.4	24.4	19.3	16.6	11.4	1-27-88
5	B6	41.8	41.9	33.8	25.5	23.0	21.1	19.8	3-7-88
14	B7	40.4	39.4	31.4	23.3	20.6	19.6	16.7	3-7-88

All LADs used for flight-qualified modules performed acceptably upon delivery to MSFC. Following the initial performance test, the LADs continued the test program. Results from additional runs of TPS-26 will be discussed later in this section. Figure 3.3 shows the above results in a graph format.

b. LAD Pressure Check and Pumpdown — TPS-46

The LAD pressure check and pumpdown (TPS-46) was executed for the purpose of determining the pressure internal to the LAD volume, and also to evacuate the LAD to a pressure of 30 milliTorr or less. Several repetitions of the procedure over an extended period of time yield data from which any leaks in the hermetic seal may be detected. High (several hundred Torr) internal pressure inside the LAD can lead to a hydration of the NaI crystal, which severely degrades performance, or a deformation of the LAD assembly from exposure to the vacuum of space (or a vacuum chamber). Initially, volatiles outgas from materials internal to the LAD, so this test was repeatedly performed to remove these substances.

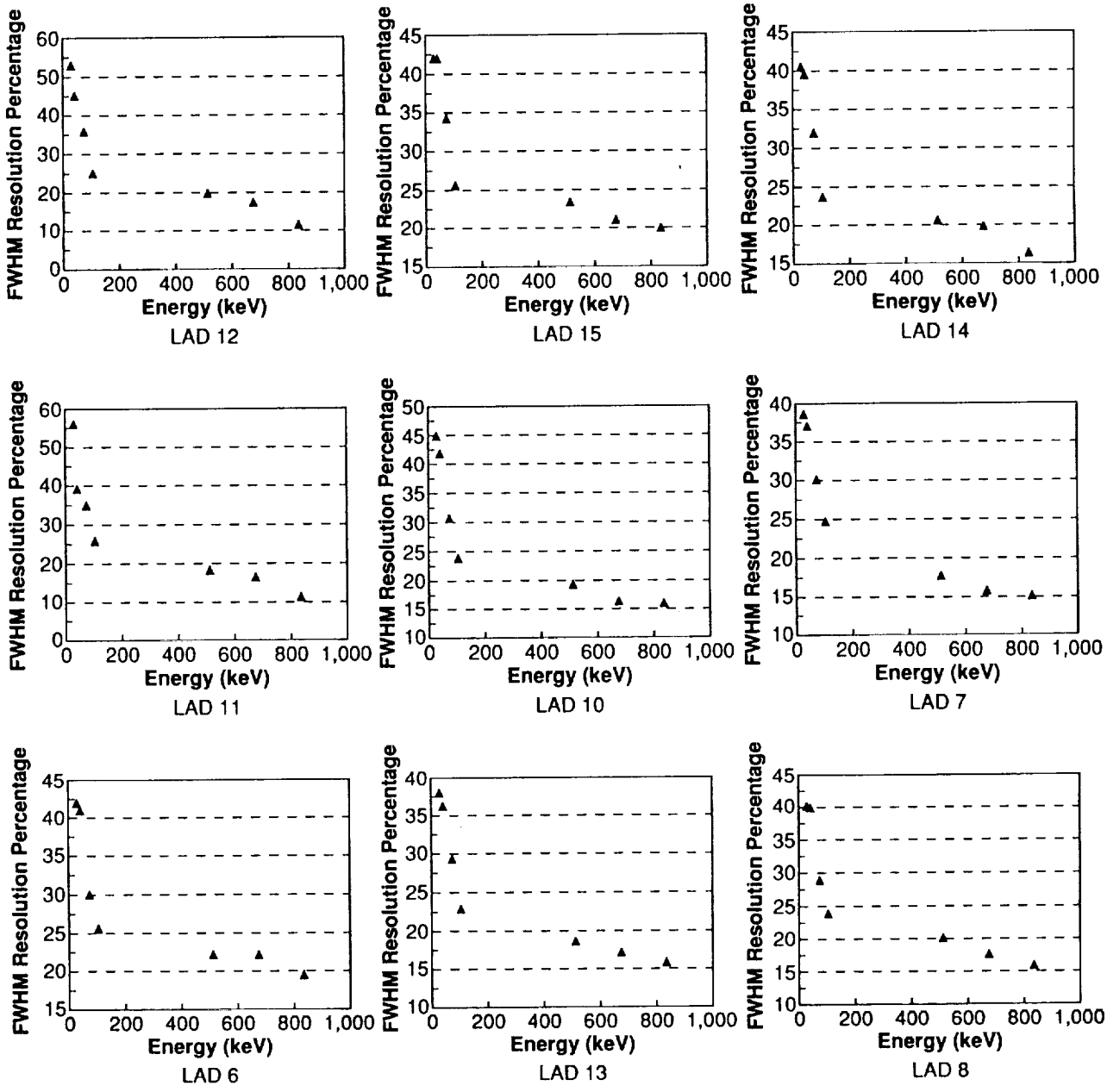

Figure 3.3. TPS-26 Initial FWHM Resolution Measurements.

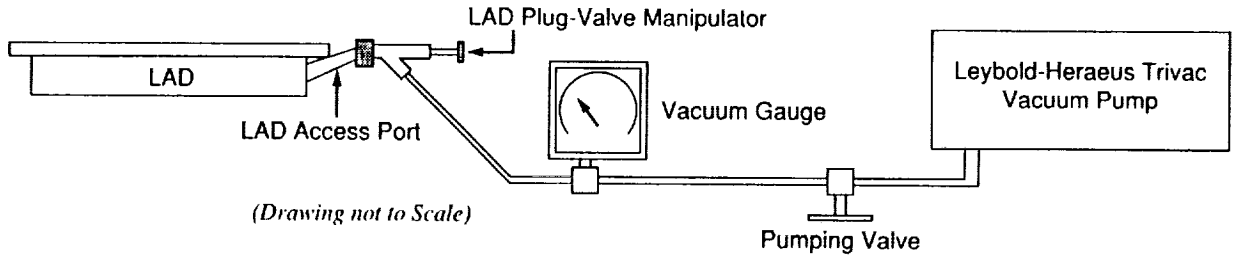

Figure 3.4. TPS-46 Arrangement.

TPS-46 was performed by placing the LAD onto a flat, padded surface with a rotary pump, a vacuum manifold, a vacuum gauge, and the BATSE LAD-plug valve operator. The manifold was connected to the pump, a Leybold-Hereaus Trivac D 1.6B model, and also was connected to the LAD venting port with the plug valve operator. The manifold could be sealed off from the pump with an adjustable pump valve. The vacuum gauge read the pressure inside the manifold. With the LAD valve closed, the pump was started to evacuate the manifold. The manifold was evacuated to a pressure of less than 5 milliTorr. When that pressure was reached, the valve was closed, isolating the manifold from the pump. The pressure was allowed to stabilize, then the LAD valve was opened. The resultant pressure was recorded. Knowing the initial pressure in the manifold, the volume of the manifold, the volume of the LAD, and the resultant pressure allows one to calculate the initial pressure inside the LAD. The pump valve was then opened to allow the pump to evacuate the interior of the LAD. The entire procedure lasted approximately 90 minutes.

Over a long period of time, it is desirable that the internal pressure of the LAD continue to decline. This result indicates that the pumping is removing volatiles which outgas from internal materials. It was not unusual, however, to experience higher internal pressures than normal following thermal balance tests (or thermal vacuum tests in the case of the entire detector module). The thermal cycling encourages the material inside the LAD to outgas faster, and thus produce a higher internal pressure. A complete history of the evacuation test results is provided in Appendix B.

This procedure was executed in MSFC Building 4481 until the LADs were installed onto the detector module.

c. LAD Vibration Test

The vibration test of the BATSE Large Area Detector was performed by the Test Laboratory at MSFC in the vibration facility, Building 4619. Each LAD was vibrated in three axes. The X and Y axes lie in the plane of the LAD, and the Z-axis is normal to the detector plane. The LAD was bolted to the vibration fixture with the optical window face-down. All of the perimeter bolt holes were used to fasten the LAD into place. The vibration was random for a duration of 60 seconds with the following specifications:

Table 3.2. BATSE LAD Vibration Specifications

X-Axis	Y-Axis	Z-Axis
20 Hz at 0.0001 g^2/Hz	20 Hz at 0.0001 g^2/Hz	20 Hz at 0.00005 g^2/Hz
60-80 Hz at 0.15 g^2/Hz	60 Hz at 0.01 g^2/Hz	225-260 Hz at 0.4 g^2/Hz
100-200 Hz at 0.04 g^2/Hz	100-125 Hz at 1.0 g^2/Hz	700-1300 Hz at 0.0005 g^2/Hz
300-1400 Hz at 0.004 g^2/Hz	200-900 Hz at 0.005 g^2/Hz	2000 Hz at 0.00005 g^2/Hz
2000 Hz at 0.002 g^2/Hz	2000 Hz at 0.0001 g^2/Hz	
Composite 4.17 g-rms	Composite 7.2 g-rms	Composite 7.2 g-rms

Following the vibration in three axes, the LAD was thoroughly inspected for any cracks in the NaI, separations from the housing, or debonds in the optical coupling between the NaI and the quartz window. Several LADs were damaged during vibration, including one which had the quartz window smashed to pieces after an error in the Z-axis vibration levels. No LAD which was damaged during vibration was placed onto a detector module. The table below summarizes the LAD vibration tests which took place at MSFC.

Table 3.3. BATSE LAD Vibration Test Dates and Results

LAD #	B#	Test Date	Result
8	P-F	11-10-87 and 11-24-87	Pass
13	B0	2-8-88 and 3-24-88	Pass
6	B1	10-15-87	Pass
7	B2	12-15-87	Pass
10	B3	12-15-87	Pass
11	B4	2-1-88	Pass
12	B5	2-1-88	Pass
15	B6	4-1-88	Pass
14	B7	2-8-88 and 3-24-88	Pass

Detectors which show two vibration tests were re-tested following a failure in the thermal stress test (see next section). These LADs, after passing the vibration test, were sent to the thermal test and cracked during the test. Further vibration testing was done to determine if additional cracking or debonding would appear because of the vibration. For the LADs shown in the table above, no additional problems were found. The second vibration test was done exactly in the same manner as the first.

d. LAD Thermal Stress Test

The second environmental test for the large area detector was the thermal stress test (TPS-38). The test was performed in MSFC Building 4476 by Test Laboratory personnel. Three complete thermal cycles were initially performed between the temperatures of -10 and 40 °C. After experiencing several LAD cracks during the test, the end-points were changed to -5 and 35 °C. LAD #6, installed on B1, is the only LAD on the GRO which was tested between -10 and 40 °C. It did not crack. In addition, a 6-hour soak was performed at the hot and cold temperatures.

The LAD was mated to a test-cone, in identical fashion to the flight configuration. The cone-LAD assembly was then placed on a rack inside the thermal chamber. The assembly was laid on its side so that the orientation of the LAD was such that the plane of the detector was nearly vertical. Temperature sensors were located at several positions on the LAD. Exact locations for each LAD are sketched in the notebook of the respective detector. The figure below details the thermocouple locations for the LAD #6 test on October 19, 1987. This is representative of all LAD thermal stress tests.

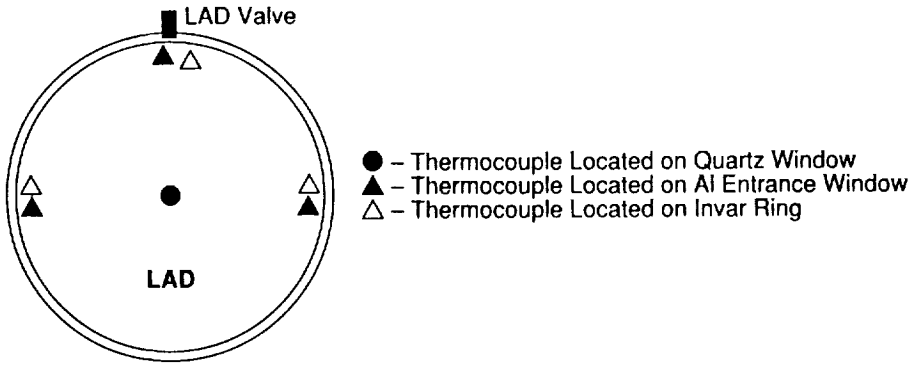

Figure 3.5. TPS-37 Thermocouple Locations (LAD #6 - 10/19/87).

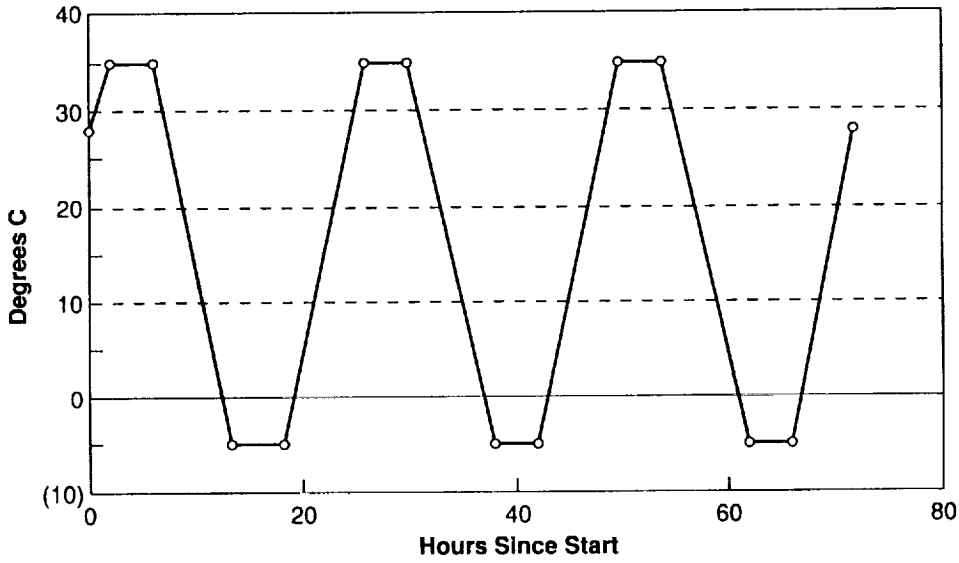

Figure 3.6. BATSE TPS-37 Temperature Profile.

The cone to which the LADs were mated for this test had a hole in the location where the three PMTs are mounted on the flight cone. The hole allowed for the viewing of the LAD's NaI crystal throughout the entire test. A video recorder was used on later tests to document the entire test and capture any cracking events which might occur. The entire cone-LAD assembly was padded with foam rubber, and the cone was capped with transparent plastic. This prevented any convection currents inside the chamber from creating hot or cold spots on the crystal, and also helped keep the temperature slope within the desired 5 °C per hour region. The entire three cycles and soak periods took approximately 96 continuous hours. The table below lists the times of first-run thermal tests for the nine LADs installed onto flight modules.

Table 3.4. Results of TPS-37 Initial Tests on LADs

LAD #	B#	Initial Test Date	Result
8	P-F	11-13-87	Cracked
13	B0	2-17-88	Cracked
6	B1	10-19-87	Pass
7	B2	12-15-87	Pass
10	B3	12-15-87	Pass
11	B4	2-4-88	Pass
12	B5	2-8-88	Pass
15	B6	4-4-88	Pass
14	B7	3-11-88	Cracked

Problems with the LADs appeared early in the test program, as many LADs cracked during thermal cycling. Many efforts were made with the design team, scientists, and manufacturers to determine what was causing the failure. No factor was ever positively identified in determining why some LADs cracked and others did not. Fortunately, a crack in a LAD turned out not to be as severe a problem as was originally thought; no effect on the detector performance was observed.

After the crack in LAD #8 appeared, a detailed examination of the NaI crystal was made. All visible features of the NaI were noted and sketched, including cracks, debonds, and non-uniformities. The LAD was taken from the thermal chamber to the vibration facility where the vibration test was performed again. After vibration in three axes, no further cracking or debonding could be identified. A second thermal stress test was then performed. The LAD was cycled six times (twice normal) between the temperatures of -5 and 35 °C. Six-hour soak periods were executed at all hot and cold temperatures during the cycling. This test took place on December 4, 1987. After 7 days of thermal cycling, no further cracking or debonding was apparent in the NaI crystal. It became evident that once the initial stress in the NaI was released through the cracking of the detector, no further degradation in the structure of the LAD occurred. All of the cracked LADs were re-vibrated with no additional cracks, debonds, or changes in the visible structure. The dates of these second vibration tests were given in Table 3.3.

e. Second Performance Test of all LADs (TPS-26)

Following completion of the environmental test portion of the LAD program, an additional TPS-26 was performed on each of the LADs. This test determined if the vibration and thermal stress tests caused any degradation of the detector's performance. The conditions of this test were identical to that of the first test. The results presented here represent data from the final TPS-26 in the test program. Some detectors had more than two performance tests executed. The results of these intermediate tests will be given in the final section of the LAD test sequence which deals with deviations from the standard sequence.

Table 3.5. BATSE TPS-26 Post-Environmental Test Results

		FWHM Resolution % (energy in keV)							
LAD #	B#	23	32	60	88	511	662	835	Test Date
8	P-F*	51.6	39.3	30.8	23.7	19.3	17.7	16.7	12-14-87
13	B0*	40.5	38.1	30.0	22.3	17.4	17.2	12.1	3-25-88
6	B1	43.7	41.6	31.4	24.2	19.5	18.5	17.8	10-27-87
7	B2	38.4	38.2	28.6	22.8	19.2	16.0	12.5	12-23-87
10	B3	43.2	37.7	30.0	23.5	19.0	18.2	16.7	12-21-87
11	B4	40.9	39.4	30.2	23.0	21.3	19.1	12.5	2-8-88
12	B5	42.1	41.8	35.0	25.6	23.4	21.5	20.8	3-2-88
15	B6	44.6	46.0	36.0	28.4	23.3	23.5	19.6	4-11-88
14	B7*	41.5	40.1	31.8	23.9	21.3	19.8	17.6	3-25-88

*Cracked LAD.

Table 3.6. Change in FWHM Resolution Percentages from Initial to Final Tests

		Change in FWHM Resolution % (energy in keV)						
LAD #	B#	23	32	60	88	511	662	835
8	P-F*	11.8	-0.2	2.2	-0.2	-0.4	0.1	0.7
13	B0*	2.6	1.8	1.2	-0.3	-0.6	0.7	-3.6
6	B1	2.1	0.7	1.4	-1.3	-2.3	-3.3	-1.5
7	B2	0.1	1.2	-1.2	-1.8	1.5	-0.2	-2.5
10	B3	-1.2	-3.7	-0.6	0.0	0.1	1.6	2.1
11	B4	-14.5	0.3	-4.0	-2.6	4.1	3.3	1.3
12	B5	-10.0	-2.7	-0.4	1.2	4.1	4.9	9.4
15	B6	2.8	4.1	2.2	2.9	0.3	2.4	-0.2
14	B7*	1.1	0.7	0.4	0.6	0.7	0.2	0.9

*Cracked LAD.

The results from the final iteration of TPS-26, when compared with the initial iteration, yield the differences summarized in the table above. Inspection of the data shows that the environmental test program did not have a significant effect on the resolution of the LAD crystals. For LADs #8, #13, and #14, one cannot make the argument that a crack in the NaI degrades the resolution significantly, with the possible exception at lower energies (< 23 keV). Of the cracked LADs, only #8 showed extreme degradation in the measured resolution, and that degradation came only at one energy, 23 keV. Another cracked detector, LAD #13, shows the best measured resolution at 88 and 511 keV. In light of the data shown above, it was decided that a cracked LAD could be installed onto a detector module and used for flight. Of the three cracked units, one is on the protoflight module, which is not installed on the spacecraft.

Among the detectors with no environmental test problems, the measured resolution at 88 keV is consistently below the 29.5% required. Large fluctuations in the resolutions measured for LAD #11 and #12 are strongly believed by the editor to be a measurement error in the initial test. All other measurements show good agreement with previous data, and all of the LADs appear to have the same behavioral trends and patterns. For these reasons, the LADs were declared to have successfully completed the environmental testing program with no significant degradation in their performances. Successful completion of the final pumpdown and a helium leak check would validate the LADs for use on a BATSE detector module.

f. Final Pumpdown and Helium Leak Check

After completion of the final TPS-26, each of the LADs was given another pressure check and pumpdown. This procedure is described in section III.A.1.b. Long-term results of these tests are presented as Appendix B. Internal pressures from each of the detectors were measured, and the LADs were evacuated. The LADs were then helium leak tested. After evacuation, the LADs were backfilled with gaseous helium and sealed. The LAD was then "sniffed" around its entire perimeter for any residual helium in the neighborhood of the LAD. This test was performed by Mr. J. O. Jolley of the Infrared and Cryogenic Physics Branch at NASA-MSFC. No LAD was found to exhibit a detectable leak. The helium was then removed from the LAD, and the interior was evacuated to a pressure of < 30 milliTorr. At this time, each LAD was transported to MSFC Building 4705 for installation onto a BATSE detector module.

g. BATSE LAD Anomalies and Test Flow Deviations

The flow described above was the nominal path from delivery to installation for the BATSE LADs. However, there were some significant deviations from the path described above, with each LAD tracing a somewhat different path through the system. In the following paragraphs, these differences will be presented on an individual basis, one LAD at a time.

LAD #8 -- BATSE Protoflight Module. The problems with LAD #8 were discussed a great deal in the previous sections. As the first LAD installed onto a detector module, this detector was the "test-case" to a certain extent. The problems of LAD #8 cracking during thermal stress testing, re-vibration, and subsequent additional thermal tests were all outlined above. These will not be repeated here.

LAD #8 received an additional TPS-26 (performance test) between the vibrational tests and the thermal test in which it cracked. This test was performed on November 10, 1987, and the results are tabulated below.

Table 3.7. LAD #8 Post-Vibration/Pre-Thermal Performance Results

		FWHM Resolution % (energy in keV)							
LAD #	B#	23	32	60	88	511	662	835	Test Date
8	P-F*	44.6	48.9	34.2	24.4	21.4	16.6	14.1	11-10-87

*Cracked LAD.

LAD #8 received an additional vacuum check between the completion of the vibration tests and the beginning of the thermal stress test in which the LAD cracked. This vacuum check was performed on November 12, 1987, and yielded good results.

LAD #13 -- BATSE B0 Module. This LAD, like LAD #8, cracked in the thermal stress test. The additional vibration test of LAD #13 was discussed in the preceding pages. Immediately after the LAD cracked in the thermal chamber, and the test was completed, TPS-26 was performed to check the resolution prior to vibration. This test was performed on March 14, 1988, and its results are summarized below.

Table 3.8. LAD #13 Post-Thermal Resolution Prior to Re-Vibration (Cracked)

		FWHM Resolution % (energy in keV)							
LAD #	B#	23	32	60	88	511	662	835	Test Date
13	B0*	39.7	39.3	30.1	22.3	17.5	17.1	14.2	3-14-88

*Cracked LAD.

The results from LAD #13's re-testing are better than most LADs without cracks.

LAD #6 -- BATSE B1 Module. No Anomalies.

LAD #7 -- BATSE B2 Module. LAD #7 arrived at MSFC with some minor abrasions on the quartz window. These abrasions were noted and sketched into the flight data pack, which remains on file with the instrument until launch. After launch, the data pack will return to MSFC and will be available for inspection. The quartz window problem showed no apparent effect on the detector performance. No further anomalies or deviations occurred with this LAD.

LAD #10 -- BATSE B3 Module. Because LAD #10 was put into the thermal chamber at the same time as LAD #7, and there was only one standard test-cone for all LADs, LAD #10 was mated to a different cone for this test. The cone used for the test was taken from the ES62 supernova balloon flight instrument, detector #1. The LAD-to-cone interface on this cone is mechanically identical to a BATSE flight detector module light collection cone in every way.

LAD #11 -- BATSE B4 Module. An additional TPS-26 was performed on LAD #11 between the vibration test and the thermal stress test. This TPS-26 run was executed on February 2, 1988. Results from this test are presented below.

Table 3.9. LAD #11 Post-Thermal Resolution Prior to Vibration

		FWHM Resolution % (energy in keV)							
LAD #	B#	23	32	60	88	511	662	835	Test Date
11	B4	40.2	39.7	30.0	23.5	20.9	18.0	16.3	2-2-88

LAD #12 -- BATSE B5 Module. As was done with LAD #11, LAD #12 also received an additional TPS-26 test between vibration testing and thermal stress testing. The results of the test, completed on February 3, 1988 are given below.

Table 3.10. LAD #12 Post-Thermal Resolution Prior to Vibration

		FWHM Resolution % (energy in keV)							
LAD #	B#	23	32	60	88	511	662	835	Test Date
12	B5	40.8	41.7	31.4	24.6	23.2	21.1	19.3	2-3-88

LAD #15 -- BATSE B6 Module. LAD #15 was delivered to MSFC and started through the test program normally. However, upon arrival at the vibration test facility, the LAD could not be mated to the shaker-plate because of an error in the bolt hole locations. The Invar flange of LAD #15 had to be re-drilled to put the bolt holes in the proper location. After the drilling was performed, a second performance test was executed prior to vibration and thermal stress testing. The results from this test are shown below. LAD #15 has the poorest resolution of all LADs at 88 keV.

Table 3.11. LAD #15 Resolution after Hole Drilling on Invar Flange

		FWHM Resolution % (energy in keV)							
LAD #	B#	23	32	60	88	511	662	835	Test Date
15	B6	43.3	45.0	36.4	27.3	24.5	22.4	20.9	3-31-88

LAD #14 -- BATSE B7 Module. LAD #14 cracked during the thermal stress test, was re-vibrated (as described above), and had a final performance test executed on the LAD. The results of all LAD #14 testing have been presented previously.

2. BATSE Spectroscopy Detector Assembly

The BATSE spectroscopy detector assembly (SD) was approved for inclusion in the experiment in 1983, after the preliminary design for the main BATSE experiment was completed. The detectors were designed at the University of California-San Diego (UCSD) and the housings were fabricated there. The NaI crystals were encapsulated at Bicron Corporation. The completed assemblies were sent to UCSD for further test and calibration. Following this testing, the units were shipped to MSFC for installation onto the BATSE detector modules. After assembly, a spectroscopy detector performance test (TPS-16) was executed. This same test was used as an acceptance test at MSFC. The test was used to characterize the detector gain by measuring the +HV required to obtain a standard output for the Cs 137 662 keV line. In addition, the test was used to obtain resolution measurements and check for any detector degradation which might occur. One particularly important mode of degradation is the formation of a dead-layer on the NaI crystal near the beryllium window. This development would reduce the detector efficiency at low energies.

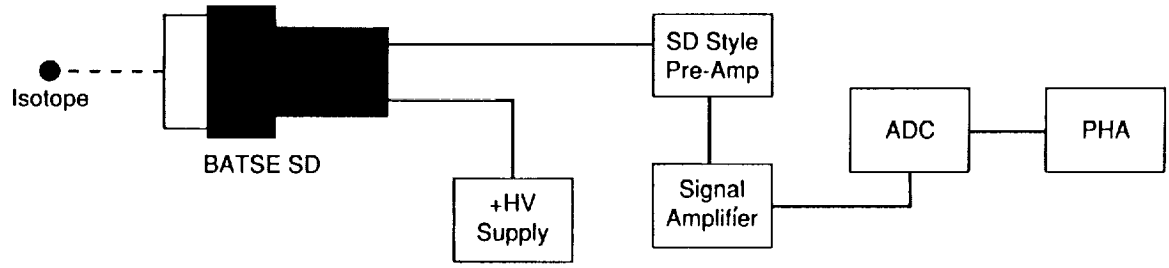

Figure 3.7. BATSE TPS-16 Equipment Configuration.

The SD to be tested was connected to a spectroscopy-style pre-amp and an +HV power supply. The pre-amp is the front-end of the MQT board, IC's #1 and #2, and is used to measure the nominal operating +HV. The signal from the pre-amp was fed to an amplifier which passed the amplified signal to ADC. A 2048 channel PHA was used to analyze the output of the ADC and build a spectrum. A standard oscilloscope was used to monitor the signal out of the SD.

The test equipment was configured as shown in Figure 3.7, and a Cs 137 source (a few μCi in activity) was placed 12.0 cm from the detector window, on-axis. The +HV was powered and then adjusted so that the 662-keV line produced an output of 0.66 V ± 0.01 V. The output was checked and adjusted to produce the same output over time. After the SD displayed stability at this value for 1 hour, the test continued. The applied +HV required to produce the 0.66 V output was recorded as the "nominal operating +HV."

Resolution measurements were taken using the same Cs 137 source at a 12.0-cm distance. The FWHM resolution of the 662-keV line was measured and recorded. The Cs isotope was removed, and a Cd 109 source was installed at a distance of 20.0 cm. Resolution measurements were taken at 23 keV. The final source used was Fe 55, placed 7.6 cm from the detector window. Measurements of the 5.9-keV peak were taken.

Data collected at MSFC were stored onto a Tracor-Northern Pulse-Height Analysis System which has been difficult to maintain in a reliable operating condition at times. The spectra taken are no longer available for inspection. However, each of the individual test procedures provided ample locations for the recording of data, calculations, and comments. These test procedures are on file as portions of the detector module notebooks. The table below contains the results from testing of the BATSE SD flight units.

Table 3.12. TPS-16 Results for Flight Spectroscopy Detectors

SD Serial No.	B#	FWHM Res. % 5.9	23	662	Nom.+HV	Date	Location
112184-11	P-F	43	25	6.8	1273	12-16-84	UCSD
	...	25	xx	6.5	1236	2-24-87	MSFC
112298-03	B0	32	27	6.9	1376	4-2-86	UCSD
	...	xx	28	7.1	1346	6-13-86	MSFC
	...	27	27	7.1	1346	7-23-86	MSFC
112280-12	B1	46	27	7.2	1392	11-26-86	UCSD
	...	37	27	6.9	1392	12-16-86	MSFC
112407-08	B2	45	28	7.3	1373	7-31-86	UCSD
	...	45	28	7.5	1365	10-16-86	MSFC
112276-07	B3	42	27	7.3	1270	8-1-86	UCSD
	...	49	28	7.5	1259	10-27-86	MSFC
112406-10	B4	45	27	7.4	1335	1-5-87	UCSD
	...	24	19	6.8	1311	2-17-87	MSFC
112399-09	B5	xx	26	7.2	1221	12-11-86	MSFC
112175-01	B6	47	27	7.1	1312	3-25-86	UCSD
	...	xx	30	7.3	1320	6-11-86	MSFC
	...	44	26	7.3	1320	7-31-86	MSFC
112173-02	B7	xx	28	7.6	1419	7-14-86	MSFC
	...	44	28	7.7	1419	7-25-86	MSFC

The data obtained from TPS-16 are incomplete to a large extent. Certain portions of spectral resolutions were not computed, because of the difficulty in obtaining measurements at 5.9 keV, for example (marked by xx in the table). For two of the SDs, the results from initial tests performed at UCSD are not available. Large discrepancies exist in the measured resolutions between UCSD and MSFC, especially at low energies. Because the test was done over a period of nearly 2 1/2 years, variations in equipment, personnel, and other factors may have influenced the test results.

The interested user is encouraged to consult detector module or experiment-level testing when searching for the best quality SD calibration data. TPS-16 does, however, provide a benchmark resolution at 662 keV against which future performances can be judged. The 662-keV solution numbers presented above are reliable as one indicator of the detectors performance. These numbers closely resemble resolutions measured for SDs when installed on the spacecraft. Future SD calibrations included resolution measurements at a large number of incident energies, photopeak separations from isotopes with neighboring lines, and measurements taken at no fewer than four different gain settings. There exists no record of additional tests performed on the SD units until they were installed as one component of a detector module.

3. BATSE Charged Particle Detector

a. TPS-15 — CPD Acceptance Test

After the charged particle detector (CPD) was fully assembled, the unit was given a thorough acceptance test (TPS-15). This test ensured that the CPD was light-tight, that both PMTs were contributing equally to the generation of signals, that the CPD had no "dark" regions, and that a threshold of 0.6 x muon-deposition energy could be reached with less than 1860 V applied to the PMTs. Figure 3.8 describes the equipment configuration for TPS-15.

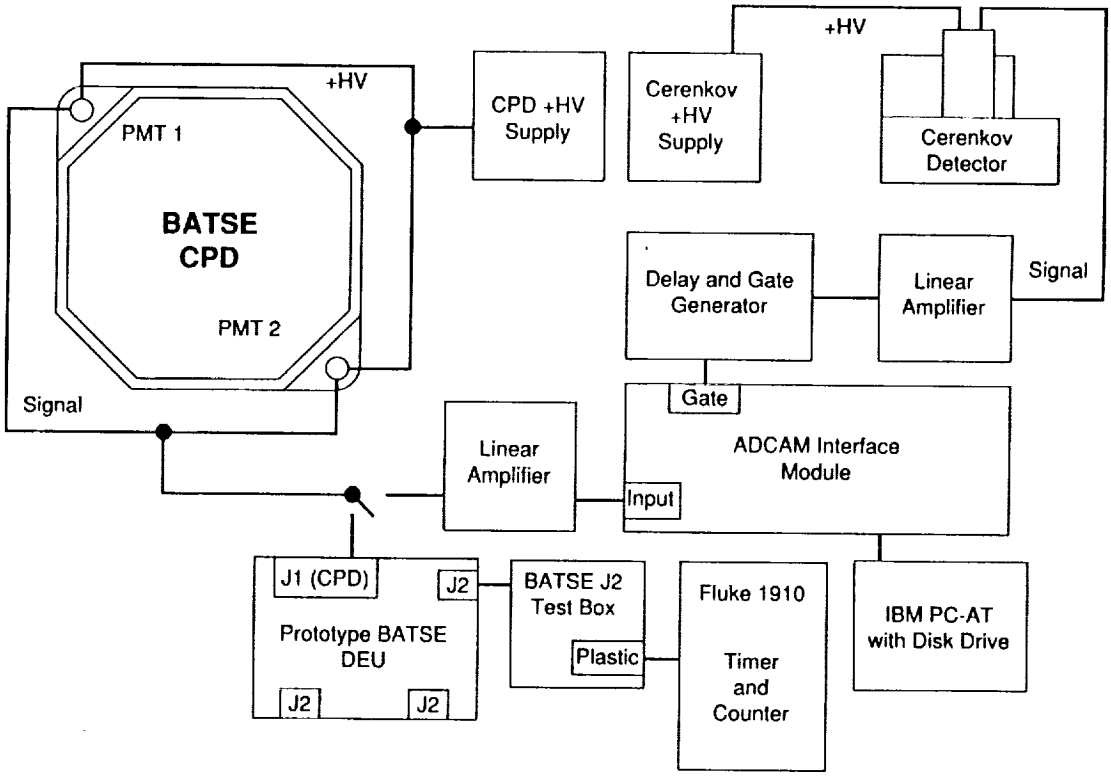

Figure 3.8. TPS-15 Equipment Configuration.

The CPD was connected to one +HV supply which regulated both PMTs simultaneously. The signal from the PMTs was summed and sent to both a linear amplifier and to a DEU prototype box. The amplifier sent an input signal to an ADCAM interface module which allowed the acquisition of spectra onto an IBM PC-AT computer with ADCAM software. The DEU produced an output signal which was counted by a Fluke timer/counter. A Cerenkov detector, with its own +HV supply, served as the input to a delay and gate generator which gated the ADCAM module. All signals were visible on an oscilloscope.

Following configuration of the hardware, the CPD was powered up, and a high-intensity flashlight was used to illuminate the entire CPD, checking for a light leak. If no leak was found, the face of the CPD was "mapped" using a small Co 60 source. The isotope was placed at 11 different locations over the surface, and a 60-second integration was obtained at each location. These spectra were stored onto disk.

With the isotope removed, the Cerenkov detector was then placed in the center of the CPD, and a 3600-second spectra was taken with the CPD gated by the output of the Cerenkov detector. In this way, a spectrum was generated which contained only "verified" muon events. This spectrum was also stored onto disk. The output of the CPD was then sent to the DEU, whose PLASTIC rate was determined through the Fluke multimeter. The DEU only provides an integral rate, with no energy information. Once the rate from the DEU was determined, the coincidence spectrum could be examined and a channel found where the integral rate above that channel matched the rate from the DEU. This channel was then the location in energy of the DEU threshold. By comparison with the muon peak, the energy of the threshold relative to a muon-deposition energy was calculated. If necessary, the +HV was adjusted on the CPD to raise or lower the gain such that the DEU threshold would lie at 0.6 x the muon deposition energy. In this way, one could ensure that most of the muon events would be detected by the CPD and anti-coincidenced in the electronics. After the first voltage was established, other thresholds were attained through a similar matching of the count rate from the spectrum with that on the Fluke. The voltages required to attain these thresholds were recorded. The following table summarizes the results from all of the CPDs used on flight-qualified detector modules.

Table 3.13. TPS-15 CPD Acceptance Procedure Results

		+HV Required to Obtain n x Muon Energy								
CPD #	B#	0.4	0.6	0.8	0.9	1.0	1.15	1.3	1.5	Date
06	P-F	1525	1405	1350	1329	1305	1275	1250	1214	10-6-87
03	B0	1520	1430	1365	1335	1310	1280	1250	1226	11-24-87
02	B1	1440	1335	1275	1255	1235	1215	1180	1155	10-20-87
01	B2	1330	1245	1190	1162	1148	1124	1100	1065	11-24-87
04	B3	Missing Test Results								
05	B4	1325	1240	1190	1170	1149	1132	1110	1087	11-30-87
09	B5	1285	1221	1155	1143	1125	1096	1073	1050	11-25-87
07	B6	1385	1302	1235	1215	1200	1167	1153	1120	11-27-87
08	B7	1289	1208	1163	1132	1115	1096	1073	1050	11-25-87

CPD 04, which was installed onto detector module B3, was tested on 11-25-87 (Editor's notebook); however, the test procedure is missing, and the various voltages are unobtainable. All spectra generated during these tests, including those for CPD 04, are stored on 5.25" floppy disks in the BATSE library and are available for inspection. Unlike most spectra, the CPD spectra are in ADCAM format and require a PC with suitable software.

In practice, the +HV setting for the CPDs is obtained through the use of data obtained during the BATSE science tests, not from the results of TPS-15. On orbit, the eventual setting will most likely be driven primarily by the charged particle rate. Despite these, TPS-15 offered a well-defined standard against which to measure the performance of each CPD, allowed the BATSE team to establish that the CPD was operating properly, and exhibited behavior similar to the CPDs fabricated prior to the one under test.

b. CPD Triple Coincidence Tests

Following the successful completion of TPS-15, the BATSE team designed a test to obtain a low background measurement of the energy resolution of the CPD. CPDs 01, 05, and 07 were used in this test, which was not an original part of the CPD calibration program. The three CPDs were "stacked" vertically with a 1-meter separation between them. The orientation of the detectors was such that their planes were perpendicular to the local vertical. CPD 05 was the top detector, with 07 on the bottom, and 01 in the middle. The center CPD was connected to the ADCAM module and coincidence-gated with both of the other CPDs. To register an event in the center CPD, an event also had to be registered by the other two CPDs. The coincidence gating, along with the vertical stacking of the detectors, allowed almost exclusive counting of muon events and rejection of other events. Spectra were accumulated from the center detector, each with a live time of 65,250 seconds. The voltages on the two gating-CPDs were set to

produce a threshold at 1.0 x muon deposition for the first accumulation and 0.8 x muon deposition for the second accumulation. Resolutions of 42% and 43% FWHM were obtained from the two accumulations. This number is representative of the FWHM resolution of all BATSE CPDs.

c. CPD Rapid Pumpdown Test (TPS-67)

The BATSE system thermal vacuum test (see section III.C) revealed that sufficient venting of the interior of the CPD was not provided. During the slow pumpdown and return to atmosphere, the aluminum faceplate of the CPD on module B6 (DM #0/8 at the time) buckled and separated from the honeycomb interior. If the only method by which the CPD could vent its interior during a slow pumpdown was through structural deformation, the result during the rapid ascent of launch could be easily forecast. In addition, after pumpdown in the thermal vacuum test, the CPD rate would drop to zero (or a very low number) for a period of time, and then gradually return to the proper value. This behavior was attributed to the internal pressure in the CPD forcing the PMT upward, compressing the wave-washer in the back, and separating the tube face from the DC-93-500 optical coupling. As the internal pressure was bled-off, the wave-washer would relax, forcing the tube face back against the optical coupling.

Each of the CPDs were fitted with the two sintered bronze vents shown in the CPD diagram in section II.C. A test was then devised to determine if the CPD was properly vented and could withstand the shuttle ascent pumpdown rate. TPS-67 was performed on CPD 02 on September 15 and 16, 1988. The CPD, along with a DEU and an HVPU, were placed into a small vacuum chamber. The small chamber was connected through a manually adjustable manifold to a large vacuum chamber. The CPD was equipped with sensors on the top of both PMTs and in the center of the CPD body on both sides. These sensors measured the displacement of the various portions of the CPD and were visible at all times during the test. Furthermore, a complete set of electrical GSE was located outside the chamber to monitor the rates, voltages, and currents in the CPD assembly as the chamber was being evacuated. The rapid drop in pressure was accomplished by evacuating the large vacuum chamber, and then opening the valve on the smaller chamber to expose its interior to vacuum. The rate of pressure drop was controlled by an operator manipulating the valve.

Three separate pumpdowns were executed. The first two evacuations were at a rate slower than that of the shuttle ascent, and were done to verify the structural integrity of the CPD. The third pumpdown was executed at a rate representing the shuttle ascent rate. The rate used was derived from the BATSE-GRO ICD. During each of the pumpdowns, the count rate and deflection sensors were monitored. The CPD rate was required not to drop below a statistically significant amount during depressurization. The PMT displacement limit was set at 0.051 cm, and the face-sheet displacement limit was set at 0.102 cm.

The shuttle rate pumpdown sustained depressurization at an average rate of 0.22 psi/sec, traversing from 14 psi to 1 psi in a little more than 60 seconds. During this time, the pumpdown

rate reached a maximum value of nearly 0.3 psi/sec, falling from 14 psi to 11 psi in only 10 seconds. The maximum deflection of the PMTs was recorded to be 0.0013 cm. The face-sheet was displaced a distance of 0.01 cm, while the count rate was unaffected by the depressurization. Complete results of this test are on file in the BATSE library.

4. BATSE Photomultiplier Tube Screening Tests

The photomultiplier tubes used on BATSE, procured and tested during 1984-1987, were purchased from Thorn-EMI-Gencom, Inc. The specifications that are a part of the procurement document require that certain tests be successfully completed prior to acceptance of the PMTs for flight. Certificates of conformity were provided with each PMT, along with supporting data. Additional tests were performed at MSFC, either to confirm the data provided by the manufacturer, or to perform tests that would have been too costly if performed by them.

As a result of the testing performed at MSFC, approximately 33% of the 12.7-cm (5") PMTs and 24% of the 5.08-cm (2") PMTs were returned to the manufacturer for replacement. Table 3.14 lists these returns by cause.

Table 3.14. Breakdown of BATSE PMTs Returned to EMI by Failure Mode

	Number of PMTs Returned	
	12.7 cm	5.08 cm
Foreign particles exceeding maximum size	9	0
Construction defects	5	2
Unstable gain	5	2
Unsatisfactory energy resolution	5	0
Gain unacceptable (too low)	1	3

Table 3.15. EMI Testing Specifications and Acceptable Ranges of Values

Parameter	Acceptable Range
HV for 50 A/Lumen	1300-1800 V
Dark current	< 10 nA
Resolution (FWHM) at 662 KeV (with MSFC-supplied NaI crystal)	8.0 %
Quantum efficiency at 410 nM	0. 24 %

The table above lists the parameters measured at the manufacturer for each of the 12.7-cm PMTs fabricated for use in the BATSE Instrument. These tests were performed twice at the manufacturer, once after construction of the PMTs, and once after a random vibration test, consisting of 1-minute exposures for each of three orthogonal axes. The exposure, detailed in the following table, produces a composite 5.2-gm level.

Table 3.16. EMI Vibration Specifications of PMT Tests at the Manufacturer

20 - 80 Hz	+15 dB/octave
80 - 200 Hz	0.08 g^2/Hz (constant)
200 - 400 Hz	-6 dB/octave
400 - 600 Hz	0.02 g^2/Hz (constant)
600 - 2000 Hz	-10 dB/octave

These tests were performed a third time, following an aging process which consisted of thermal soaks of 20 hours at temperatures of 23, 45, and 23 °C. At each step, values for the dark current, resolution, and gain were measured. PMTs which passed these screening measures were shipped to MSFC.

Upon arrival at MSFC, a second series of tests were perfomed to verify that the hardware complied with the required specifications. This sequence began with a visual inspection under 10X magnification. This inspection was performed a minumum of two times on each PMT, once at the beginning and again at the end of the screening process. Confirmation of the proper PMT size was made by passing the tube through metal plates of the maximum sizes, for both the dynode and cathode diameters. Proper length and concentricity were verified using another machined plate. Five of the 12.7-cm PMTs and two of the 5.08-cm PMTs were rejected on the basis of internal contamination exceeding the specified limits.

Subsequent to the initial visual inspection, PMTs were placed into a light-tight diffuse-reflecting box. Up to ten PMTs were tested simultaneously, each with a PMT base similar to that used for BATSE, but without Zener diodes in the last two stages. A commercial magnetic shield was used around each PMT. Two of the PMTs were retained throughout all batches, to serve as reference tubes. The temperature was digitized and stored with the spectral data.

A green LED was mounted in the same plane as the tubes and was pulsed at a frequency of 1 kHz. Events synchronous with the LED drive pulse were digitized and summed using a CAMAC data system. Spectra obtained could be viewed using a remote-controlled digital-input PHA.

Stability of the PMTs was determined by integrating data for 2 minutes and storing the spectra to disk for a continuous duration of approximately 24 hours. A minumum of two runs were obtained for each batch of PMTs. Tubes which showed anomalous behavior relative to the reference PMT or the temperature measurement were not retained as flight candidates.

By varying the rate of the green LED, a sequence of anode currents could be generated in each PMT to obtain a measurement of the fatigue experience by the PMT. Table 3.17 lists the currents and time durations.

Table 3.17. Anode Current Exposure Times Used During MSFC PMT Screening

Time Interval (hr)	Current (μA)
5	0.01
4	0.1
4	0.01
8	2.0
24	0.01

Gain response to this fatigue exposure ideintified two classes of tubes, with approximately one-third of the tubes being reduced in gain during the 2 μA exposure, and two-thirds showing an increase. Recovery times for both classes were comparable, typically 3-6 hours. An example of each type is shown in Figure 3.9. The gain variations for the flight PMTs is shown in Figure 3.10.

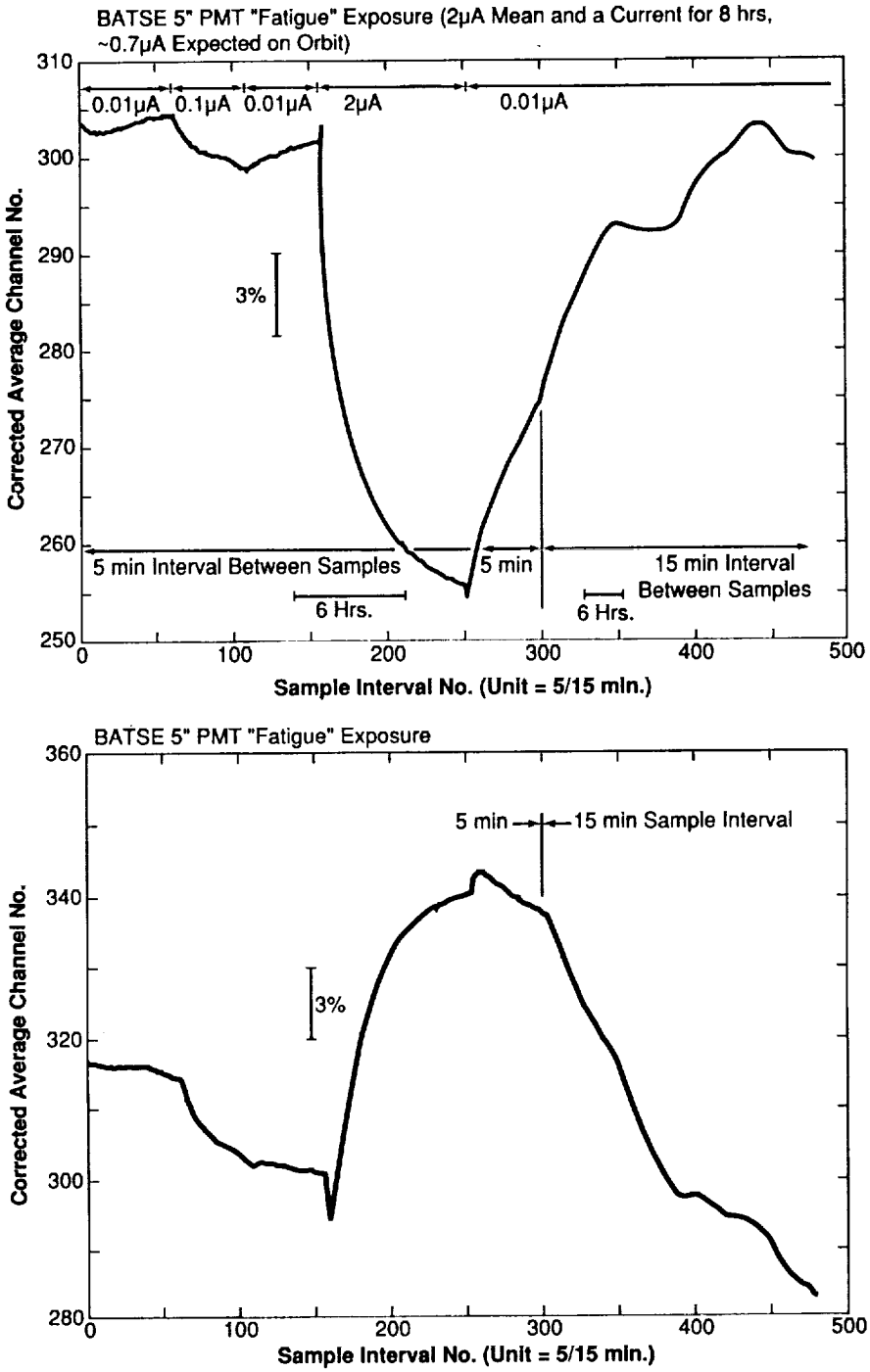

Figure 3.9. Gain Response to Fatigue Exposure (Two Types) Observed During MSFC PMT Screening Tests.

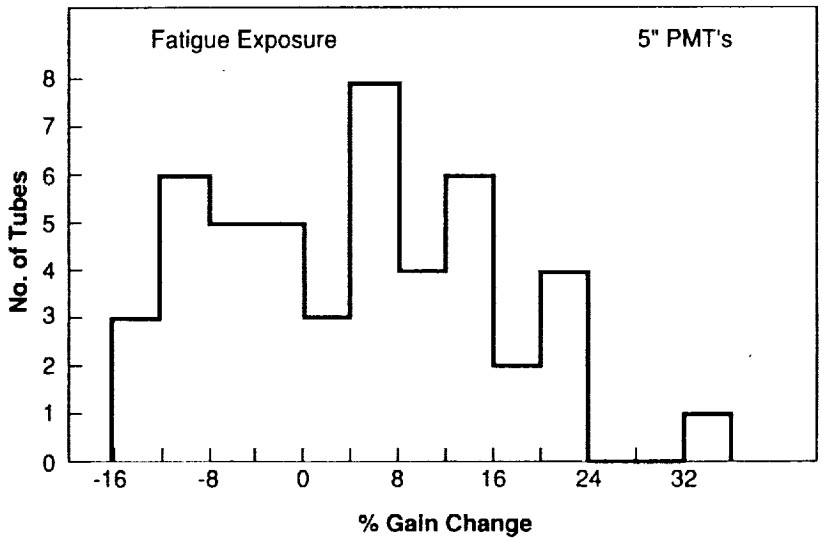

Figure 3.10. Gain Response to Fatigue Exposure for BATSE Flight PMTs.

Tubes undergoing test were also exposed to light levels (while powered off) that would have produced anode currents of more than 15 μA if the +HV were on. This exposure was conducted in intervals of 20 minutes, followed by 70-minute "recovery" intervals, thereby simulating passage in and out of the South Atlantic Anomaly. These cycles were repeated for two additional intervals. The +HV on/off cycle was repeated for 8 more hours, but with no LED light exposure. Typical PMTs showed gain changes of a fraction of 1%, with recovery to the initial gain in 30-60 minutes. Similar data accumulations were performed for +HV on/off cycles where no light exposure occurred. Similar gain variaitons of a fraction of 1% were also observed during this test.

The final test performed during acceptance testing was a measurement of the resolution. The best of the 12.7-cm PMTs were selected for use on the BATSE spectroscopy detectors. Each tube was subject to a measurement of the FWHM energy resolution using a 5" x 5" NaI Detector and a Cs 137 isotope. The following figure shows the distribution of the results obtained during the resolution testing.

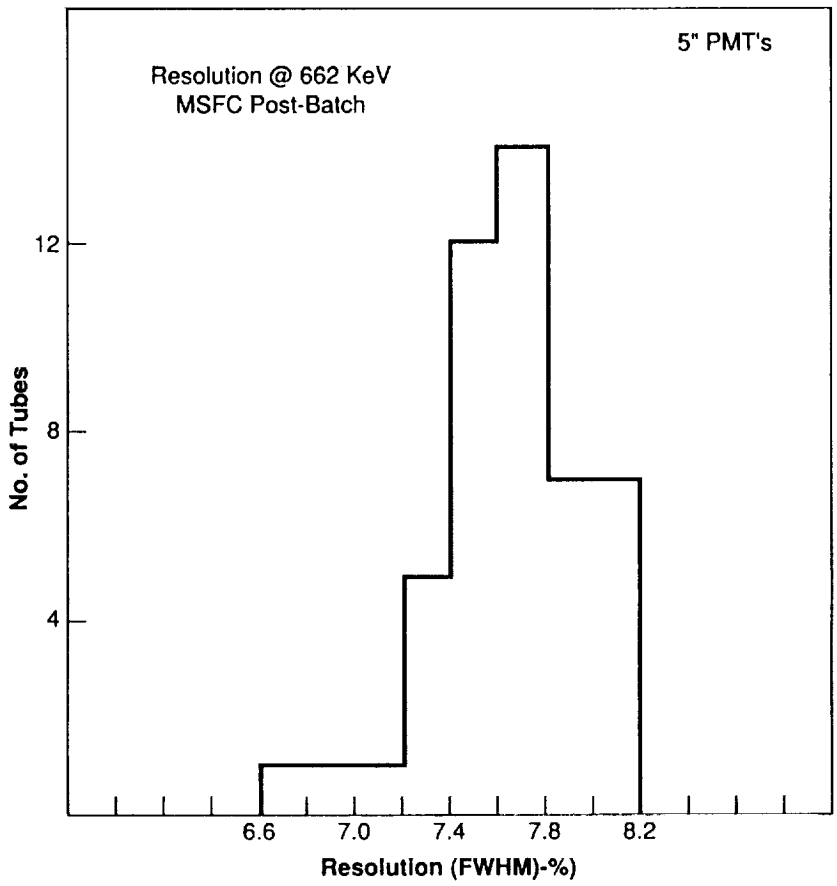

Figure 3.11. Measured 662-keV FWHM Energy Resolution Distribution for 12.7-cm PMTs.

5. BATSE DEU Board-Level Testing

a. CEU/DEU Interface and LED Driver Board — TPS-32

TPS-32, the CEU/DEU interface and LED driver board test, was performed by personnel from Space Science Laboratory at NASA-MSFC. A full prototype DEU was assembled and configured for the test as shown in Figure 3.12. All portions of the assembly were non-flight, except the board which was under test at the time. The interested reader may wish to consult BATSE drawing numbers 42A30491 and 42A30493 for a detailed look at the layout of this board.

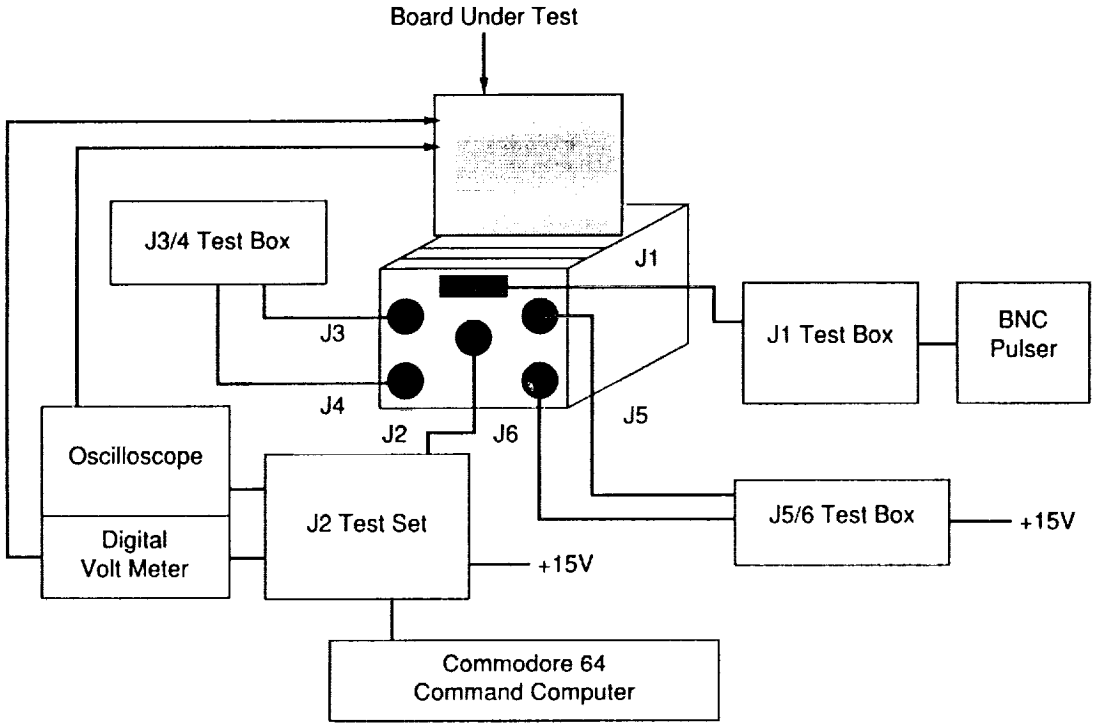

Figure 3.12. Test Configuration for BATSE TPS-32 CEU/DEU Interface and LED Driver Board Test.

Following the establishment of the testing configuration, power was applied to the test set. The signal generator was set to a frequency of 1.5-1.6 MHz and a duty cycle of approximately 30%. This simulated the MQT and FMQT signals from the LAD and SD boards. The correct reproduction of the input signal was verified at the outputs of the line drivers on the card for all associated signals, ensuring that the appropriate output was being generated for input to the CEU.

Subsequent testing verified the proper operation of the LED digital-to-analog converter. The LED amplitude was commanded to level zero, and RP3 was adjusted to produce 0 V ± 5 mV. With the LED commanded to each of the remaining 15 levels, the proper analog voltage was verified according to the table below. After verification of the proper voltage levels, the LED pulse shape was examined and verified while at command level #8.

Table 3.18. Acceptable Analog Voltage Levels for LED Digital-to-Analog Converter - TPS-32

Command Level	Acceptable Range (volts)
1	0.612-0.637
2	1.225-1.275
3	1.837-1.912
4	2.450-2.550
5	3.062-3.187
6	3.675-3.825
7	4.287-4.462
8	4.900-5.100
9	5.512-5.737
10	3.125-6.375
11	6.737-7.012
12	7.350-7.650
13	7.962-8.287
14	8.575-8.925
15	9.187-9.562

The next portion of the test adjusted potentiometers RP4, RP5, and RP6 to establish the proper output reference voltage for the module's 15-, 3-, and 6-V HKG measurements. Following completion of this portion, the SD LLD was adjusted. With the LLD commanded to value zero, RP1 was adjusted to produce an output of 0 V, ± 5mV. The LLD was then commanded to full-scale (255 decimal), and RP2 was adjusted to -6.0 V, ± 5mV. Each of the LLD command bits were then tested and verified to produce the proper voltage output according to the table below.

Table 3.19. Acceptable Voltage Levels for SD LLD Command Values TPS-32 - CEU/DEU Interface and LED Driver Board Test

Command Level	Acceptable Range
1	-23 mV ± 5 mV
2	-47 mV ± 10 mV
4	-94 mV ± 10 mV
8	-188 mV ± 10 mV
16	375 mV ± 10 mV
32	-750 mV ± 10 mV
64	-1.5 V ± 10 mV
128	-3.0 V ± 10 mV

The final portion of the test examined and verified the proper output of the various FAST discriminators and MQT signals generated from a given input. The pulser was used to simulate the input from the LAD and SD MQT boards and the PLASTIC signal. The associated output signals passed to the CEU by the interface board were then examined at the output of the J2-box for proper amplitude and duration. This completed TPS-32.

b. DEU HKG and Command Logic Board — TPS-33

TPS-33 utilized the same GSE configuration as TPS-32, with the exception that the only flight hardware in the DEU was the HKG and command logic board under test. All other hardware was prototype. Drawing numbers 42A30488 and 42A30490 detail the layout of the HKG and command logic board. Using a Commodore 64 computer, each of the strobe (serial command) lines were verified to appear active only at the desired point when utilized, that each of the strobe lines were isolated, and that the proper destination of the strobe line was reached. For strobe 0 (command 0), a continuous sweep through the data bits was executed to verify that the output exhibited binary counter operation at the time of the strobe.

Following the verification of the serial command strobe and data lines, the LAD LLD digital-to-analog converter was adjusted and checked in an identical manner to the SD LLD adjustment described in the previous section. Each of the command bits for the LAD LLD were exercised, and the proper output voltages were verified. These output voltages are identical to the SD LLD values. The test concluded with a check of all multiplexed HKG parameters. Each of the 32 values were polled, and a proper HKG return was verified. This completed the testing of TPS-33.

c. SD MQT Board Test — TPS-33

TPS-34 also used the same GSE configuration as the previous two board-level tests and replaced the prototype SD MQT board with a flight unit. Unlike the previous two tests, a PMT and NaI assembly were used as the input to the DEU at the J1 connector. The PMT was a 12.7 cm diameter, nine-stage tube with a BATSE flight-like base. Optically coupled underneath the PMT was a 12-cm NaI crystal. A voltage of 1000 V was used for the phototube. In this manner, actual NaI-generated pulses could be used to establish the proper shaping of the baseline-restoration circuit which serves as the input to the MQT integrated circuit. The baseline-restoration circuit was adjusted for critical damping of the input NaI signal by adjusting RP1 on the board. The interested reader may wish to consult BATSE drawing numbers 42A30494 and 42A30968 for a more extensive look at the SD MQT board. The PMT-NaI arrangement was disconnected at this point and replaced with a pulser and shaping box for the remainder of the test.

Following the adjustment of RP1, each of the flash-encoding discriminators (SFASTn) were examined for proper reference voltages. SFAST3 and SFAST4 were verified to turn-on near the desired voltages of 1.5 and 3.0 V, respectively. SMQT pedestal and full-scale adjustments were subsequently made in identical fashion to those described in section III.B.1.h. Finally, the SFMQT signal was examined to verify that it properly prevented the processing of SMQT signals when active.

d. LAD MQT Board Test — TPS-35

The GSE configuration for TPS-35 mirrored that of the previous tests, again with the only flight component being the board under test. BATSE drawing numbers 42A30905 and 42A30970 will provide the interested reader with a more detailed look at the LAD MQT board. The same PMT-NaI hardware used in TPS-34 provided input to the LAD MQT board during TPS-35. Following configuration of the GSE, the LAD baseline-restoration circuit shaping was executed as described in the previous section. Potentiometer RP1 was adjusted to provide the proper shaping.

After removal of the PMT-NaI assembly, and substitution of a pulser and shaping box, the next section of the test examined the LAD flash-encoding discriminators (FASTn). Each of the discriminators was checked for the proper firing voltages. FAST2, FAST3, and FAST4 were verified to fire near 56, 112, and 337 mV, respectively. The FAST1 threshold is determined by the LLD setting. Reference voltages for each of the LLD command bits were also measured for proper performance. The final discriminator test verified the differential nature of the four FASTn discriminators.

The LAD MQT was subsequently adjusted to provide a pedestal of 400 ns and a full-scale duration of 24 μs. These adjustments were accomplished by manipulation of RP3 and RP2 on the LAD MQT board, in identical fashion to the description of TPS-60 in section III.B.1.h.

Following MQT adjustments, the CPD signals were simulated by a pulser, and the proper PLASTIC signal amplitude and duration was verified. The proper anti-coincidence operation of PLASTIC with the MQT signal was also examined. Finally, the FMQT signal was checked to verify that it properly inhibited the processing of MQT signals during the duration in which it was active. This concluded TPS-35.

B. BATSE Subsystem Test Program

1. BATSE Detector Module Testing

The detector module test and calibration program was an extensive and complex series of events. In addition to the many tests which needed to be done on each detector module, the situation was further complicated by the fact that nine modules were at some stage of the program at any given time. The results of this program for each module will be presented. The results here include only data which were obtained during tests in which the detector module was considered a stand-alone piece of hardware. Any tests during which a module was connected to another piece of flight hardware (e.g., the CEU) will be presented elsewhere. The presentation contained here will progress somewhat chronologically, with deviations, exceptions, and special tests noted where appropriate.

a. Overview of Detector Module Test Flow

The BATSE detector modules were fabricated in MSFC Building 4705 under a contract to Ver-Val Enterprises, Inc. Science-related hardware, including PMTs, LADs, and SDs was assigned to a module by personnel from the BATSE Science Team. The first module (protoflight) completed fabrication and was ready for testing on January 21, 1988. Module B6 was the final module, starting the test flow on May 26, 1988. The flow for each detector module is described by Figure 3.13.

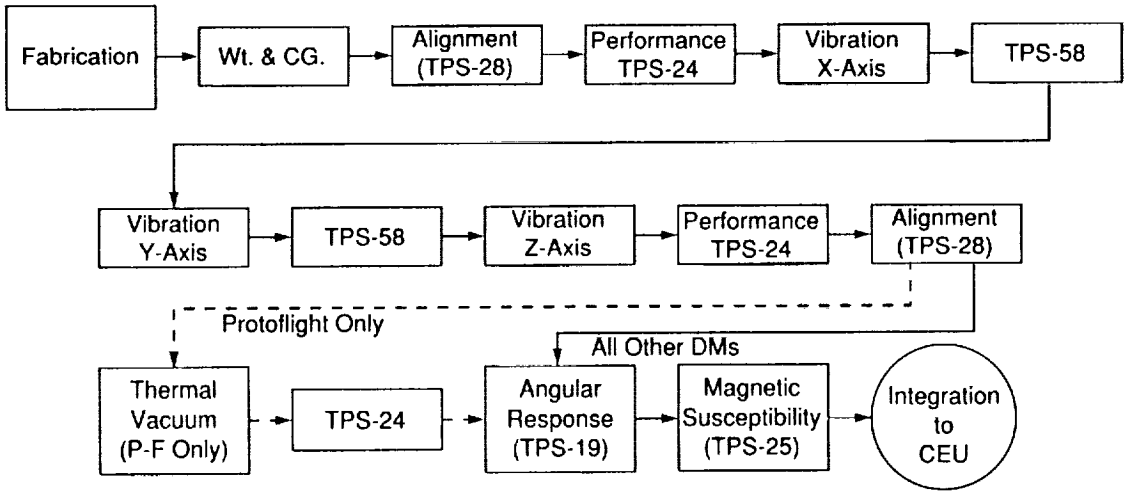

Figure 3.13. BATSE Detector Module Test Flow.

Following assembly, each detector module was weighed and had center-of-gravity measurements performed. Alignment of the LAD and SD with respect to an optical alignment fiducial was then measured in TPS-28. The module was then powered-up for its initial performance test. This test, TPS-24, included a check of every module function. The detector module was then sent to the vibration facility for vibration tests in all three axes. Between the vibration tests, an abbreviated version of TPS-24 was performed. A second alignment measurement and a full-scale TPS-24 were then performed following successful completion of the vibration tests. The protoflight module was taken to the thermal balance and thermal vacuum tests at this point. All other modules proceeded to the next portion of the test flow. The module was taken to the angular response test facility for angular response (TPS-19) and magnetic susceptibility (TPS-25) tests. After completion of the test program, the module was integrated to the CEU for system-level testing.

b. BATSE Detector Module Weight and Center of Gravity Measurements

The first stop for a detector module following assembly was to the north end of Building 4705 for initial weight measurements and center of gravity determination. These properties of the detector module are of obvious importance in determination of the properties of the overall spacecraft. This test is the only time that the modules were weighed, and the only addition to the detector module after this point was the sintered bronze vents added to the CPD assemblies. The coordinate system used for the center of gravity measurements (U,V,W) is a right-handed system, with the U-V plane containing the detector module base. The U-axis points directly out the front of the module; the W-axis is the normal to the baseplate. The figure below details the orientation of the coordinate system.

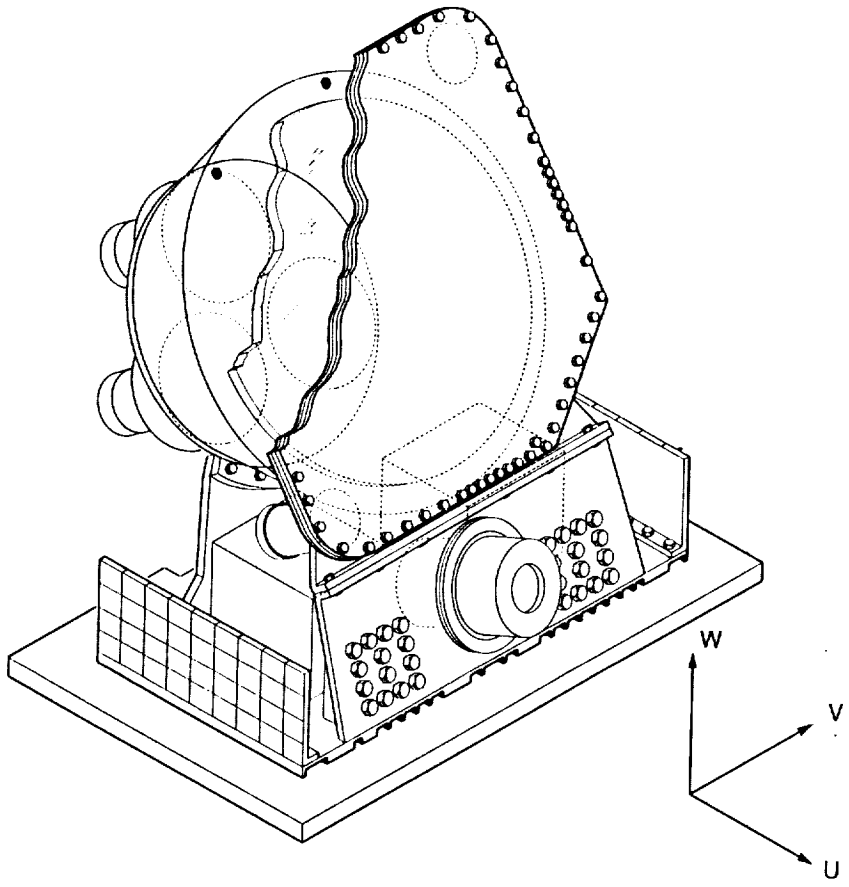

Figure 3.14. BATSE U,V,W Detector Module Coordinate System.

The results from the weight and center of gravity measurements of the nine flight-qualified detector modules are summarized in Table 3.20.

Table 3.20. Detector Module Weights and Center of Gravity Locations

		Center of Gravity (cm)		
Detector Module	Weight (lb)	U	V	W
Protoflight	194.75	23.114	-0.287	28.560
B0	196.10	22.984	-0.246	25.580
B1	196.13	23.061	-0.175	28.565
B2	195.63	23.094	-0.287	28.626
B3	193.90	23.127	-0.269	28.593
B4	196.93	23.005	-0.183	28.504
B5	195.11	23.017	-0.119	28.438
B6	196.15	23.012	-0.262	28.468
B7	195.20	23.068	-0.188	28.514
Flight cables	173.00			
Detector insulation	58.00			

c. Detector Module Alignment Measurements — TPS-28

The next phase of the test and calibration program for the detector modules was TPS-28. The purpose of this test was to determine the orientation of the BATSE large area detector and spectroscopy detector to a detachable, non-flight alignment fixture. This fixture consisted of a corner-cube reflector and a flat mirror. Each of the fixtures are serialized and assigned to a particular module throughout the entire lifetime of the detector. This test was repeated at several locations during the test and calibration program to determine the effects, if any, of the environmental tests on the alignment of the BATSE detectors. The data from this series of tests were then used in conjunction with spacecraft measurements to determine the pointing aspect of each LAD in the GRO coordinate frame.

Determination of the BATSE LAD internal pointing aspect was made on a granite slab using a Nikon-model autocollimator and an optical bench. The serialized alignment fixture is tilted to the top of the detector module and aligned to it by precision locating pins. The attachment is made to the LAD cone flange, which is also the support point for the LAD crystal housing. The alignment fixture is installed in this location so that there is minimum flexure between the alignment assembly and the crystal. The repeatability of the accurate installation of the fixture has been verified. The entire detector module is then installed into its holding fixture. Figure 3.15 illustrates this entire arrangement.

The light-emitting diode (LED) calibration assembly is removed from the back of the LAD cone so that the rear face of the optical window of the LAD assembly can be viewed directly. The parallelism of this surface with the front surface of the LAD crystal was determined during the LAD assembly process at the Bicron Corporation facility. The detector module is then placed on its side, and the optical bench and collimator are arranged as shown in Figure 3.16.

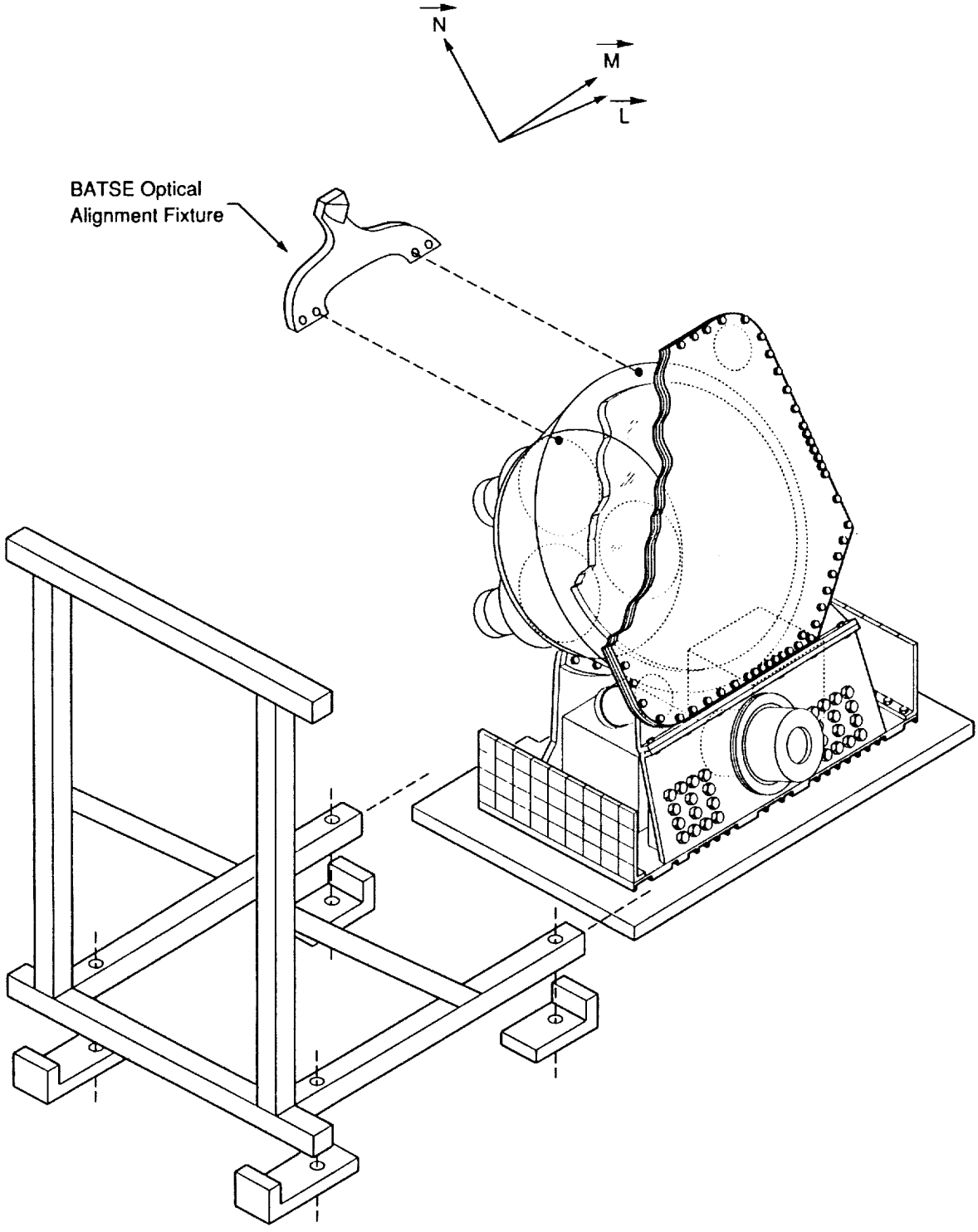

Figure 3.15. BATSE TPS-28 Fixtures and Detector Module.

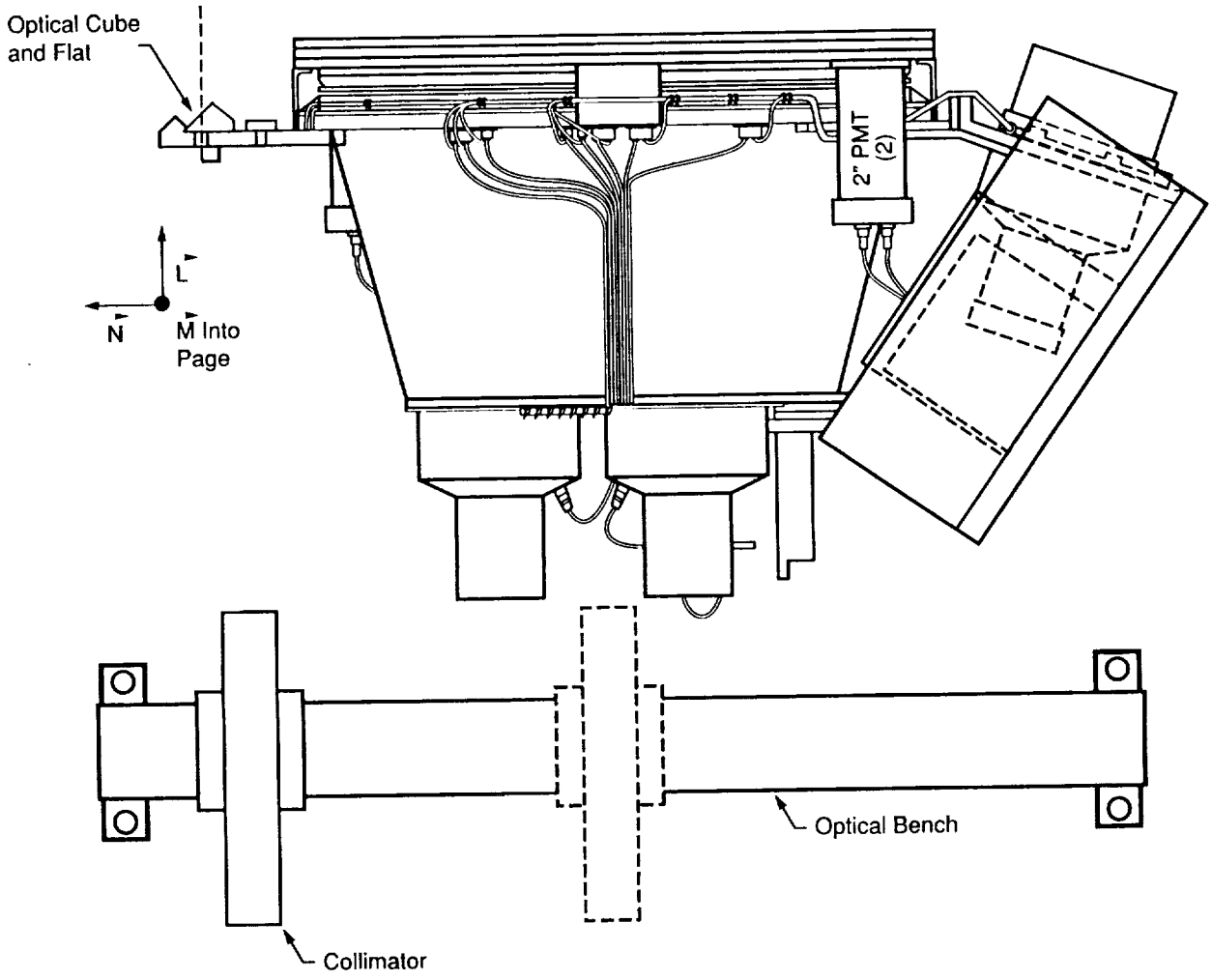

Figure 3.16. BATSE TPS-28 Measurement Configuration.

The coordinate system in which these initial measurements are taken, labeled (L,M,N), is right-handed and is fixed onto the alignment fixture (see Figure 3.16). The L-axis is the normal to the surface of the mirrored flat behind the optical corner-cube. The M-axis is parallel to the precision-machined edge against which the corner-cube is seated for installation. These two axes are orthogonal to within the tolerances of the precision milling machine on which the fixtures are constructed. The N-axis is perpendicular to these two axes.

The quantities measured in this test are the offset in pitch-angle and yaw angle of the normal to the LAD with respect to the normal to the mirrored flat (L-axis). Pitch angle is measured as an offset from the L-axis in the LN plane, and is defined such that a positive angle is an offset from the L-axis toward the N-axis. Similarly, the yaw offset is measured in the LM plane, and is defined as positive when the offset is in the direction of the M-axis. From these two angles, the three components of the LAD pointing vector can be constructed in the LMN system. The measurement is obtained by first aligning the autocollimator so the line of sight is along the L-axis. When this is accomplished, the returned image from the optical flat will fall directly on the center of the autocollimator viewfinder. The autocollimator is then translated along the axis on the optical bench until the returned image from the LAD is present in the viewfinder. The pitch and yaw angles are recorded. The measurement is repeated to insure accuracy.

When taking initial measurements, the true orientation of the detector module is somewhat difficult to establish in all three axes. The L-axis is obviously the easiest, because it can be read directly off the autocollimator through the reflection from the optical flat. The M- and N-axes are more difficult and may vary slightly from the local vertical and local horizontal because of play in the system. It is estimated that this error is on the order of a few arc minutes, and does not contribute to a significant degradation of the measurement.

Internal alignment measurements were performed three times; the first after the module was constructed, the second after the vibration test, and the final measurement following the shipment of BATSE to TRW prior to the detector modules' installation onto the spacecraft. All three of these measurements were consistent. For the final calculations to determine the pointing of the LADs in GRO coordinates, the data from the last internal measurement at TRW were used. The offset angles in pitch and yaw are summarized in Table 3.21.

Table 3.21. BATSE LAD Pitch and Yaw Offsets Measured in LMN Coordinates (Data from Final TPS-28, November 1988, California)

Detector Module #	Pitch Offset (degrees)	Yaw Offset (degrees)
B0	-0.26027	0.01527
B1	-0.12638	0.03805
B2	-0.00388	-0.01777
B3	0.12861	0.02844
B4	-0.08333	-0.04972
B5	0.14861	0.02250
B6	0.16888	-0.04111
B7	0.09111	0.07166

From the values in the table above, one can construct the LAD pointing vector in LMN coordinates using the following equation:

$$\underline{\text{LPOINT}} = (\cos(\text{Tp})\cos(\text{Ty}))\,\underline{\text{L}} + (\cos(\text{Tp})\sin(\text{Ty}))\,\underline{\text{M}} + (\sin(\text{Tp}))\,\underline{\text{N}}, \qquad (3.1)$$

where LPOINT is the LAD pointing vector, Tp is the measured pitch angle offset, Ty is the measured yaw angle offset, and $\underline{\text{L}}$, $\underline{\text{M}}$, and $\underline{\text{N}}$ are unit vectors parallel to each of the three defining axes. Substitution of the values from the table above into the equation above yields the components of the LPOINT vector. These components are summarized in Table 3.22.

Table 3.22. BATSE LAD Unit-Length Pointing Vector Coordinates in LMN Space (Data from Final TPS-28, November 1988, California)

Detector Module #	L	M	N
B0	0.999989	0.000266	-0.004543
B1	0.999997	0.000664	-0.002206
B2	0.999999	-0.000310	-0.000068
B3	0.999997	0.000513	0.002245
B4	0.999998	-0.000867	-0.001454
B5	0.999996	0.000392	0.002594
B6	0.999995	-0.000717	0.002948
B7	0.999998	0.001250	0.001591

Having determined the LAD pointing vectors in the LMN coordinate system, these vectors can be transformed into any other coordinate system through a series of coordinate transformations. The next step in the alignment measurements is to transform these pointing vectors into an alignment cube-based coordinate system. This calculation, and others required to obtain the LAD pointing vectors in GRO coordinates, will be discussed in the section concerned with spacecraft alignments. As mentioned, the data presented in this section are concerned only with measurements taken on detector modules as stand-alone units. The detailed alignment calculations with respect to the GRO spacecraft are described in another document.

d. Detector Module Performance Test — TPS-24

TPS-24 was designed to be a thorough test of all detector module hardware and functions. This test procedure served as the standard for detector module testing throughout the program. The test consisted of several sections: initializations, spectroscopy detector tests, large area detector tests, charged-particle detector tests, and housekeeping checks. Each of these sections will be discussed in detail.

The detector module required a large amount of ground support equipment for this test. The equipment provided power to the module and allowed for the examination of individual signals from the detectors. Figure 3.17 shows the test configuration.

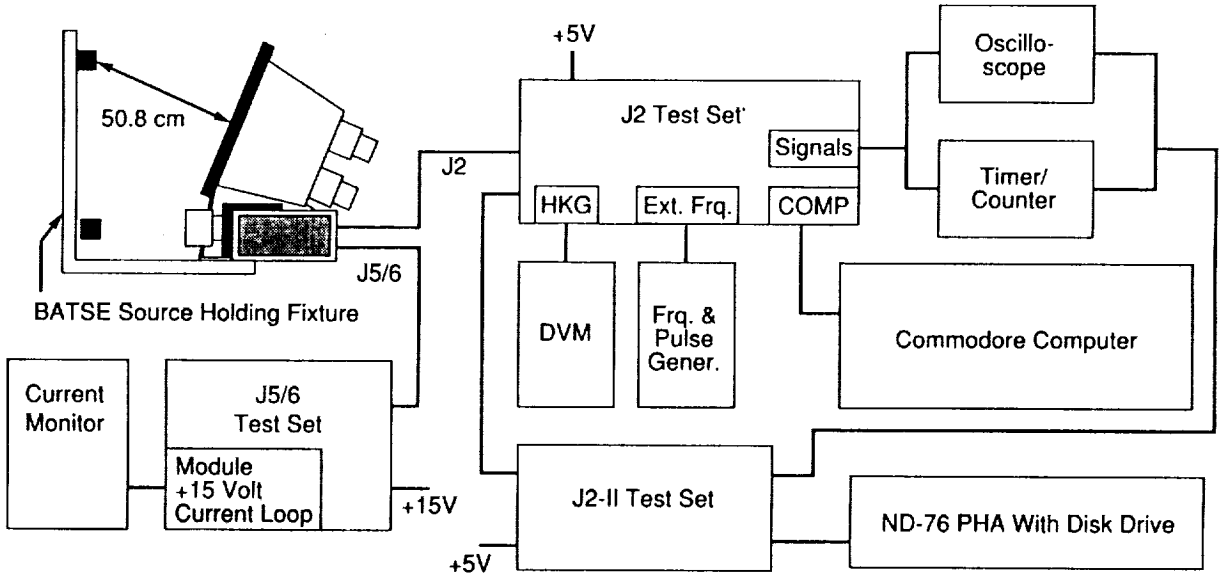

Figure 3.17. TPS-24 Test Configuration.

The J2 box is a part of the GSE which serves primarily as a breakout of all signals which the module generates and transmits through its J2 connector. These include all LAD signals (FAST1-4, LAD-MQT, FASTID), CPD signals (PLASTIC), SD signals (SMQT, SFAST1-4), housekeeping voltages, and heater status resistances. J2 also allows for the input of an external frequency to drive the LED calibration assembly. The J2-II box serves as the interface between the MQT signals and the pulse-height analyzer. This box also allows for the viewing of the other event-generated signals. The J5-6 box is the power interface for the detector module. Commands are sent to the detector module through a Commodore computer containing software which generates serial commands to the module either individually, or from predetermined command files stored on floppy disks.

Radioactive isotopes are used during TPS-24 to generate gamma ray events in the detectors. These sources are always located at a distance of 50.8 cm from the center of the detector under test and on the axis of the detector. This location is obtained through the use of a source-holding fixture constructed specially for this test. The fixture consists of aluminum tubing, and is seated against the detector module baseplate in one of two pinned positions (depending on whether the LAD or SD is being tested). The isotopes are mounted onto 5.1 x 5.1 cm cards which slide into a slot on the holding fixture. This arrangement provides a repeatable isotope test location which is uniform from module to module.

(1) Initializations

The test begins with the power-up of the detector module. The module is monitored immediately upon power-up to verify the proper current is being drawn (< 500 mA). This initial turn-on current is different each time the module is powered because of the uncertain state of the five +HV supplies. After the safe operating current of the module is verified, all +HV supplies are powered off, and the PMTs are then balanced. The balancing of the LAD is accomplished using a small Cs 137 source placed into the holder at the standard 50.8-cm distance. The isotope's 662-keV line is used as the reference. Each PMT's +HV supply is individually commanded so that the three PMTs contribute equally to a summed gain which has a dispersion of 5 keV/channel. The CPD voltage is set at the value needed to obtain 0.6 x muon deposition energy, and is determined in TPS-15 (see section III.A.3.a). For the SD, three different gains are obtained. High voltages required for dispersions of 1 keV/channel, 4 keV/channel, and 10 keV/channel are determined. The 4 keV/channel gain is considered nominal, with the other two providing gains of 4X and 0.4X nominal. After the voltages are determined, the +HV supplies are set at nominal values, command files are generated, and the PMTs are allowed 30 minutes to stabilize. Table 3.23 displays the initial +HV values for all supplies and all gains.

Table 3.23. TPS-24 Initial High Voltage Values

	Detector Module Number								
HV Supply	P-F	B0	B1	B2	B3	B4	B5	B6	B7
PMT-A	1538	1402	1504	1441	1480	1496	1539	1373	1551
PMT-B	1526	1409	1488	1413	1508	1539	1520	1280	1535
PMT-C	1524	1409	1504	1469	1484	1535	1559	1308	1575
CPD	1405	1429	1335	1245	1276	1240	1221	1304	1209
SD-1X	1160	1272	1303	1248	1161	1232	1130	1225	1311
SD-4X	1269	1559	1610	1535	1421	1500	1386	1511	1626
SD-0.4X	1003	1134	1146	1098	1024	1017	1012	1095	1150

Comparison of the CPD voltages with those from Table 3.13 shows variations of 1-2 V from the values obtained in TPS-15. The command resolution of the HVPU is 4 V; therefore, the CPD could not be commanded exactly to the value desired in all cases. For TPS-24, the closest value possible was used regardless of whether it was greater or less than the value desired. The initialization section of TPS-24 is complete following the 30-minute warm-up period.

(2) Spectroscopy Detector Tests

Section two of TPS-24 involves testing of the SD and its associated electronics. A verification of the stabilized PMT is executed by the collection of two Cs 137 spectra 15 minutes apart. A change in 662-keV photopeak location which is less than or equal to 1.25% is considered stable. After stability is established, SFAST1-4 are examined. The bi-polar nature of all four discriminator signals is verified, and each of the signals' amplitudes and durations are measured on an oscilloscope. Typical amplitudes and durations for the SFAST signals are 0.42 V and 0.44 μs, respectively. The SMQT signal is then examined. The bi-polar nature of this signal is verified, and the minimum duration of the SMQT signal is measured. This minium duration is a direct measurement of the SMQT pedestal.

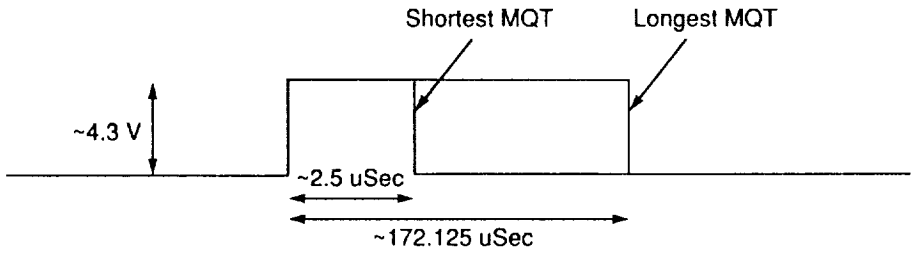

Figure 3.18. Schematic of the SMQT Signal.

For very short-time-duration MQT signals, the digitization of the signal is non-linear. To avoid these complications, the BATSE team decided that the minimum-duration MQT signal should be 2.0 μs, plus some margin. The final minimum duration arrived at was 2.5 μs. Each μs of duration in the MQT signal correlates to 16 linear SD channels. Thus a "zero-energy" event in the SD will produce an MQT signal of approximately 2.5 μs in duration, and increment channel 40 by one count. Upon connection of the schedule to the CEU, the science data function subtracts the first 32 channels, and the offset becomes approximately 8 channels in the resulting data. The offset is fine-tuned to the proper value through the use of a potentiometer on the SMQT board in the DEU of each detector module. Results of the procedure to fine-tune the pedestal are presented in a subsequent section of this document.

The SD +HV was next commanded to the 4X gain value, and a Th 228 source was placed into the holder. After a check of the proper voltage value, a 120-second integration was obtained and stored to disk on the ND-76 system. Following the 4X spectrum, the Th 228 source was replaced with a Na 22 source, the SD was commanded to the 0.4X value, and another 120-second integration was obtained.

TPS-24 continued with a mapping of the SD programmable lower-level discriminator (LLD). The LLD is commandable to 255 different values, each with a specific cut-off energy. Each bit (eight total) of the LLD was tested. Additional measurements to provide higher resolution near the expected operating value were also executed. Fifteen different command values were used at the 1X gain setting, with seven values used at the 4X and 0.4X gains. At each of the LLD settings, the threshold channel was recorded, the SFAST1 rate was recorded, and a 120-second spectrum was accumulated and stored to disk. A Na 22 isotope was used to raise the count rate to obtain good statistics over a shorter period of time. LLD values below 12 decimal usually were in the system noise and produced ringing of the discriminator. Table 3.24 shows results from detector module B1 testing on February 24, 1988, for the SD at 1X gain. These values are typical for all nine flight-qualified modules.

Table 3.24. Detector Module B1 SD LLD Channel Measurements (1X Gain, TPS-24, 2-24-88)

Discriminator Value (HEX)	SFAST1 Rate (cps)	SMQT Threshold Channel (linear)
2	-------	Ringing
4	-------	Ringing
8	17000	Ringing
C	2800	45
10	2700	46.5
12	1700	47.5
14	1600	48.5
15	1500	48.5
16	1500	49
18	1500	49.5
1C	1400	51
20	1400	52.5
40	1400	64.5
80	1200	92
FF	1000	154

Following the mapping of the SLLD at the three gain settings, the detector was thoroughly checked for any light-leak which may be present. While viewing SFAST2 on the oscilloscope and timer-counter, a high-intensity light was used to illuminate the SD over its entire surface area. As the light was moved around, the rate meter and oscilloscope were examined for any sign of the light being detected by the PMT. No SD was found to have a light-leak.

The final section of the SD portion of TPS-24 was the measurement of photopeak resolutions with various isotopes. This measurement marked the first time the photopeak resolution was measured while the SD and its flight DEU were operated together. In addition, these were the first measurements taken of the SDs since the TPS-16 results presented in Table 3.12. For some detectors, this was a time span of nearly 16 months between measurements.

Resolution measurements started by commanding the SD to the nominal (1X) gain setting and removing all sources so that a 300-second background accumulation could be obtained. This background was stored to disk and used in the subtraction from source spectra. Isotopes of Cd 109, Cs 137, Na 22, Co 60, and Th 228 were used in the measurements. In addition to the FWHM resolutions of the various photopeaks, a "peak-to-valley" ratio measurement was obtained by division of the number of counts in the 1.173-MeV peak from Co 60 by the number of counts in the minimum channel between the 1.173- and 1.332-MeV peaks. This number offers a good handle on how well the two peaks are separated, and thus the resolution of the detector. For each of the nine flight-qualified modules, the results of this section from their initial TPS-24 are presented in Table 3.25.

Table 3.25. Initial TPS-24 FWHM Resolution % Measurements for SDs at 1X Gain

	FWHM Resolution % (Energy in keV)							Peak-to-Valley
Detector Module	88	511	662	1275	1173	1332	2614	Ratio
P-F	11.4	7.9	6.7	5.2	5.5	5.2	4.1	16.4
B0	17.9	8.5	7.1	5.2	6.4	5.5	2.6	14.5
B1	14.7	8.3	7.0	5.7	6.4	5.5	4.5	8.8
B2	15.6	8.1	7.4	6.2	6.2	6.0	4.8	8.2
B3	12.9	8.2	7.1	5.7	6.2	5.6	4.3	8.8
B4	27.3	8.2	7.5	5.5	6.2	6.0	3.1	9.0
B5	16.7	8.2	7.3	6.1	6.0	5.8	3.6	7.7
B6	18.7	8.1	7.5	5.7	6.4	5.6	4.4	11.8
B7	25.0	8.2	7.0	5.7	6.2	5.8	4.4	8.3

The editor cautions those using the 88 keV numbers shown in Table 3.25. The gain of the SD was established using the 662-keV line from the Cs 137 isotope. For the measurement of the 88-keV line, the local dispersion was calculated using the location of the line and the measured "zero-energy" channel from the oscilloscope. The 23-keV line usually was below the cut-off of the LLD. The measurement of this zero-channel from the scope is highly dependent on the person doing the measuring. Examination of the test procedures indicates dispersions from 3.5 to over 5.0 keV/channel were used in the calculation, when the gain was set to almost exactly 4.0 keV/channel, verifiable from two-peak measurements taken at the same time. Since the response of the SD is nearly linear, the dispersion does not change by a large amount over an energy range of 500 keV. This linearity and the validity of the two-peak dispersion measurements call into question the validity of the dispersion measurements made using only the 88-keV line and the oscilloscope-measured pedestal channel.

For measurements at energies of 511 keV and higher, the dispersion is measured from two photopeaks of known energy, providing a much more reliable number with which to calculate the resolution. Comparison of the 662-keV FWHM resolution measurements above with those from Table 3.12 indicates that the SDs perform in a manner consistent with previous measurements at this energy. The resolution measurements marked the completion of the SD testing in TPS-24.

(3) Large Area Detector Tests

The testing of the large area detector was performed in the second section of TPS-24, and began with a check of the electronic signals, similar to what was done with the SD. The bi-polar nature of the four LAD FASTn signals was verified through observation on an oscilloscope. The duration of each of these pulses was measured and verified to exceed 50 ns. A

typical duration for a FASTn pulse is approximately 165 ns. The differential nature of these four signals was verified by examining the FASTn signals one at a time. While examining one particular FASTn signal, the oscilloscope was triggered with the other FASTn signals sequentially. While stepping through the FAST signals with scope-triggers from the other three signals, the test conductor verified that only one FAST signal was present at any given time, and that the discriminators were in fact differential. The energy boundaries of each of the signals were measured in a later test.

The LAD MQT signal was examined next. Functionally identical to the SMQT signal, the bi-polar nature of the pulse was verified, and the minimum duration was measured. Unlike the SMQT signal, with its 40-channel offset, the LAD MQT has approximately a six-channel offset. The non-linear digitization effect which is present at the low-end of the MQT signal occurs in the LAD as well as in the SD. However, incorporation of a large offset (longer MQT pulse) introduces a larger dead-time per event. Longer pulses require a longer period of time for the electronics to process the signal. With the SD, this is not a large problem, because the intrinsic rate is lower due to the smaller collection area. For the LAD, however, the count rate is sufficiently high that inclusion of a large offset would introduce unacceptably high dead-times. Because the high dead-time would outweigh the benefit of linear digitization, it was decided to place the LAD pedestal at 400 ns. This corresponds to a linear "zero-energy" channel of 6.4. (Subsequent system-level tests on the GRO spacecraft showed that the "zero-energy" channels ranged between 5.4 and 7.3 for different LADs.) The MQT was measured to verify the minimum duration at 400 ns ± 100 ns. A light-leak check was then performed on the LAD in the same way as was done on the SD. No LADs were found to have a light-leak problem.

Measurements of the LAD electronics continued with a mapping of the programmable LAD-LLD. This measurement was done in a fashion similar to that of the SD. Each bit of the LLD was checked for operation, and a mapping of the discriminator setting vs. linear channel was made. The dynamic range of the LAD-LLD is much less than that of the SD-LLD. Full-scale setting of the LAD LLD corresponds to approximately channel 25, while a full-scale setting of the SD-LLD placed it near channel 150. The mapping for the protoflight module's LLD taken from a test on February 19, 1988, is shown in Table 3.26.

Table 3.26. Sample LAD-LLD Command Setting to Linear Channel Relation (Data from TPS-24 of 2-19-88, Protoflight Module)

LAD LLD Setting (HEX)	Linear Channel of LLD
0-10	6
20	8
40	10
80	15
FF	24

Mapping of the LAD-LLD was followed by photopeak resolution measurements of the LAD. Unlike TPS-26, these measurements involve all flight components of the LAD system, not just the LAD crystal assembly. The LAD +HV supplies were commanded to the nominal (5 keV/channel) gain settings and verified. A 300-second background accumulation was collected and stored to disk. This background accumulation was used for subtraction from isotope spectra prior to calculation of the resolution. Isotopes of Cd 109 and Na 22 were used for these measurements. The data were collected in the same fashion as was done with the SD. The source was placed into the LAD source holder, a 300-second accumulation was obtained, background was subtracted, and the spectrum was stored onto disk. Results from the initial TPS-24 of all nine flight-qualified modules are presented in Table 3.27.

Table 3.27. Initial TPS-24 LAD FWHM Photopeak Resolution Percentages

	FWHM Resolution %		
Detector Module	88 keV	511 keV	1275 keV
P-F	34.8	16.9	16.5
B0	26.3	17.2	17.0
B1	32.2	17.6	18.4
B2	23.2	16.7	15.9
B3	29.4	19.2	19.9
B4	28.4	20.4	16.8
B5	38.0	21.9	21.8
B6	31.6	24.0	22.5
B7	34.5	20.0	19.7

The reader is cautioned about the validity of the measurements taken at 88 keV. The dispersion was again calculated using the location of the 88-keV photopeak and the measured "zero-channel" from the oscilloscope. The subjectivity of the oscilloscope measurement leads to possible errors in the dispersion. Because the gain of the LAD is 20% lower than the SD at 1X, errors in the measurement of the "zero" channel play a less significant role in the calculation, as the baseline is effectively larger. This is reflected in the smaller "spread" in measured resolutions from the LAD compared to the SD. However, the LAD range from 23.2% to 38.0% is still large, and reflects some problems in the measurement. Comparison of the 511-keV data with TPS-26 LAD acceptance test data shows good agreement in the resolution measurements, with no indication of degradation. The measurements taken at 1275 keV were computed using 1240 keV as the energy of the incident gamma ray line. The incorporation of 1240 keV instead of the correct value of 1275 keV into the computation of the resolution introduces a small error in the result.

Resolution measurements from TPS-24 are less than ideal. Test conditions and environments varied significantly from module to module, and as many as ten different individuals conducted these tests. These factors lead to results which, although not wholly

inaccurate, are not suitable for scientific calibrations or detailed determination of the instrument's performance capabilities. TPS-24 was designed to verify that all parts of the detector module were operating properly, and also to show that the module performed within certain a priori criteria. It was not the purpose of the test to determine exactly where inside the boundaries the modules performed. These measurements were executed during the BATSE science tests, which will be discussed later in this document. Perhaps the best module-level resolution measurements come from TPS-59, taken at TRW in California over a 1-week period with the same two test conductors performing all tests. These results will be detailed at the end of the detector module section.

The next section of TPS-24 involves testing of the LED calibration assembly. The LED can be commanded to pulse at 15 different intensity levels through the use of four bits in a serial command. Each bit was checked for proper operation, and the LED locations in the spectra were mapped against each commandable level. Because of differences in the intrinsic light output of the LEDs, and the use of different neutral density filters, each detector has a different LED response for any given command. Table 3.28 details the LED response from detector module B5 during a TPS-24 test on April 28, 1988. This behavior is representative of all the detector modules. LED positions in HER data as seen through the CEU are presented in the instrument testing section of this document.

Table 3.28. LED Channel Locations for Commanded Values from TPS-24 (Detector Module B5, 4-28-88)

LED Command Value	Uncompressed Peak Channel
15 (decimal)	532
14	506
13	460
12	413
11	364
10	316
9	267
8	217
7	167
6	119
5	73
4	32
3,2,1	OFF

For an approximate equivalent energy for the LED location, subtract 6 from the channel number and multiply by 5 keV. After integration with the CEU, the PMTs are re-balanced, and spectra in the HER data type are subjected to the quasi-logarithmic compression, which changes the values of LED location for a given commanded value. Initial tests of the LED showed that

the diode was intrinsically too bright for the detector to handle. Therefore, a change was made in the hardware to install several layers of Kodak neutral-density optical filters in front of the LED to lower the amplitude of the light output.

(4) Charged Particle Detector Tests

The CPD was the final section of detector testing executed in TPS-24. In this section, the main focus was to determine that the CPD was operating properly, and that all (anti-) coincidence circuitry was functioning normally. This portion of the procedure began with the collection of a 300-second LAD spectrum with the CPD on and in anti-coincidence mode. This spectrum was stored to floppy disk. Next, the CPD was powered off, and another LAD spectrum of 300 seconds was accumulated. This spectrum was also stored and subtracted from the previous spectrum. The difference in counts between these two spectra is due to the lack of CPD rejection in the second integration. From the difference, a charged-particle rejection rate was determined.

The CPD was then commanded into the coincidence mode, and the +HV on the LAD PMTs was lowered until the gain allowed the analysis of muon events in the LAD. A third 300-second LAD integration was accumulated and stored to disk. If the CPD and its associated circuitry were operating properly, the count rate in the coincidenced spectrum above 0.6 x muon peak energy (CPD threshold) should be approximately equal to the CPD rejection rate derived from the first two spectra. The analysis had to be done in this fashion because of the mono-channel nature of the CPD PLASTIC signal from which a spectrum is not obtainable. The table below presents the CPD rejection rates and coincidence count rates from the initial TPS-24 performed on all flight-qualified detector modules.

Table 3.29. CPD Rejection and Coincidence Rates from Initial TPS-24 Runs

Detector Module	CPD Rejection Rate (cps)	Coincidence Rate (cps)
P-F	28.6	26.4
B0	25.9	23.4
B1	28.3	25.4
B2	29.6	28.3
B3	29.6	28.4
B4	24.4	26.7
B5	25.5	27.5
B6	19.8	19.5
B7	27.0	24.4

The expected CPD rate from muons in the atmosphere can be obtained by multiplying the rate of muons per square centimeter per steradian by the cosine-squared distribution of muons and integrating over the solid angle. Using a value of 0.01 $cm^{-2}s^{-1}sr^{-1}$ for all muons > 200 MeV in energy, one obtains a rate of 0.021 $cm^{-2}s^{-1}$. The projected area of the CPD to the vertical is approximately 1170 cm^2. Multiplication of the projected area by the rate per unit area yields an expected rate of approximately 24.6 counts per second from muons. This number is in good agreement with the results from TPS-24. The rates obtained from the CPDs are affected by other factors including the rate of accidental coincidences, the geomagnetic latitude, and the amount of mass overhead which absorbs incoming muons. This measurement completed the CPD section of TPS-24.

(5) Housekeeping Measurements

The final section of this test procedure was to check all detector module housekeeping functions. Module housekeeping is placed into one word in each packet of BATSE data, and this word is multiplexed 32 deep. For each location on the multiplexer, the status of one particular element on the module is reported. The first 10 of these are module +HV values and currents, which depend on the commanded state of the +HV supplies. The final 17 are measurements of temperatures, module low voltages, and ground offsets. Several spare locations are included.

The last 17 housekeeping measurements were checked first and compared to expected values. Following the check of these measurements, each +HV supply was individually tested and mapped to housekeeping measurements. With all other +HV supplies off, the supply under test was commanded to check each bit of the 8-bit setting command. While commanded at each of the eight values, the two housekeeping measurements related to that supply were obtained. This sequence was repeated for all five supplies on the detector module. Testing in this fashion insured that all bits in the +HV commands were functional, that the housekeeping functions for that supply were operating, and allowed for a mapping of commanded value to voltage and rent. This mapping was then compared to the desired linear relationship of commands to voltage between 1,000 and 2,000 V. Table 3.30 contains the relationship for PMT A on detector module B3, obtained in a TPS-24 measurement taken on February 25, 1988.

Table 3.30. Voltage and HKG Values for Selected Commands
(Detector Module B3, PMTA -- TPS-24, 2-25-88)

+HV Commanded Value	Voltage	Analog/Raw HKG Voltage
255 (decimal)	1993	4.982
128	1496	3.741
64	1246	3.116
32	1121	2.803
16	1056	2.640
8	1027	2.568
4	1012	2.529
2	1004	2.510
1	1000	2.500
0	OFF	0.000

(6) Pass/Fail Criteria and Data Storage

The detector module testing in TPS-24 was completed at the end of the Housekeeping section described in the previous paragraphs. The module was then passed or failed based on the following criteria:

(a) The resolution of the LAD at 88 keV shall not exceed 35.0% FWHM as specified in MSFC-SPEC-697D.

(b) The resolution of the SD at 662 keV shall not exceed 8.0% FWHM as specified in MSFC-SPEC-697D.

(c) The CPD must function as tested, with coincidence and rejection rates agreeing to within 10% of each other.

(d) The LED must function at all command levels, and all bits of the LED command must operate.

(e) All analog HKG values must be read in the proper fashion and correspond to proper states of detector module parameters.

(f) All commands sent to the module must be received and executed properly, with no drop-outs or cross-talk on the command lines. Each bit of each command must function properly and initiate the proper response in the module's housekeeping and telemetry.

In all cases, failures of the module on requirements (a) or (b) were shown to be measurement errors caused by the test conductor. Each module's FWHM resolutions meet or exceed these requirements. All CPDs were shown to function normally in each of the TPS-24 executions. After the installation of the neutral density filters, all module LEDs operated

nominally. Individual anomalies or discrepancies will be discussed at the end of the module section.

Data from iterations of TPS-24 are located in two places. First, each test procedure contained blanks where the test conductor was required to fill in information, calculations, or test results. These completed procedures are stored in the detector module notebooks which are located in the BATSE library. Second, all accumulated spectra were stored to RX-50 compatible floppy disks which are readable on a ND-76 PHA with disk drive. These spectra are not located with the detector module notebooks, but do reside in the BATSE library. Each disk is labeled with the test, date, and module number. These data are available from the editor.

e. Detector Module Vibration Testing

The vibration test of the BATSE detector module was conducted in a similar fashion to the vibration of the BATSE LAD crystal assembly. The testing occurred in MSFC Building 4619 and was executed under the direction of the Test Laboratory. The entire detector module was bolted to the vibration table for the test. Each module was subjected to a sine-sweep and random-mode vibration tests in all three axes. Unlike the LAD, the entire detector module was subjected to the same levels of vibration for the X-, Y-, and Z-axes. The specifications for each of the vibration tests are summarized in Table 3.31.

3.31. BATSE Detector Module Vibration Test Specifications

Sine Evaluation	Random Mode
5 Hz to 2000 Hz at 0.25 g peak	20 Hz at 0.000047 g^2/Hz
2000 Hz to 5 Hz at 0.25 g peak	120 Hz to 600 Hz at 0.01 g^2/Hz
	2000 Hz at 0.00025 g^2/Hz
Sweep Rate = 1 octave/minute	Composite = 2.8 gm
	Test time = 60 seconds

Detector Module Aliveness Test Between Axes -- TPS-58. Between axes of the vibration test, the detector module was functionally tested using BATSE-ES-62-TPS-58. This operation is an aliveness test and is an abbreviated version of TPS-24 discussed in the previous section. TPS-58 uses the same GSE as TPS-24 and was executed twice per module while the module was bolted to the shaker-table.

The test flow of TPS-58 was similar to that of the detector module functional test. After powering the module, all SD electronic signals were checked in an identical fashion to the previous test. Measurements of the four SFAST signals were made, and the SD-MQT signal was examined for changes in minimum duration and/or amplitude. Spectra from the SD were accumulated at 0.4X and 4X gains. The SD programmable LLD was tested and mapped at command values of 8, 16, 32, and 64. A light-leak test was done on the SD.

Large area detector tests consisted of a full checkout of the LAD FAST signals and the LAD-MQT pulse, as was done in TPS-24. A light-leak test and LLD mapping check were done on the LAD as well. Operation of the LED was verified at command levels of 1, 8, and 12. The CPD was tested in the same fashion as in TPS-24. Heater resistances and the final 17 housekeeping values were tested to complete the procedure. All results from TPS-58 were compared to TPS-24 results for consistency.

Resolution measurements were not made during this test, and checking of each bit of each command was not executed. Verification of the +HV housekeeping was done throughout the procedure, as the supplies were checked for proper voltages and currents after power-up. The purpose of this test was to verify that the detector module had completed the vibration in one axis without major effects to the health and behavior of the hardware. After completion of TPS-58, the module was disconnected from the GSE, and the next axis of vibration was excuted. All completed procedures and spectra generated are stored in the BATSE library, in identical fashion to those from TPS-24. No degradation in the detector module performance due to the vibration tests was found in any execution of TPS-58.

f. Post-Vibration Alignment and Performance Tests — TPS-28, TPS-24.

Upon completion of the vibration testing in MSFC Building 4619, the detector module was moved back to Building 4705 for tests to determine the effect, if any, of the preceding environmental testing. Both a detector module alignment (TPS-28) and performance (TPS-24) test were executed on the module. Both tests were carbon-copies of the tests done previously on the module.

The results from TPS-28 indicated that no major changes in LAD orientation were detectable following vibration in three axes. All measurements were consistent with previous data obtained subsequent to module fabrication. In addition, TPS-28 provided an opportunity to directly observe the LAD crystal and assembly. The LAD was examined for any debonding or cracking which may have occurred during vibration. Especially close attention was paid to those LADs which were cracked during the LAD thermal stress test. No visible indication of cracking, debonding, or structural deficiencies from the module vibration were found with respect to the LAD crystal assembly. This result further re-enforced the idea that LAD crystals could maintain their structural integrity after initially suffering cracks during thermal cycling.

The results from TPS-24 were equally important. The test executed on the module was identical in every way to the test done before vibration. The same procedure, GSE, and personnel were used in the testing after vibration. Results from this second test were consistent with those from the first run. No sign of degradation in module performance was apparent from the vibration. Resolution measurements from the SD and LSD, as well as CPD coincidence and rejection rates, are provided in Tables 3.32, 3.33, and 3.34.

Table 3.32. SD FWHM Resolution % from TPS-24 After Vibration

	FWHM Resolution % (energy in keV)							Peak-to-Valley
Detector Module	88	511	662	1275	1173	1332	2614	Ratio
P-F	12.1	8.0	6.7	5.2	5.5	5.2	4.3	17.4
B0	23.5	7.9	7.0	5.6	5.6	5.4	3.9	14.3
B1	---	7.6	6.9	5.7	6.3	5.8	3.5	7.5
B2	25.7	8.3	7.3	5.9	6.3	5.8	5.1	7.7
B3	17.1	7.4	6.8	5.2	7.0	6.0	4.2	7.5
B4	----	8.9	7.5	6.4	6.8	7.4	3.5	---
B5				--- Missing ---				
B6	25.4	7.9	7.3	5.9	6.4	5.7	4.0	10.0
B7	19.1	8.9	7.8	6.0	6.6	6.1	4.4	7.7

Table 3.33. LAD FWHM Resolution % from TPS-24 After Vibration

	FWHM Resolution % (energy in keV)		
Detector Module	88	511	1275
P-F	31.8	17.1	17.1
B0	30.0	22.7	20.4
B1	----	17.4	15.9
B2	27.4	16.7	14.5
B3	29.6	18.3	16.3
B4	29.4	19.2	17.1
B5		---Missing ---	
B6	31.6	23.9	22.4
B7	29.4	20.1	19.5

Table 3.34. CPD Rejection and Coincidence Rates from TPS-24 After Vibration

Detector Module	CPD Rejection Rate (cps)	Coincidence Rate (cps)
P-F	30.4	27.4
B0	26.0	24.7
B1	25.3	28.2
B2	26.1	23.8
B3	25.6	33.8
B4	26.7	28.8
B5	-- Missing --	
B6	29.1	24.8
B7	27.5	23.4

Several items regarding the data displayed above are worth mentioning. First, the test procedure for detector module B5 is missing from the data archive. Therefore, no measurement results are included here. The spectra, however, are available from the BATSE library if required. Second, several items in the test procedures were not filled in by the test conductors. These entries have also been left open in the tables above. Furthermore, the same caveat concerning the lowest energy measurements which was mentioned regarding other TPS-24 results applies here as well. The reader is encouraged to use TPS-59 results because of the better measurement conditions.

Despite the measurement problems at low energies, the results do indicate that the performance of the detector module was not degraded by the vibration testing. SD and LAD resolutions show no major changes from pre- to post-vibration. The CPD table shows good agreement with the expected muon rate and compatible rejection and coincidence rates.

At this point, the test flow for the protoflight module deviates from that of the other modules. Following the post-vibration tests, the Protoflight was moved to MSFC Building 4476 for thermal balance and thermal vacuum testing. All other modules, upon completion of the post-vibration tests, were moved to the Angular Response Test Facility, or tested in integrated fashion with the CEU prior to further module testing. The details of the protoflight thermal tests will be discussed in the following section.

g. Protoflight Thermal Balance and Thermal Vacuum Testing

(1) Test Configuration and Overview

The thermal balance and thermal vacuum test on the protoflight module began on March 2, 1988. The detector module was fitted with several test-only heaters and moved to chamber #7 in MSFC Building 4476. A flight thermal insulation blanket was installed over the detector module to simulate conditions on the spacecraft. A full set of electrical GSE was connected through the chamber wall to the module using a new and longer set of cables than for all previous tests. These longer cables proved to be important later on in the test. The detector module heaters were activated and monitored through a heater break-out box and the J5/6 test set. The data from the heaters were collected on the Test Laboratory's SCATS system. Finally, an isotope holder and drive system was installed in the chamber, and controlled through a power supply and switch mounted outside. Figure 3.19 details the configuration for the detector module test.

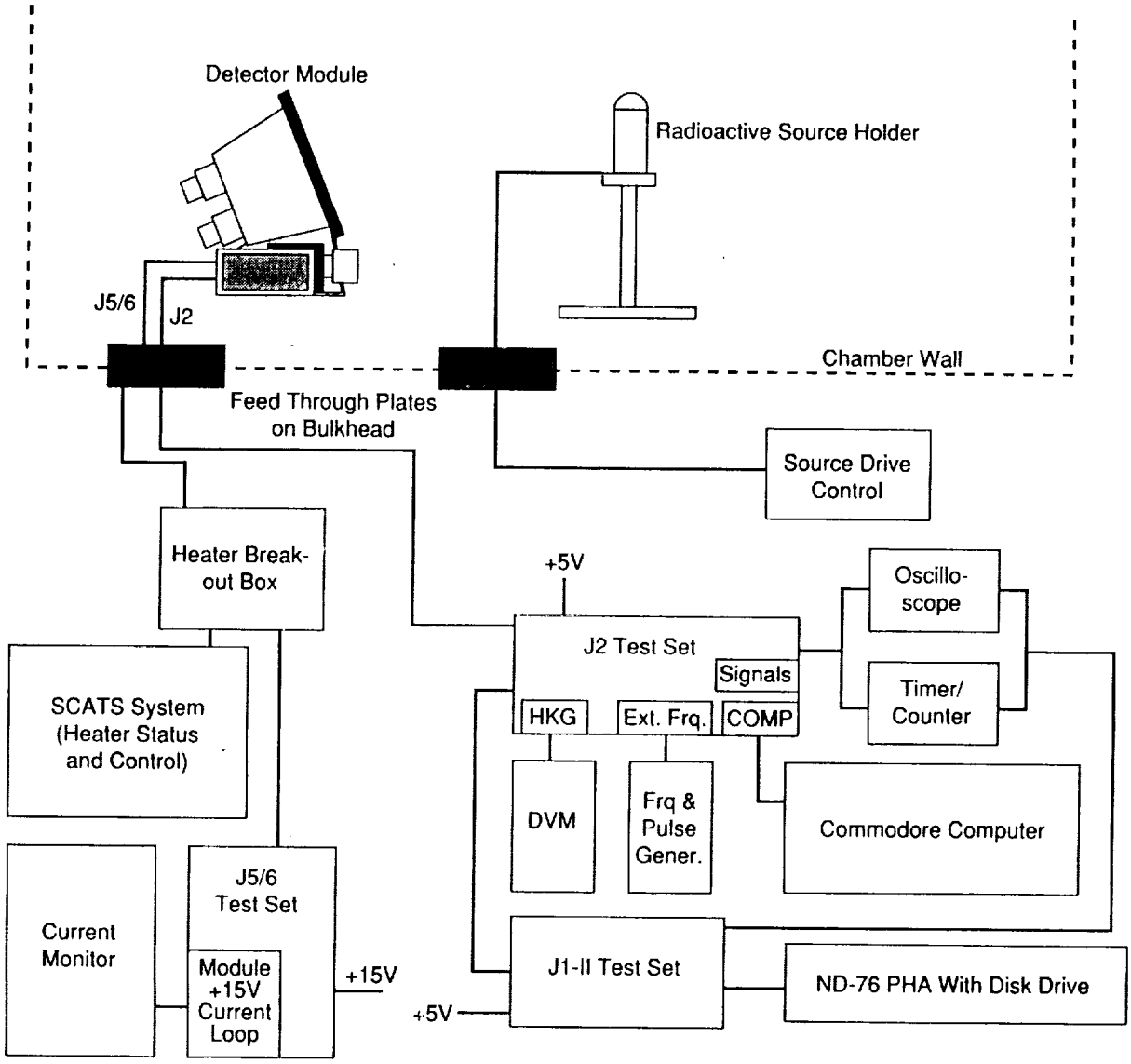

Figure 3.19. Detector Module Thermal Vacuum Chamber Configuration.

The use of radioactive sources was required for the test, and the chamber wall was too thick to efficiently illuminate the detector module without the use of extremely active samples. To overcome this problem, a special source holder was developed which was placed inside the chamber. The holder consisted of a deep aluminum cup, with an outer diameter of 9.53 cm and a height of 22.23 cm. The aluminum wall was 0.635 cm thick, which allows gamma rays of moderate energy to escape easily. At one end of the housing, the aluminum cup was flanged outward, where six holes allowed for the fastening of the cup to an aluminum base-plate. The interface was sealed with a small O-ring.

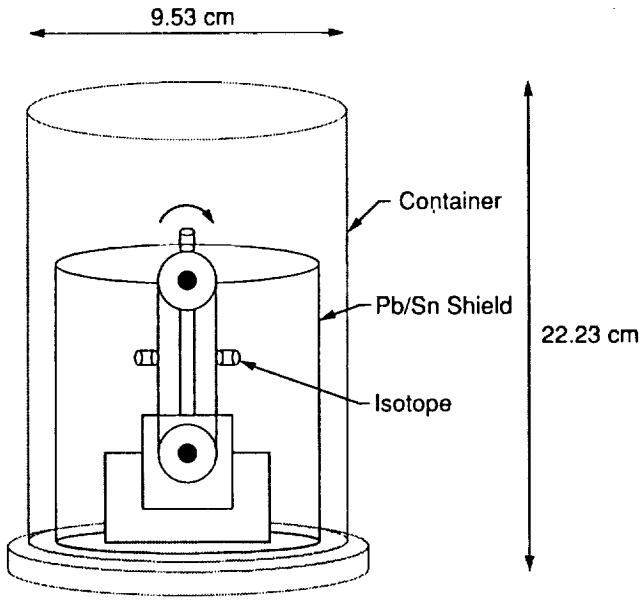

Figure 3.20. Thermal Vacuum Chamber Source Holder and Manipulator.

Interior to the holder, a small dc motor was connected to a rubber conveyor belt. This belt was oriented in the vertical direction and wound around a small pulley at the top of the holder. Three radioactive isotopes, Cs 137, Co 60, and Cd 109, were glued to the belt, each with a 90° phase-separation between them. The fourth location was empty, allowing for all sources to be shielded. This entire internal assembly was surrounded by a cylinder of lead and tin, except for near the top pulley. The dc motor was controlled by a power supply outside the chamber. To expose a source, the test conductor powered the motor until the desired isotope was at the top of the upper pulley, unshielded by the lead and tin wrapping. Each location was identified by a resistance-encoded shaft which indicated the position of the source through a unique resistance measurement. In this fashion, the test conductor could fully control the exposure of isotopes to the detector module without seeing or handling any radioactive material outside the chamber. Unfortunately the mechanism did not operate as well as hoped. Problems occurred at cold temperatures with the motor, and isotopes came unglued from the conveyer belt. The test was interrupted on two occasions to fix the holder.

(2) Pumpdown and Thermal Balance Testing

The thermal balance portion of the test was executed first, commencing on March 2, 1988. After the module was placed inside the chamber, an iteration of TPS-58 was executed to insure that the module was healthy following the transportation from Building 4705. With this test completed, the detector module was left powered on, and the chamber was pumped down. TPS-56 was then initiated to monitor the +HV and count rates as the pressure went through the corona region. Leaving the +HV on during the pumpdown and through the "corona-region" was done to verify the integrity of the BATSE +HV system, which consists of potted components,

+HV cable, and Reynolds-sealed connectors. Rates were monitored by using a frequency counter and an oscilloscope. These rates were continually checked throughout the evacuation of the chamber.

Section III.A.3.c. of this document references the CPD rapid pumpdown test (TPS-67) and the sintered bronze vent which was added to the CPD following evidence of insufficient venting. The evidence cited there is two-fold, namely the damage to the CPD which occurred in the system thermal vacuum test, and the loss of count rate due to the separation of the PMTs from the DC-93-500 optical coupling. This behavior should have been apparent in the protoflight module at the time of pumpdown, since the CPD on the module is no different than those on other detector modules. Review of the test log from the protoflight test indicates that this behavior possibly was present, but attributed to another cause. A short time after the pumpdown began, a short-circuit and loss of a transformer occurred in the SCATS GSE rack. However, the event that caused a large noise and a small amount of smoke from the GSE rack was not serious. Prior to this time, the rates on the detector module were being monitored every hour. Since the SCATSs ystem was connected to the detector module through the GSE boxes, all +HV on the module was powered off after the incident as a precaution. When the +HV was re-powered, the rates on the CPD were noticeably lower than before. The CPD was powered off. It was thought that the incident with the SCATS system had somehow affected the +HV supply or the PMTs on the CPD. Because the incident happened late in the evening, the CPD remained off for approximately 14 hours until the BATSE lead engineer could view the problem. Other rates were nominal; therefore, the +HV to the other supplies remained on. When the CPD was powered again, all rates were nominal. The distinct possibility exists that the drop in rates was unrelated to the SCATS problem, except the unfortunate coincidence of timing, and that instead it was due to a separation of the PMTs from the optical coupling as was seen later in the full-system, thermal vacuum test.

The thermal balance portion of the test was under the control of the BATSE thermal engineer, Mr. Dave Clark (ED63). The purpose was to determine the thermal behavior of the detector module and to verify the thermal design. Configuration of the detector module was altered depending on the needs of the thermal engineers to correctly assess the module's behavior. A minimum, maximum, and nominal power configuration were used. These power states differed in the level to which the +HV was commanded. The total power dissipation of the +HV is rather small, however. Nominal settings of the +HV only attain a dissipation of approximately 1 W in the module. Under normal operations, each module draws about 0.31 A at +15 V for a power dissipation of about 4.5 W. Through the thermal balance test, it was shown that the detector module has the capability to easily radiate this energy away through the mirrored radiator, and that the thermal blankets function well in maintaining a safe operating temperature range for the detectors and a low temperature rate of change.

(3) Thermal Vacuum Testing of the Protoflight Module

The thermal vacuum portion of the test immediately followed the thermal balance testing. The test consisted of six complete cycles in temperature, ranging from +40 °C to -10 °C.

At all times, the rate of change of temperature was kept below 5 °C/hr to protect the NaI crystals on the detector from further damage. The health of the detector module was assessed at many points throughout the test with the use of TPS-57, the performance test in thermal vacuum. The test is very similar to TPS-24, but proceeds in a slightly different order. The first measurements after power-up were a full check of all housekeeping values and temperature measurements. After proper temperature readings were verified, a check of each bit of the five +HV supplies was executed, and their proper housekeeping values were checked. Count rates were computed for FAST1, SFAST2, and PLASTIC, and a 30-minute stabilization period was begun. At the end of ths stabilization period, rates were compared to those computed at the beginning for consistency. If stable, a full check of the SD electronics (identical to that of TPS-24) was begun. This included checks of the SMQT minimum duration, and each bit of the programmable LLD was mapped at the three SD gains. Resolution measurements were taken (when the source holder was functioning) in the same fashion as in TPS-24. Large area detector tests and charged particle detector tests were identical to the tests done in TPS-24. This test concluded with another check of the 32 housekeeping parameters and temperature measurements. The entire test duration was approximately 4 hours. The temperature of the module was maintained at a constant value throughout TPS-57.

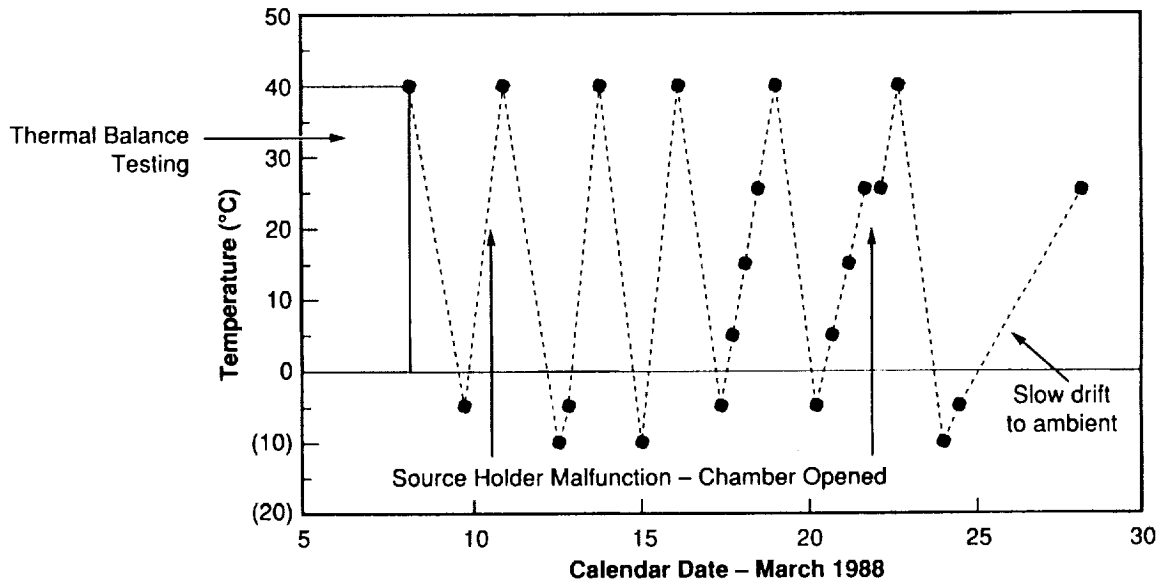

Figure 3.21. Temperature Profile of the BATSE Protoflight Thermal Vacuum Test.

The module's performance in thermal vacuum was tested a total of 22 times while the module was inside the chamber. Two of these tests were done at ambient temperature and pressure to verify the module's health before and after depressurization of the chamber. Table 3.35 details the times, dates, and temperatures at which this test was performed.

Table 3.35. Iterations of TPS-57 During Protoflight Thermal Vacuum Testing.

Iteration	Thermal Cycle	Chamber Temp.	Conditions	Date
1	Pre-Test	Ambient	Ambient	3-2-88
2	1	40 °C	Hot Case	3-8-88
3	1	-5 °C	Cold Start	3-9-88
4	2	40 °C	Hot Case	3-11-88
5	2	-10 °C	Cold Case	3- 2-88
6	2	-5 °C	Cold Case	3-12-88
7	3	40 °C	Hot Case	3-13-88
8	3	-10 °C	Cold Case	3-15-88
9	4	40 °C	Hot Case	3-16-88
10	4	-5 °C	Cold Case	3-17-88
11	4	5 °C	Cold Case	3-17-88
12	4	15 °C	Mid-Range	3-18-88
13	4	25 °C	Mid-Range	3-18-88
14	5	40 °C	Hot Case	3-19-88
15	5	-5 °C	Cold Case	3-20-88
16	5	5 °C	Cold Case	3-20-88
17	5	15 °C	Mid-Range	3-21-88
18	5	25 °C	Mid-Range	3-21-88
19	6	40 °C	Hot Case	3-22-88
20	6	-10 °C	Cold Case	3-24-88
21	6	-5 °C	Cold Case	3-24-88
22	6	Ambient	Ambient	3-28-88

During the test, the radioactive source holder and drive assembly did not operate as planned. The chamber was repressurized and the test interrupted on March 10 and March 22, 1988, for repair of the source holder. Consequently, the data from TPS-57 are not consistent from test to test in the number of isotopes used and spectra accumulated. At different times, one or more of the three isotopes may not have been available to illuminate the detector. After the detector module reached its final cold-case state, it was allowed to warm up without the impetus of additional heaters or input energy. This was done at the request of the thermal engineers who used this behavior in constructing the BATSE thermal model. The slow ramp rate to ambient is a direct result of allowing the module to simply "drift" upward to the ambient temperature. The final iteration of TPS-57 comes approximately 4 days after the previous test.

(a) Results of Thermal Vacuum Testing

The protoflight thermal vacuum test was the first opportunity for the BATSE team to examine the operation of the detector module over a wide range of temperatures and under vacuum conditions. TPS-57 was used to monitor the health of the module, identify all hard failures which may occur during the test, and obtain a broad characterization of the module performance over the range of temperatures. This test was primarily an engineering test, and consequently the results are of relatively little scientific interest. These results are important, however, and are outlined in Table 3.36.

Table 3.36. BATSE Protoflight Thermal Vacuum Test Result Summary

- Detector module thermal control system design was verified
- Detector module thermal model was constructed
- +HV system basic design was verified in vacuum*
- Detector gains were stable to < 5% over the temperature range
- Detector resolutions vary by < 2% (size of error in measurement) over the temperature range
- Temperature sensors operate properly over the temperature range
- Detector module heaters and thermostats operate properly
- Detector module electronics (MQT, FASTn, LLD) function normally over the temperature range
- LED light output was stable over the temperature range
- Detector module hot and cold start capabilities were verified

* Subsequent minor design changes were made after the system thermal vacuum test.

The record copies of the 22 executions of TPS-57 are on file in the BATSE library with other data from the protoflight module. These documents contain all housekeeping, resolution and count rate measurements made during the test at the various temperatures. TPS-57 generated a large amount of detector spectra, and these are also available for inspection in the BATSE library. The spectra are contained on 5.25" floppy disks, in RX-50 format. They are directly readable onto an ND-76 PHA with the appropriate disk drive.

(b) BATSE Large Area Detector "Notch" Anomaly

The first paragraph of section III.B.1.g(1) mentions the use of long cables to connect the detector module to the GSE. Extensions were required for the data and power connections to the module because of the isolation of the detector module inside the vacuum chamber. The cables used were of approximately the same length as those cables used on the GRO to connect the eight modules to the CEU. With the longer cables, the detector module was in more of a flight-like configuration than with the shorter test cables used in all previous testing. The use of these longer cables uncovered a serious anomaly in the LAD spectra which was not detectable using the shorter connections.

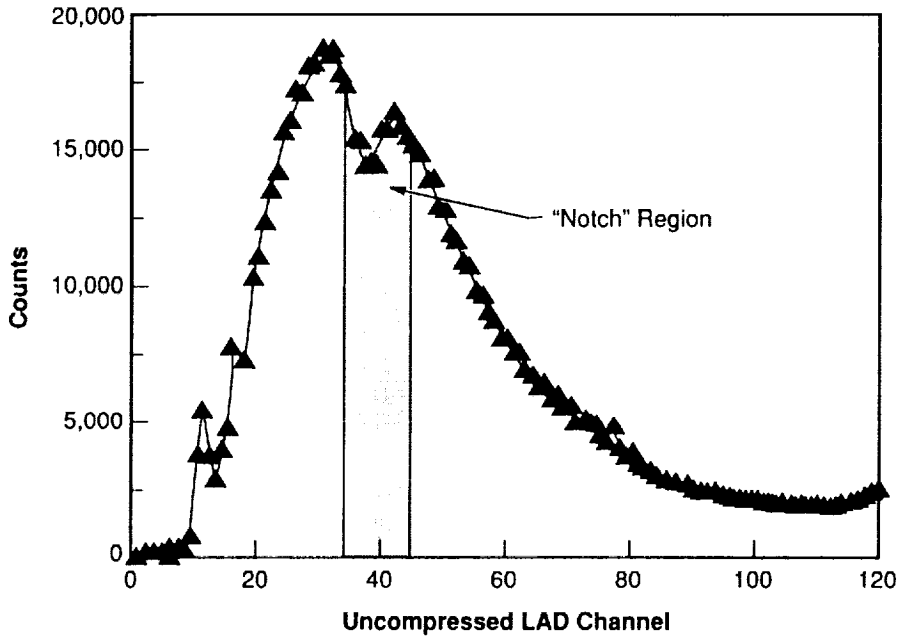

Figure 3.22. BATSE Large Area Detector Spectrum with "Notch" Feature.

Figure 3.22 shows a LAD background spectrum taken from the 12th execution of TPS-57 at a temperature of 15 °C. The spectrum shows a distinct "notch" feature at approximately channel 37. This feature was not present in any detector module spectra prior to the introduction of the long cables in the thermal vacuum test. Other detector modules, when connected with long cables (for example in the angular response test), show identical features in the LAD spectra. The feature is best described as a differential non-linearity that was limited to the 100-200 keV (uncompressed channel 25-45) region. Both the depth and the location of the "notch" were dependent on temperature and the setting of the programmable LLD. As the temperature was increased, the "notch" location moved higher in channel space, but became less pronounced. At temperatures near 40 °C, the feature was not always present. After extensive work by Mr. Robert W. Austin, BATSE lead engineer from the Space Science Laboratory of MSFC, the problem was traced to coupling of the digital outputs of the FAST discriminators into the analog circuit of the MQT, which digitizes the signals from the LAD PMTs. A small amount of charge was coupled into the analog path for signals meeting the threshold of the FAST2 discriminator on the LAD. This produced a "depressed region" in the charge-to-time conversion (spectrum) of the LAD because the additional charge coupled into the analog path caused these events to be digitized into a higher channel number than was appropriate in this region (and

above). This problem was never seen in the BATSE SD spectra, with or without the long cable connections.

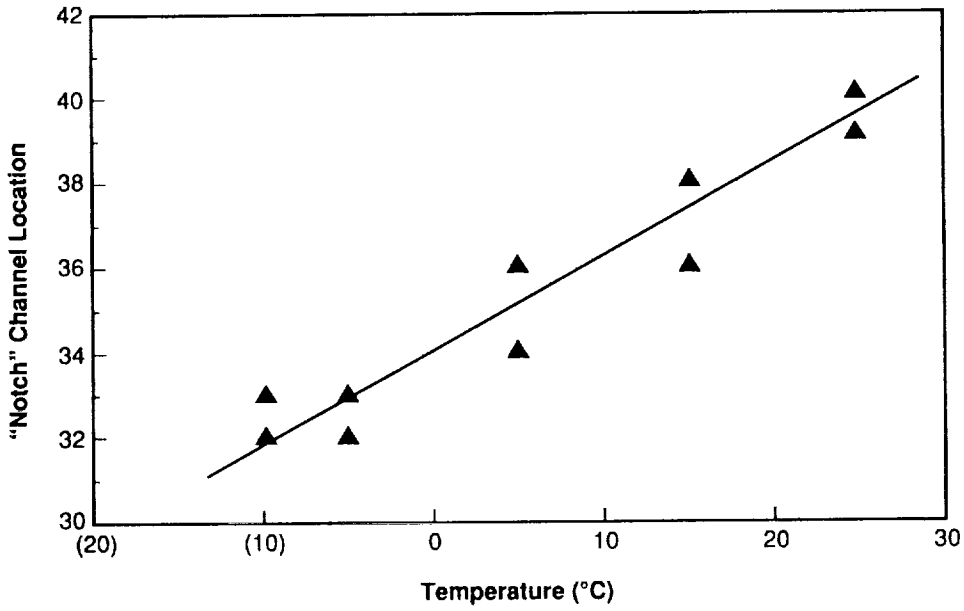

Figure 3.23. Energy Channel-Temperature Dependence of the "Notch" Feature.

The solution to the "notch" problem was to provide additional isolation between the signal and ground paths associated with both of the circuits involved. This isolation was accomplished by re-routing the analog signal grounds within the DEU box, increasing the signal isolation resistor (R9) on the 42A30970 (LAD) board from 200 Ohms to 2.49 kOhms, and removing the coupling caps (C14 - C17) at the FAST discriminators. Corresponding changes were made to the 42A30968 (SPEC) board. The resistor changed on this board is referenced as R9, and the associated SFAST coupling caps are designated C10 - C13. The reader is encouraged to examine the drawings of these boards if further information on the re-work is needed. DEUs from each of the nine modules were modified in this manner to correct the problem. Because the work involved changes to both the LAD and SD data circuits, extensive amounts of re-testing were required. The details and results of these tests are outlined in a subsequent section.

h. DEU Analog Board Adjustments for LAD and SD—TPS-60

In order to effect the modifications described in the previous section, it was necessary to remove the covers and boards from each of the nine DEUs. Additionally, previous tests had shown that not all module spectra exhibited the same pedestal channel, and that the four FAST discriminators from the LAD and SD were not corresponding to the same energy channel in all detector modules. It is important to have each of the FAST discriminators from the various modules starting and ending on the same energy boundaries. If different detectors have different FAST thresholds, the burst data, which are summed from different detectors in many cases, will be convoluted with counts from different energies being added together in the same energy bin. This condition would cause a large amount of difficulty in the analysis of data. The BATSE team decided that while the DEUs were open, the opportunity to fine-tune all adjustments was conveniently available. Furthermore, this test would provide a chance to measure the energy thresholds of the SD's FAST3 and FAST4 discriminators, which lie above the energy range of the SMQT. In light of these considerations, TPS-60, the BATSE DEU/DM SD, and LAD analog board adjustment procedure was executed.

The GSE for the procedure is identical to that of TPS-24 (see Figure 3.17). The ND-76 PHA is gated with the output from the J2-II box, which is dependent on the module signal selected. The LAD was adjusted first. Adjustments were made to potentiometers RP2 and RP3 on the 42A30970-1 (LAD MQT) board. RP2 is the potentiometer which sets the MQT pedestal. RP3 adjusts the gain of the MQT. Gain adjustments of the MQT were required to set the upper energy threshold of FAST3, because the threshold of the discriminator is not adjustable. Only the lower level of FAST1 is programmable, while the trigger levels of the others are fixed. FAST3 is the higher of the two burst channels, and is desired to have an upper threshold of 300 keV. At a dispersion of 5 keV/channel with a pedestal of 6 channels, this boundary lies at MQT channel 66. Thus the adjustment was made to the MQT gain so that MQT channel 66 corresponded to the upper edge of the fixed FAST3 discriminator. Changing the MQT gain invalidates the previous +HV values used to set the energy to channel relation. The adjustments of RP2 and RP3 are not independent, so that adjusting one affects the settings of the other. Consequently, these adjustments were iterated until both criteria were met. At the completion of this section of TPS-60, the LAD MQT pedestal was located at channel 6, and the upper edge of the FAST3 discriminator was located at MQT channel 66. Two 300-second integrations were obtained with the ND-76 gated on FASTID and on FAST3 to document the location of these thresholds.

Adjustments of the SD potentiometers proceeded in a different fashion. Because only SFAST2 lies within the range of the SMQT, only potentiometer RP3 on the SMQT board was adjusted. The setting of this potentiometer locates the pedestal of the SMQT, and was adjusted to place the pedestal in channel 40. The rationale for the pedestal at this location was discussed in section III.B.1.d(2).

Following adjustment of the pedestal, SFAST3 and SFAST4 were each connected to a timer/counter and a 1000-second integration was performed. An average rate for each of the two

discriminators was computed. This rate was compared to a 57,600-second integration generated with a flight-like SD in a different electrical configuration. The flight-like SD was powered through an adjustable +HV supply, and its gain was set low enough to bring 100-MeV events onto the scale of the PHA. An energy calibration and integral rate was computed for every channel in the spectrum obtained through the flight-like SD. To determine the energy threshold of the SFAST3 and SFAST4 discriminators, the rates obtained in the 1000-second integration were compared to this reference spectrum. The channel in the reference spectrum which possessed the same integral rate as the SFAST integration was deemed to be the location of the SFAST threshold. The energy of the SFAST threshold is then determined by the energy-channel calibration of the reference spectrum. Obviously the answer obtained is dependent on the +HV value to which the flight SD is commanded. All of the TPS-60 measurements were done with the SDs commanded to the 1X gain settings obtained in TPS-24. The results of the SFAST energy measurements for the eight flight detector modules are contained in Table 3.37.

Table 3.37. SFAST3 and SFAST4 Threshold Energies Measured at 1X Gain in TPS-60

	Energy Threshold (MeV)	
Detector Module	SFAST3	SFAST4
B0	28.2	45.0
B1	26.6	46.9
B2	29.4	45.9
B3	28.8	47.2
B4	26.3	42.5
B5	29.1	39.3
B6	29.1	48.5
B7	29.4	48.2

The data presented in the table above were taken after the pedestal adjustment was made to RP3 on the SMQT board. Adjustment of the pedestal effectively changes the gain of the detector slightly. The +HV must be adjusted to compensate for the MQT gain change if the standard dispersion of 4.0 keV/channel is to be maintained. These measurements were accumulated with the old +HV values, but a slightly changed MQT gain. In all cases, however, the adjustment to align the pedestal into channel 40 was minimal. Consequently, the effect on the measured threshold of the SFAST discriminator is small. Measurements of these thresholds at other gain settings were taken at TRW prior to spacecraft integration, and after installation on the GRO. These results will be presented in subsequent sections of this document.

i. Detector Module Performance Test After DEU Modification—TPS-59

After modifications were made to each DEU, a full-scale detector module performance test was required. The BATSE team determined that the modifications made to the DEU did not invalidate the vibration tests performed on each module; therefore, these were not repeated. The performance test flows much in the same vain as TPS-24. The configuration of the GSE required

for this test is identical to that of the previous performance test. Because of the long period of time needed to characterize, isolate, identify, and fix the problem of the "notch" in the LAD spectra, the iterations of TPS-59 were not complete until July 1988. Table 3.38 indicates the time of execution of TPS-59 for each of the eight flight detector modules.

Table 3.38. Dates of TPS-59 Iterations Following DEU Modifications

Detector Module	Date of First TPS-59
B0	July 1, 1988
B1	June 17, 1988
B2	June 27, 1988
B3	June 29, 1988
B4	June 29, 1988
B5	June 24, 1988
B6	July 6, 1988
B7	June 30, 1988

(1) Initializations

As with TPS-24, this test begins with a determination of all +HV values required to meet particular pre-determined gain settings. Because the pedestal and (in the case of the LAD) the gain of the MQT were adjusted, new voltage values were required to obtain the desired dispersions in the detectors. Voltage values for the LAD were determined at a dispersion of 5 keV/channel, and for the SD at 1 keV/channel, 4 keV/channel, and 10 keV/channel. These gains are the same as those used in TPS-24. Table 3.39 contains the revised voltage values for these gain settings.

Table 3.39. Revised +HV Values for Standard Gains - TPS-59

	Detector Module Number								
HV Supply	P-F	B0	B1	B2	B3	B4	B5	B6	B7
PMT-A	1665	1480	1614	1508	1559	1610	1646	1453	1654
PMT-B	1650	1480	1591	1476	1587	1642	1602	1350	1626
PMT-C	1646	1559	1610	1535	1571	1665	1638	1390	1677
CPD	1406	1429	1335	1245	1276	1240	1221	1304	1209
SD-1X	1181	1256	1303	1248	1169	1220	1138	1232	1319
SD-4X	1449	1543	1606	1531	1429	1496	1386	1512	1622
SD-0.4X	1051	1106	1150	1106	1035	1083	1012	1094	1165

Table 3.40. Changes in +HV Values from TPS-24 to TPS-59

	Detector Module Number								
HV Supply	P-F	B0	B1	B2	B3	B4	B5	B6	B7
PMT-A	127	78	110	67	79	114	102	80	103
PMT-B	124	71	103	63	79	103	82	70	91
PMT-C	122	150	106	66	87	130	79	82	102
CPD	These values were not adjusted for TPS-59								
SD-1X	21	-16	0	0	8	-12	8	7	8
SD-4X	180	-16	-4	-4	8	-4	0	1	-4
SD-0.4X	48	-28	4	8	11	66	0	-1	15

Table 3.40 displays the changes in +HV values from TPS-24 to TPS-59. Inspection of the table shows that the LAD +HV values were changed significantly more than the SD values. The contributors to the need for +HV adjustment are the re-work to fix the notch problem, adjustment of the LAD pedestal, and changing the MQT gain to align FAST3 and MQT channel 66. The change in the MQT gain was the largest perturbation to the previous gain setting. The SD, which had no change of the MQT gain, required little +HV adjustment (with the exception of the P-F module), indicating that the other two operations affect the gain much less severely. The protoflight module was the most maladjusted of all the modules. The changes in LAD +HV values for each module are all of the same "family." Selection of the PMTs for flight on each module was heavily dependent on matching of PMT behavioral characteristics. The closeness of the required adjustment for each PMT on a given module is an indication that the PMTs were operating in the same manner, with no tube displaying divergent behavior from the others on that particular module.

(2) Spectroscopy Detector Measurements

Spectroscopy detector measurements began with a check of the stabilization of the SD PMT, similar to what was done in TPS-24. Amplitude and duration measurements of the four SFAST discriminator signals were made, in addition to a check of the bi-polar nature of these signals. Typical amplitudes and durations were measured to be 4.25 V, and 0.42 μs, respectively. A measurement of the SMQT signal was also executed. Unlike TPS-24, however, the measurement consisted simply of a check of the dual-polarity of the signal and examination by inspection of the general form of the signal. Because this test was executed immediately after TPS-60 (in some cases on the same day), which set the pedestal of the SMQT signal, the BATSE team felt no need to measure the pedestal again.

After a check of the SD PMT stability, which was identical to that of TPS-24, the LLD was tested at 1X and 4X gains. Three isotopes, Cd 109, Cs 137, and Co 57, were placed into the source holder to provide energy references across the region of the SD spectrum.

Spectra of 60-second duration were accumulated at nine different settings of the LLD with the detector at 1X, and then 4X gain. The 0.4X gain setting was not used in the check of the programmable LLD.

(a) 4X Gain Resolution Measurements

Following the check of the programmable LLD, the SD was commanded into the 4X gain mode to provide a dispersion of 1 keV/channel in the uncompressed SHER spectrum. The desired voltage was verified, and a 300-second background accumulation was obtained. This background spectrum was stored to floppy disk and used in subtraction from subsequent source-spectra at this gain. Isotopes of Co 57 and Cs 137 were used in these accumulations to provide measured resolutions at 14 keV, 32 keV, and 662 keV while the detector was commanded to the 4X gain setting. These measurements were the first low-energy determination of the photopeak resolution since the initial SD TPS-16 performance tests. Unlike previous resolution measurements where the dispersion was calculated using an oscilloscope measurement of the pedestal, calculations here used two photopeaks of known energies in determining the number of keV per channel. This affords a more accurate determination of the resolution by eliminating the subjective observation of the pedestal channel in an oscilloscope. Determination of the SD resolution in the energy region exploited by the 4X gain is an important part of predicting BATSE science capabilities, especially in light of the discovery of cyclotron absorption lines in some gamma ray burst spectra near 20 and 40 keV. Results from the 4X gain resolution measurements are provided in Table 3.41.

Table 3.41. Spectroscopy Detector FWHM Resolution % at 4X Gain -- TPS-59

	Energy Resolution % (FWHM) (in keV)		
Detector Module	14	32	662
B0	25.7	21.4	6.7
B1	25.8	23.3	7.1
B2	35.7	24.2	7.7
B3	49.8	21.9	7.2
B4	40.7	27.4	7.3
B5	40.2	25.5	7.3
B6	38.6	25.9	7.5
B7	35.8	26.6	7.3

The results presented in Table 3.41 compare favorably with the results obtained in TPS-24 before and after the environmental tests. Measurements taken at 14 keV were difficult to obtain in several cases because of the photopeak's proximity to the lower-level discriminator cutoff. Nonlinearity in the digitization of PMT signals near the threshold of the LLD may distort the normal Gaussian profile of the photopeak, leading to inaccuracies in the measured resolution at 14 keV.

(b) 0.4X Gain Resolution Measurements

The spectroscopy detector was commanded to the 0.4X gain setting following the completion of the previous resolution measurements at high dispersion. The voltage used at the 0.4X gain setting provides a dispersion of 10 keV/channel in the uncompressed region of the SHER spectrum. Isotopes of Na 22 and Cs 137 were used to obtain resolution measurements at energies of 511 and 662 keV. Each accumulation lasted 300 seconds, and a background spectrum was also obtained. These spectra were stored onto floppy disk. Results from these measurements are summarized in Table 3.42.

Table 3.42. Spectroscopy Detector FWHM Resolution % at 0.4X Gain - TPS-59

	Resolution % (FWHM) (energy in keV)	
Detector Module	511	662
B0	7.9	7.5
B1	8.7	7.9
B2	8.8	8.6
B3	8.5	8.1
B4	9.8	8.2
B5	8.3	7.3
B6	9.6	8.3
B7	9.5	7.3

The measurement accuracy of the results presented in Table 3.42 is not as high as the accuracy obtained at higher dispersion. Because of the compressed gain, the photopeaks are contained almost entirely within a region of 5 or 6 channels. Inside this region, it is difficult to determine exactly where the half-maximum point of the photopeak is located. An error as small as one-half of a channel in the location of the FWHM creates a 20%-order error in the width used to determine the resolution. The reader is encouraged to consult measurements made at nominal or 4X gain for more accurate results.

(c) 1X Gain Resolution Measurements

The most comprehensive set of photopeak resolution measurements taken at the module level on the spectroscopy detector were acquired during TPS-59. The 1X gain measurements were executed with isotopes of Cd 109, Na 22, Cs 137, and Co 60. These sources provided photopeaks ranging from 88 keV to 1.332 MeV. All dispersions were calculated using two photopeaks of known energy, adding to the reliability of the calculation. In addition to resolution measurements, a photopeak separation measurement was done with the Co 60 isotope. Each of the integrations taken were 300 seconds in duration, and the sources were placed at the standard 50.8-cm distance from the detector. Background accumulations were taken, stored to disk, and used in subtraction from isotope spectra. The results from the first iteration of TPS-59

following the detector electronics re-work are summarized in Table 3.43.

Table 3.43. Spectroscopy Detector 1X FWHM Resolution % from TPS-59

	FWHM Resolution % at Energies Shown (keV)					
Detector Module	88	511	662	1173	1275	1332
B0	11.8	8.0	7.2	5.8	5.3	5.5
B1	13.9	8.2	7.2	6.6	5.7	6.0
B2	12.7	8.3	7.5	6.7	5.7	5.9
B3	15.9	8.5	7.9	7.3	6.5	6.3
B4	15.5	8.4	7.3	6.4	5.8	5.8
B5	14.8	7.9	7.1	6.2	5.8	5.7
B6	17.0	8.3	6.4	6.2	5.5	5.5
B7	14.1	8.5	7.5	6.8	5.9	6.1

The results in Table 3.43 represent the most reliable measurements of SD photopeak resolution taken to that point in the testing program. Each of the tests were executed with the same GSE in a span of 15 days, and with the exception of B6, were done by the same three test conductors. Comparison of these results to those of TPS-16, the initial performance test, shows no detectable degradation in the performance of the SD at 662 keV. The resolutions measured in this iteration of TPS-59 served as the benchmark resolutions for the detector module test program.

(3) Large Area Detector Measurements

(a) LAD Electronics Testing

As was done in TPS-24, the large area detector portion of the test followed the spectroscopy detector measurements. The first portion of this section involved testing of the LLD. Isotopes of Cs 137 and Cd 109 were placed in the source holder to provide energy references to the various LLD settings. Eight settings were checked and a 120-second integration obtained at each. These spectra were stored onto floppy disk. Following the check of the discriminator, LAD signals were tested. The four FAST discriminators were checked for bi-polarity, and the differential properties of the discriminators were verified. The FAST discriminators were then mapped in MQT space through the use of the ND-76. The PHA was fed the MQT signal, but gated with the four discriminators. A spectrum was thus produced only over the energy region of the discriminator used to gate the PHA. The channel boundaries were determined and recorded for each of the FAST signals. Table 3.44 summarizes the results of this measurement.

Table 3.44. Mapping of FAST Discriminator Boundaries into MQT Channel from TPS-59

Detector Module	FAST1	FAST2	FAST3	FAST4
B0	LLD - 15.5	15.5 - 26	25.5 - 66	66 and higher
B1	LLD - 16	16 - 25.5	26 - 64	65 and higher
B2	LLD - 16	16 - 25.75	25.5 - 66	66 and higher
B3	LLD - 16	16.5 - 26	26.5 - 66	67 and higher
B4	LLD - 16.25	16.5 - 25.75	27 - 66	67 and higher
B5	LLD - 16.5	16.5 - 26	26.5 - 67	67.5 and higher
B6	LLD - 15.5	16 - 25	26 - 66	67 and higher
B7	LLD - 17	17.5 - 26.5	28.5 - 66	70 and higher
Typical Energy	25-50 keV	50-100 keV	100-300 keV	> 300 keV

The lower level of FAST1 is determined by the setting of the programmable LLD. The channels listed in Table 3.44 are linear MQT channels and were determined by inspection from the 120-second spectra obtained with the gated PHA. The boundary channel was deemed to be at the location which contained half as many counts as the first channel where the FAST discriminator was fully present. Therefore, for those discriminators which appear in the above table to have "gaps," there is still some continuation of the discriminator beyond the channel shown.

FAST1 was designed to cut-off at linear MQT channel 16, corresponding to an energy of 50 keV. FAST2 and FAST3, the burst trigger channels, were intended to cover the region of 50 - 300 keV, or linear channel 16 - 66. FAST4 would then contain all counts above 300 keV. Table 3.44 indicates that the measured locations of the discriminators are well correlated to the desired locations. Exceptions are detector module B7, where FAST1 was measured to start in channel 17.5 (107.5 keV) and detector module B1, where FAST3 ends in channel 64 (290 keV). These measurements were repeated at TRW prior to spacecraft integration.

The LAD MQT signal was observed by the test conductor, who checked for bi-polarity and verified the shape of the signal was nominal. Having recently completed TPS-60, the BATSE team chose to eliminate measurements of the MQT pulse which were done in the previous test in greater detail.

(b) LAD Resolution Measurements

Measurements of LAD FWHM photopeak resolutions were executed in the next section of TPS-59. Isotopes of Cd 109, Na 22, and Cs 137 were individually placed at the standard 50.8-cm location, and 300-second integrations were obtained. A 300-second background spectrum was subtracted from the source integration, and the resolutions were computed. All dispersions were calculated using known photopeak energies, instead of the previous oscilloscope measurement of the pedestal channel. The results from the initial iteration of TPS-59 are contained in Table 3.45.

Table 3.45. LAD FWHM Photopeak Resolutions from TPS-59

	FWHM Resolution % (energy in keV)			
Detector Module	88	511	662	1275
B0	23.5	17.8	16.9	18.8
B1	26.8	18.5	16.3	14.6
B2	22.5	15.6	15.1	14.9
B3	25.6	18.6	16.7	17.0
B4	30.5	19.8	18.8	20.1
B5	28.9	22.5	21.1	20.4
B6	29.8	22.8	21.5	21.7
B7	26.6	20.6	19.0	22.2

Following the measurements of photopeak resolutions, a 120-second integration was obtained from each of the PMTs on the LAD. With two PMTs powered off, the remaining tube was commanded to its nominal +HV value. A Cs 137 source was placed in the holder, the spectrum was accumulated, and stored onto floppy disk. This process was repeated for the remaining PMTs. The three spectra were compared for balance, resolution, and PMT uniformity. These spectra, like all from TPS-59, are available in the BATSE library for inspection.

(c) Other LAD Measurements

The LAD section of TPS-59 concluded with a mapping of the LED at five different command settings. The LED was driven with an external wave-form generator at a frequency of 1.0 kHz, in an identical manner as was done in TPS-24. For each of the five amplitude settings, a 60-second integration was accumulated and stored to floppy disk. The LEDs were found to perform in a manner consistent with pre-modification results.

(4) Charged Particle Detector Measurements

TPS-59 contained a test of the charged particle detector which was the same as the measurement of TPS-24. A 300-second spectrum was accumulated from the LAD with the CPD on, and in anti-coincidence mode. A second integration of 300 seconds with the CPD off was

subtracted from the first. The difference in the two spectra is a measure of the rate at which the CPD electronics rejects events. A third spectrum of 300-second duration was taken with the LAD gain lowered to bring muons onto the scale of the MQT, and the CPD in coincidence mode. If the CPD and its associated circuitry are functioning properly, the integral rate in this spectrum above 0.6 x the peak muon deposition energy will be approximately the same as the rejection rate obtained from the first two spectra. The magnitude of the rate is dependent on test conditions, such as the amount of mass overhead. Results from this iteration of TPS-59 are presented in Table 3.46.

Table 3.46. CPD Coincidence and Rejection Rates from TPS-59

Detector Module	CPD Rejection Rate	CPD Coincidence Rate
B0	19.9	19.3
B1	19.6	19.5
B2	20.1	20.1
B3	20.0	19.8
B4	20.0	19.7
B5	19.7	19.4
B6	19.8	19.5
B7	20.2	19.5

The data in Table 3.46 indicate that the CPDs operated in an excellent manner during the test. The coincidence rate and rejection rates are in good agreement, and the magnitude of the rate is approximately what one would calculate from muons incident on the detector at a 54.7° angle from the zenith. The CPD testing concluded TPS-59. An extensive measurement of all command bits in the HVPU was not done. A systematic check of all other data from the module was not included in this iteration of TPS-59. However, voltages, currents, and other housekeeping values were verified throughout the test.

j. Detector Module Angular Response Calibration—TPS-19

The BATSE detector module angular response calibration (TPS-19) was the first pure calibration executed on the detector modules. To this point in the program, all testing was primarily of a functional, or engineering nature, designed to verify proper operation or to verify compliance with certain specifications. TPS-19 had no pass-fail criteria, but instead served to collect data for use in the construction of the BATSE detector response matrices. The test was performed on four of the detector modules during the Spring and Summer of 1988. For several of the modules, this was prior to re-work done to remove the notch in the LAD spectrum. Although the notch feature was present in the spectra, the BATSE team was primarily concerned with the relative heights of photopeaks taken from isotopes at different incident angles. The presence of the notch feature does not affect the number of counts in the photopeak of any given isotope, as long as the photopeak is not in the same region of the spectrum as the notch feature.

The test returned data concerning the response of the LAD and SD to different energy gamma rays at a large number of incident angles. The radioactive isotopes used in this test are summarized in Table 3.47.

Table 3.47. Isotopes used in BATSE Angular Response Calibration -- TPS-19

Isotope	Activity (mCi)	Photon Energy(ies) (keV)
Barium 133	10	80, 356
Selenium 75	10	265, 136, 280
Cobalt 57	10	122, 136
Cobalt 60	10	1173, 1332
Cadmium 109	10	23, 88
Cesium 137	2	32, 662
Americium 241	20	60

The calibration was performed in MSFC Building 4705, a large open high-bay. The bay was set up with two scaffolds, separated by a distance of 12.2 meters (40 feet). One scaffold was used to hold the radioactive source, and the other was used to support the detector module and some associated equipment. Each scaffold was elevated to a height over 4.6 meters. This was done to help eliminate the scattering of gamma rays off of the floor into the BATSE detectors. Figure 3.24 illustrates the organization of the high-bay during the test.

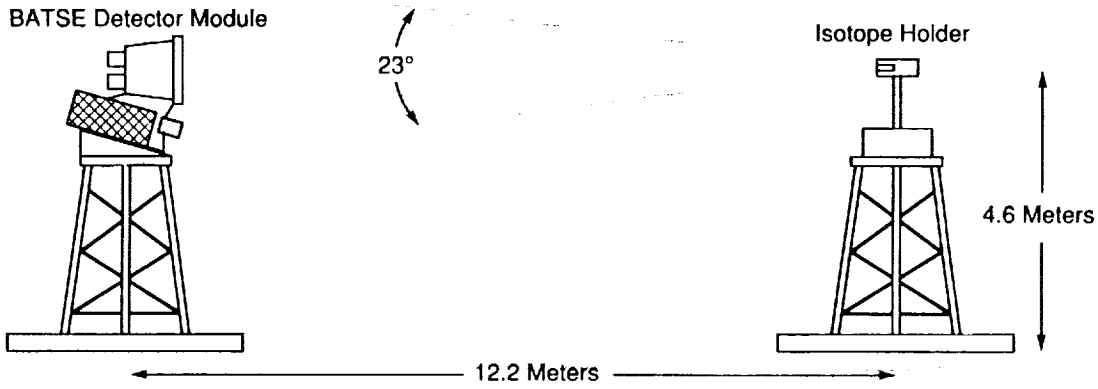

Figure 3.24. BATSE Angular Response Calibration Facility.

The scaffold on the east end of the high-bay was used to hold the radioactive isotope fixture. The fixture is a thick lead annulus, 14.6 cm in length, and 9.5 cm in diameter, with an

inner diameter of 2.54 cm. Both the inner and outer surfaces of the holder were lined with 0.16 cm of tin to absorb any k-shell x-rays from the lead. The source itself is a stainless steel button mounted on the head of a screw. This screw was affixed to a 4.4-cm plug which slides into the lead annulus. The first 1.9 cm of the plug near the source is brass, with the remainder of the plug fabricated from lead. With the source inside the holder, the opening angle of the radiation beam is 23°. The entire annulus is mounted onto a Celestron telescope mount for accurate pointing. The alignment of the radiation beam to the detector module was accomplished by transmission of a laser beam from the source holder onto the optical alignment fixture. When the holder and module were aligned, the beam was reflected back onto itself. After this pointing was established, the source holder was not moved throughout the entire test of the module. Figure 3.25 illustrates the source holder's construction.

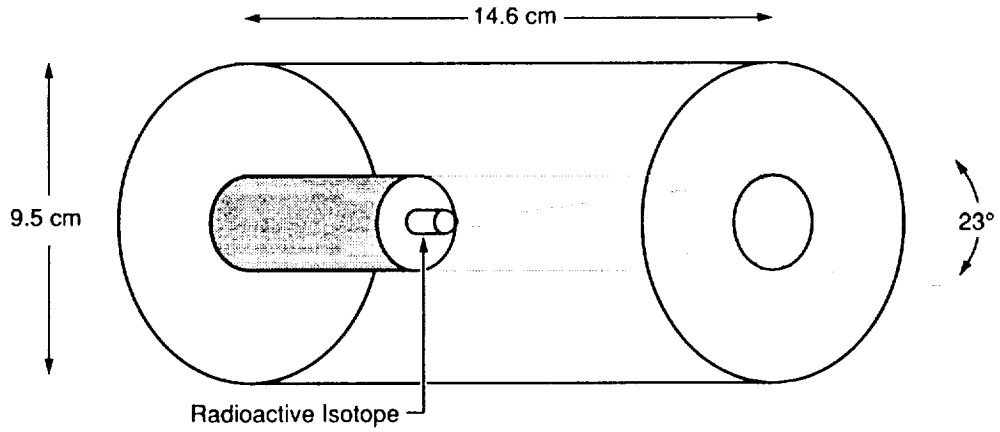

Figure 3.25. BATSE Angular Response Isotope Holding Fixture.

The detector module was bolted to an adjustable inclined wedge so that the large area detector was oriented in the local vertical plane, perpendicular to the incident radiation. Following the completion of the LAD testing, the module inclination was changed so that the face of the SD was vertical. The SD was then tested. The entire module-fixture assembly was mounted onto a rotating table, driven by a precision stepper-motor. This motor was computer-controlled, so that any desired angle could be obtained to the nearest 0.1°. The orientation of the detector with respect to the radiation beam was controlled by this computer from a remote location in the high-bay. A television camera mounted on the detector scaffold platform allowed the test conductor to determine the detector position without having to climb the scaffold, or enter the radiation beam.

The radiation environment near the detector module was monitored through the use of three 7.6 cm x 7.6 cm Harshaw NaI detectors. One detector was placed over the top of the detector module, with the other two placed on either side. These detectors were operated

simultaneously to the LAD and SD to insure that the radiation beam illuminated the module evenly. For each LAD or SD spectrum taken during this test, there is a corresponding spectrum from each of the three peripheral detectors.

Data from the LAD were accumulated at 40 different angles for each of the seven isotopes and for background. Spectroscopy detector spectra were taken at only 12 angles. The response of the LAD as a function of angle is critical for burst location; therefore, a detailed collection of data was warranted. The SD, on the other hand, is not used for burst location, and has a more uniform angular response because of its geometry. Figure 3.26 details the angles at which LAD and SD spectra were accumulated using background and isotopes.

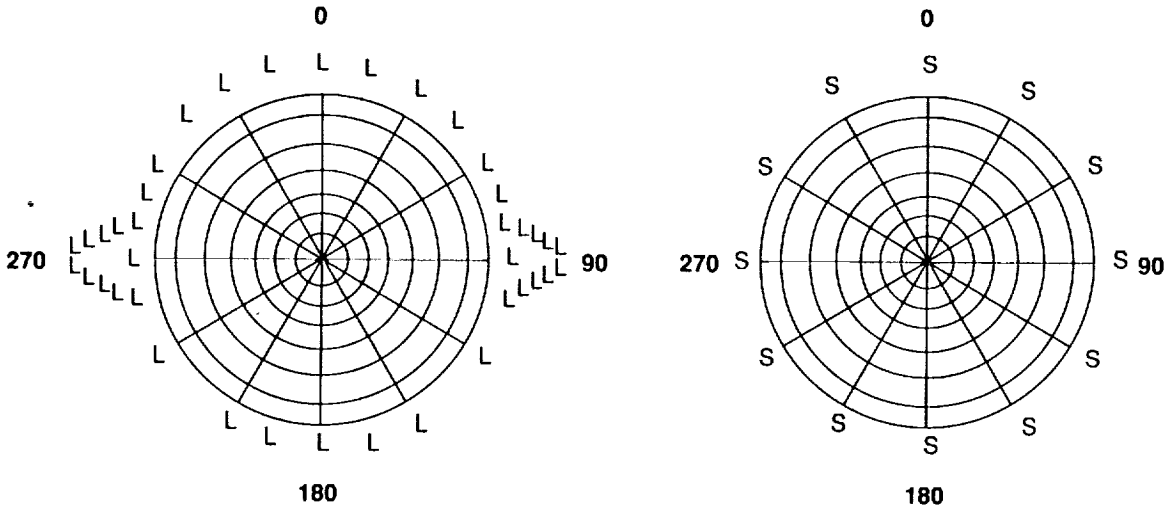

Figure 3.26. Incident Beam Angles for LAD and SD Spectra Taken During BATSE Angular Response Calibration (TPS-19).

Test angles for the LAD were concentrated near 90° and 270°. The response of the detector is highly dependent on angle in this region. For a large number of gamma ray bursts, one or more detectors will view the burst nearly edge-on. Because the response of the LAD is most sensitive at these angles, the edge-on detectors can provide important information in the localization of gamma ray bursts on the sky.

Each of the 300-second integrations from the LAD and SD were stored onto floppy disk and onto the Space Science Laboratory VAX computer for analysis. The primary data reduction was done by Dr. Geoff Pendleton of the University of Alabama, Huntsville, and by Dr. Patrick Lestrade of Mississippi State University. Figure 3.27 shows the response of the LAD as a function of incident angle for two different input energies.

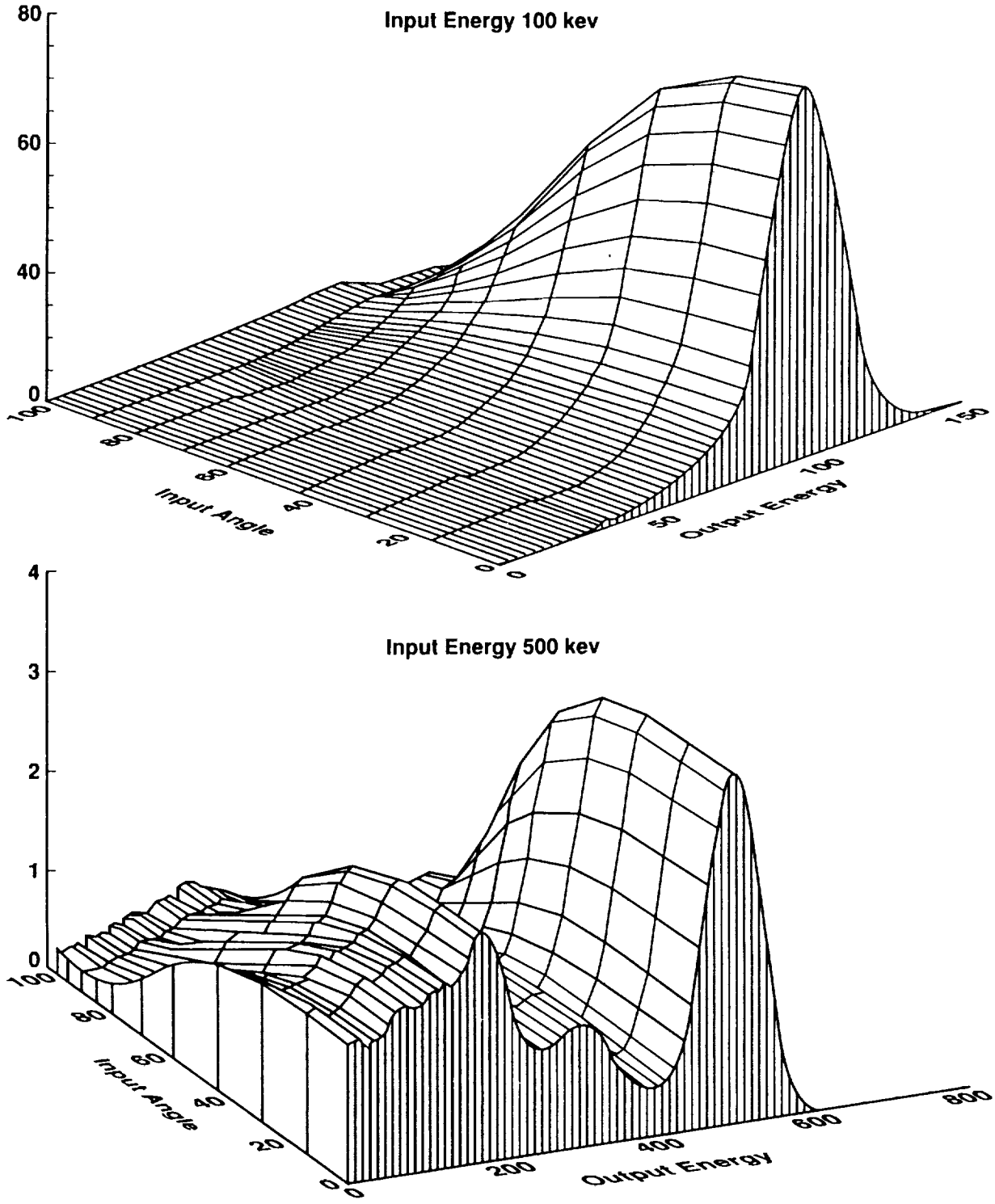

Figure 3.27. LAD Response Profiles from TPS-19 at 100 and 500 keV Incident Energies.

The dominant contribution to the response of the detector is the projected area. The near-cosine response curve at small incident angles is indicative of this effect. However, the response does not drop off as fast as a cosine function. Higher energy photons (662 keV for example) produce a fairly flat response in the detector over the range of 0° - 50°. In this region, the projected area is getting smaller with increasing angle; however, the effective thickness of the detector is increasing. This tends to offset the decreasing amplitude of the photopeak produced by a smaller projected area. The LAD has a finite thickness (1.27 cm); therefore, the photopeak does not vanish when the incident radiation is orthogonal to the detector face. Shielding from the CPD, a non-uniform radial response across the face of the LAD, and other factors introduce perturbations to the response at various angles. The spectra taken with the LAD facing away from the isotope (angles between 90 and 270) show the effectiveness of the lead-tin lining of the LAD light collection cone. The passive shielding is very effective up to energies approaching 300 keV. At 280 keV, the height of the photopeak is reduced from the face-on spectrum by a factor of nearly 4. Near 662 keV, the photopeak height is only reduced by a factor of 2, and a large number of photons are seen to Compton-scatter in the cone, but still deposit energy in the detector. The local minimum in the photopeak height centered at 180° is caused by the shielding of the three photomultiplier tube assemblies at the back of the cone.

Figure 3.28 shows the response of the spectroscopy detector over the range of angles used in the calibration. The SD is offset from the front of the detector module and is exposed from the side. Also, the presence of the beryllium window complicates the response at low energies where the window is more transparent than the aluminum housing.

The response of these detectors was parametrized in a functional form which yields the intensity in count-space at a given energy as a function of incident energy and angle. This parametrization is given below.

Large Area Detector:

$$\begin{aligned} I(\text{E-out}) = A &+ B*\{\text{COS}(\theta^2 + 0.2618 \text{ radians})\} \\ &+ C*\{\text{COS}(\theta^2 + 0.2618 \text{ radians})\}^2 \\ &+ D*\{\text{COS}(\theta^2 + 0.2618 \text{ radians})\}^3 \end{aligned}$$

Spectroscopy Detector:

$$\begin{aligned} I(\text{E-out}) = A &+ B*\{\text{COS}(\theta + 0.2618 \text{ radians})\} \\ &+ C*\{\text{COS}(\theta + 0.2618 \text{ radians})\}^2 \\ &+ D*\{\text{COS}(\theta + 0.2618 \text{ radians})\}^2 \end{aligned}$$

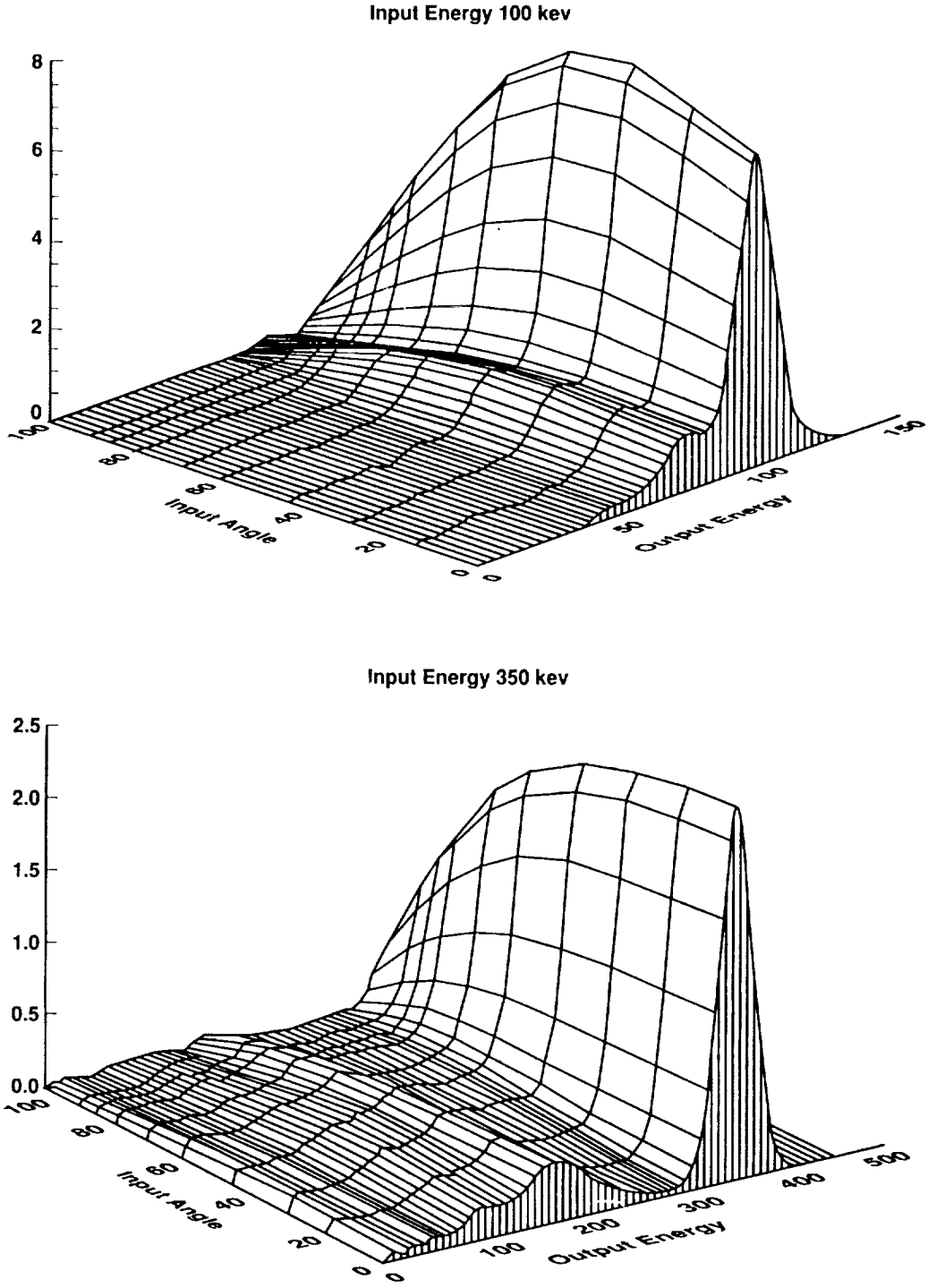

Figure 3.28. Protoflight SD Response Profile vs. Incident Angle for TPS-19.

The quantity I(E-out) is the intensity in count-space which the detector reports at energy E-out for a 1.0 photon/cm^{-2} incident plane-wave of monochromatic gamma rays at a given input energy (E-in). The coefficients A, B, C, and D are a set of four parameters unique to the desired incident energy and output energy. Despite the detector similarities, each one has a completely unique set of parameters A, B, C, and D for every given combination of input and output energy.

The user of the parametrization defines the incident energy (E-in) at the detector and the energy of interest in the detector (E-out). These two energies uniquely define a set of A, B, C, and D from which the detector response I(E-out) can be determined as a function of angle using the parametrization on the previous page. This scheme has been implemented into BATSE mission operations and data analysis software packages.

k. Detector Module Magnetic Susceptibility Calibration—TPS-25

The magnetic susceptibility calibration (TPS-25) was the final planned test in the Detector Module test and calibration sequence. This procedure provided data used to determine the effect of changing magnetic fields on the gain of the PMTs in the BATSE detectors. As the GRO orbits the Earth, the orientation and intensity of the Earth's magnetic field changes, producing changes of gain in the PMTs. From the data derived in this test, the gain change in the detector could be determined as a function of the surrounding magnetic field's direction and intensity.

This calibration was performed in the same facility as the angular response testing. The detector module was located on the floor, away from any large metallic objects. A large wood cubic frame was installed over the detector module so that the PMTs from the LAD were approximately in the center of the cube. The cube measured 2.5 m on each side, and all six of the cube faces were wound with wire coils which produced a magnetic field perpendicular to the cube face when current was passed through them. Each of the six coils were controlled by individual power supplies so that the magnetic field inside the cube could be manipulated in three dimensions. Figure 3.29 outlines the configuration of the TPS-25 calibration.

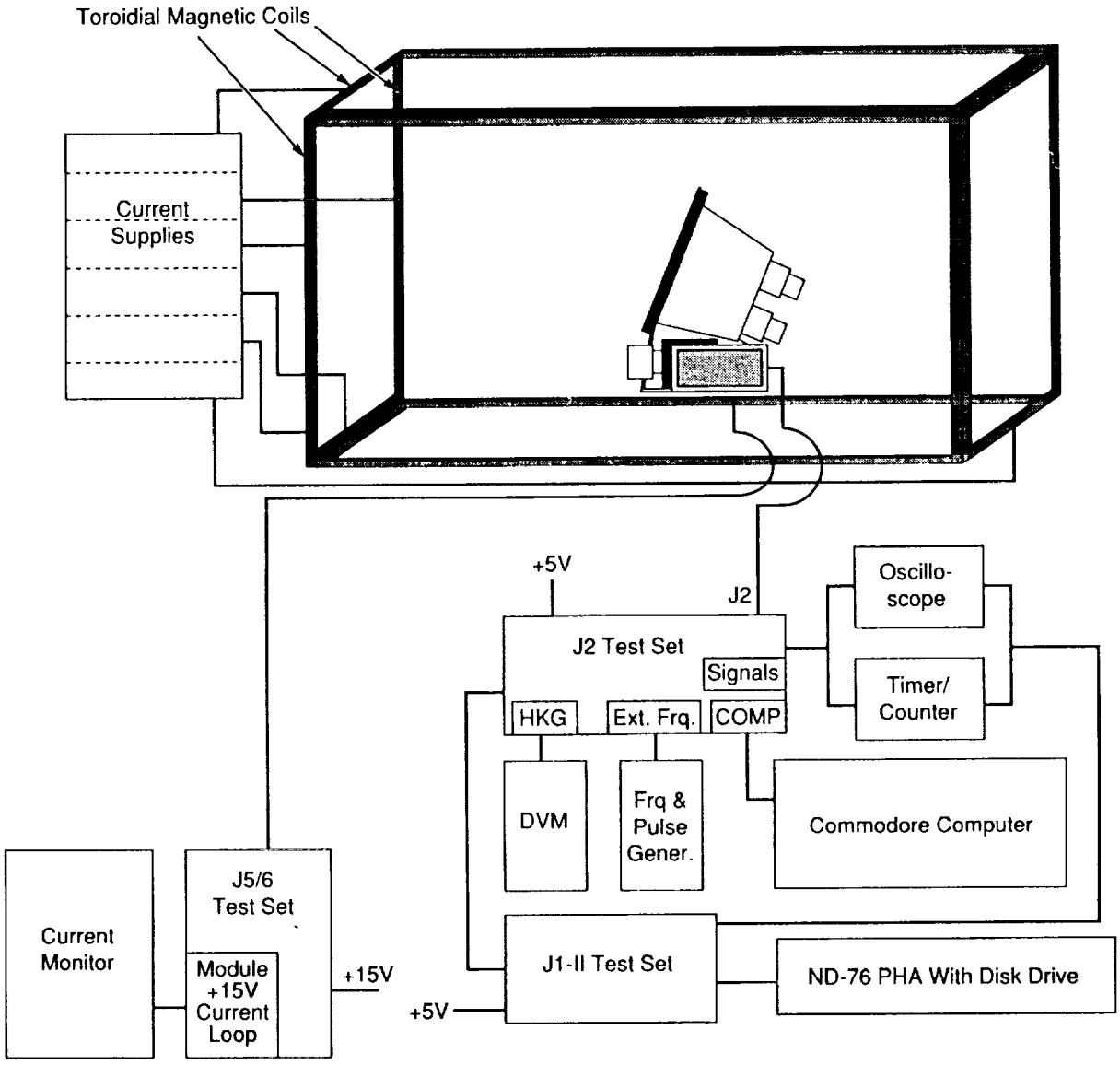

Figure 3.29. Detector Module Magnetic Susceptibility Calibration (TPS-25) Equipment Configuration.

The test began with data collection in the ambient magnetic field of the Earth. The module was powered up, and a 300-second LAD spectrum was accumulated. A Cs 137 source was then placed at the standard 50.8-cm test location, and another integration completed. After background subtraction, the spectrum's parameters were recorded and used as the baseline. This measurement was repeated for the SD.

After data collection in the ambient magnetic field of the Earth, the coils were powered up and adjusted to exactly counter the Earth's field. This effectively removed any magnetic field from the center of the cube where the PMTs were located. Background and source spectra were accumulated in the same manner as before. This measurement sequence was executed for the LAD and SD in all of the following magnetic field configurations:

Table 3.48. Magnetic Field Orientations for TPS-25

- Ambient Earth Magnetic Field
- Zero Magnetic Field
- 0.5 Gauss East Direction
- 0.5 Gauss West Direction
- 0.5 Gauss North Direction
- 0.5 Gauss South Direction
- 0.5 Gauss Directly Upward
- 0.5 Gauss Directly Downward
- 1.0 Gauss East Direction
- 1.0 Gauss West Direction
- 1.0 Gauss North Direction
- 1.0 Gauss South Direction
- 1.0 Gauss Directly Upward
- 1.0 Gauss Directly Downward

The changing magnetic field produced less of an effect on the detector module than was thought prior to the test. The LAD was more profoundly affected than the SD, as expected because of the lack of magnetic shielding beyond the front face of the PMT, and showed approximately a 3% variation in the location of the 662-keV peak over the range of magnetic field configurations. Changes to the magnetic field in the vertical and forward direction appear to have a larger effect on the module than side-to-side changes in the orientation of the magnetic field. The figure below contains 662-keV photopeak locations for the LAD on Detector Module B2 in several magnetic field configurations.

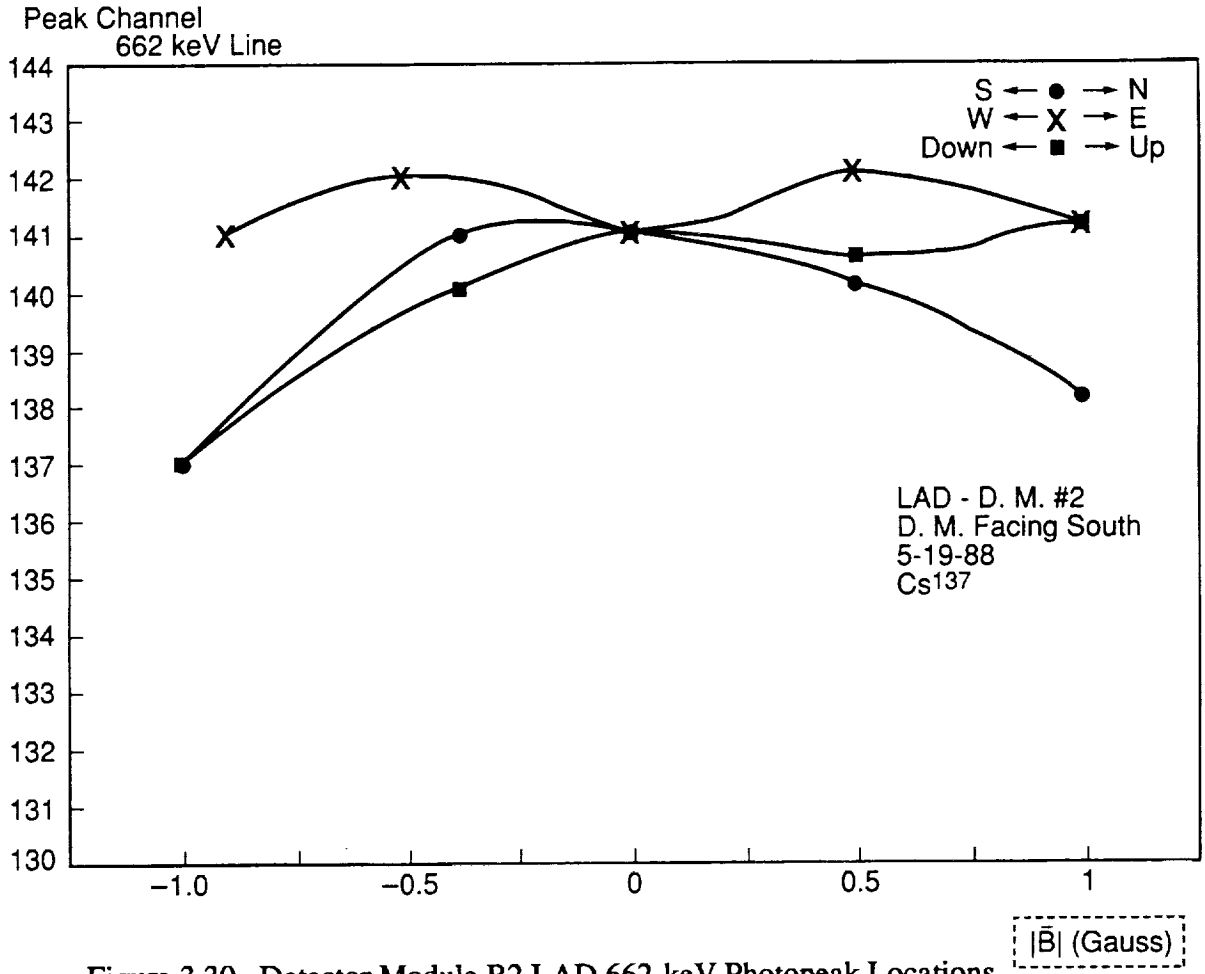

Figure 3.30. Detector Module B2 LAD 662-keV Photopeak Locations in Various Magnetic Field Configurations from TPS-25.

After examination of the results from the first few detector modules, the BATSE team decided that this calibration was not needed for all of the modules. There were several reasons for this decision. First, the results from module to module were consistent in the scale of the effect (approximately 3% in the LAD) produced by the magnetic field, but not terribly predictable in terms of the direction of the effect. One LAD could show an increase in gain for one magnetic field configuration, and the next module would show a decrease for the same configuration. The amount of change, however, would be similar in scope. Second, the effect of a temperature change on the module was thought to be perhaps as large as 1% per °C. In thermal vacuum tests, this was found not to be the case; however, at the time, a maximum 3% change from the magnetic field seemed like a small portion of the total gain change which BATSE was to experience on orbit. BATSE is equipped with automatic gain control (AGC) which is enabled to hold the gain of the LAD steady. A 3% change over half of an orbit (45 minutes) is easily controlled with the use of the AGC. Furthermore, the presence of the massive spacecraft structure will affect the magnetic susceptibility, decreasing the usefulness of these calibrations. Last, a monitoring of magnetic susceptibility can be performed in orbit on all detectors through the use of the background 511-keV line. For these reasons, the test was not performed on the final five modules. Data from the tests performed are available for inspection in the BATSE library.

l. Detector Module Testing at TRW

Following transport of the BATSE flight hardware by truck from Marshall Space Flight Center to TRW in Redondo Beach, California, a series of detector module tests were performed prior to spacecraft integration. These tests were done to verify that the modules encountered no problems or damage during the trip from Huntsville, Alabama. The experiment arrived at TRW on October 26, 1988, and was unpacked in the high-bay of Building R7A. Eight of the nine modules constructed were shipped, while the protoflight module remained in Alabama for further testing and use as a science model. Table 3.49 lists the tests performed on each of the eight modules prior to experiment integration.

Table 3.49. BATSE Detector Module Tests Performed at TRW

- TPS-28 -- BATSE Detector Module Optical Alignment Procedure
- TPS-46 -- BATSE Detector Module LAD Vacuum Level Measurement and Pumpdown Procedure
- TPS-59 -- Procedure for Performance Testing of the BATSE Detector Module at TRW

(1) Detector Module Optical Alignment—TPS-26

The first test performed on the detector module after arrival in California was the optical alignment procedure, TPS-26. The test proceeded in the same manner as the alignment measurements made in Alabama. The module was placed on a level granite slab in the R7A high-bay for these measurements. When the LED calibration assembly was removed from the back of the LAD light collection cone, a thorough inspection was made of the LAD NaI crystal. The BATSE team performing the test examined the LAD for any sign of cracking or debonding which may have occurred during transportation. No large area detector was seen to exhibit major signs of degradation or damage as a result of the transportation of the experiment. The alignment procedure produced data which were in agreement with measurements taken on the detector modules in Huntsville. Results from these iterations of TPS-59 in California are presented in Tables 3.21 and 3.22, where the mechanics of this test are described. These results were used in conjunction with GRO spacecraft measurements of module positions to calculate the LAD pointing vectors in GRO coordinates after the detector modules were installed onto the spacecraft.

(2) LAD Pressure Check and Pumpdown—TPS-46

Following optical alignment measurements and LAD visual inspections, the eight large area detectors were subjected to a pressure check and an evacuation. The test is identical to the pressure check and pumpdown test described in section III.A.1.b, requiring the same GSE, and configuration. The LADs were examined for excess internal pressure which might indicate a failure in the hermetic seal. The measured residual pressure was also compared to previous

measurements to verify that the residual outgassing rate was decreasing over time. Finally, the LAD was evacuated to a minimum residual pressure. The entire pumpdown history of the LADs is presented in Appendix B in graphic form for easy use. Measured residual pressures and final pumpdown pressures are given in Table 3.50 for this iteration only.

Table 3.50. BATSE LAD Pressure Check Data from TPS-46 at TRW - November 1988

Detector Module	Residual Pressure (mTorr)	Final Pressure (mTorr)
B0	1400	17
B1	900	19
B2	525	16
B3	900	23
B4	3500	13
B5	800	19
B6	400	18
B7	400	13

The data derived from TPS-46 indicate that all LAD seals were in good condition following delivery to California. All eight of the measured average outgassing rates declined, indicating that the amount of volatile material inside the LAD was decreasing with each evacuation. This was the final evacuation procedure performed on the detector modules prior to the installation of the detectors onto the spacecraft.

(3) Detector Module Performance Test—TPS-59

The final performance test of the detector module as a stand-alone unit was performed with TPS-59 at TRW. This iteration of TPS-59 utilized the same GSE configuration as the previous iterations, with a few procedural changes and additions. This test was the most comprehensive test of the detector modules, designed to detect any flaws in the hardware performance and to provide some final calibration measurements prior to installation on the spacecraft. In the following sections, a detailed presentation of the results from these tests is provided. All results from these tests are available for inspection in the BATSE library.

(a) Initializations

In the same manner as previous iterations of TPS-59, the test begins with the establishment of +HV values to obtain desired dispersions in the detectors. All PMTs were rebalanced to nominal gains with the use of a Cs 137 source at the standard 50.8-cm test location. The 662-keV line from this isotope was used as the reference marker. The new +HV values from this iteration of TPS-59 are contained in Table 3.51.

Table 3.51. Revised +HV Values for Standard Gains - TPS-59

	Detector Module Number							
HV Supply	B0	B1	B2	B3	B4	B5	B6	B7
PMT-A	1494	1629	1511	1576	1613	1657	1462	1652
PMT-B	1493	1610	1487	1591	1647	1630	1366	1626
PMT-C	1565	1610	1540	1571	1674	1660	1396	1680
CPD	1514	1474	1329	1306	1325	1260	1416	1258
SD-1X	1260	1291	1257	1179	1224	1145	1227	1322
SD-4X	1545	1595	1530	1441	1506	1396	1501	1620
SD-0.4X	1115	1142	1128	1045	1084	1016	1083	1166

Most of the PMTs required slightly higher voltages to obtain the desired dispersion than were needed in earlier iterations of TPS-59. Voltages for the CPD were obtained through calibrations done during the BATSE Science Testing Program at MSFC. These new voltages were arrived at through the use of radioactive sources, instead of determining the 0.6 x muon deposition energy. Isotopes provided a better knowledge of where the CPD threshold was located in energy. The procedure for determining these values is described in the system-level testing portion of this manual. None of the PMTs on the detector modules showed a major change in the voltage required for nominal gain settings. In addition, each PMT on a given module shows approximately the same voltage adjustment. These two observations indicate that the PMTs were operating nominally, with no divergent behavior from others on the same module.

(b) Spectroscopy Detector Measurements

The spectroscopy detector measurements began with a measurement of the electronic signals, similar to the previous module tests. The four SFAST signals were measured for proper amplitude and duration. Both polarities of the four SFAST discriminators were checked and verified by the BATSE test conductor. The SMQT signal was also examined for both polarities. In addition, the SMQT signal's minimum duration was verified to be longer than 2.5 μs. This ensured that the pedestal of the SMQT would fall in channel 40 or higher. An MQT duration of 1 μs corresponds to a linear channel number of 16. The stability of the spectroscopy detector PMT was verified prior to the measurement of photopeak resolutions.

-1- 4X Gain Resolution Measurements

The photopeak resolution measurements began with the spectroscopy detector at the 4X gain setting. This gain provides a dispersion of 1 keV/channel in the uncompressed SHER spectrum. After verification of the proper gain setting, a 300-second

background accumulation was obtained and stored to disk. Curiously, the radioactive background in California was found to be substantially higher than in Alabama. The background accumulated here was subtracted from all source spectra prior to calculation of the resolution. Isotopes of Co 57 and Cs 137 were used at this dispersion to provide measurements at energies of 14, 32, and 662 keV. This portion of the procedure was executed in identical fashion to that of section III.B.1. The results from the measurements at 4X gain are summarized in Table 3.52.

Table 3.52. Spectroscopy Detector FWHM Resolution % at 4X Gain -- TPS-59
(Data Obtained at TRW in November 1988)

	Energy Resolution % (FWHM)		
Detector Module	14 keV	32 keV	662 keV
B0	32.1	24.4	6.9
B1	37.8	27.1	7.1
B2	38.3	24.9	7.4
B3	32.8	21.9	7.5
B4	37.1	26.8	7.3
B5	54.3	23.8	7.0
B6	37.0	26.5	7.1
B7	34.5	24.0	7.4

These values of measured FWHM resolution are comparable to those of the previous TPS-59 displayed in Table 3.41. The resolution of the detectors at 14 keV shows an increase across the board from previous values. This increase is due to a higher LLD setting for the second measurements than was used for the first. Near the energy of the LLD, the digitization of the MQT is nonlinear, and counts in that region are distorted. This leads to a broadening of the resolution at these energies. One may notice that detector module B5 shows an SD resolution considerably higher at 14 keV than the other detectors, which are in quite good agreement. The development of a dead layer on the surface of the NaI would cause a significant degradation of the resolution at lower energies. However, the resolution measured at 32 keV for this detector shows no indication of degradation, and the poor resolution measurement is attributed to the effect of the LLD. Results from this iteration of TPS-59 at 32 and 662 keV are in excellent agreement with previous measurements and well within the specifications required. Table 3.53 summarizes the change in measured resolution between the TPS-59 conducted at MSFC and the TPS-59 executed in California after delivery of the BATSE hardware.

Table 3.53. Change in FWHM Resolution % at 4X Gain from TPS-59 in Huntsville to TPS-59 in California

	Change in Energy Resolution % (FWHM)		
Detector Module	14 keV	32 keV	662 keV
B0	6.4	3.0	0.2
B1	12.0	3.8	0.0
B2	2.6	0.7	-0.3
B3	17.0	0.0	0.3
B4	3.6	-0.6	0.0
B5	14.1	-1.7	-0.3
B6	-1.6	0.6	-0.4
B7	-2.9	-2.6	0.1

- 2- 0.4X Gain Resolution Measurements

Following the measurements taken at 1 keV/channel (uncompressed), the SD voltage was commanded to the value required for a 10 keV/channel dispersion in the uncompressed SHER spectrum. A 300-second background accumulation was obtained first at this new setting and stored to disk. Cesium 137 and Na 22 isotopes were placed at the 50.8-cm test location, and individual integrations of 300 seconds were obtained with each source. From the background-subtracted spectra, the results of Table 3.54 were calculated.

Table 3.54. Spectroscopy Detector FWHM Resolution % at 0.4X Gain - TPS-59

	Resolution % (FWHM)	
Detector Module	511 keV	662 keV
B0	9.5	8.2
B1	9.1	7.9
B2	9.3	8.1
B3	8.9	7.8
B4	9.7	8.5
B5	8.7	7.6
B6	8.9	7.9
B7	9.3	8.2

Because of the compressed gain, the photopeaks are condensed into five or six channels, making an exact determination of the half-maximum location more imprecise than at other dispersions where the photopeak occupies more channels. This measurement uncertainty was discussed in section III.B.1.i(2)(b) and applies here, as well. Despite the problem of measurement, the results in Table 3.54 agree well with those from the previous iteration of TPS-59 at the Marshall Space Flight Center.

- 3 - 1X Gain Resolution Measurements

At the 1X gain portion of the spectroscopy detector measurements, this iteration of TPS-59 deviated from previous tests. In prior operations, the programmable LLD was tested prior to any resolution measurements. In this iteration, the LLD was mapped after the resolution measurements at 4X and 0.4X gains. Each bit of the programmable discriminator was tested for operation, and 14 values of the LLD were tested. At each value, a 120-second integration was obtained with Cs 137, Co 57, and Cd 109 isotopes all located at the 50.8-cm test position. These spectra were stored onto floppy disk, as were all integrations from this test. Seven command-values of the LLD were mapped at 0.4X and 4X gains.

The SD was next commanded back into the 1X gain mode, and a light leak test was done. It was conceivable that during the transit of the detector modules and other flight hardware, damage could have occurred which, although small, may have caused a light leak in the detector. For this reason, eachy of the detectors were checked with a high intensity light at TRW for any sign of a leak. The results for all of the SDs were negative.

The final portion of the SD testing was reserved for photopeak resolution measurements at 1X gain. These measurements used isotopes of Cd 109, Na 22, Cs 137, and Co 60. As with previous measurements, all integrations were 300 seconds in duration, and the isotopes were placed at the standard 50.8-cm test location. Dispersions were calculated using photopeak locations with known energies. The results from this iteration of TPS-59 are contained in Table 3.55.

Table 3.55. Spectroscopy Detector 1X FWHM Resolution % from TPS-59 at Redondo Beach, California - November 1988

	FWHM Resolution % at Energies Shown (keV)					
Detector Module	88	511	662	1173	1275	1332
B0	14.3	7.8	6.9	5.8	5.4	5.4
B1	15.3	8.5	7.3	6.7	5.7	6.0
B2	11.3	8.2	7.4	6.4	6.1	5.9
B3	12.7	8.1	7.1	6.2	5.8	5.8
B4	16.9	8.5	7.4	6.3	5.9	5.9
B5	12.1	8.1	7.2	6.1	5.8	5.9
B6	11.0	8.3	7.0	6.4	5.7	5.9
B7	12.0	8.4	7.5	6.7	6.2	6.2

These results are nearly identical to those from the earlier iteration of TPS-59. The B6 measurement from the previous TPS-59 indicated a resolution of 6.4% at 662 keV. This was most likely an error on the part of the test conductor. The value of 7.0%, obtained in the latest

test, is more reasonable. The B6 measurements at other energies are in good agreement. A similar case can be made for the B3 measurements from the first TPS-59. At all energies, the previous resolutions appear poorer than the other detectors. The latter TPS-59 measurements show that the resolution for B3 is similar to other detectors, and are in good agreement with measurements made at other gains. Table 3.56 details the change in measured resolution between the TPS-59 test done at MSFC and the test done in California.

Table 3.56. Change in FWHM Resolution % for SDs at 1X Gain from TPS-59 at MSFC to TPS-59 in California

	Change in FWHM Resolution % at Energies Shown (keV)					
Detector Module	88	511	662	1173	1275	1332
B0	2.5	-0.2	-0.3	0.0	0.1	-0.1
B1	1.4	0.3	0.1	0.1	0.0	0.0
B2	-1.4	-0.1	-0.1	-0.3	0.4	0.0
B3	-3.2	-0.4	-0.8	-1.1	-0.7	-0.5
B4	1.4	0.1	0.1	-0.1	0.1	0.1
B5	-2.7	0.2	0.1	-0.1	0.0	0.2
B6	-6.0	0.0	0.6	0.2	0.2	0.4
B7	-2.1	-0.1	0.0	-0.1	0.3	0.1

These data represent the final measured resolutions of the spectroscopy detectors prior to detector module installation on the GRO. These data are believed to represent the best set of SD photopeak resolution measurements taken throughout the entire test program of the BATSE experiment. All modules were tested within a period of 48 hours by the same test conductors in a test environment that was highly controllable and uniform from module to module. These same conditions were not present to this extent anywhere else during the course of the test flow. Mechanical constraints may have prevented the precise location of an isotope, different test conductors may have executed tests on different modules, or a long period of time may have elapsed between module tests. The presence of any of these factors would contribute to lower the quality of the measurements as a set.

(c) Large Area Detector Measurements

The LAD measurements began with a full check of the electronics and signals associated with the detector. Each of the FAST discriminators were examined to verify bi-polarity and to measure the duration of the signal. Typical FAST discriminator durations were measured to be 150 ns. The differential nature of the four FAST signals was also verified. A mapping of FAST discriminators to MQT channel was then executed using the gated pulse-height analyzer. This portion of the test was configured in the same fashion as before, and is described in section III.B.1.i(3)(a). The MQT channels' correspondence to the four FAST discriminators is shown in Table 3.57.

Table 3.57. Mapping of FAST Discriminator Boundaries into MQT Channel from TPS-59 in California - November 1988

Detector Module	FAST1	FAST2	FAST3	FAST4
B0	LLD - 13.5	13.5 - 23.5	24.5 - 65.5	64 and higher
B1	LLD - 15	15 - 24.5	25 - 64	63.5 and higher
B2	LLD - 14	14 - 24	24.5 - 66	65.5 and higher
B3	LLD - 15.75	15.75 - 25.75	26 - 66.5	66 and higher
B4	LLD - 15	15.5 - 25	25.5 - 65	64.5 and higher
B5	LLD - 15	15.5 - 24.5	25 - 65.5	65.5 and higher
B6	LLD - 15.5	16 - 25.5	25.5 - 66	66 and higher
B7	LLD - 16	17 - 25.75	26.5 - 66.5	66.5 and higher

The measurements inTable 3.57 agree with earlier results to within a channel (5 keV) in most cases. Notable exceptions are the FAST1 discriminator in detectors B0 and B3. These were measured to each start two linear channels earlier than before. Detector B7's FAST4 discriminator was measured to start in channel 66.5 compared to channel 70 in the previous TPS-59 measurement. To determine the approximate energy correlation of these channel numbers, subtract 6 from the channel in question, and multiply by 5 keV.

LAD testing continued with a check of the MQT signal similar to the previous tests and a light leak check of the entire LAD assembly. All of the LAD assemblies were verified to be light-tight following shipment from Alabama.

Each bit of the programmable LLD was then exercised, and the location of the LLD was mapped into MQT channel space for 15 different settings. With a Cs 137 and a Cd 109 isotope at the standard 50.8-cm test location, a 60-second integration was obtained for each of the 15 settings. The channel number corresponding to the LLD cut-off was recorded and the spectrum stored onto floppy disk. Each of the LLDs were verified to be fully functional.

Photopeak resolution measurements constituted the next section of TPS-59. Isotopes of Cd 109, Na 22, and Cs 137 were used to produce photopeaks at 88, 511, 662, and 1275 keV. A 300-second background accumulation was also acquired and used in the subtraction from source spectra. The results of these measurements are contained in Table 3.58.

Table 3.58. Change in LAD FWHM Photopeak Resolution % from TPS-59 Iterations

	Change in FWHM Resolution % (Energy in keV)			
Detector Module	88	511	662	1275
B0	2.0	0.9	0.4	-1.0
B1	1.5	0.4	1.2	-12.3
B2	0.8	1.0	0.2	0.9
B3	-0.2	1.0	1.0	2.4
B4	-1.6	-0.3	-0.8	0.6
B5	2.8	1.2	0.4	0.5
B6	-0.3	0.6	0.1	0.4
B7	0.4	-0.1	0.2	-3.4

Changes in the measured resolution from one iteration of TPS-59 to the next are small, less than 1% or 2% in most cases. The exceptions are at the highest energy measurements, where the measured resolution is degraded severely by the radial response of the detector. Photons which deposit their energy in the center of the LAD do not produce the same response in the detector as photons which interact near the edge. The effect is a severely broadened photopeak that resembles two overlapping Gaussian profiles. The locations of the half-maximum points are dependent on how severe the broadening is, and what channel one chooses as the photopeak maximum channel (which may have neighboring channels on both sides with more counts). An extensive test was included in the BATSE science testing for calibration of this effect. Despite the fluctuations at 1275 keV, the overall performance of the LADs was not detectably degraded by transport of the hardware from Alabama to California.

Large area detector testing continued with a mapping of the LED into MQT channel space. Six levels of the 4-bit commandable LED were exercised, and each bit of the command was verified to be operational. As in previous tests, the LED was driven with a 1 kHz pulse of 1 μs width, and a 60-second integration was obtained. All eight LEDs were verified to be fully operational in this test.

(d) Charged Particle Detector Measurements

The CPD tests for this iteration of TPS-59 were identical to those of previous module performance tests. A 300-second spectrum was obtained from the LAD with the CPD in anticoincidence mode, followed by another 300-second accumulation with the CPD off. The difference in counts between these spectrum was due to the rejection of the CPD. The LAD was then placed in coincidence mode and the gain adjusted to bring muons onto the scale of the MQT. A third 300-second spectrum was accumulated. The count rate in this spectrum was then compared to the previously derived rate for agreement. The results are contained in Table 3.59.

Table 3.59. CPD Rejection and Coincidence Rates from TPS-59 in California

Detector Module	CPD Rejection Rate	CPD Coincidence Rate
B0	20.6	21.0
B1	19.4	20.4
B2	21.4	20.2
B3	21.2	20.6
B4	20.8	20.6
B5	20.9	20.7
B6	21.5	20.4
B7	20.8	20.4

The rejection and coincidence rates shown in Table 3.59 are in close agreement, indicating that the charged particle rejection system is working well. Furthermore, the rate of rejection is comparable to the rate expected for the inclined CPD (see section III.B.1.d(4)). The new CPD voltages and different test location make it difficult to compare these numbers to those from previous testing, however. The module-to-module correlation in coincidence rate is an indication that all of the CPD thresholds are close to one another in energy. In addition to this standard check, the CPD was examined for a light leak in a manner analogous to the LAD and SD. No light leaks were found.

(e) TPS-59 Conclusions

TPS-59 concluded with a measurement of all housekeeping parameters. The final section began with a check of the passive analog thermistors. These temperature sensors provide measurements to the spacecraft RIU and are included in GRO engineering telemetry. However, they are not routed through the DEU and are not visible anywhere in BATSE data. The resistance of the thermistors and associated circuitry was measured to verify proper operation of these elements.

Table 3.60. Passive Analog Thermistor Measured Resistances - TPS-59

Detector Module	Resistance Measured (Ohms) PAT RIU-A	PAT RIU-B
B0	2647	2643
B1	2601	2598
B2	2635	2637
B3	2596	2594
B4	2697	2697
B5	2580	2580
B6	2657	2657
B7	2663	2653

The second portion of the housekeeping check was a read of HKG values 15-31. These multiplexed values contain the housekeeping for the module's low voltages and temperatures. All measured HKG parameters were compared to expected values.

Finally, each bit of all five +HV supplies was checked for proper operation. A simultaneous verification of the expected current and voltage measurements in housekeeping was done. At the full-scale +HV setting (command data = 255 decimal), the HVPS +5V current was measured to verify that the HVPS was not in an over-current condition. Typical current values for the HVPS with one supply at full scale were 0.08-0.1 A. The conclusion of the test marked the final time that any of the eight flight modules was powered on as a stand-alone unit. All subsequent powering of the modules was accomplished through use of the BATSE power module, or through the BPM simulator. Following the completion of TPS-59, each detector module was integrated to the CEU and BPM.

m. Detector Module Auxiliary Tests

At several times in the detector module test program, the BATSE team performed auxiliary tests on the detectors. These were one-time-only types of tests which were performed on only one module and were not part of the pre-planned test flow. The protoflight module was the subject for most of this testing because of its easy accessibility during the time it was located in the Space Science Laboratory. A brief summary of the important tests is provided in the following sections.

(1) Protoflight Out-of-Balance Testing

In May 1988, a day of testing was given to the protoflight module to determine the single PMT performance for balancing using a simulated 511-keV line and to determine the effect of an out-of-balance condition on the detector resolution. The original plan for on-orbit balancing of the PMTs called for the use of a small Am 241 light pulser installed onto the face of

the LAD in view of the PMTs. However, the light pulsers were very unreliable. The behavior of the light pulsers was unpredictable, environmental changes distorted their performance by a large amount, and they degraded rapidly over time. For these reasons, they were omitted from the final configuration of the detector modules, and the BATSE team decided to use the on-orbit 511-keV line for PMT balancing.

The module was placed on the top of the shipping container and connected to the same GSE configuration which was used for TPS-24 and TPS-59. A Co 60 source of 3 μCi activity, and a Na 22 source of 1 μCi activity were placed at the rear corner of the detector module to simulate the anticipated on-orbit spectrum and 511-keV line. With the LLD set to 32 (hex), a total count rate of approximately 3800 counts per second was registered in the LAD. The intensity of the 511-keV line compared to the level of background was less than the level registered by BATSE-like detectors flown on the third MSFC Supernova 1987A Balloon Flight from Alice Springs, Australia.

After the isotopes were put into place, the PMTs were balanced at the proper 5 keV/ channel gain. The PMTs were easily balanced by the test conductor using the 511-keV line. Digital voltage commands of 162, 157, and 155 were required for PMTs A, B, and C, respectively. This result confirmed that on-orbit PMT balancing using the 511-keV line could be accomplished with little difficulty.

Following the balancing of the PMTs, single-tube spectra were accumulated from PMT-A to determine the +HV values necessary for gain adjustments of -10%, -20%, and -40%. These spectra were stored to disk, and a similar sequence was executed for PMT-B at values of +10%, +20%, and +40% gain change. The voltage command values required to adjust the individual PMT gains to the prescribed values are summarized in Table 3.61.

Table 3.61. Voltage Command Values Required for Gain Adjustments on the BATSE Protoflight LAD

Gain Change	PMT-A Command Value	PMT-B Command Value
Zero (nominal gain)	162	157
-10%	157	----
-20%	151	----
-40%	136	----
+10%	----	160
+20%	----	165
+40%	----	179

The spectra accumulated from PMT-A and PMT-B were taken with the source configuration simulating the anticipated on-orbit spectrum. After accumulating these individual PMT

spectra, all three PMTs were powered on for the collection of spectra in four different gain configurations. PMTs A and B were adjusted to one of the off-nominal gain states, while PMT-C remained at the nominal voltage setting. In this manner, spectra of the simulated on-orbit spectrum were taken with known out-of-balance conditions. The PMT gain configurations used in this portion of the test are summarized in Table 3.62.

Table 3.62. Out-of-Balance PMT Gain Combinations Used in Spectra With Anticipated On-Orbit Background Source Configuration

PMT-A Gain	PMT-B Gain	PMT-C Gain
Nominal	Nominal	Nominal
-10%	+10%	Nominal
-20%	+20%	Nominal
-40%	+40%	Nominal

After the completion of these spectral integrations, a 1 μCi Na 22 isotope was placed at the center of the CPD on the protoflight module, and the "on-orbit" source configuration was removed. The gain combinations detailed in Table 3.62 were repeated, and spectra were accumulated. In addition, individual PMT spectra were obtained with the tube commanded to nominal-gain voltage values. Next, a final set of spectra were accumulated using a 10 μCi Cs 137 source at the standard 50.8-cm test location. The PMT voltage configurations used in the Na 22 accumulations were repeated with the Cs 137 source.

The results of the test were two-fold. First, the BATSE team demonstrated that the PMTs on the LAD could be balanced through the use of the on-orbit 511-keV line. No problems were encountered using a line intensity less than that seen in flight data from the BATSE-like LADs flown on high-altitude balloons. This allowed for the removal of the Am 241 light pulsers while maintaining confidence that the PMTs could be easily balanced on-orbit. Second, the effect of an out-of-balance PMT on the overall detector resolution was shown to be small. Degradations in the resolution of the detector were not noticeable in any of the gain-combination spectra (Table 3.62) until the 40% out-of-balance condition was imposed. Even with this large disparity in PMT gain settings, the resolution was only degraded a few percent. This was a surprising result. All data and spectra from this test are available for inspection in the BATSE data library.

(2) Protoflight SD Low Energy Resolution Measurements

On May 11, 1988, the BATSE protoflight module was tested to measure the FWHM photopeak resolution at low energies. In TPS-24 and TPS-59, these low energy peaks were often below the threshold of the programmable LLD, or difficult to measure because of other test considerations. The GSE required for this testing was identical to that of TPS-24 and was configured in the same manner. The SD was commanded to the 4X gain setting (1 keV/ channel uncompressed), and a 300-second background acquisition was obtained. Subsequent

300-second integrations were made with a Cd 109 and a Co 57 isotope located at the standard 50.8-cm test location. The background spectrum was subtracted from the two source spectra, and the FWHM resolution was calculated. The resolution at 14 keV was determined to be 44.6%, with the resolution at 23 keV measured to be 26.2%.

(3) Plastic Fraction Calibration

The plastic fraction calibration was performed on the BATSE protoflight module in May 1988. The test was executed in order to determine the ratio of the number of gamma rays detected in the CPD to the number of gamma rays detected in the LAD as a function of gamma ray energy and angle of incidence. The data collected in this test are to be used to help determine the setting of the parameter PFRAC on-orbit. PFRAC is a parameter in the BATSE CEU which is used to prevent burst triggering if the CPD rate indicates a charged particle event.

The protoflight module was connected to the standard test GSE in the TPS-24 configuration. In addition, the FAST2 and FAST3 discriminators were connected to a timer/counter. The PLASTIC rate was also input to a timer/counter. Power was applied to the module, and nominal +HV values were established. Background rates for the CPD and burst trigger channels (FAST2 + FAST3) were determined from a 100-second integration of their counts. Next, Co 60 and Co 57 isotopes were individually placed at angles of 0°, 45°, and 70° from the detector normal, and at a distance of 90 cm. The rate determination was repeated for each of these six configurations. Table 3.63 contains the rates from the test.

Table 3.63. Data from Plastic Fraction Calibration on the Protoflight Module

Source	Angle (°)	Plastic Rate	Burst Chan. Rate	PFRAC
None		63.0	1318.7	
Co 60	0	207.9	2292.8	0.15
Co 60	45	262.6	2489.4	0.17
Co 60	70	186.3	1913.2	0.21
Co 57	0	62.5	4709.2	0.00
Co 57	45	61.8	4576.9	0.00

The value PFRAC is calculated by first subtracting the background rates from the source rates. This yields the rate at which the gamma rays from the source interact in both the CPD and LAD burst trigger channels. Dividing the plastic source rate by the LAD source rate yields the fraction of events which are seen in both the LAD burst channels and the CPD. Because the threshold of the CPD was set well above the energies of the Co 57 isotope emission (14, 122, and 136 keV), no gamma rays which interact in the CPD from this isotope cause a source count to appear in the PLASTIC rate. PFRAC is therefore equal to zero, and the last planned location for this source was omitted.

n. Detector Module Unique Attributions and Anomalies

The flow of each of the detector modules through the planned test program was unique. Throughout the course of this flow, the modules experienced anomalies and non-conformities not present on the other detector modules. In this section, each of the modules' quirks, failures, non-conformities, and unique features are discussed.

(1) Protoflight Detector Module

The protoflight module was the first module fabricated and tested in the series. Released for testing on January 21, 1988, this module received the most extensive testing throughout the program at MSFC. The protoflight module contains LAD #8, which was cracked in thermal stress testing. In the initial testing of the module, a cross-wiring of LAD and CPD signals was noticed in the connection to the DEU. An EO was written to rectify the mix-up, and the problem was corrected the next day. Because of the long protoflight thermal vacuum test, this module contains the largest amount of spectra characterizing the LAD "notch" phenomenon discussed earlier. Throughout the test program at MSFC, the module was referred to as DM #0. The original plan in the numbering system was to call the protoflight module "DM #0," and all subsequent modules DM 1-8. These numbers would then correspond to their eventual location on the spacecraft; however, that plan changed later in the program.

(2) Detector Module B0

This detector module was named DM #6 throughout the testing program. A decision was made by the BATSE team upon arrival at TRW to switch the location of DM #6 and DM #8 on the spacecraft. The primary impetus for this decision was the desire to place the superior module DM #6 at the +X,+Y,+Z location (B0) for more frequent coordinated observations with the OSSE Instrument. DM #8 was then placed in the B6 location on the GRO. B0 contains LAD #13, which was cracked during initial thermal stress testing at MSFC. No performance anomalies were present in B0 throughout the test flow.

(3) Detector Module B1

Released approximately 2 weeks after the protoflight, detector module B1 had a hardware error after manufacturing. When TPS-24 was executed, the LAD was found to be inoperative. The CPD and SD were functioning normally; however, the LAD was connected to a blank port on the DEU. The signals from the LAD PMTs were not reaching the electronics; therefore, the detector was not functional. This problem was repaired in 2 days. B1 was the module used in the DM-CEU-BPM electromagnetic compatibility and interference tests prior to the full BATSE instrument test. This test is discussed in a subsequent section of this document, and produced evidence of module susceptibility to radiation in the 50-60 MHz and 150-170 MHz bands. B1 contains LAD #6, which showed a tremendous increase in the average outgassing rate following GRO thermal vacuum testing. The rate of outgassing pressurization went from approximately 0.3 Torr/month to 1.8 Torr/month. Although each of the LADs average outgassing

rate increased because of the thermal cycling and vacuum conditions, none were as dramatic as B1. Subsequent measurements indicated no problems with the B1 LAD hermetic seal or leakage.

(4) Detector Module B2

During the initial TPS-24, the LAD PMTs were inadvertently operated with the LED calibration assembly removed from the back of the cone. No apparent short-term or long-term effects were noticed from the 45 seconds of operation in this condition. B2 had one of the shortest duration test flows. Testing started on February 23, 1989, and was completed by March 7. No testing anomalies were attributed to B2 during the module test program. The resolution of the LAD on detector module B2 is the best of the flight modules.

(5) Detector Module B3

Detector module B3 was among the few modules with no anomalies or unusual operations during the test flow prior to integration with the CEU and BPM. Test data in the BATSE library for this module are labeled DM #3. Module B3 is 2 pounds lighter than any of the other detector modules. The reason for the discrepancy in weight is not known.

(6) Detector Module B4

Like detector module B3, B4 also exhibited no anomalies during its pre-integration testing. All performance, engineering, and environmental test results were acceptable.

(7) Detector Module B5

Detector module B5 completed manufacturing with a defective +HV power unit. With a supply commanded to full scale (command data = 255), the HVPS would enter into an oscillation and draw an unacceptably large amount of current. When the module was initially powered up for the test, the test conductor recorded an initial module +15 V current of 500 mA, which is very high. At the point in the test where each bit of the supplies and the HKG are tested, the erroneous current was noted on both the SD and CPD +HV supplies. The problem was fixed by replacing the entire HVPU with serial number 006. HVPU #8, which was originally on B5, was repaired and installed onto B6. The repair process was completed in 9 days. This replacement supply functioned normally throughout the remainder of the module testing program. The LAD on B5 is the detector with the poorest resolution on the spacecraft. In April 1990, PMT C on this module failed at KSC. It was replaced with a tube from the protoflight module. The details of this failure and replacement are contained in a later portion of this manual

(8) Detector Module B6

Detector module B6 spent most of its early life under the name DM #8. As the eighth flight module, it was scheduled to be installed into the +X,+Y,+Z location on the GRO. However, after arrival at TRW, it was decided to install this module in the B6 location, and place DM #6 in the B0 spot, switching the detector modules (see section III.B.1.n(2)). B6 contains LAD #15, which arrived at MSFC with a problem in the spacing of the mounting holes on the Invar ring. These holes were re-drilled to match the LAD cone interface.

(9) Detector Module B7

Detector module B7 contains LAD #14, which cracked during the thermal stress testing at MSFC. It is the only other module (with B0) containing a cracked LAD. All results from the testing program were acceptable for B7, and no hardware problems were found.

o. BATSE Detector Module Parts Listing

Table 3.64 details the contents of each of the nine BATSE detector modules fabricated at MSFC. Serial numbers for all major components are provided.

Table 3.64. Detector Module Parts List by Serial Number

	LAD#	CPD# (PMTs)	PMT-A	PMT-B	PMT-C	SD PMT	LED ASSEMBLY#	DEU#	HVPU#	MODULE SERIAL #
Protoflight Module	8 (cracked)	6 (192164-10 & 193166-15)	112306-13*	112302-14	112297-10	112184-11	8 (A273922)	5	4	001
DM B0	13 (cracked)	3 (192152-08 & 192187-03)	112177-03	112179-04	112413-22	112298-03	4 (A373927)	6	7	007
DM B1	6	2 (192165-07 & 192188-04)	112398-19	112311-05	112351-06	112280-12	7 (A373928)	8	3	002
DM B2	7	1 (192162-02 & 192375-19)	5003-27	112819-25	112356-16	112407-08	9 (A373906)	7	10	003
DM B3	10	4 (192145-09 & 192378-22)	112193-07	112584-21	5012-26	112276-07	1 (A373905)	9	2	004
DM B4	11	5 (192139-05 & 192274-17)	5002-28	112405-12	112290-11	112406-10	6 (A373910)	4	5	005
DM B5	12	9 (192346-14 & 192376-20)	112378-23	112310-08	112402-17**	112399-09	2 (A373929)	3	6	006
DM B6	15	7 (192190-11 & 192273-13)	112176-01	112409-15	112411-20	112175-01	11 (A373939)	10	8	009
DM B7	14 (cracked)	8 (192374-18 & 192377-21)	112304-09	5011-24	112312-30	112173-02	3 (A373912)	1	9	008

*This PMT was removed from the P/F module and installed into the "C" location on B5.
**This PMT was removed from B5 and replaced with PMT-A from the P/F module in June 1990.

2. BATSE Power Module Testing

a. Introduction

The BATSE power module was subject to a test program entirely different from that of the BATSE detector modules. The BPM testing which was performed focused on a listing of requirements which the power module had to meet or exceed. Data obtained from the testing are of a pass-fail, binary nature. An example of this type of data is whether a certain command to the BPM opens a relay or not. In this test environment, either the relay opens, or it doesn't. No data obtained from the BPM tests contain calibration information or other information beyond the compliance with a pre-determined requirement. The detector module data, on the other hand, not only determine whether the module performs according to specifications, but also tell how well and in what manner the module behaves.

For this reason, section III.B.2 is brief compared to the section on detector module testing. In the following paragraphs, the BPM acceptance test will be discussed, along with the requirements which the BPM performed against in the test.

b. BATSE Power Module Acceptance Test

The BPM acceptance test was written and performed under the direction of the Test Laboratory at MSFC. The test procedure was released October 21, 1988, with the document number MTCP-FC-BTSE-305D. Other BATSE flight hardware such as the detector modules, the CEU, and heater interfaces were simulated by load panels connected to the BPM. The power module was connected to the SCATS data acquisition system through the BPM test set, a fuse panel, a power distribution panel, and patch distributors. Power to the BPM was supplied by a simulated GRO power supply, 0-40 Vdc, and 15 A. A similar power supply provided power for the heater circuits.

The test started with the application of GRO-1 power (primary power simulation). Proper voltages and currents were verified for the CEU simulator load panel. The CEU and BPM temperature readings were verified through the SCATS as well. Detector module power relays were then cycled through, and full functionality of these relays with both GRO-1 and GRO-2 power was verified.

Section two of the procedure checked the STS heater circuits and thermostats. Control of the heater circuits was accomplished by a GSE cable to J16, where the IFJ is installed for flight. Combinations of circuit states were tested for all eight detector module heater circuits. Following the checkout, the cable was removed and the IFJ installed to verify the proper voltage state with all thermostats open. Detector module thermostats were then simulated to close with input through the module ports, and the proper voltage readings were verified.

The third section of the test involved the verification of detector module primary heater circuits and thermostat closure simulations. Status voltages and power voltages were monitored and verified in all configurations of thermostat closure and open states. A similar check was done for the backup thermal control heater circuits and both sets of make-up heater circuits.

Completion of the heater circuits marked the conclusion of the acceptance test. The procedure run prior to any connection of the flight hardware components into the BATSE unit. Examples of this occurrence were prior to thermal vacuum testing, science testing, and integration at TRW. Copies of the as-run procedure are available in the BATSE data library.

3. Central Electronics Unit Testing

The central electronics unit (CEU) is the most complex portion of the BATSE flight hardware. As such, the CEU received a large number of specialized tests to check and verify proper operation of each of its components and functions. The assembly and testing of the CEU was exercised under the direction of the Information and Electronic Systems Laboratory (EB) at MSFC. Mr. Jon R. Rehage, designer of the CEU, served as the primary test engineer throughout the program.

CEU data obtained in these tests are similar to BPM test data, because they are primarily of a binary nature. As discussed before, in these types of tests, data generated simply indicates a pass/fail status. In the following paragraphs, each of the CEU tests performed during the program will be discussed. These include the CEU environmental tests which were performed prior to experiment integration.

Each test presented in this section was executed under the same configuration with minor changes for the individual tests as required. The CEU was placed on a table and connected to several pieces of ground support equipment. Two test-program function boxes were connected to J46 and J47. The microprocessor development unit and CEU test set were also connected in this area. Ports J30-J32 were connected to the BPM simulator. Detector modules were simulated by a piece of GSE designed to emulate the DEU in each module. This simulator was connected to ports J10-J17. The spacecraft interface, at J34-J39 and J40-J45, was made between the CEU and the GRO simulator. This simulator contained two remote interface units (RIU) and transmitted data and commands to the BATSE IGSE computer system. Figure 3.31 is a schematic of this test configuration.

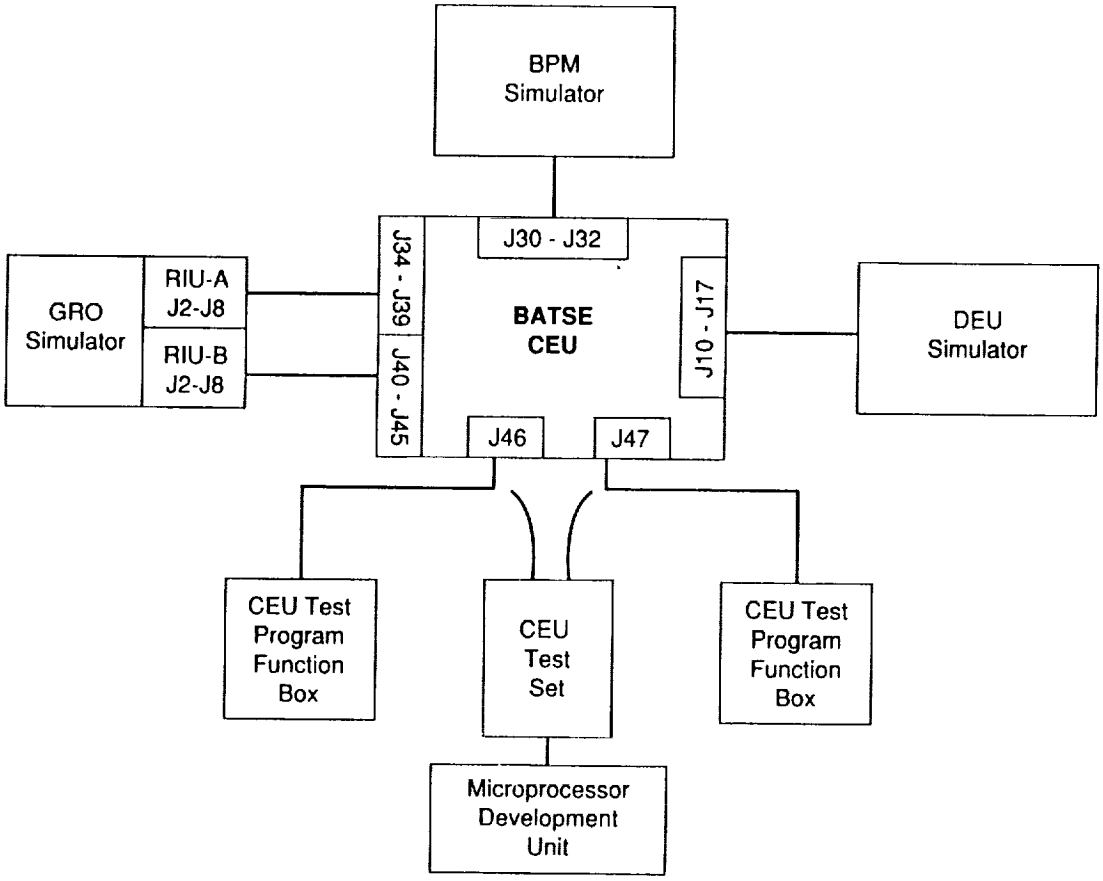

Figure 3.31. CEU Stand-Alone Testing Configuration.

a. CEU Assembly Procedure

The CEU assembly procedure was released under the number MSFC-PROC-1348. The CEU was assembled in a piece-wise fashion by installing one function at a time and executing a short test to verify the basic operation of the function and the CEU as it existed at the time. Each flight board was tested and verified inside the CEU breadboard, so that these tests were essentially a verification of the flight box and its wiring. To protect the flight boards from any damage caused by wiring errors in the flight box, CEU breadboard functions were tested first wherever possible.

This test was performed using several pieces of GSE, namely the BPM simulator, a GRO simulator, and a DEU simulator which emulated the eight detector modules. The BPM simulator provided power to the CEU for the test. An extensive CEU test set was also employed for this and most other CEU tests.

The CEU chassis backplane wiring was checked first, using a point-to-point continuity measurement using drawing #42A30412, the BATSE wire list for the CEU backplane. Both

BPM connectors (J30 and J31) were checked, along with the power routing to each of the board locations. Cable signal returns, cable shields to CEU chassis wiring, differential signal wiring, and all system logic signal wiring was tested.

After successful checking of proper CEU box wiring, the functions were installed, starting with the power control function (PCF). The BPM and GRO simulators were connected to J30 - J32, and J34 - J35, respectively. Table 3.65 details the boards installed and their locations for this portion of the test.

Table 3.65. Number and Location of Boards Installed During PCF Installation

Board Type	Board Number	CEU Location
PCF 1	42A30467-1	A1
PCF 2	42A30469-1	B1
PCF 2	42A30469-1	C1
PCF 2	42A30469-1	C2
BSF	42A30966-1	C3

After installation, the BPM simulator was powered up, and the proper voltage to the CEU was verified. At the GSE console, a program "CEUSTAT" was run. This program sent discrete commands to all of the CEU functions, to help verify that the function could be turned on and off with the proper discrete command. The power control was monitored by the test conductor who measured the voltage between pins A61 and B61 for each of the functions' board locations.

The BPM simulator was powered off after the PCF installation, and the CEU control function A was then installed. Table 3.66 details which CEU boards were installed here and which locations they went into.

Table 3.66. Number and Location of Boards Installed During CCF-A Installation

Board Type	Board Number	CEU Location
GROI	42A30964-1	A2
CCF1	42A30952-1	A3
CCFM	42A30962-1	A4
CCF2	42A30954-1	A5
CCF3	42A30956-1	A6
CCF4	42A30958-1	A7
CCF5	42A30938-1	A8
FIFO	42A30930-1	A9

After all boards were installed, a short test of the CCF-A function was executed. The CCF memory and watchdog timer were tested using the CEU test set. The interface between CCF-A and the GRO was verified, as was the HER burst memory.

CCF-B was installed following the completion of CCF-A. The hardware installed into the CCF-B function is identical to that of CCF-A, and the testing done to verify the function was exactly the same. Table 3.67 details the locations of the boards installed for the CCF-B function.

Table 3.67. Number and Location of Boards Installed During CCF-B Installation

Board Type	Board Number	CEU Location
GROI	42A30964-1	B2
CCF1	42A30952-1	B3
CCFM	42A30962-1	B4
CCF2	42A30954-1	B5
CCF3	42A30956-1	B6
CCF4	42A30958-1	B7
CCF5	42A30938-1	B8
FIFO	42A30930-1	B9

Following successful installation and checkout of the CCF-B function, the ADF was installed into the CEU flight box. Both ADF boards were installed at the same time with power off, and the eight DEU simulator cables were connected to J10 - J17 during installation. Table 3.65 lists the boards that were placed in the CEU during ADF installation.

Table 3.68. Number and Location of Boards Installed During ADF Installation

Board Type	Board Number	CEU Location
ADF	42A30940-1	A10
ADF	42A30940-1	B10

When these two boards were installed, a program was run with the CEU test set to verify the operation of the ADF. The results of the test were compared to satisfactory results included in the test procedure.

The DCH function was installed next in the CEU. Table 3.69 lists the 16 boards that were placed in the CEU flight box, and subsequently tested using an automated test program from the CEU test set.

Table 3.69. Number and Location of Boards Installed During DCH Installation

Board Type	Board Number	CEU Location
DCH1	42A30948-1	A21
DCH2	42A30950-1	A22
DCH1	42A30948-1	A23
DCH2	42A30950-1	A24
DCH1	42A30948-1	A25
DCH2	42A30950-1	A26
DCH1	42A30948-1	A27
DCH2	42A30950-1	A28
DCH1	42A30948-1	B21
DCH2	42A30950-1	B22
DCH1	42A30948-1	B23
DCH2	42A30950-1	B24
DCH1	42A30948-1	B25
DCH2	42A30950-1	B26
DCH1	42A30948-1	B27
DCH2	42A30950-1	B28

The sixth function installed into the CEU flight box was the MER/pulsar function. After installation, an automated test program was run from the CEU test set to verify that these functions were operating properly. Output from this test program was compared to the expected values which are listed in the test procedure. Table 3.70 lists boards that were installed in the CEU box for this function.

Table 3.70. Number and Location of Boards Installed During MER/Pulsar Installation

Board Type	Board Number	CEU Location
MPC	42A30944-1	A16
MPM	42A30934-1	A17
MPM	42A30934-1	A18
MPM	42A30934-1	A19
MPM	42A30934-1	A20
MPC	42A30944-1	B16
MPM	42A30934-1	B17
MPM	42A30934-1	B18
MPM	42A30934-1	B19
MPM	42A30934-1	B20
PSRB	42A30932-1	C17
PSRB	42A30932-1	C18
PSRB	42A30932-1	C19

The remaining functions, the TTS, the HER memory, TTE, and STTE, were installed following MER/pulsar. In a similar fashion, each of these four functions were tested individually before the next function was installed into the CEU box. Successful completion of the remaining four function installations marked the conclusion of the CEU assembly procedure.

Table 3.71. Number and Location of Boards Installed During TTS Installation

Board Type	Board Number	CEU Location
TTSC	42A30960-1	A13
FIFO	42A30930-1	A14
FIFO	42A30930-1	A15
TTSC	42A30960-1	B13
FIFO	42A30930-1	B14
FIFO	42A30930-1	B15

Table 3.72. Number and Location of Boards Installed During HER Memory and TTE Installation

Board Type	Board Number	CEU Location
FIFO	42A30930-1	C5
FIFO	42A30930-1	C6
FIFO	42A30930-1	C7
TTEC	42A30946-1	C8
FIFO	42A30930-3	C9
FIFO	42A30930-3	C10

Table 3.73. Number and Location of Boards Installed During STTE Installation

Board Type	Board Number	CEU Location
STTEC	42A30936-1	C11
FIFO	42A30930-1	C12
FIFO	42A30930-1	C13
STTEC	42A30936-1	C14
FIFO	42A30930-1	C15
FIFO	42A30930-1	C16

b. CEU Functional Test Procedures

Each of the CEU functions were verified after installation through the use of a test procedure designed to test the operation of one specific function. Thus each function had its own test procedure to run. These procedures were operated under the same general configuration as the CEU assembly procedure. The CEU was connected to the BPM simulator, its own test set, a GRO simulator, and simulators for the detector modules.

These procedures consisted primarily of automatic programs and computer sequences which autonomously tested the functionality of the CEU element under examination. Data were printed by the program and compared to acceptable results listed in the test procedures. These data are not of a form which is easily presented in a table, and most are of a binary pass/fail nature. For this reason, an extensive discussion of these test results will not be presented here. All other CEU tests involve additional pieces of flight hardware and will be presented in the instrument-level portion of this document. The procedures summarized in Table 3.74 are available for inspection in the BATSE data library.

Table 3.74. BATSE CEU-Element Functional Test Procedures

Procedure	Number
CEU PCF Functional Test Procedure	MSFC-PROC-1352
CEU GRO Interface Functional Test Procedure	MSFC-PROC-1353
CEU CCF Functional Test Procedure	MSFC-PROC-1354
CEU ADF Functional Test Procedure	MSFC-PROC-1355
CEU DCH Functional Test Procedure	MSFC-PROC-1356
CEU SDH Functional Test Procedure	MSFC-PROC-1357
CEU MP Functional Test Procedure	MSFC-PROC-1358
CEU TTS Functional Test Procedure	MSFC-PROC-1359
CEU HER/SHER Burst Memory Functional Test Procedure	MSFC-PROC-1360
CEU TTE Functional Test Procedure	MSFC-PROC-1361
CEU STTE Functional Test Procedure	MSFC-PROC-1362

C. BATSE Instrument Sub-Level Testing

Throughout the course of the BATSE test program, several procedures were executed involving portions of the complete BATSE instrument flight hardware. Most of these procedures involved the BPM, the CEU, and one or more detector modules. These tests were done to verify interfaces, check certain performance features on a small scale, or to obtain characteristics of behavior prior to the full-scale instrument test. In this section, each of these tests will be discussed, and results will be presented where applicable.

1. CEU-BPM Interface and Functional Test

This test, MSFC-PROC-1551, was designed to show that the CEU/BPM power control function could properly control the power of each BATSE detector module and BPM power supplies. In addition, the bi-level status provided to the GRO (simulator) and each BATSE data-packet was verified to be present for all CEU/BPM power control functions. The test further insured that the CEU and BPM could be controlled through either of the two RIUs, and that the CEU could measure the following housekeeping items:

- CEU +5 V voltage
- CEU +5 V current
- DEU +15 V current (sum of all detectors powered on)
- BPM power supply temperature

The CEU and associated GSE were configured as shown in Figure 3.31; however, the BPM simulator was replaced with the flight power module. With the BPM and GSE powered up, an automatic test program was started, and the results of this program were compared to the satisfactory results in the test procedure. Because the results of this testing are contained in a computer printout in the BATSE data library, they will not be discussed here.

2. Detector Module Interface Test

Following the completion of the detector module test program, an interface test was performed for each of the modules to verify compatibility and proper operation with the CEU and BPM. The test was a modified version of BATSE-ES-62-TP-100, the BATSE system engineering test. The detector module was connected to its proper ports on the CEU and on the BPM. The CEU and BPM were powered through the GRO simulator.

The BATSE system test software was started, and commands were sent to power up the module which was undergoing test. At power-up, the +15 V current was verified to lie within the region 200 mA ±50 mA. If the current exceeded 250 mA, the power would be removed from the module. No instances of overcurrent were present at the initial power-on of the detector module using the BPM and CEU.

Following power-up, each bit of each +HV supply was exercised through serial commanding. During the operation, the voltage and current readings in housekeeping were recorded. In this manner, the operation of serial commands, the operation of the +HV supplies, and any cross-talk on the command lines could be tested. Each of the modules performed flawlessly during this portion of the interface testing. Table 3.75 shows the recorded voltage and current housekeeping measurements for each bit of the +HV supplies on detector module BO.

Table 3.75. Housekeeping Values for Detector Module BO Interface Test +HV Supply/Cross-Talk Check

	High Voltage Command Setting (Hex)								
Mnemonic	01	02	04	08	10	20	40	80	
HV1VLT	1000	1005	1012	1028	1059	1122	1247	1497	(PMTA)
HV2VLT	999	1003	1011	1027	1058	1121	1246	1497	(PMTB)
HV3VLT	1000	1004	1012	1027	1058	1121	1247	1497	(PMTC)
HV4VLT	999	1003	1011	1027	1056	1120	1246	1497	(CPD)
HV5VLT	1001	1005	1013	1028	1059	1122	1247	1498	(SD)
HV1CUR	61.3	61.9	62.6	64.0	66.7	72.1	83.0	104.8	
HV2CUR	61.3	61.6	62.3	63.7	66.4	71.9	82.8	104.6	
HV3CUR	61.3	61.6	62.3	63.7	66.4	71.8	82.7	104.6	
HV4CUR	58.3	58.5	59.0	59.9	60.1	65.4	72.8	87.3	
HV5CUR	61.4	61.8	62.5	63.8	66.6	72.0	82.8	104.7	

Note: HVnVLT reading is in volts, HVnCUR reading is in μA.

After the proper operation of the +HV supplies was verified, an eight-set integration was obtained at nominal +HV through the CEU to determine the properties of spectra taken through the CEU. The nominal +HV values were taken from the TPS-59 procedure performed prior to

integration. This test marked the initial collection and printout of HER and SHER spectra from the flight module through the central electronics. Spectra were examined for consistency, accuracy, count rate, and other parameters. Two of the detector modules were integrated to the CEU prior to the repair of the "notch" anomaly described in section III.B.1.g(3)(b). This feature was present in the spectra taken through the CEU for these modules. The spectra obtained here were printed and are currently stored with the test procedure in the BATSE data library.

The next section of the integration test operated the programmable lower-level discriminators on the LAD and SD. Values of 08, 09, 0A, 0C, 10, 20, 40, and 80 Hex were used in the test. This checked each bit of the programmable LLD and also allowed for the test conductor to verify that no cross-talk was present on the command lines. At each discriminator setting, a one-set integration was obtained from the LAD and SD. Rates from the NaI and FAST discriminators were printed. After completion of the spectral accumulation, the data were printed out, and the next command value was tested.

A test of the LED followed the LLD check. The LED was commanded to a rate of 1 kHz, and spectral accumulations of one-set duration were obtained for LED amplitudes of 4, 5, 6, 8, A, C, E, F, and 0. As in previous tests, this verified the operation of the LED amplitude command bits and allowed for a calibration of LED to HER channel for the Detector Module under test. After this was completed, the LED rate was doubled to 2 kHz, and another integration obtained at amplitude 8. The rates were compared to verify that the number of counts in the LED peak was approximately double the first and that the peak channel was the same for both integrations. This test verified the proper operation of the LED frequency circuitry in the CEU and its coordinated operation with the flight detector module.

The final portion of the test placed the detector module into coincidence mode. A spectrum was accumulated for one set of HER data, and examined to verify that each channel had a low number of counts, and that all were less than the overflow channel 127. Inspection of the spectrum allowed the test conductor to determine if the coincidence circuitry was working properly. Temperature measurements and other HKG parameters were accumulated during this spectral integration. These parameters were compared to expected values and to the detector module environment to verify proper operation.

3. Detector Module EMC/EMI Tests

The detector module EMC/EMI testing involved the CEU, BPM, and detector module B1. This test was performed in the R/F test facility at NASA/MSFC in Building 4705. Testing was performed on April 1-2, 1988. The test consisted of four major parts: conducted emissions, conducted susceptibility, radiated emissions, and radiated susceptibility tests. These tests were performed to determine the effect of these operations at the module level and to give an indication of effects on the overall system performance prior to the full-scale system EMC/EMI tests. Testing was performed under the direction of the Test Laboratory, with BATSE personnel from Space Science Laboratory monitoring the effect of the testing on the hardware.

Conducted emissions and susceptibility tests were performed first. These tests involved sending positive and negative pulses on each lead of the power supply to determine any effect on the hardware performance. No anomalies were found in any of the conducted emissions or conducted susceptibility portions of the test.

A measure of the radiated emissions of the hardware was found to be 21 dB above specifications in the region near 1 MHz. This emission most likely stems from a clock in the CEU. After the exceedence was found, the detector module was powered off, and the test repeated with the CEU and the BPM. The out-of-limits condition was found to still be present with the detector module powered off. This excess of emissions near 1 MHz is not considered serious, and has not been found to affect the operation of any other piece of flight hardware on the instrument or the spacecraft.

The radiated susceptibility test proved to be the most difficult conditions for the hardware to properly operate. The CEU and BPM were not affected by the incident radiation; however, the detector module exhibited pronounced abnormalities in two particular frequency bands. The LAD and SD count rates and several HKG measurements were affected by the test. When the anomalies occurred, several deviations were made to the planned sequence of events to determine the extent of the R/F interference.

The first frequency range which exhibited problems was the band from 55 MHz to 65 MHz. The initial sweep of through this region at 2 V/meter produced excessive count rate indications in SFAST1, erroneous temperature measurements, and also produced a count rate deficiency reading in the LAD discriminator channels. Following the initial sweep, several iterations of the frequency range at different field strengths were done to isolate these problems. Nine additional sweeps were performed, each with a different purpose.

A second sweep in this frequency range was performed to see if the problem of excess counts appearing in the SFAST1 data could be repeated. This sweep reproduced the problem. The rate indication increased approximately 25% in the SFAST1 data when the problem existed.

The third iteration was done to determine the effect of this anomaly on the SHER data. A spectrum of SHER data was generated during the frequency sweep, and showed no visible anomalies. This is not a totally surprising result, for two reasons. First, the discriminator channel which shows the excess count rate indication lies below the threshold of the MQT generating the SHER spectrum. Second, the high rates only occur over a few packets. This time span is not long enough to have a large influence on the spectrum, because the integration time is much longer (typically 49 seconds).

A fourth sweep was done while logging data from the second SFAST channel in addition to the first. The first LAD FAST discriminator channel was also monitored. The LAD discriminator rate apparently dropped to zero near 56 MHz, while the SFAST1 rate apparently fell 50%. Near 62 MHz, the SFAST1 channel displayed an increase in count rate of nearly 25%. The SFAST2 channel also showed an apparent increase at this frequency.

The fifth iteration was done to determine the repeatability of the LAD rate drop near 56 MHz. Both LAD and SD anomalies were present in the fifth sweep. A sixth sweep investigated the effect on the HER data. Although the LAD and SD rate anomalies were repeated, the HER data spectrum was not noticeably affected in this frequency band.

Temperature values were examined in the seventh sweep of the frequency band. At 56 MHz, the housekeeping returned a value of 233 °C for the right radiator temperature, and -274 °C for the MQT temperature. Because of the multiplexed nature of the temperature telementry, it was difficut to obtain readings for all temperature measurements. Affected temperature values would only show an anomalous reading if the MUX were reading that particular sensor at the time of anomaly.

The eighth sweep in the range was done at a reduced intensity of 1 V/meter. No anomalous LAD or temperature data were found; however, the SFAST1 rate indicator showed an increase for one packet near 62 MHz. The ninth sweep increased the field strnegth to 1.5 V/ meter, and the SFAST1 rate anomaly increased in severity. No LAD or temperature anomalies were recorded at this field strength.

The final sweep was a repeat of the eighth sweep at 1 V/meter. Two packets of data showed anomalous SFAST1 rate indications near 62 MHz.

The second band of R/F which affected the operation of the module was in the region of 130 MHz to 155 MHz. The problems encountered in this region were similar to that of the previous frequency band. LAD and SD rates were affected, along with temperature measurements. The SD rates were more severely affected in this band than the previous one. After the initial anomaly identification, this region was re-swept in the manner described in the following paragraphs.

The second sweep was done to examine the effect of the anomaly on the SHER data. This was done in the same manner as before. At 146 MHz and 156 MHz, SFAST1 displayed a large apparent increase in the count rate. The increases were more intense and occurred over a wider frequency range than in the 55 - 65 MHz band. SHER data were not noticeably affected by the anomaly in the SFAST data. Temperature values were examined on the third sweep, and an anomalous event was received at 146 MHz.

The fourth sweep was executed at a reduced field strength of 1 V/meter. The SD was still profoundly affected near 154 MHz.

The frequency band tested here ended near 155 MHz. Because the anomalies were seen near the edge of the planned test region, a new band of 150-170 MHz was implemented. This allowed the BATSE test team to determine the upper frequency of the disturbance which became apparent near 154 MHz. A sweep in this region at 2 V/meter determined that the region in which the data were affected extended up to nearly 161 MHz. This region, from 154-161 MHz, was the most profoundly disturbing region of the entire EMC/EMI test. Two subsequent sweeps at 1

V/meter and 0.5 V/meter were done to determine the lower threshold field strength which would produce a problem. Both field strengths caused anomalies in the data. The final run, executed at 0.3 V/meter, did not generate any problems in the BATSE data.

These frequency bands were the only ones in which the BATSE hardware experienced any operational difficulties. During the full instrument EMC/EMI test, these bands again caused anomalous behavior from the BATSE flight hardware. A summary of the instrument EMC/EMI test is presented in a later section of the document.

4. BATSE Burst Trigger Verification Test

A test of the BATSE burst trigger was made in the clean room of MSFC Building 4705 during the first week of June 1988. Four detector modules, along with the CEU and BPM, were used for this test. To this point in the BATSE test program, all activations of the burst trigger were done through commands to the central electronics, or by signals from the LEDs contained in the detector modules. This test was done to verify that counting rates from a gamma ray source would produce the proper burst triggering response in the CEU. This test marked the first time that a radioactive isotope was used in the production of burst data. Chip Meegan and John Horack were the test conductors for this operation.

The four detector modules were placed on tables and arranged to each face in a different direction from each other. This arrangement replicated one hemisphere of the LAD octahedron configuration present on the GRO. A Cesium 137 isotope was placed at a height of approximately 300 cm directly above the center of the module arrangement. This isotope was housed in a metal box and could be exposed rapidly to provide the count rate change necessary for burst triggering. With the isotope in place, the four detector modules were powered on, and the background computations were made by the CEU. Subsequently, the source was rapidly exposed to the four detectors. The CEU successfully recognized the exposure of the source and properly triggered the "burst." Data were accumulated from the burst readout for the next 1.5 hours.

This short test was not the only test in which a burst was triggered through the use of a radioactive isotope. Other tests at the instrument and spacecraft level provided more comprehensive examination of the burst data generated and the contents therein. These tests are discussed in subsequent sections of this document.

D. Experiment Testing

The majority of the testing done on BATSE hardware took place under the full instrument configuration. These tests are also referred to as "system-level" tests. Eight flight detector modules, the BPM, and the CEU were used in these tests which occurred both on and off the spacecraft. The electrical configuration of the Instrument is the same as shown in Figure 2.13. Numerous "canned" procedures were used to test and calibrate the various facets of instrument performance. In this section of the document, these procedures will be discussed first, followed

by a summary of experiment testing off the spacecraft. The initial discussion of the procedures used will eliminate the need to describe them every time their results are presented. Procedures which were one-time-only tests, or which were related to a particular test (e.g., thermal vacuum) will be covered in the applicable section. System thermal vacuum testing will follow, with science testing, TRW testing, and KSC testing concluding this section. The overall presentation of material in this section is principally in chronological order.

1. Primary Instrument-Level Test Procedures

a. TP-100 Engineering Test

The BATSE engineering test (TP-100) was executed after each connection between the Detector Module and the CEU was established. The procedure was run with any number of modules connected to the CEU and also served as the detector module interface verification test (see section III.C.2). This procedure provided the most comprehensive examination of the BATSE interfaces and hardware operations and was used to test the flight cables prior to their shipment to Redondo Beach, California.

Testing commences after all electrical connections have been made. The interface between the CEU and the BPM has already been verified. The CEU is powered on, either through the GRO simulator, or by the spacecraft, depending on the configuration. After packet output and proper currents are verified, the testing begins.

The first section of TP-100 is iterated for each detector module in the configuration. With all other modules off, the first detector module is powered through the appropriate discrete command sequence, and all +HV is off. After completion of the power-on sequence, the +15V current is checked for the proper value. When all of the modules in the configuration have been checked out, they are powered up, and the total +15V current is verified for the number of modules under test. With all eight detector modules and +HV off, this current is approximately 1.5 A.

While all of the detector modules are on, every +HV supply in the configuration is tested. Starting with +HV supply A on the first module, serial commands are used to test each bit of the supply. For each of the commanded levels, the proper HKG return is verified. The entire instrument is monitored to ensure that the commanding of one +HV supply causes no interference or cross-talk or results in any other portion of the flight hardware. When all eight bits of the +HV supply have been tested and the HKG verified, the supply is left at command value 80 Hex, and the next supply is tested in the same way. Upon completion of all five supplies on the detector module, they are powered off, and the next module is tested. This rather long and tedious sequence ensures that each supply can be commanded to any of its 255 states and that commanding of a supply through serial commands causes no other unwanted effects in the instrument.

In the second section of the procedure, a comprehensive check of all LLDs is executed. All of the +HV supplies are commanded to their nominal values, and spectra are taken at LLD settings of 20, 21, 22, 24, 28, 30, 40, and 80 Hex. Each of these spectra are approximately 48 seconds in duration. As the LLD values are incremented, the spectra are examined to verify that counts are progressively being removed from the lower channels, as the LLD cuts off data from higher and higher energies in both the LAD and the SD. All detector modules are tested simultaneously.

The third section of TP-100 is an accumulation of a background spectrum. All +HV supplies and LLDs are commanded to their nominal values. The integration of HER and SHER data consists of eight sets of data, each approximately 48 seconds in duration for a total of slightly more than 6 minutes. Each of the accumulated spectra from the SDs and LADs are examined, printed, and stored to disk for later reference.

Part four of TP-100 consists of a test of the LEDs on each of the detector modules. The LEDs are commanded to a rate of 1 kHz by means of serial commands. Each bit of the LED amplitude command is then tested. At each level, a spectrum is accumulated from all LADs, and the peak channel is recorded from the spectra. In this manner, a mapping of LED command to HER channel is obtained. After exercising each bit and nine total command levels, the LED rate is commanded to 2 kHz. Another spectrum is obtained at amplitude 8. This new spectrum is compared to the previous amplitude-8 spectrum to verify that there are approximately twice as many counts in the LED peak at the 2 kHz rate than in the 1 kHz rate spectrum. This verifies that all bits of the LED command are operational, that the LED control circuitry is operating properly, and that the LED pulses are accounted for in the data.

Section five is the final portion of TP-100. The modules are commanded into coincidence mode, and a spectrum is accumulated from each. These spectra are examined to verify that the counts reflect data obtained in the coincidence mode. The test concludes with a collection of the two passive analog temperature measurements from each of the detector modules. These data are compared with the environment to verify correctness.

b. TP-105 - Detector Module Test

The detector module test, TP-105, is a test designed to check all detector module functions. Some of the operations performed here are also done in TP-100, but those here are not as extensive. Like TP-100, this test begins with a verification of +HV control. However, unlike TP-100, the supplies are all tested together. Each bit of each +HV supply command is tested, with all supplies operating simultaneously. Proper HKG return from the supplies is verified.

The LLD check in TP-105 is identical to that of TP-100, with values of 20, 21, 22, 24, 28, 30, 40, and 80 Hex being tested for all modules in the configuration. Following this portion of the test, the LLDs are returned to their nominal values.

As with TP-100, the LEDs are tested next; however, this portion of the test is not as extensive as the engineering test. LED amplitudes of 4, 5, 6, 8, and 0 are used in this test, and peak channels are recorded for each setting and module. The LED is operated at 1 kHz throughout the accumulation of all spectra, and no comparison of spectra with different LED pulse rates is done.

TP-105 concludes with a coincidence test and temperature check which is identical to that of TP-100. The primary motivation for TP-105 was to exercise all functions tested in TP-100, and verify their operation in a shorter time frame. TP-100 lasts nearly 10 hours, while TP-105 can be executed in about 2 hours.

c. TP-110 - Power-Up and Aliveness Test

As the name suggests, this procedure is used every time that power is applied to the BATSE instrument. The purpose of this operation is to bring BATSE to a nominal operating configuration from the power-off state and to perform a brief check of the instrument's major functions. The procedure contains three major sections, which must be performed in the order presented. Section one applies power to the BATSE instrument, and configures the GSE for reception of data from the flight hardware. Section two powers the detector modules and sets parameters to nominal values. The third section is a brief check of major functions.

After the GSE is properly configured, the system test software (STS) is started. At this point, the test conductor chooses the remote interface unit (RIU) through which the instrument is to operate. All CEU relays are then configured, after which the CCF, ADF, and TTU are selected. Primary or backup power is then applied to the instrument according to the configuration of the power relays. After power is applied either by a switch on the GRO simulator, or by the GRO test conductor, the +5 V current is monitored for any out-of-limit conditions. Heater power may also be applied in the first section at the discretion of the BATSE test conductor.

In the second section, the detector modules are powered on through discrete commands sent from the STS console. Following power, the LLDs and +HV supplies are commanded to their desired settings by the test conductor. All limit checking is subsequently enabled in the STS, and the test conductor verifies that there are no out-of-limit conditions.

The final section of the procedure is the aliveness test. All analog housekeeping values are examined for acceptable readings. These values include detector module +HV voltages and currents, module low voltages, temperature readings, and instrument currents. A printout of all values is produced. LAD and SD discriminator (FAST and SFAST) rates are examined for proper operation. PLASTIC and NAI rates are examined in the same manner. Science data are examined for the proper content of an HER or SHER spectrum, and the auxiliary data are checked to verify that the correct start and end times are present. Continuous data are also examined for proper content. If no error conditions exist, the LED is commanded to an amplitude of 4, and a rate of 1 kHz. A 48-second spectrum is accumulated from each of the

LADs and SDs. This spectrum is printed out, and the peak channels of the LED are recorded from the LAD spectra. At the conclusion of the test, the LED is powered off.

Through the use of TP-110, the BATSE instrument can be taken from a state of complete power-off to a nominal operating condition in approximately 20 minutes.

d. TP-120 - Coincidence Test

The purpose of TP-120 is to verify that count rates exceeding the burst trigger threshold occur at the expected rate for statistical fluctuations. This insures that the burst trigger thresholds are being computed correctly, and that the large area detectors do not exhibit spurious high counting rates. The test begins by setting the burst trigger levels to one of several options, depending on the length of time available for the test. With the instrument powered up and running, the STS is set to accumulate counts of the parameter EXFLAGS, which is the count of individual detectors above burst threshold. The STS also is set to accumulate COINC, which is the count of instances when two or more detectors exceed burst threshold simultaneously. These values are collected for the entire duration of the test.

After accumulation of the data, the average background rate from each LAD is determined for each of the three triggering time scales (64 ms, 256 ms, and 1.024 s). These rates are compared to the computed thresholds. The number of standard deviations for each threshold is computed. The values obtained are slightly lower than the prescribed values because of round-off in the calculations. The average number of detector sigmas is entered into the table.

The mean time between accidental triggers for one detector and coincidence triggers in two or more detectors is computed from an assumed Poisson-like background distribution for each time scale . The expected number of accidental triggers is then found by multiplication of the expected rate by the time duration in which EXFLAGS were accumulated. The number of observed single detector and coincidence triggers are verified to lie within 3σ of the number expected.

This test can last anywhere from 1 to 8 hours, depending on the time available.

e. TP-125 - Background Run

TP-125 is a brief and simple procedure which instructs the test conductor to accumulate a background spectrum, print it out, and store it onto disk. This test was often run simultaneously with TP-120 when time permitted. The duration of the integration is left to the discretion of the BATSE test conductor.

f. TP-140 - Long Calibration

The long calibration (TP-140) is designed to provide a complete energy calibration of all large area and spectroscopy detectors. This test serves as the primary calibration procedure outside those science tests performed at MSFC and TRW with express calibration purposes.

With all detector modules powered in nominal configuration, the test starts with the accumulation of a 40-set background spectrum. The duration of this integration is approximately 32 minutes. After background acquisition, the spectrum from each of the detectors (LAD and SD) is stored onto disk for future reference. A small, 1 μCi sample of Ba 133 is then placed in front of each of the detectors. The location is approximately 50.8 cm from the LAD, and on axis. In several instances, the precise location of the isotope with respect to the detector was difficult to discern because of the presence of the multi-layer insulation blanket. A similar 40-set integration is obtained during the time the Ba 133 sources are in place. All eight modules are tested simultaneously. The spectra are stored to disk, and the process was repeated for Cd 109, Co 60, and Cs 137 isotopes.

After the completion of the Cs 137 40-set spectrum, single-PMT spectra are obtained for each of the 12.7-cm PMTs on all eight LADs at nominal +HV settings. The Cesium isotope remains in place for these spectra, which are approximately 16 minutes in duration. When this spectrum is completed, high voltages are raised by 100 V across the board, and another Cs 137 spectrum is accumulated. From these spectra, the PMT exponent (% gain change divided by % high voltage change) for each LAD tube is calculated.

The CPD calibration section is performed next in the test sequence. With the Cs 137 isotope still in place, CPD rates are obtained from each of the detectors at eight different voltage settings. In this manner, a plot of rate vs. +HV is constructed for each of the CPDs. The location of the Cs 137 peak in the rate plot allows the test conductor to locate the threshold of the CPD in energy and adjust the +HV if necessary.

After calibration of the CPD, another 40-set background spectrum is obtained with all PMTs commanded to nominal +HV values. The final section of TP-140 is the LED calibration. In this segment, the LED rate is commanded to 1 kHz, and each of the 16 amplitudes are utilized. At each amplitude, a spectrum is accumulated and the peak channel recorded into a data table. In this manner, a determination of LED location in HER channel space is determined for each of the possible LED amplitude settings.

TP-140 normally takes 6-8 hours to execute.

g. TP-150 - Short Calibration

As the name indicates, this test provides a short calibration of the LAD and SD for each detector module. The spectra accumulated in the first section of TP-140 are repeated in this test; however, the duration of the integrations is only 16 minutes instead of the 32-minute runs from

the previously described test. The LED, CPD, and PMT calibrations are not exercised during TP-150. Usually, this test was not run during the same period of test time in which TP-140 was executed. TP-150 lasts approximately 2 hours.

h. TP-170 - CPD Calibration

TP-170 consists of a collection of eight, 5-minute spectra from the LADs while operated in the coincidence mode with the CPDs. For each of these eight spectra, the CPDs are commanded to a different +HV value. During the time of spectral accumulation, a count rate vs. +HV plot can be constructed. This method is identical to the CPD calibration detailed for TP-140. From the rate plot, the BATSE test conductor can determine the location of the CPD threshold, and determine if the +HV requires adjustment. Table 3.76 shows the +HV values used in the eight spectral accumulations and rate determinations.

Table 3.76. CPD +HV Values for Rates Obtained in TP-170

CPD Run	+HV Value for CPDs
CPDHV1	Nominal +96 V
CPDHV2	Nominal +32 V
CPDHV3	Nominal +16 V
CPDHV4	Nominal
CPDHV5	Nominal -16 V
CPDHV6	Nominal -32 V
CPDHV7	Nominal -64 V
CPDHV8	Nominal -96 V

i. TP-171 - CPD/LAD Coincidence Run

TP-171 is executed in order to verify proper operation of the coincidence and anti-coincidence mode circuitry on each of the eight detector modules. The test proceeds very much like the CPD test done in TPS-59 at the detector module level. The +HV on all modules is commanded into nominal states, and LADs are in anti-coincidence mode to start the test. An 8-set integration is accumulated and stored to disk for later reference. Next, the CPDs are all powered off, and the integration sequence is repeated. The first spectrum is subtracted from the second, with the difference in counts in the upper channels coming from the lack of CPD rejection. From the number of counts in these upper channels, and the duration of the integration, an average CPD rejection rate is computed. The final spectrum is accumulated with the LAD and CPD in coincidence mode. The +HV on the LAD is sufficiently low so that muons are brought onto the scale of the MQT. From this coincidence spectrum, the counting rate in the LAD above an energy near 0.6 x muon deposition energy can be computed. This counting rate is compared to the CPD rejection rate for each of the eight modules. At the conclusion of the test, all parameters are returned to their nominal values. The duration of TP-171 is approximately 30 minutes.

j. TP-180 - Burst Data Test

The burst data test serves the purpose of verifying the proper operation of the BATSE burst data types. The data types checked in this test are DISCSC, PREB, MER, TTS, TTE, STTE, HERB, and SHERB. There are three options for this test.

Option 1 creates a burst in detectors B0 and B1 and keeps burst storage parameters at their default values. Option 2 produces a burst in detectors B2 and B3 and optimizes the parameters for weak bursts. The final option creates a burst in detectors B4 and B5, while optimizing the parameters for a strong burst.

After selecting the option desired, the BATSE test conductor turns on the LEDs to verify their presence in the burst trigger channels (FAST2 and FAST3). Revisions to the LED amplitudes can be made if necessary. The LED is then turned off.

The burst is triggered by a command file which enables the burst trigger, turns on the LEDs in the proper detectors, decreases the LED frequency by 1000 counts per second every 10 seconds, and finally turns off the LED after 100 seconds. The burst readout is then accumulated to archive tape for post-processing analysis. In this analysis, the test conductor examines the burst readout for several features.

The first packet of the burst readout (DISCSC) is examined to verify that the burst trigger time (rise in rate) is contained and visible in the packet. The location of the LEDs in the continuous (CONT) data is recorded. The pre-burst (PREB) data are compared to LAD discriminator rates previous to the burst trigger for all eight detector modules to verify that the PREB count rate is approximately 1/16 of the LAD discriminator rates. The PREB data type contains four-channel data rates per 0.064 second for all modules. All 16 MER channels are examined to verify that only those channels which contain LED counts in CONT data also contain counts from the LED in MER data. Furthermore, the MER data are examined to verify the proper number of LED counts both before and after the change in integration time. TTS data are examined by the BATSE test conductor to verify that the LED is appearing in the proper discriminator channels and that the time to spill in these channels is much shorter than in channels without the LED. HERB and SHERB data are examined for proper detector output and time scale parameters. The TTE data are examined to verify that the first quarter of the memory contains data from all detectors prior to the burst, and also to verify that the final three quarters contain data only from those burst-selected detectors. Lastly, the STTE data are examined for proper data content.

Each iteration of TP-180 requires approximately 1.5 hours to accumulate and 30 minutes for data analysis. Customarily, all three options were executed during a set of functional testing.

k. TP-188 - Coordinated BTS/SF Signal Test

TP-188 is the only BATSE standard test which requires the cooperation of the other experiments on the GRO. The test is executed primarily to verify the function of the GRO burst trigger signal and solar flare trigger signal. Solar flare parameters in the BATSE CEU are set to "don't care" values for this test. With other instruments on-line, a burst is triggered using the LED in the sun-facing detectors. The burst trigger signal and the solar flare trigger signal are thereby activated. Start times and load times of the triggered burst are provided to the other experimenters by the BATSE test conductor. Redundancy in these signals is tested by switching BATSE over to ADF-B and repeating the test when the other instruments are ready. The entire duration of each signal test is approximately 10 minutes, with 30-35 minutes between the A and B side tests due to the other instruments' reconfigurations. This procedure is done for every spacecraft functional test.

l. TP-190 - Pulsar Data Test

As the name suggests, the pulsar data test is designed to verify proper generation and output of pulsar data. Pulsar data are accumulated into both memories at the LED rate and then read out in the output schedule. The BATSE test conductor then examines these data in the post-processing mode to verify the proper data parameters. This test has two options, each of which exercises the A and B pulsar memories, but alternates the source of the data (i.e., LAD or SD). Option A patches data from LAD B0 and B1 to the A memory, while patching SD B6 and B7 to the B memory. All LEDs are on, with B0 and B1 set at amplitudes of 4 and 5, respectively. All other LEDs are at amplitude F. In this manner, incorrect patching of LAD data into the memory would easily be identifiable in the upper pulsar data channels. Option B is similar; however, LAD B4 and B5 are patched to the B memory, and SD B2 and B3 are patched to the A side. The eight LEDs are again on, with the unused LEDs at amplitude F. B4 and B5 LEDs are commanded to amplitudes of 6 and 7, respectively.

After collection of the data, the BATSE test conductor determines the CONT data channels in which the LED appears for all eight LADs. The pulsar data are then examined to verify that LED counts appear only in the pulsar data channels which correspond to the CONT data for the selected detectors. All other pulsar data channels are verified to be void of LED pulses. Furthermore, the pulsar data are counted to verify the proper number of LED pulses in the correct channels given the pulsar parameters in place during the accumulation.

The entire pulsar data test lasts approximately 20 minutes per option, including data reduction time. Customarily, both options are executed during BATSE functional testing.

m. TP-192 - Pulsar Clock Frequency Calibration

TP-192 is a test devised to determine the difference in frequency between the GRO spacecraft clock and BATSE's internal pulsar clock. The test procedure was developed in May 1989 for initial use in the GRO thermal vacuum test later that summer. That opportunity allowed

the BATSE team to determine the behavior of the two clocks as a function of temperature. Since that time, this procedure is executed as a standard portion of the BATSE functional test sequence.

The test begins with the sending of a command file to create the proper test environment. Pulsar data are accumulated at a period of 1 second with 1000 scans. After accumulation, the data is read out in the full-A data type. At the completion of the data accumulation and readout, the pulsar auxiliary data are examined. The auxiliary data contain both the start and end time for the pulsar accumulation, according to the spacecraft clock. According to the BATSE clock, the time of accumulation is exactly 1000 seconds. The GRO clock, however, is slightly different. The elapsed time on the spacecraft clock is computed simply by subtraction of the auxiliary time words. The ratio of these two clock values yields the frequency percent difference.

Results from this test are presented throughout the remaining portions of this document, with the most interesting results obtained in GRO thermal vacuum testing. Because BATSE has two independent clocks in CCF-A and CCF-B, the test is usually done on each side during functional testing. The duration of this test is approximately 20 minutes.

n. TP-195 - Data Consistency Tests

TP-195, the data consistency test, is the procedure through which the BATSE test conductor can verify that summations of BATSE data packets over identical energy and time intervals yield consistent detector counting rates, within the precision permitted by the data collection time. Because BATSE has a large number of different data types, each with varying temporal and energy ranges, it is important to verify that each data type is consistent with the true incident counting rate at the detector and that each data type is consistent with all of the others.

BATSE is placed into a normal operating mode, at nominal +HV and LLD settings. Large area detector rates are compared to NaI and PLASTIC rates to verify that the anti-coincidence circuitry is operating properly. A commanded burst is then executed to generate all of the burst data types for later analysis. Following a complete burst readout (1.5 hours), pulsar data are generated, along with several dumps of the instrument memory.

After the data are collected, the test conductor unfolds each of the data types off-line and examines them for consistency with the incident counting rate in the desired energy region and for consistency with all other data types.

o. TP-199 - End of Shift Procedure

This test procedure allows the BATSE test conductor to power down the instrument, save all data to tape or disk, and power off the IGSE in an orderly fashion. The test leaves the BATSE flight hardware in a power-off configuration which is suitable for the initiation of operations again through TP-110. Usually, the BATSE test conductor can perform an orderly shut-down of the instrument in approximately 5 minutes. Because this test does not produce any unique data or results, most executions of this procedure are not on file in the BATSE library.

p. TP-200 - Power Control Functional Test

TP-200 is the test by which each of the power control function (PCF) relay switching circuits and status verification circuits are exercised and validated. Each of the PCF relays in the CEU are configured into the primary and redundant on/off states through commands sent from the GSE. After each command file is executed, the status response in the BATSE packet data, and in the GRO spacecraft engineering telemetry, is verified. At the conclusion of this test, all relays are left in the nominal configuration.

The procedure begins with BATSE powered on and operating through RIU-A. A command file to set all relays to nominal positions is executed, and the telemetry response is verified correct. In this configuration, all CEU boards are powered on, with the exception of the alternate ADF. Detector modules are off. After a nominal starting configuration has been established, the ADF functional element is tested. ADF-B and ADF-A are both powered individually into their primary and redundant configurations. A similar mode of testing is used for the detector modules, followed by DCH/SDH functions, MER/PSR memory functions, PSR-B memory functions, STTE/HER functions, SHER and MPC functions, the TTE function, CCF-A and CCF-B, steering and control relays, and finally primary and backup power.

After completion of the test, the instrument is switched to utilize RIU-B, and the entire procedure is repeated. TP-200 lasts approximately 1.5 hours and exercises each of the relays in the CEU to all primary and redundant power configurations.

2. Engineering and Qualification Tests

The primary engineering and qualification tests performed on the BATSE hardware were done for detector module integration verification and flight cable testing and to allow the BATSE team to become familiar with the operations of the hardware and associated procedures. These operations were executed during the time period of May-June 1988 and were performed in MSFC Building 4705. Preparations for the upcoming system-level EMC/EMI and thermal vacuum tests were being made, and no other types of testing were planned for this period. The integration of detector modules into the system was discussed in section III.C.2 and will not be repeated here.

Fabrication constraints on the GRO spacecraft required that the BATSE flight cable harnesses be delivered to TRW in California and installed onto the GRO a significant period of time before the remainder of the instrument. On May 20 and 21, 1988, the BATSE team performed a full test of the flight cable harnesses which connect the BPM and CEU to all eight detector modules. The TP-100 procedure was used for this test. Through this test, the BATSE team verified pin-to-pin continuity and isolation for each of the harness sets, and also verified that no cross-talk existed in any of the cables. The flight cables had previously been thermal cycled and vacuum tested. They received thermal vacuum testing in conjunction with the rest of the GRO spacecraft and BATSE instrument during the GRO thermal vacuum test in July and

August 1989. This execution of TP-100 marked the final use of the flight cables during the BATSE test program until installation of the flight hardware onto the GRO spacecraft.

The BATSE team used the remainder of this time period to become familiar with the operations and procedures surrounding the BATSE flight hardware test environment. The IGSE system had to be learned, and significant bugs needed to be worked out. Development of the procedures detailed in section III.D.1 was done at this time. Execution of the procedures showed the BATSE team where changes needed to be made for future iterations of a particular test.

All test results and data from this period are on file in the BATSE data library. No results are presented here because of the exploratory and deterministic nature of the operations performed during this test time.

3. System-Level EMC/EMI Testing

The BATSE system-level EMC/EMI test was performed in July 1988 in the MSFC R/F test facility located in Building 4705. The flight hardware was moved from the clean room facility in which the engineering and qualification testing had been done, and all interfaces were re-mated. After reintegration of the hardware, a complete TP-100 was executed to verify that the connections had been made properly, that no damage to the hardware had been done during the transport, and to insure that the instrument was ready to proceed with the environmental test at hand.

The EMC/EMI test proceeded much like that of the module-level testing described in section III.C.3 of this document. This operation determined the effect of conducted emissions, conducted susceptibility, radiated emissions, and radiated susceptibility tests on the entire BATSE instrument, operating as one unit. As with the previous EMC/EMI tests, the operations were directed by personnel from NASA/MSFC Test Laboratory, with Space Science Laboratory personnel monitoring the instrument for any anomalous effects.

Conducted emissions and susceptibility tests were executed first, producing the same results as the module-level test. Signals were injected onto the positive and negative leads of BATSE power lines with frequencies ranging from 30 Hz to 50 MHz with no noticeable effect on the instrument performance or operation.

Radiated susceptibility tests again caused anomalies in the instrument performance at several frequencies. This portion of the testing was conducted with the entire BATSE instrument bathed in R/F radiation at a strength of 2 V/m. The first two frequency bands, 14-150 kHz and 150 kHz-15 MHz, produced no anomalous effect on the operation and performance of the hardware. This result was consistent with the previous sub-system EMC/EMI test results. The third frequency band ranged from 15 to 220 MHz. In this region, numerous anomalies in rates and temperature readings were found, like those in the module-level test. Erroneous temperature readings began near 42 MHz, and were present through 220 MHz. The field strength of the incident radiation was lowered to 0.5 V/m, and the test was repeated. At this lower intensity, no

anomalous rates or temperature readings were observed. The system-level results in this region differed from those of the module-level test in the sense that the anomalies occurred over a slightly larger frequency band (42-220 MHz). In the detector module test, the susceptible regions were confined to 55-65 MHz and 130-155 MHz. Presumably each of the detector modules are susceptible near these frequencies. However, each of the detector modules have slightly different properties, such as the length of the temperature sensors, exact configuration of cabling, R/F environments, etc. These differences most likely lead to variations in the particular frequencies at which each module is susceptible. When all of the modules are combined into a system, one expects a band of frequencies over which the entire Instrument shows susceptibility.

Radiated susceptibility tests continued up to frequencies of 15 GHz with no further anomalies, and the region from 42 to 220 MHz was the only one in which difficulties occurred. Because this behavior had been seen before, and was an acceptable condition, no further attention was directed toward investigating the details of the behavior. Results from the system-level EMC/EMI test are available for inspection in the BATSE library.

4. BATSE System-Level Thermal Vacuum Test

a. Test Overview

The BATSE system-level thermal vacuum test was conducted in the Sunspot Space Simulation Chamber located in MSFC Building 4619. The chamber was closed on August 1, 1988, and the test was scheduled to last 8 1/2 days. Problems with the flight hardware, repair, and retesting caused extensive delays. BATSE successfully completed thermal vacuum testing on September 27, 1988. During the test, the detector modules were exposed to six temperature cycles between 0-35 °C, while the CEU and BPM were cycled twice between -10 °C and 50 °C. Temperature rates of change were kept below 5 °C per hour, and temperature soaks were executed at each extreme for a minimum duration of 4 hours after stabilization. The protoflight module did not participate in this test. During most of the hot-to-cold transitions, BATSE power was removed to expedite the test. Figure 3.32 displays the temperature profile of the BATSE thermal vacuum test.

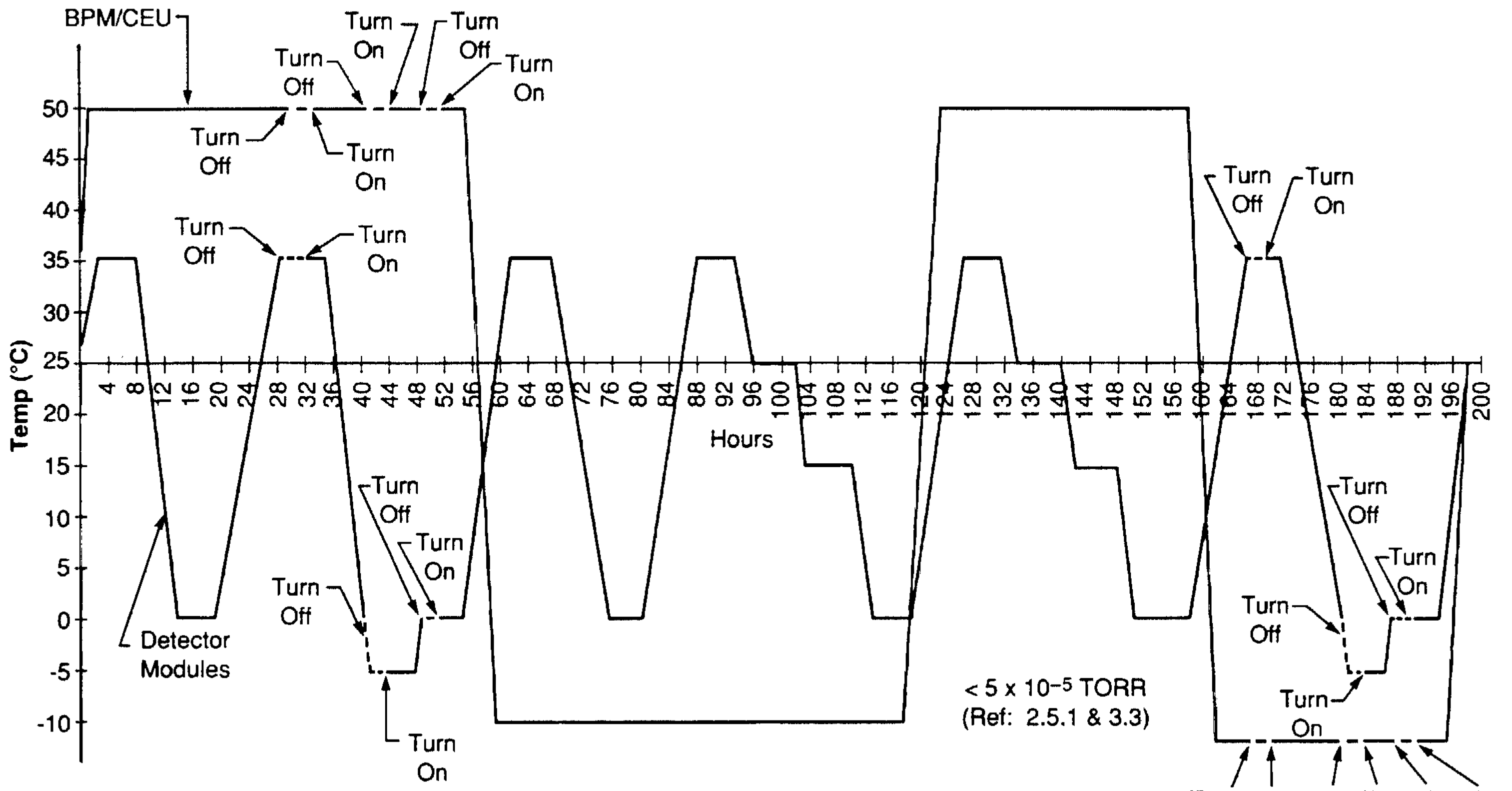

Detector Modules

Ramp rate ≤ 5°C/hr; soaks at extreme temperatures after stabilization for 4 hours minimum
6 Cycles 2 normal; 2 hot starts; 2 cold starts (1 of each with BPM/CEU hot and 1 of each with BPM/CEU cold)
MLI blankets on; at low temperature turn-on operate for 1 hour then raise temperature to 0°C
2 Calibration cycles (1 with BPM/CEU hot, 1 with BPM/CEU cold)
Calibrations at +35°C, +25°C and 0°C stopping on hot to cold transition

BPM/CEU

Ramp rate ≤ 20°C/hr

Figure 3.32. BATSE System Thermal Vacuum Test Temperature Profile.

Three separate tasks were to be accomplished during this testing. The first was to verify the proper operation of all BATSE hardware throughout the desired temperature range, and under vacuum conditions. Second, the BATSE team obtained calibrations on temperature-dependent portions of the instrument behavior. Temperature soaks and plateaus were added to the timeline to aid in the acquisition of calibration data. Third, and somewhat less important, the T/V test offered the opportunity to execute additional testing which the science team desired, but were not necessarily temperature or vacuum related.

The mechanical configuration of the chamber system, the flight hardware, and associated GSE took nearly 2 weeks to complete. Each detector module was fitted with its flight thermal blanket, numerous test-only heaters, and temperature sensors. Because of limited space in the chamber, the detector modules were placed in specially fabricated support racks which supported two modules each, one above the other. In this configuration, the centers of the two module LADs were separated by a vertical distance of 118.25 cm (46.55"). Once the detector modules were installed, the rack was lifted with a crane and placed into the chamber. Figure 3.33 details the configuration of BATSE hardware inside the sunspot chamber.

The CEU and BPM were mounted to a cold plate which was separate from any detector module support MGSE, and placed onto the floor of the chamber. The modules were arranged to face the center of the chamber where a small calibration source was located. This source was contained in the same canister which was used for the protoflight thermal vacuum test. However, no motor drive or movable apparatus was included. The isotope used was 1.105 μCi of Na 22, shielded with 0.686 cm (0.270") of lead. Combined with a location in the center of the chamber approximately 70° off-axis from the upper detector modules, at a distance of approximately 122.5 cm, the source simulated the anticipated on-orbit strength of the 511-keV line, while providing each of the eight large area detectors with approximately the same flux. In this fashion, the BATSE team could obtain a feel for the difficulty of balancing the LAD PMTs using the on-orbit 511-keV line.

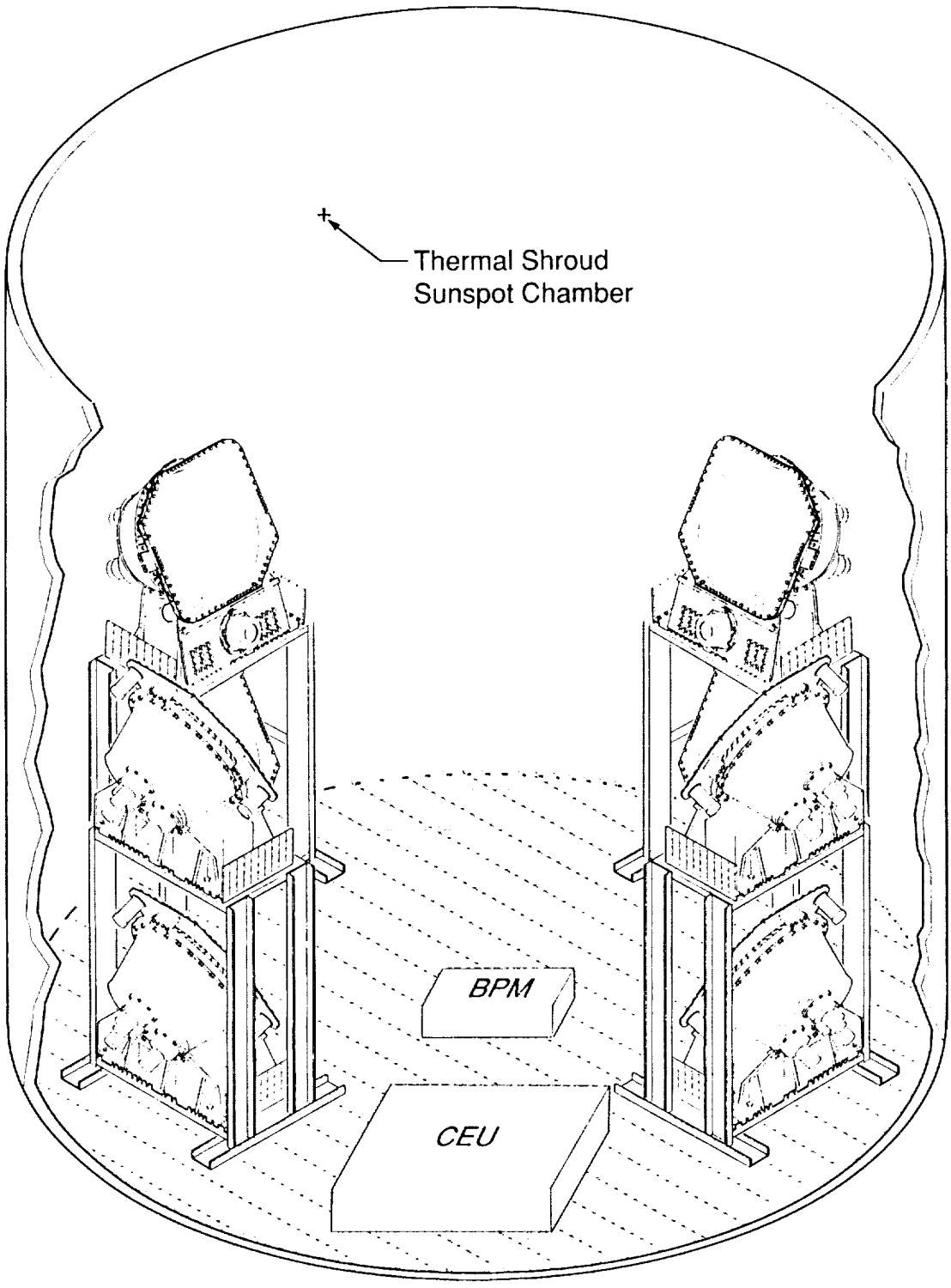

Figure 3.33. BATSE System Thermal Vacuum Test Chamber Configuration.

b. Test Flow and Description

(1) Pre-Test Checkouts

Mechanical and electrical configuration of the BATSE flight hardware and associated GSE was completed on July 29, 1988. At this time, a functional test of the BATSE instrument was done prior to the start of the test to validate all electrical interfaces, and to again verify the instrument readiness to begin the thermal vacuum test. CEU and BPM stand-alone functional tests were executed with no anomalies. BATSE personnel from Space Science Laboratory then proceeded with a full eningeering test (TP-100), checking all detector module interfaces and performance. Results from these tests are on file in the BATSE library. The flight hardware was declared ready for chamber closure at 7 p.m. on August 1, 1988.

(2) Thermal Cycle #1

The thermal vacuum chamber evacuation began shortly after readiness was declared on August 1, 1988. BATSE power and high voltage remained on throughout the entire pumpdown phase of the test. This was done to validate the potted +HV system, which was designed to be able to operate in the corona region. No anomalies associated with the +HV were evident during the initial pumpdown phase. At 3- hour intervals during the first cycle, and throughout the remainder of the test, BATSE personnel executed BATSE-ES-62-TPS-63, the BATSE thermal vacuum monitoring procedure. The test allowed for the collection of temperature-dependent calibration data and to verify that the instrument state-of-health was acceptable during the test. TPS-63 begins with power already applied to the hardware and the instrument in normal operating conditions. The LEDs are commanded to predetermined amplitudes, and a 16-set integration is obtained. Rates, voltages, and other pertinent data are printed for archival purposes.

Six iterations of TPS-63 were executed prior to arrival at 35 °C. The hot-case temperature was reached at 11:15 a.m. on August 3, 1988. After a 1-hour soak at this temperature, BATSE personnel executed a short functional test sequence which included TP-110 and TP-105 (see sections III.D.1.b and III.D.1.c for a description). In addition, two other tests were performed. TPS-65, the BATSE thermal vacuum source resolution procedure test, was executed by placing a Ba 133 source and a Cs 137 source on the top of the chamber, and obtaining 8-set integrations of each. These sources were 10 mCi and 2 mCi in strength, respectively, and were the same isotopes used in the BATSE angular response calibration (TPS-19). A background spectrum was also obtained, subtracted from the two source spectra, and all were stored to disk. The second additional test procedure was TP-156, a PMT gain and gain-exponent measurement. This operation is identical to the PMT measurements made in TP-140; however, here, the small Na 22 source in the center of the chamber was used. All spectra collected in this test were also stored to disk for future reference. These two procedures were executed at all temperature plateaus throughout the test. During this thermal cycle, RIU simulator A was used, as was the primary GRO power input.

Table 3.77. BATSE System T/V Test Cycle #1 Important Events

Date	Time	Event
8-1-88	19:00	Begin pumpdown of thermal vacuum chamber
8-2-88	17:00	TPS-63 first iteration
8-2-88	--------	CPD rates on several modules low (near zero)
8-3-88	11:15	Arrive at 35 °C, begin 1-hour soak
8-3-88	12:15	Begin short BATSE functional
8-3-88	15:45	Complete short functional, begin transition to cold
	-- Power off during cold transition --	
8-4-88	11:45	Arrive at cold-case temperature (0 °C)
8-4-88	12:45	Begin short BATSE functional
8-4-88	16:45	Complete short functional, begin transition to hot
8-4-88	20:00	PMT C on DM 0 (B6) enters overcurrent, powered off
8-5-88	01:00	CPD rates begin to normalize, apparent improvement
8-5-88	04:00	Complete Cycle #1

Two major anomalies were uncovered during the first cycle of the test. The CPD rates on nearly every module were extremely low, in many cases at or near zero in any one second interval. This anomaly was found later to be caused by insufficient venting of the CPD. Gases trapped inside the CPD placed pressure on the PMT and wave washer, causing a separation of the PMT face and the optical coupling. This anomaly, the CPD vent repair, and re-qualification are discussed thoroughly in section III.A.3.c.

The second major anomaly in this thermal cycle was the manifestation of a high voltage problem in vacuum conditions. At 20:00 on August 4, the BATSE test conductor on duty noticed an overcurrent condition in PMT C on detector module DM #0 (later B6). This anomaly was caused by a +HV breakdown somewhere in the PMT supply cable system. The +HV supply was powered off immediately. For the remainder of the test, PMT C on DM #0 would operate in an intermittent fashion.

(3) Thermal Cycle #2

Cycle #2 began at approximate 04:00 on August 5, with the transition through 25 °C. By 11:00 on the same day, the final hot-case temperature of 35 °C had been reached, and BATSE was powered off for a 2-hour soak. At 13:00, BATSE was powered to configure power relays for GRO secondary (backup) power. After reconfiguration, the instrument was turned off for a second 2-hour soak period. At 15:00, the second hot-case functional test was performed.

Table 3.78. BATSE System T/V Test Cycle #2 Important Events

Date	Time	Event
8-5-88	04:00	Begin Cycle #2 at 25 °C
8-5-88	11:00	Power off -- arrival at hot plateau
8-5-88	13:00	Power on to reconfigure for backup power, power off
8-5-88	15:00	Power on, begin short BATSE functional
8-5-88	16:15	CPD DM #7 (B7) high voltage anomaly
8-5-88	19:00	Complete short functional, begin transition to cold
		-- Power off during cold transition --
8-6-88	11:15	Arrive at cold-case temperature (-5 °C)
8-6-88	16:15	Power on, configure for primary power, power off
8-6-88	18:15	Begin short BATSE functional
8-6-88	20:30	Complete short functional, begin rise to 0 °C
8-7-88	03:45	Arrive at 0 °C, power off for soak
8-7-88	05:45	Power on, configure for backup power, power off
8-7-88	07:45	Begin long BATSE functional
8-7-88	15:40	Finish long functional, switch to RIU-B, CCF-B, ADF-B, TTU-B, begin rise
8-7-88	21:00	Enable automatic fain control
8-8-88	00:30	Complete Cycle #2

At the hot-case plateau, a short BATSE functional test was performed, following a 2-hour soak period at 35 °C. The subsequent cold transition terminated at -5 °C, 5° lower than the previous cold temperature. This lower temperature was a planned phase of the thermal vacuum testing. A short BATSE functional was executed at this temperature, after which the temperature was raised to 0 °C. Following a 4-hour soak at 0 °C, an extensive functional test of the BATSE instrument was performed. Functional testing here included iterations of TP-110, TP-105, TP-170, TP-171, and TP-120. The results from these tests are on file in the BATSE library. When the long functional was complete, all BATSE subsystems were switched to the B-side, and the temperature transition to hot-case was started.

One major anomaly was present during the second thermal cycle. The CPD on detector module DM #7 (B7) suffered high voltage breakdown. The anomaly was the second high voltage problem encountered under vacuum conditions during the test. This failure manifested itself through a current-limiting condition in the +HV circuit and a tremendous jump in the registered counting rate from the CPD. Behavior similar to this was seen during the previous +HV breakdown anomaly on detector module 0 (B6) PMT C. The CPD on DM #7 (B7) remained intermittent in its behavior throughout the rest of the thermal vacuum test.

(4) Thermal Cycle #3

The third cycle of the test mirrored the first cycle in profile. This cycle began at approximately 00:30 on August 8, with a transition through 25 °C. Iterations of TPS-63 continued at the standard 3-hour intervals. The BATSE automatic gain control function was utilized throughout all power-on activities in this thermal cycle. Hot-case functional testing at 35 °C began at 07:45 on August 8, following a 2-hour soak at this temperature. By 12:45 of the same day, the transition to the cold-case was started. A check of the failed +HV supplies on detector module #0 (B6) and #7 showed that the +HV system still exhibited the anomalous conditions described previously. They were immediately powered off. Table 3.79 highlights the major events in the third thermal cycle.

Table 3.79. BATSE System T/V Test Cycle #3 Important Events

Date	Time	Event
8-8-88	00:30	Begin Cycle #3 at 25 °C
8-8-88	05:45	Arrival at hot plateau
8-8-88	07:45	Begin short BATSE functional test
8-8-88	12:45	Begin cold transition, power on
8-8-88	13:00	Examination of DM #0 PMT C and DM #7 CPD +HVs
8-9-88	05:00	Arrival at cold-case temperature (0 °C)
8-9-88	07:30	Begin long BATSE functional test
8-9-88	13:50	Complete long BATSE functional, begin rise to hot-case
8-9-88	14:00	Execute HVPS/PMT stress test
8-9-88	14:50	DM #1 SD +HV anomaly
8-9-88	23:00	Complete Cycle #3

At the cold plateau, a long functional test was executed, including procedures TP-180 and TP-190, the burst and pulsar data tests. Because of the problems seen with the +HV supplies on detector module #0 and #7, it was decided that a stress test of the +HV system was warranted. This test placed all +HV supplies at their maximum attainable value of 2000 V for a period of approximately 90 minutes. A third +HV failure was induced during this test on the SD of DM #1 (B1). When commanded to full scale, the supply returned a value of 1041 V, indicating that some of the eight command bits had failed. The third thermal cycle ended on August 9, with a transition through 25 °C.

(5) Thermal Cycle #4

The fourth thermal cycle differed from the first three with the introduction of two intermediate plateau temperatures at which calibration data were obtained. These plateaus occurred at temperatures of 25 °C and 15 °C during the transition to cold-case. The hot-case plateau was reached at 05:00 on August 10, with a short functional test commencing 2 hours afterward. Transition to the first plateau began at 15:45 of the same day. During this cycle, BATSE was powered off for all cold transitions to aid in a more rapid change of temperature.

The 25 °C plateau was reached at 20:45 on August 10, following which, a short functional was executed. An identical test was completed at the 15 °C plateau at 00:30 of the following day. A temperature of 0 °C was reached at 09:00 on August 11, and was followed 90 minutes later by a long functional test similar to those performed before. This cycle was completed at 03:00 on August 12.

Table 3.80. BATSE System T/V Test Cycle #4 Important Events

Date	Time	Event
8-9-88	23:00	Begin Cycle #4 at 25 °C
8-10-88	05:00	Arrival at hot plateau
8-10-88	07:00	Begin short BATSE functional test
8-10-88	15:45	Begin cold transition
		-- Power off during cold transitions --
8-10-88	20:30	Arrival at 25 °C plateau, short functional
8-11-88	00:30	Arrival at 15 °C plateau, short functional
8-11-88	00:45	SFAST discriminator 3 on B7 intermittent failure
8-11-88	09:00	Arrival at 0 °C cold-case
8-11-88	10:30	Begin long BATSE functional
8-11-88	16:00	Complete long BATSE functional, begin rise to hot-case
8-12-88	03:00	Complete Cycle #4

One major anomaly occurred during this cycle. Spectroscopy discriminator channel 3 on detector module #7 (B7) experienced a partial failure. As described in the initial portion of this mocument, the four SFAST discriminators are integral and contain all counts above a particular threshold, even those which are also contained in discriminators which begin at higher energies. Consequently, SFAST3 should always report an equal or greater number of counts than SFAST4. At the 15 °C plateau, and throughout remaining portions of the test, this integral nature of SFAST3 was lost. Counts would sometimes appear in channel 3; however, there would be fewer counts than in channel 4, indicating that the discriminator was not functional for the entire duration of the readout or that its operation was intermittent. At this point in the test, the exact location of the failure (i.e., in the detector module or in the CEU receiving circuitry) could not be determined.

(6) Thermal Cycle #5

The fifth thermal cycle was identical to cycle four, with the exception that BATSE was operated on primary power instead of the redundant supply. Of the six cycles in the first T/V test, this was the most trouble-free. The cycle began at 03:00 on August 12 at the transition through 25 °C. The hot-case plateau (35 °C) was reached shortly after 5:30 the same day. Two hours later, a long BATSE functional was executed, which included burst and pulsar data tests. This testing was completed by 15:30 that afternoon, and the transition to the first plateau (25 °C) was begun. At both the 25 °C and 15 °C plateaus, a short functional test of TP-110, TP-105, and

TPS-65 was executed. These proceeded in identical fashion to the previous thermal cycle. The cold-case plateau of 0 °C was reached at 09:30 on August 13. After a 1-hour soak period, the BATSE test conductor executed yet another short functional test. This series of tests was completed by 13:45, at which time the rise to hot case was started. Cycle #5 was completed with no additional anomalies at 03:00 on August 14, 1988.

Table 3.81. BATSE System T/V Test Cycle #5 Important Events

Date	Time	Event
8-12-88	03:00	Begin Cycle #5 at 25 °C
8-12-88	05:30	Arrival at hot plateau
8-12-88	07:30	Begin short BATSE functional test
8-12-88	15:30	Begin cold transition
8-12-88	20:00	Arrival at 25 °C plateau, short functional
8-13-88	00:15	Arrival at 15 °C plateau, short functional
8-13-88	09:00	Arrival at 0 °C cold-case
8-13-88	11:30	Begin short BATSE functional
8-13-88	14:00	Complete short BATSE functional, begin rise to hot-case
8-14-88	03:00	Complete Cycle #5

(7) Thermal Cycle #6

The final thermal vacuum cycle of the initial test was started on August 14, 1988, with the transition through 25 °C. Unlike the previous two cycles, this period had no intermediate plateaus. Instead, a transition to -5 °C followed the hot-case soak and functional testing. Hot-case functional testing began at 08:15 on August 14, following a switch to primary power and a 4-hour soak at 35 °C. This testing was completed by 11:30 that day, and the instrument was released for the transition to -5 °C. BATSE was powered off at 04:00 on August 15 when a temperature of 5 °C was reached. The hardware was then left to settle into the final temperature of -5 °C with power off.

Table 3.82. BATSE System T/V Test Cycle #6 Important Events

Date	Time	Event
8-14-88	03:00	Begin cycle #6 at 25 °C
8-14-88	04:30	Arrival at hot plateau
8-14-88	08:20	Begin short BATSE functional test
8-14-88	11:30	Begin cold transition
8-15-88	08:30	Arrival at -5 °C cold-case
8-15-88	10:30	Switch power relays to redundant supply
8-15-88	12:30	Begin short functional
8-15-88	16:00	Complete short functional, begin rise to 0 °C
8-15-88	19:00	Arrive at 0 °C, power off BATSE
8-15-88	21:00	Switch power relays to primary supply
8-15-88	23:00	Begin 0 °C short BATSE functional
8-16-88	02:00	Complete short BATSE functional
8-16-88	13:15	Arrive at ambient temperature, begin ambient short functional
8-16-88	16:00	Complete ambient functional, begin chamber repressurization

Following 2 hours at the -5 °C plateau, BATSE was briefly powered to switch to the redundant power configuration. Another 2-hour soak followed, after which a short functional was executed. When the temperature of the instrument reached 0 °C, an identical sequence of steps was executed, with the power relays being switched back into the primary position. At 13:15 on August 16, ambient temperature was reached, and the final short functional was executed. Upon completion of this testing, the thermal vacuum chamber was pressurized to 1 atmosphere and opened. Thermal cycle #6 was completed with no additional anomalies.

c. First Thermal Vacuum Retest Operation

(1) Overview and Motivation

The first BATSE system thermal vacuum test had produced several anomalies. The SFAST discriminator of detector module #7 was not operating properly. High voltage system failures occurred on PMT C of detector module #0 and on the CPD of detector module #7. Because of the isolation of the hardware inside the vacuum chamber, troubleshooting was limited to operations which could be done in the current instrument configuration. At the times of these anomalies, the BATSE team was unable to discern whether, for example, the failure of the SFAST discriminator was located inside the detector module or inside the CEU receiving circuitry. Likewise, a breakdown in the +HV system could be located inside the PMT, inside a cable, or at any of the +HV junctions and connectors. To facilitate the localization of these anomalies, the BATSE instrument was re-configured into the mode detailed in Figure 3.34.

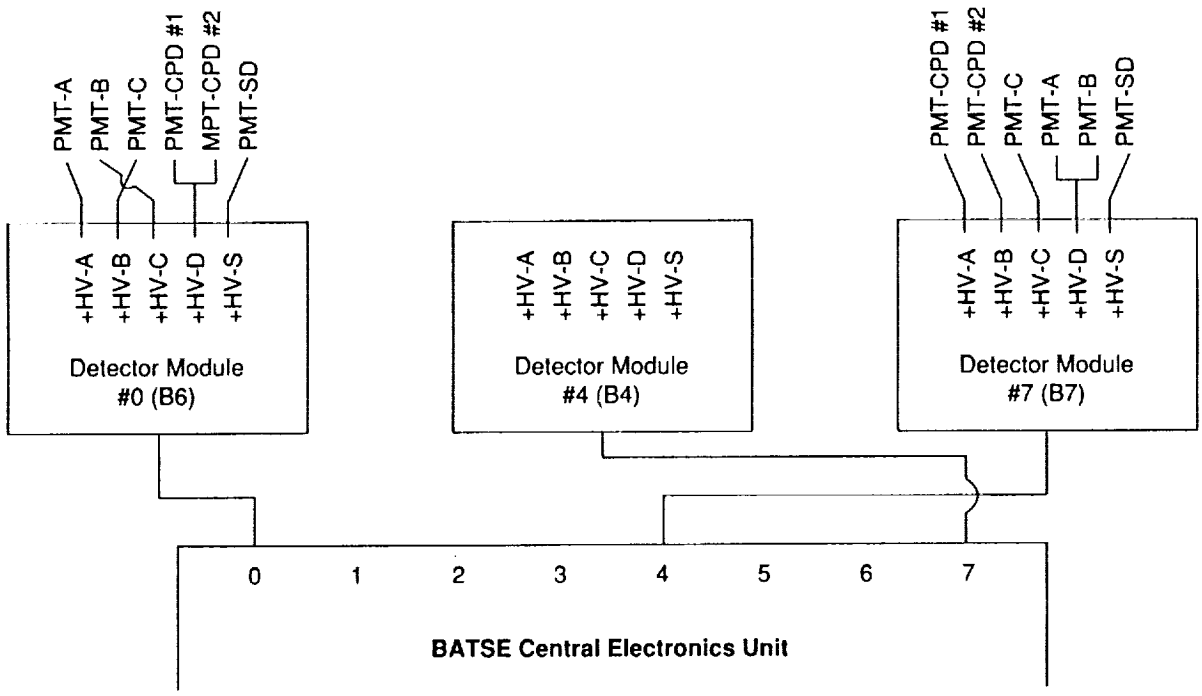

Figure 3.34. BATSE Thermal Vacuum Troubleshooting Test #1 Instrument Configuration.

On detector module #0, the +HV supplies from PMT B and PMT C were effectively swapped by interchanging the connectors at the HVPS box. If the anomaly followed the switch, and appeared on the supply formerly used for PMT B, the difficulty would be localized outside the HVPS box, nearer the phototube. To localize the SFAST discriminator problem, detector modules #4 and #7 were interchanged at the CEU. If the problem with the SFAST discriminator was inside the detector module, it would manifest itself now through CEU port #4. Lastly, the configuration of the CPD +HV system on detector module #7 was changed to power each of the CPD phototubes individually, using supplies A and B. PMT A and B on module #7 were powered through the CPD supply, +HVD. If the anomaly occurred in this configuration, it would be immediately associated with an individual component of the detector module.

This first troubleshooting test in thermal vacuum was intended to last for one thermal cycle in order to isolate all failures found during the previous six cycles. The test began on August 18, following a period of 24 hours in which the BATSE hardware was reconfigured.

(2) Test Flow and Description

BATSE was powered on August 18, 1988, at 10:30 for the start of the troubleshooting test under vacuum conditions. A complete power-up and aliveness test (TP-110) was executed, along with a detector module test (TP-105) to check each bit of all +HV supplies. Immediately upon powering of the instrument, several anomalies were present. The rates of four CPDs were exceptionally low, and the CPD on detector module #6 (B0) entered an overcurrent condition, indicating a breakdown of the +HV system. This particular +HV supply and PMT set exhibited no problems during the first six cycles.

At 17:24 on August 18, approximately 7 hours after the beginning of the test, +HV supply B on detector module #0 indicated an overcurrent condition. Because PMT C was connected to that supply and PMT C had demonstrated this behavior before, the anomaly was located to the PMT/cable system. Twenty minutes later, PMT C on detector module #5 was noticed to have the wrong voltage for the command entered. Investigation into the anomaly showed that the upper and lower bits of the higher-order byte in the command setting had failed.

Another +HV failure occurred at 22:30 on the same day. Detector module #7's CPD suffered +HV breakdown and failure. This failure isolated the anomaly to PMT #2 on the CPD, determined because each PMT was individually powered according to the scheme above.

The SFAST3 discriminator problem re-appeared at 00:05 the next morning. Because the anomaly was apparent on detector module port #7, this failure was isolated to the receiving circuitry in the CEU or the cable, not the detector module. The characteristics of the SFAST3 anomaly were identical to those from the previous test.

An already busy evening became even more so when the SD +HV supply on detector module #1 began reporting an erroneous voltage in the housekeeping at 02:05 on August 19. This supply showed no anomalies during the previous testing, and troubleshooting indicated that two bits of the higher-order byte in the command had failed. The two bits which failed were on detector module #5.

The final +HV anomaly occurred at 11:15 on the morning of August 19, approximately 24 hours after the test began. The CPD on detector module #5 tripped into an overcurrent condition because of a breakdown in the +HV system. The test was concluded at 14:25 the same day. In a period of shortly more than 24 hours, each of the anomalies from the first test had been repeated and identfied, and three new +HV were generated.

d. Second Thermal Vacuum Troubleshooting Test

(1) Overview and Motivation

In an effort to further isolate both the problems which became apparent in the first test and the new problems, a second troubleshooting test was executed following repressurization of the chamber. In this test, significant changes were made to the configuration of BATSE. Detector Module #7 was reconnected to CEU port #7; however, module #4's cable was used. Module #4 received DM #7's cable. This was done to further isolate the SFAST3 problem. At that point, the possibility existed that the SFAST3 anomaly was due to a cable problem. Evidence of a problem on SFAST3 of detector module #7 would now positively indict thye CEU as the source of the anomaly.

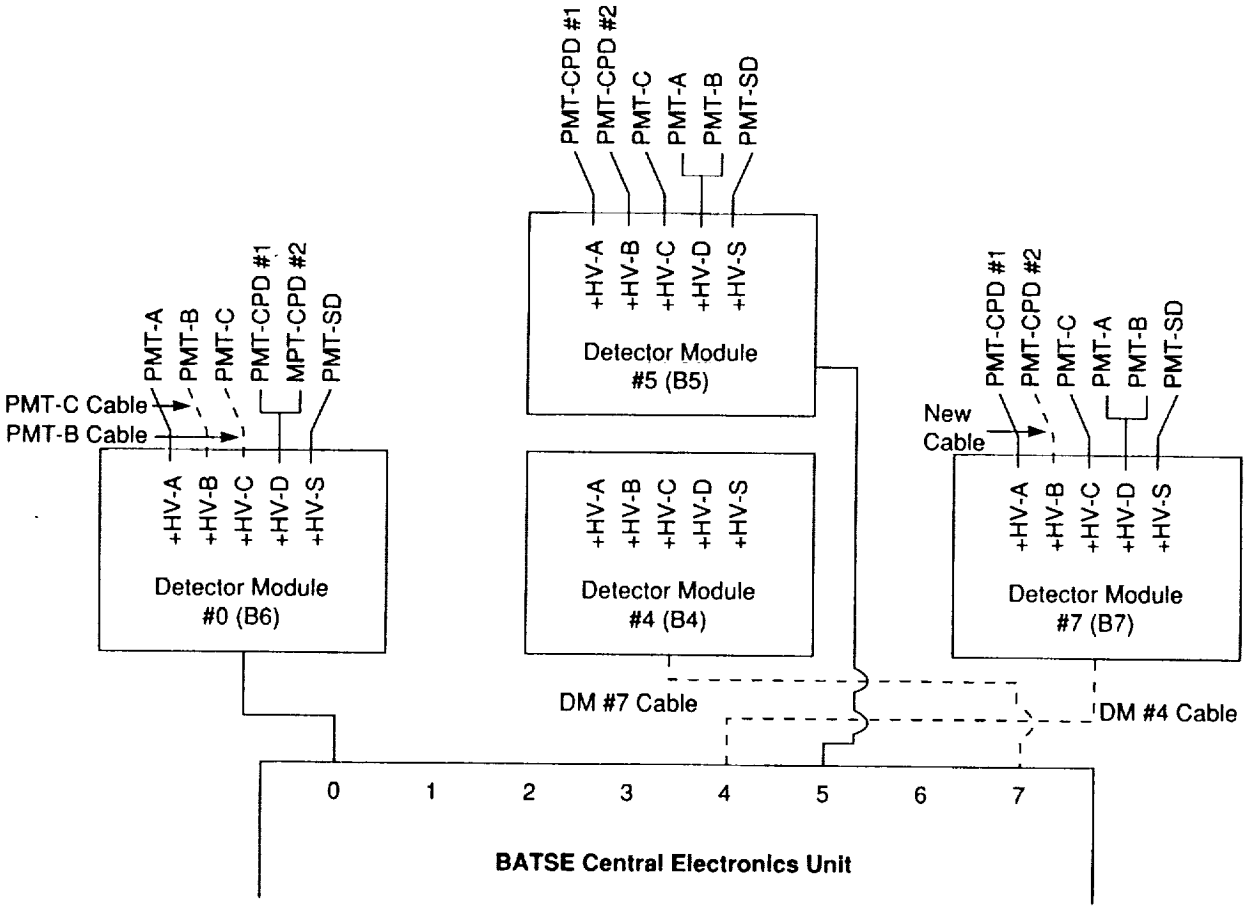

Figure 3.35. Second Thermal Vacuum Troubleshooting Test Instrument Configuration.

PMT #2 on the CPD of detector module #7 received a new +HV cable. Further evidence of a problem with this +HV system would indicate that the PMT was the source of the anomaly. Detector module #5 was internally reconfigured to match the first retest configuration of detector module #7. The final configuration change was made to PMT A, B and C on detector module #0. PMT A received the +HV cable from PMT C and was connected to the B +HV supply. PMT B retained its cable, but was connected to HV supply C. PMT C received a cable from PMT A and was connected to PMT A's +HV supply. In this manner, if PMT C displayed an overcurrent condition, the problem would be positively isolated to the phototube itself.

(2) Test Flow and Description

The second troubleshooting test began on August 23, 1988. After reconfiguration of the BATSE hardware as shown in Figure 3.35, the instrument was powered up at ambient pressure. The CPD on module #6 displayed the +HV breakdown problem seen previously at vacuum. The PMT C +HV supply on module #5 exhibited a bit failure problem, as did the SD and CPD supplies on module #1. At normal pressure and temperature, SFAST3 was fully operational.

Evacuation of the chamber began at 13:30 on August 23. By 19:30, the chamber pressure had reached 30 Torr, and two more +HV supplies had failed. Both HVPS A on module #7 and HVPS B on module #0 exhibited command bit failures. During the pumpdown, the count rate on each of the CPDs exhibited the sharp decline seen during the previous two transitions to vacuum conditions. Before the end of the day, four more +HV supplies either suffered breakdown or were found to have non-functional command bits in the supply.

BATSE remained under vacuum until the afternoon of August 24, at which time the test was terminated. During the previous 3 weeks of testing, the instrument had suffered severe anomalies on nearly one-third of the +HV supply systems onboard. It became apparent that there was an inherent problem with the +HV system, which, if left unattended, would lead to the eventual failure of all BATSE +HV after a short period of time at vacuum conditions.

e. Recovery and +HV System Repair

The BATSE flight hardware was removed from the thermal vacuum chamber on the afternoon of August 25, 1988. Damage to the CPD on module #0 was evident immediately upon removal of the thermal blanket. A lack of adequate venting caused the outer face of the CPD to separate from the honeycomb structure which supports it. The deformed face plate was conclusive evidence that the CPD was poorly vented, and most likely the cause of the paucity of counts during the initial stages of the pumpdown. Although a small redesign effort was necessary, the first problem encountered during the test appeared to be under control. The application of a sintered bronze vent to each of the CPDs and the qualification testing which followed is detailed in section III.A.3.c and will not be described here.

The effect of the anomaly seen in the SFAST3 discriminator was minor. The behavior of the discriminator was intermittent and not of great impact to science operations. Because of the integral nature of the discriminators, much of the information given in SFAST3 could be reconstructed by examination of the difference between SFAST2 and SFAST4. For these reasons, no effort was made to repair the SFAST3 receiving circuitry in the CEU. The BATSE team felt that the reward for fixing the anomaly did not justify the time, effort, and risk to flight hardware that would be undertaken in the event of a repair. This anomaly was seen again in the GRO thermal vacuum test at cold-case.

Efforts to solve the +HV problems were not quickly rewarded. Mr. Robert Austin and Mr. Richard Acker of MSFC led the investigation into the +HV problems. Each of the PMT HV cable systems which suffered an anomaly in the thermal vacuum test were dissected and examined. In addition, several of the failed 4050-IC chips, which control the +HV command bits, were removed and analyzed. Inspection of the cables and connectors in the +HV system yielded some surprising results. Many of the interfaces were blackened with a carbon-like deposition, indicating some form of electrical breakdown or arcing across the +HV interface. In many instances, dirt, contamination, or missing O-rings were found to be the cause of this breakdown. When the command bit ICs under inspection were placed into a scanning electron microscope, many of the inputs showed catastrophic failure due to the passing of a large spike or transient which destroyed the IC. After extensive effort, the picture became clearer after Bob Austin identified a one-to-one correlation between evidence of +HV breakdown and damage to IC chips on the HVPS board.

During events of +HV breakdown, caused by dirty connectors, missing O-rings, or contamination, large transients were placed on the +HV line. These transients propagated through the +HV circuit from the point of breakdown via the +HV return line. The layout of the HVPS card allowed these transient pulses to not only make their way through to the return, but also to the inputs of the command bit ICs. These transients damaged or crippled the ability of a particular input to function, causing one bit of the command to be lost. Rework of the HVPS card was necessary. The reader is encouraged to consult BATSE drawing numbers 42A30879 and 42A30861 for detailed information on the layout of the HVPS card. All 40 of the BATSE flight HVPS units experienced rework to better route the +HV return from pin E6 to E3 by means of a patched wire. In addition, all 4050 IC chips were replaced with new integrated circuit units.

Testing of the repair involved powering up a non-flight supply which had been given the above modifications. The +HV output was placed onto two wires which could be manually shorted together and caused to arc. After hundreds of iterations where the test conductor simply "bounced" the wires together, repeatedly causing breakdown and arcing, damage could not be induced to any of the eight command bit inputs on either of the 4050 ICs on the board. Concurrent to the repair of the HVPS cards, Bob Austin removed, cleaned, inspected, and repaired all interface connections for the 40 +HV supplies on the flight hardware. In many instances substantial cleaning and replacement of isolation O-rings was required. Following the

rework, each of the detector modules was given an individual retest of all +HV functions. The entire process of removal, identification, repair, and retest lasted approximately 4 weeks.

f. BATSE High Voltage Vacuum Qualification Retest

All repairs and preliminary retesting of the BATSE detector modules was completed by September 20, 1988. Following the retest, BATSE was placed back into the thermal vacuum chamber in an identical configuration to the initial test in August. TP-100 was conducted on September 21 to verify the proper connection and health of all BATSE interfaces. All +HV supplies operated normally, without incidents of breakdown or non-functional command bits. Evacuation of the chamber commenced on September 22, 1988, with BATSE power off. After a 48-hour period during which the pressure in the chamber was 5×10^{-5} Torr or less, BATSE was powered up at 07:30 on September 24. All +HV supplies were commanded to 1500 V (middle of dynamic range), and tight limits were placed on all housekeeping parameters. The test plan called for a minimum of 96 hours at vacuum with thermal cycling to verify that the +HV repair was effective. During each day, a high voltage stress test was performed, where all 40 supplies were commanded to 2000 V for a period of 20 minutes. Furthermore, a check of each bit position of all supplies was executed every 8 hours.

This thermal vacuum test proceeded without high voltage anomalies and was successfully concluded at 20:00 on September 26, 1988.

E. BATSE Science Testing at MSFC

1. Overview

Despite the extensive amount of testing which had been conducted on the BATSE instrument to this point in the program, there existed the need to obtain data for use in the scientific calibration of the hardware. This class of data was not available during any other portion of the test flow. Therefore, an extensive series of science tests was developed and executed during October 1988, prior to the shipment of BATSE flight hardware to California. These operations were performed under the direction of Dr. Gerald Fishman, BATSE Principal Investigator, and are listed in Table 3.83. The duration of BATSE science testing was nearly 18 days.

Table 3.83. BATSE Science Tests and Calibrations

• Data consistency test—TP-195
• Absolute efficiency calibration—TP-118
• Radial response calibration—TP-119
• Simulated gamma ray burst test—TP-187
• CPD science calibration

All science testing was performed in the clean room environment of MSFC Building 4705. Unlike the thermal vacuum test, the protoflight detector module was included for all science tests. Because of the constraint of eight ports on the CEU, one module was disconnected at all times. The data consistency test was performed without the protoflight module. Because this test is fully described in section III.D.1.n, it will not be discussed here. The flight CEU and BPM were used for all science testing.

BATSE flight hardware was moved from the thermal vacuum chamber following the HVPS qualification test at vacuum conditions (see Section III.D.4.f) and configured in Building 4705 by September 28, 1988. After all interfaces were mated, TP-100 was executed on September 29 to verify proper connections and to determine the readiness of the hardware to begin testing. The results of this test are on file in the BATSE data library.

2. Absolute Efficiency Calibration - TP-118

The first of the science tests to be performed was TP-118, the absolute efficiency calibration. This test was executed on all nine of the flight qualified BATSE detector modules. For this test, all nine modules were placed side-by-side on a long table in the clean room. The positions of the modules were adjusted so that all nine faced the same direction to within 0.30 arc min. Of the nine modules, the module in the middle had the isotope placed on-axis. However, data were also recorded simultaneously from seven other off-axis modules. Following the completion of the center module, the detectors were re-positioned so that another module could be tested. Figure 3.36 details the configuration of the detectors during the test.

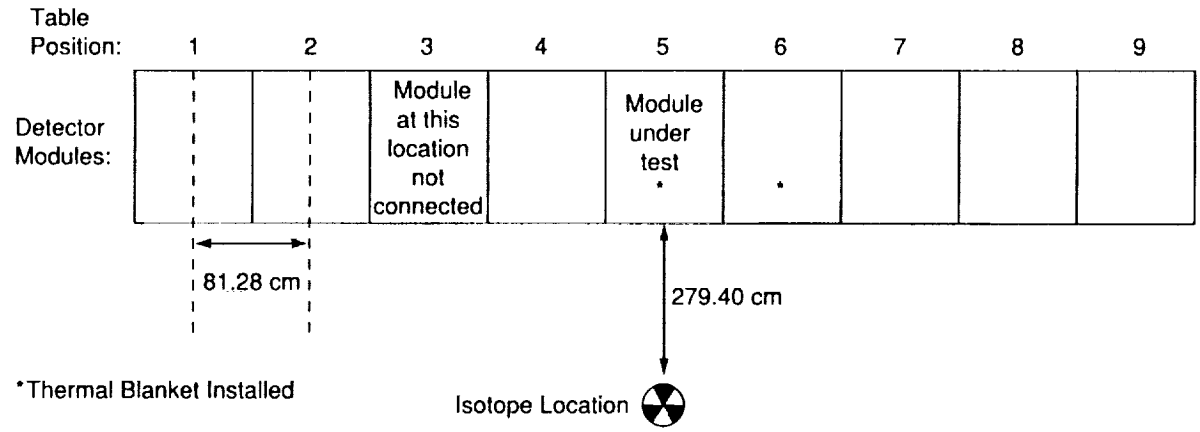

Figure 3.36. Detector Module Arrangement for TP-118 Absolute Efficiency Calibration.

The geometric arrangement of the modules during the test ensured that the scattering environment was the same for each module during its test and also allowed for coincident measurement of the off-axis radiation environment from neighboring detector modules. Detector

C-3

modules in positions #5 and #6 were fitted with a flight thermal blanket so that any absorption of incident photons by the cover would be accounted for in the calibration.

Each detector module required nearly a full day to complete. The movement and alignment of the modules was done first thing in the morning, and testing continued until completion in the afternoon. Table 3.84 describes the sequence of detector module flow for each of the 9-days required to complete the testing.

Table 3.84. Detector Module Flow Through TP-118 Absolute Efficiency Calibrations

	Table Position								
	1	2	3	4	5	6	7	8	9
Day #1	P/F	1	2	3	4	5	6	7	0/8
Day #2	1	2	3	4	5	6	7	0/8	P/F
Day #3	2	3	4	5	6	7	0/8	P/F	1
Day #4	3	4	5	6	7	0/8	P/F	1	2
Day #5	4	5	6	7	0/8	P/F	1	2	3
Day #6	5	6	7	0/8	P/F	1	2	3	4
Day #7	6	7	0/8	P/F	1	2	3	4	5
Day #8	7	0/8	P/F	1	2	3	4	5	6
Day #9	0/8	P/F	1	2	3	4	5	6	7

The numbers in Table 3.84 are detector module numbers (DM #) and correspond to the location on the GRO spacecraft in all cases except DM #0/8, which is B6, and DM #6, which is B0. The protoflight module is indicated by "P/F." All flight modules were connected to their respective CEU port. The protoflight module was connected to the port vacated by the detector module occupying table position #3.

The radioactive sources were placed into the standard BATSE test holder at a distance of 3.000 ± 0.003 meters from the center of the LAD under test and on the perpendicular bisector. Given this orientation, the LAD in the center intercepts approximately 0.0018 of the photons emitted at the source, 3 meters away.

The isotopes used were calibrated and traceable to the National Bureau of Standards, with their activities were known to ±5% or better. Two of the isotopes, Cs-137 and Co 60, were obtained from the NBS, and were calibrated to ±3%. A complete list of source-related data is given in Table 3.85.

Table 3.85. BATSE Absolute Efficiency Isotope Information

Isotope	Energies (keV)	Activity (μCi)	Date
Cd 109	88	114.6	8-1-88
Am 241	60	109.61	8-1-88
Co 57	14.4, 122, 136	114.3	8-1-88
Ba 133	81, 302, 356, 384	85.7	7-1-88
Na 22	511, 1274	114.0	9-1-88
Cs 137	32, 662	81.6	9-6-88
Y 88	898, 1836	109.9	8-5-8

The calibration started with a background collection, and then each of the isotopes were utilized for LAD data collection. Following the isotope collections, a second background spectrum was taken. A similar sequence was then followed for the spectroscopy detector at 1X gain (4 keV/channel uncompressed). After these measurements, the SD gain was changed to 4X (1 keV/channel uncompressed), and the sequence was repeated. The Na 22 and Ba 133 isotopes were not used during the SD measurements. Each of the integrations were 8-set spectra, approximately 393 seconds in duration. All data obtained during these tests are on file in the BATSE library.

Dr. Geoff Pendleton and Dr. Patrick Lestrade are the principal BATSE team members involved in determination of the absolute photopeak efficiency of the detector modules. Their work on the data set generated through TP-118 has yielded the following functional form for the module behavior.

3. BATSE Radial Response Calibration - TP-119

Early in the calibration of the BATSE large area detector (LAD) it became apparent the response of the detector was not uniform over its entire surface. Further testing demonstrated that this behavior was radially dependent. Because of variations in the scintillation light output of the NaI crystal and light collection inside the LAD cone, a gamma ray which deposits its energy in the center of the detector does not produce the same response as a photon of the same energy which interacts near the edge. This behavior ismore prevalent at high energies (> 500 keV) and is manifested by a flat-topping of photopeaks in the calibration spectra.

To calibrate this effect, the BATSE team designed and performed the BATSE radial response test, TP-119. In this test, 100 μCi of Hg 203 was placed in a specially designed holder which was mounted to a fixture across the face of the detector module. This holder was then placed at 15 different locations on the LAD diameter, and spectra were accumulated. Each spectra was integrated for a period of approximately 90 seconds. Only one diameter was tested, because of the LAD's rotational symmetry about the normal to the detector.

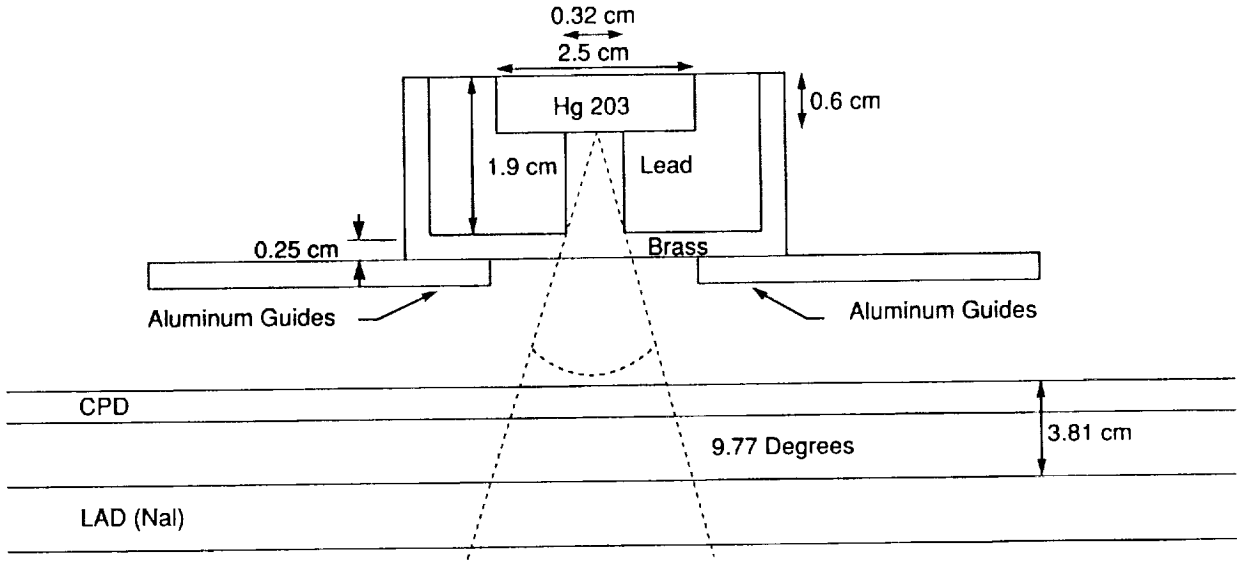

Figure 3.37. BATSE Radial Response Source Holder.

The source holder was a small lead cup, 1.9 cm in thickness, lined with 0.25 cm of brass on the outside. The radio isotope, a 2.5 cm x 0.6 cm disk, is placed into the top of the holder. Directly beneath the source is a 0.32-cm hole, which collimates the escaping photons into a beam 9.77° in aperture. This assembly rides across the face on the charged particle detector (CPD) on two aluminum guide rods. These rods are affixed to the detector module at the lifting sling points. This insures that the rods fit the same way each time they are put onto the module, and the module-to-module variation in placement is minimized.

The fifteen locations on the LAD diameter were located with seven on either side and one location in the center of the detector. The test locations were spaced closer together near the edge of the LAD to get a better calibration on the behavior near the edges, where the effect becomes more dependent on radius. Radii of 0.0, 10.0, 15.0, 20.0, 22.0, 23.0, 24.0, and 25.0 cm were used for all nine of the BATSE detector modules, including the protoflight unit. Figure 3.38 is a schematic of the test locations at the various radii.

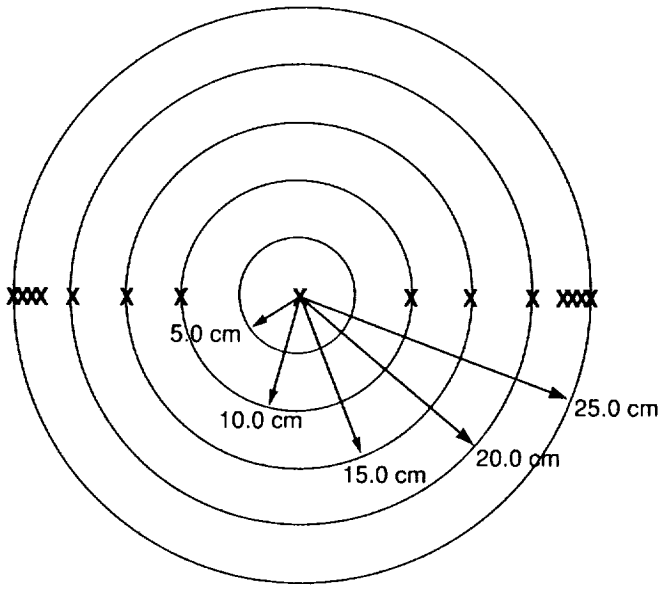

Figure 3.38. Test Locations on the Face of the BATSE LAD for TP-119.

Because of variations in the properties of the LADs, each detector module exhibits a slightly different radial response. This behavior is evident when comparing the flat-topping of higher energy (>500 keV) photopeaks generated by different modules. Some LADs exhibit a pronounced flattening, while others exhibit somewhat less of an effect. Data from this test were used to fit a parametrization to the radial response of each of the detector modules. The response of the LAD is nearly uniform from the center of the detector out to a radius CENT, which differs for each module. From this point to the edge of the LAD, the response decreases linearly to a fraction of the response in the center. The response at the edge of the detector is given by the equation,

$$\% \text{ response at edge} = (1 - \text{EDGE})*100\% , \tag{3.2}$$

where the parameter EDGE differs for each LAD and is the percent drop in response from the center to the edge of the crystal. The parametrization is therefore a two-part linear fit; a constant response from the center of the detector to a radius CENT, and a linear decrease in response from the radius CENT to the edge, where the fractional response at the edge is given by equation (3.2). The parameters CENT and EDGE are given for each module in Table 3.86.

Table 3.86. Radial Response Parameters for Each Detector Module

Detector Module	CENT (cm)	EDGE
B0	13.3	0.122
B1	15.5	0.128
B2	14.5	0.107
B3	13.0	0.126
B4	12.0	0.135
B5	11.7	0.161
B6	12.6	0.103
B7	12.2	0.143

4. BATSE Science CPD Calibration

During the test program of the BATSE flight hardware, TP-170 had been executed many times to determine the calibration of the CPDs. However, this procedure relied upon background rates and the muon spectrum as seen through the LAD to determine the location of the threshold in energy. During the science tests, each of the nine BATSE CPDs were calibrated through the use of a Co 60 and a Cs 137 isotope. These calibrations were executed on October 12 and 15, 1988.

The location of the CPD threshold must be determined indirectly because of the lack of a pulse height analyzer at the output of the CPD signal. The desired location of the threshold is approximately 700-800 keV. At this threshold, over 95% of normally-incident minimum ionizing charged particles will be detected and rejected by the anti-coincidence circuitry.

Figure 3.39 depicts the relationship between rate and high voltage for the BATSE CPD on detector module B4. Each isotope was placed at a distance of 5.08 cm from the face of the CPD in the center of the detector. Other CPDs have similar behavior; however, the location on the X-axis (voltage) differs for all CPDs. The "knee" in the two curves for Co 60 and Cs 137 arise because of the onset of detection of photons from the Compton-edged of the photopeaks of these isotopes. For Co 60, the emission is near 1.2 MeV, and for Cs 137, the line is located at 662 keV. Using these two curves, one can easily localize the threshold of the CPD near 700 keV simply by setting the voltage at a point where the Co 60 is mostly detected by the CPD and the Cs 137 is not. This is precisely what was done for all nine CPDs.

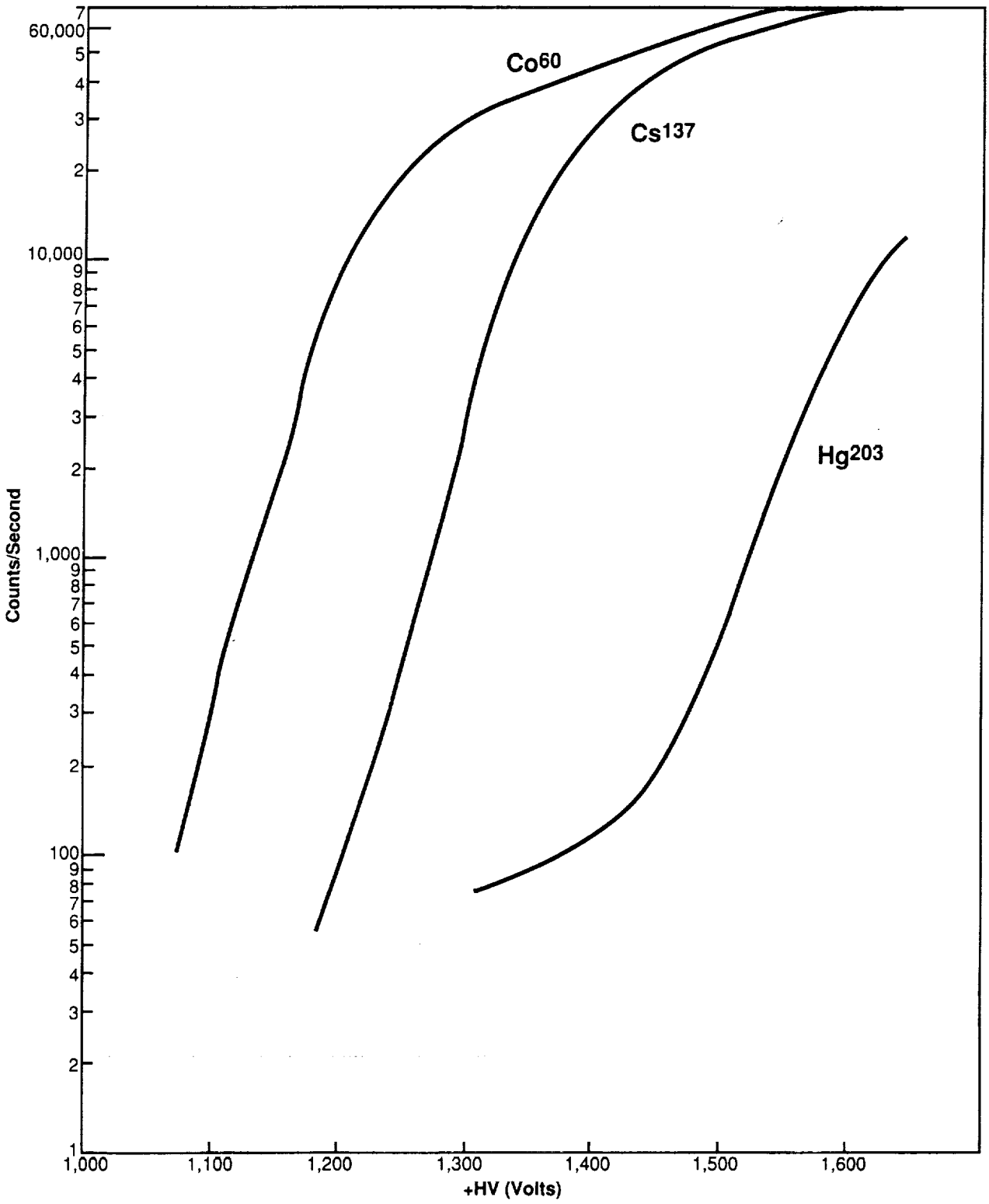

Figure 3.39. Rate vs. High Voltage for the CPD on B4 with Various Isotopes.

After generation of the data in Figure 3.39, each CPD was individually tested. A 100 μCi isotope of Co 60 was placed in front of the CPD center at a distance of 5.08 cm. The +HV was then adjusted to produce the desired count rate. The Co 60 source was replaced with a 100 μCi Cs 137 source, and the rate compared to the expected value. Fine-tuning of the voltage was necessary in all instances because of slightly different responses from each CPD. However, in this manner, the CPD threshold was easily placed in the desired location, with considerable uniformity from module to module.

Table 3.87 lists the final +HV command settings and voltages required to place the CPD threshold between the "knee" in the Co 60 and Cs 137 rate curves.

Table 3.87. CPD Voltage Values Obtained During BATSE Science Tests

Detector Module	CPD Command Value	CPD Voltage (Volts)
B0	103	1402
B1	96	1377
B2	61	1239
B3	53	1209
B4	60	1237
B5	45	1176
B6	79	1311
B7	42	1165
P/F	91	1357

5. BATSE Rotating Wheel Burst Simulation Test - TP-187

October 18, 1988, was the final day of BATSE testing at Marshall Space Flight Center. TP-187, the rotating wheel burst simulation test, was the final test executed. To this point in the test program, all burst data generated came either through a commanded burst or through an activation of the LED. No burst data existed with small-scale time structure, produced by photons. This test allowed the BATSE team to generate such data. Each of the detector modules were in the configuration from TP-118, the absolute efficiency test. Figure 3.36 details this arrangement. Detector module B7 was located in table position #9. A 10 mCi isotope of Ba 133 was located off the corner of table position #9. From this point, all LADs were visible to the source. The isotope was placed behind a slotted lead wheel which acted as a shutter in front of the isotope when the wheel was rotated. Figure 3.40 shows the construction of the slotted wheel.

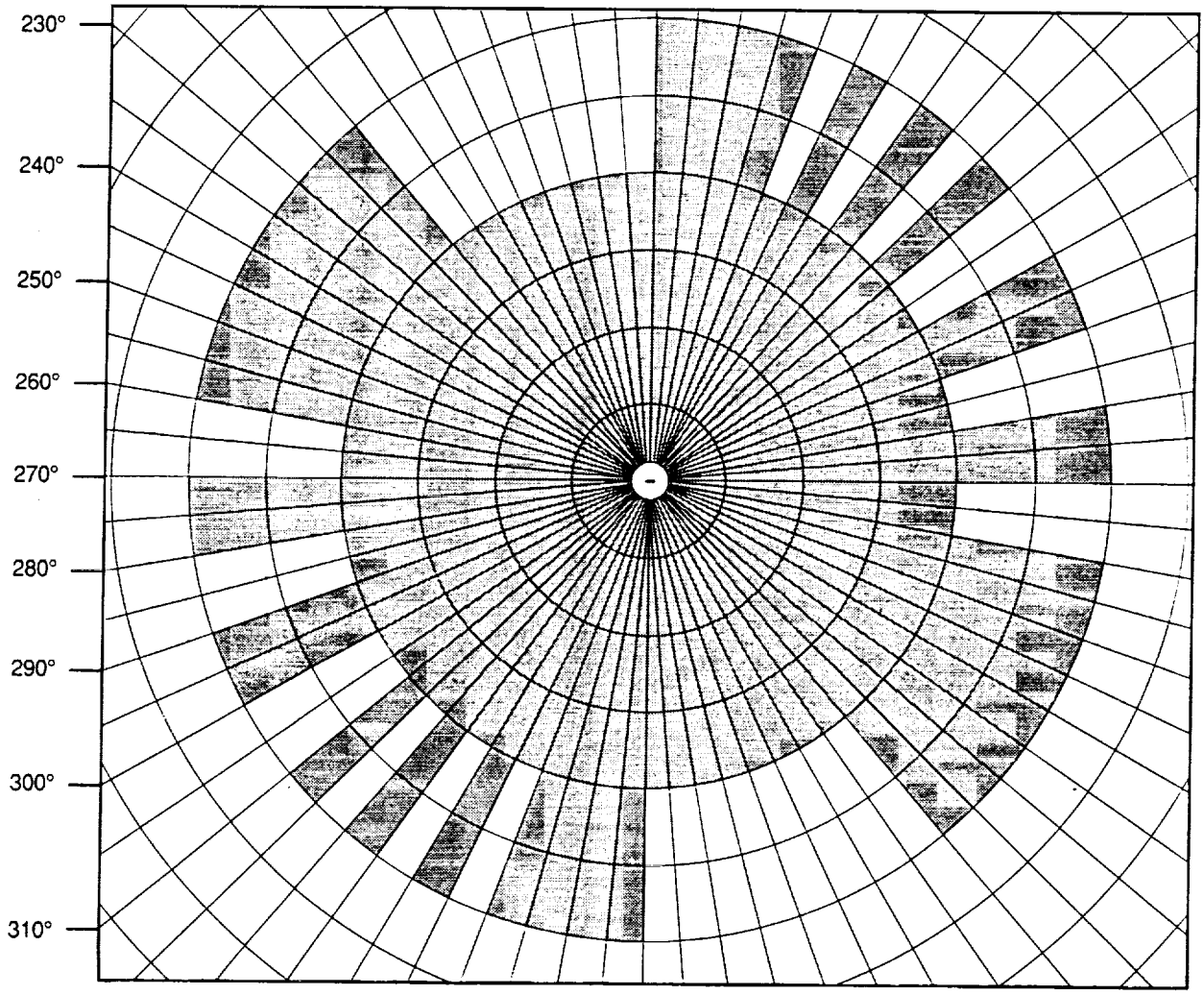

Figure 3.40. BATSE Rotating Lead Wheel Used in TP-187.

The axis of the wheel was connected to a small stepper motor which was driven by a frequency generator. By adjusting the frequency of the driving pulses, the rate at which the wheel rotated could be controlled. The wheel was symmetrically cut to expose and shield the source for various lengths of time. The smallest interval of exposure or closure on the wheel is 5° degrees, with the largest being 40°. The nominal rotation rate of the wheel was approximately 25 rpm. At this rate, the smallest interval of 5° lasted approximately 0.033 seconds, near the period of the Crab Nebula pulsar.

BATSE was powered into a nominal operating condition and allowed 1 hour for the stabilization of the PMT gains. Short background spectra were accumulated with the source exposed through the wheel, and with the source occulted by the wheel. Following the spectral accumulations, the wheel was rotated to a position which occulted the source, and the background was allowed to be recomputed by the CEU.

After background recomputation, burst triggering was enabled through serial command 4420, and the wheel was set in motion at the default rotation rate. The burst triggered nominally. After 30 seconds, the rotation rate of the wheel was decreased by a factor of 10 through a change in the pulse generator's drive frequency. The burst readout was allowed to complete, and all data types were monitored during the readout. This operation concluded BATSE testing activities at MSFC.

6. BATSE Total MSFC Testing Time

BATSE held a formal pre-shipment review at the Marshall Space Flight Center to assess the readiness of the instrument to be shipped to California. For this review, the total operation time of the instrument was determined. The number of hours in Table 3.88 are computed from the test log, which indicates the tests run and the duration. These numbers are accurate to ±5%.

Table 3.88. Summary of BATSE Operation Time at MSFC

	BATSE Power-On Time (Hours)
Non-thermal vacuum:	416
Thermal vacuum:	620
Total operation time:	1,036

F. BATSE Operations at TRW - Redondo Beach, California

Following the final science test in October 1988, preparations began to ship the BATSE flight hardware and GSE to the GRO mission contractor, TRW, in Redondo Beach, California. The hardware was packaged and shipped in an environmentally controlled air-ride van by 3-Way Van Lines. Mr. Byron Schrick and Mr. Scott Storey accompanied the flight hardware to California. The BATSE caravan left NASA/MSFC in Huntsville, Alabama at noon on October 25, and arrived in the Los Angeles area 42 hours later, on the morning of October 27. The flight hardware was subsequently unloaded from the air-ride van into the high-bay of TRW Building #R7A. BATSE remained in California until February of 1990, when it was shipped to the Kennedy Space Center as a fully-integrated part of the Gamma Ray Observatory. During this time period, BATSE was represented in California by Mr. John Horack.

In the following pages, all BATSE operations at the system level are detailed. Testing which was performed at the detector module level during November 1988 is contained in section III.B.1.l. Results from environmental, engineering, and scientific tests are presented here, along with a narrative description of major events and anomalies.

1. BATSE System Integration Bench Testing

Upon arrival at TRW, the BATSE flight hardware was off-loaded and tested to verify that the journey from Alabama caused no damage or anomalies to the instrument. Subsequent to the module-level tests presented in section III.B.1.l, the BATSE hardware components were re-integrated to the system level. This configuration was identical to that of the system-level tests conducted at MSFC. The test procedures which were used in operation of the experiment are described in section III.D.1. Table 3.89 details the tests performed on the floor at TRW.

Table 3.89. BATSE System-Level Bench Tests Executed at TRW

- TP-100 — Engineering test
- TP-105 — Detector module test
- TP-110 — Power-up/aliveness test
- TP-120 — Coincidence test
- TP-125 — Background test
- TP-140 — Long calibration
- TP-170 — CPD calibration
- TP-171 — CPD/LAD coincidence run
- TP-180 — Burst data test (three options)
- TP-188 — Burst trigger/solar flare trigger signal test
- TP-190 — Pulsar data test
- TP-195 — Data consistency test
- TP-200 — Power control functional test
- BATSE thermal control system test

Testing began on Thursday, November 10. A total of five test days were required to fully complete the functional testing and was completed on November 16. One iteration of TP-110 was executed for each of the days during which testing was performed. TP-100, the BATSE engineering test was performed first to verify that all interfaces were mated properly. This test was the first in which the detector module switch involving DM #0/8 (B6) and DM #6 (B0) was present. From this test forward, the detector modules maintained the flight configuration with respect to the CEU port at which they were connected.

TP-100 and TP-105 verified the proper operation of all 40 +HV supplies and all command bits contained therein. Each of the BATSE +HV supplies and associated PMTs operated flawlessly, with no indication of damage arising from the transportation of the hardware across the country.

Mr. Emmett Nash and Mr. John Lowery, under contract to MSFC Test Laboratory, performed a full test of all BATSE heaters and components of the thermal control subsystem.

All heater circuits were verified to be operational. Thermostats could not be cycled because of the room temperature environment.

The long calibration, TP-140, was performed on November 14, 1988. During this test, each of the modules were lined up similar to the configuration of TP-118 at MSFC, however, there were no exacting requirements on the pointing or alignment of the modules. To support the radioactive sources required for this test, a long beam was supported horizontally in front of the row of modules. Figure 3.41 illustrates the configuration as seen from the side.

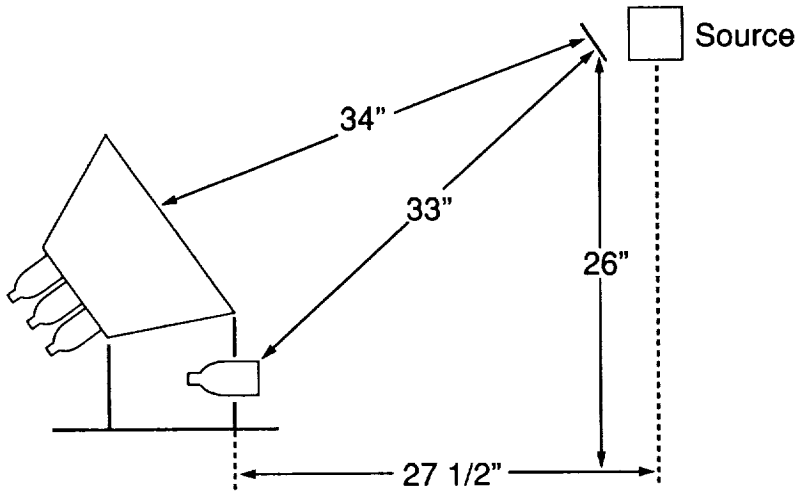

Figure 3.41. BATSE TP-140 Long Calibration Isotope Location During Bench Testing at TRW.

In this configuration, the support beam was located approximately 70 cm in front of the row of detector modules, at an elevation of 66 cm off the floor. The small isotopes were then affixed to the beam in front of each detector. At this location, each isotope was approximately 86 cm from the center of the LAD and 84 cm from the top of the SD. These measurements are accurate to within a centimeter.

TP-170, the CPD calibration, was performed on November 11 and yielded a somewhat surprising result. The counting rates for the various +HV command settings are shown in Table 3.90. These rates are about 30% higher than those seen in tests at MSFC for a given voltage setting. This behavior is exhibited in all eight of the flight CPDs. The result was due to the substantially increased level of the background radiation in California when compared to the environment at MSFC in Huntsville. Prominent background lines produced by naturally occurring K 40 and Th 228 are present in all spectra taken while at TRW. These, combined with other

high-energy background components, caused the CPD to exhibit higher rates than in previous testing.

Table 3.90. TP-170 CPD Rates at CPDHVn Voltage Settings
BATSE System-Level Bench Testing at TRW

	CPD Count Rate at Various + HV Command File Settings Detector Module							
	BO	B1	B2	B3	B4	B5	B6	B7
CPDHV1	89.8	111.3	109.4	110.4	107.4	106.4	100.6	101.6
CPDHV2	79.1	95.7	90.8	92.8	90.8	90.8	86.9	85.9
CPDHV3	75.2	91.8	86.9	87.9	85.0	85.0	84.0	81.1
CPDHV4	72.3	88.9	81.1	83.0	80.1	81.1	80.1	77.1
CPDHV5	69.3	83.0	78.1	79.1	76.2	76.2	76.2	73.2
CPDHV6	66.4	79.1	73.2	73.2	73.2	73.2	71.3	69.3
CPDHV7	59.6	72.3	66.4	66.4	66.4	63.5	64.4	60.5
CPDHV8	53.7	63.5	57.6	57.6	56.6	56.6	57.6	53.7

All three options of the burst data test (TP-180) were executed, followed by both options of the pulsar data test (TP-190). Each of these tests proceeded without anomaly. TP-200, the power control functional test, was the final exercise of the system-level bench test. All power control functions were completely checked out and verified to operate in the desired manner. Following the successful completion of these tests, BATSE was declared ready for installation and integration into the Gamma Ray Observatory (GRO).

2. BATSE Flight Hardware Installation

As previously mentioned, the BATSE flight cable harnesses were shipped to TRW early in the Summer of 1988. When the remainder of the flight hardware arrived in California, the harnesses had already been placed aboard the Observatory. OSSE was installed on November 18, spawning some jocular debate as to who actually had their hardware on the Observatory first. Nevertheless, the detector modules were the next part of the BATSE instrument to be installed. Module installation began on the afternoon of Monday, November 28, 1988. Installation of the modules located on the +Z half (top) of the spacecraft was rather simple, as the module was simply lifted from one position and placed onto its location on the GRO. Each module is affixed to the spacecraft with four titanium bolts and four annular Teflon isolators. Consultation of the BATSE/GRO Interface Control Document will provide the reader with a more detailed look at the mechanical interface between the BATSE detector module and the GRO platform. The MLI bottom "pan" was placed first, followed by the Teflon isolators. As the module was placed over the proper location, the titanium bolts were inserted. Because of the relaxation of the Teflon isolators, several torqueing procedures were required over a period of several days.

The lower detector modules (-Z locations) were not as simple to install, primarily because they had to be inverted prior to installation. Figure 3.42 schematically shows the equipment required to invert and install the detector modules into the -Z positions. The lower modules were lifted from their position by means of the standard lifting sling and placed into the inverting fixture. This apparatus resembled a swing-set and could be rotated 360° about a horizontal axis. The "seat" of the fixture contained the bolt-pattern required to affix the BATSE detector module securely. The module was bolted into the inverting fixture, and the lifting sling was removed. The fixture was then inverted manually and secured in the upside-down position with two locking pins. In an attempt to minimize the amount of torque which the inverter had to overcome, the rotation axis was designed to pass close to the center of gravity of the combined module-fixture mass. After locking the detector module into place, the second lifting fixture was attached to the crane and moved into position. This piece of equipment resembled a see-saw, with the crane interface at the fulcrum, the inverted detector module at one end, and counterweights at the other.

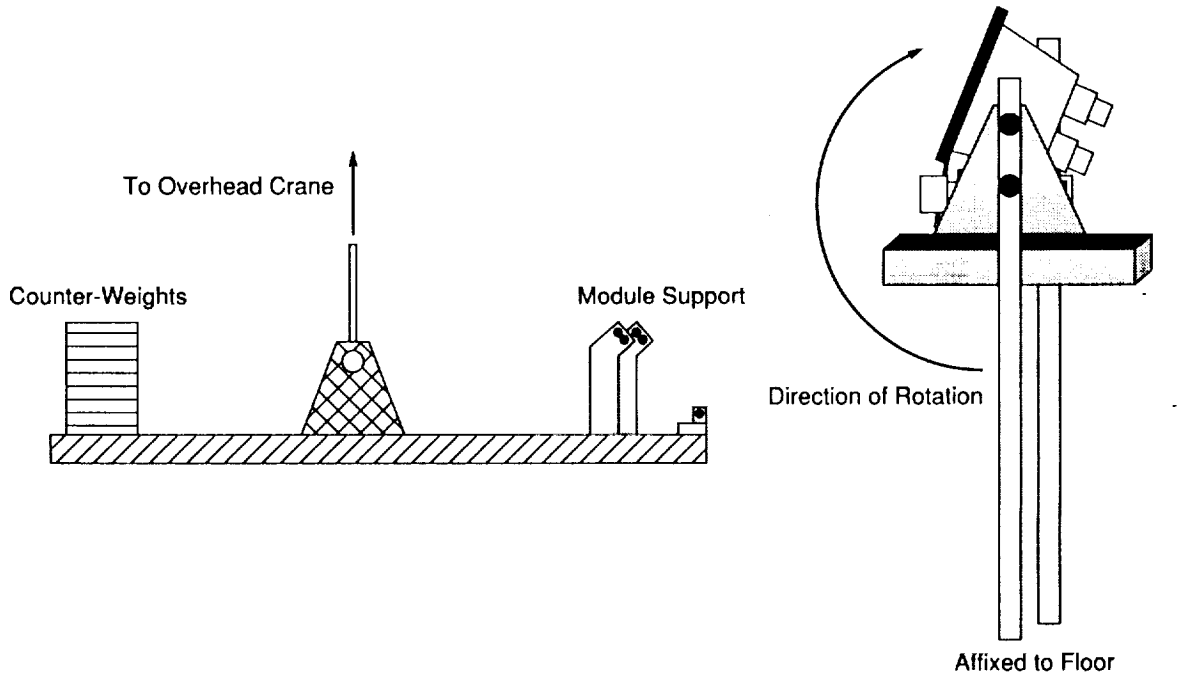

Figure 3.42. BATSE/GRO -Z Detector Module Installation Support Equipment.

The detector module end of the lifting fixture was fitted with apparatus which allowed the module to be attached at the same points as the BATSE lifting sling. With the module inverted and locked into place, the lifting apparatus was carefully positioned underneath the module and fastened to it. Counterweights were continually used to prevent any mechanical loads from being

input into the module structure and to keep the center of gravity of the module-fixture mass near the center point at which the crane was attached. After installing the lifting fixture, the module was carefully unfastened from the inverting apparatus and transported slowly to the desired position on the spacecraft. Once at the desired location, the detector module was removed from the lifting fixture in a similar process to the one described above, only in reverse.

The first modules to be installed on the spacecraft were B5 and B7. This operation was completed on November 28. B0, B4, and B6 were installed on November 29. On November 30, the remaining three detector modules (B1, B2, and B3) were placed onto the GRO.

Installation of the BATSE remote electronics (CEU and BPM) proceeded much more slowly than the detector modules. Because these boxes are located on a panel, substantial work had to be done on the panel prior to installation on the spacecraft to ease the difficulty of some tasks. Configuration of the panel, including the mounting of heaters, installation of harnesses, alignment of the panel, and fit checks of components, lasted longer than anticipated, forcing the CEU and BPM installation to be delayed a few days.

The CEU and BPM were checked for the proper mechanical interface to the panel on December 1. At the time, the BATSE panel was not on the spacecraft. All fit checks went well, and several minor modifications had to be made. Several heaters near the BPM had to be trimmed away, and a small amount of thermal paint re-work had to be done. The BPM was also verified to have four bolt holes where no blanks existed in the panel. However, these interface points were not used in compliance with the BATSE/GRO Interface Control Document.

The BATSE panel was placed onto the spacecraft on December 2, with the CEU and BPM following in the early morning hours of December 6. Detector module interface connections to the 146 and 148 brackets and all CEU-BPM connections were completed by December 7. At that point, however, BATSE could not power-up because of the lack of electrical connections to the spacecraft and the inability to connect the detector modules with the panel in the open position. Finally on December 15, 1988, the BATSE panel was closed, and all remaining interfaces were mated. Despite numerous problems with ground system software and hardware, BATSE was powered at 11:00 a.m., and TP-200 was successfully executed through the spacecraft data and command system.

3. BATSE Integration Verification Tests

Testing to verify the successful integration of BATSE flight hardware to the GRO began on January 12, 1989. In total, six testing procedures were executed, four of which were new tests to verify interfaces to the spacecraft remote interface units (RIU). BATSE test conductors were John Horack and Chip Meegan of Space Science Laboratory. Table 3.91 summarizes the testing done during this period of time.

Table 3.91. BATSE Integration Verification Test Procedures

- TP-100 — BATSE engineering test
- TP-200 — Power control functional test
- TP-204 — BATSE command and telemetry test
- TP-208 — TTU test
- TP-212 — BATSE discrete command test
- TP-216 — Passive analog test
- BATSE heater functional checkout

All testing was under the control of TRW Document XR-21S-51, the GRO Instrument to Observatory Interface Verification Procedure. This document referenced each of the BATSE TP-series tests. Under normal circumstances, nearly all testing at TRW was handled in a similar manner. TP-200 was the first test executed on the morning of January 12. This test had been executed prior to the new year without difficulty, but was repeated as part of the "official" interface verification test for completeness. During this iteration of TP-200, the power cross-strapping interface and the GRO engineering telemetry measurements were of primary interest. In engineering telemetry, the GRO reports the positions of all BATSE power control function relays, several temperatures, and currents. To this point, each iteration of TP-200 was executed without the concurrent GRO measurements because BATSE was not on the spacecraft. The simultaneous agreement of BATSE telemetry with independent GRO measurements was an important positive result of the test.

The second test procedure performed was TP-204, the RIU command and telemetry test. This entire test was performed on primary power and then repeated on backup power. In one sense, the remaining TP-200 series tests were a formality. For example, in order to successfully complete TP-200, one requires the ability to reliably send commands to the instrument and receive proper telemetry. A second command and telemetry test is somewhat superfluous. At the start of the test, BATSE is operating through RIU-A with CCF-A, and command file RLYNOM is sent to configure all BATSE power control function relays to the nominal position. This file contains approximately 100 discrete commands. After the file is executed, the telemetry is examined to verify the proper relay states, indicating a normal commanding sequence execution. Several serial commands are sent to BATSE, exercising the CCF-A command channel (channel 1). When these commands have been verified, the test conductor switches BATSE over to CCF-B by using discrete commands and repeats the serial command exercise, utilizing the channel for CCF-B (channel 2). BATSE is then configured to operate through RIU-B, and the entire test is repeated. In this fashion, both serial command channels are executed through each RIU, and approximately 100 discrete commands are sent through both RIUs. In addition, the proper GRO engineering telemetry indications of relay positions through both RIUs indicate that each is functioning properly.

The third test procedure executed was TP-208, the TTU test. This test verified the proper receipt of the serially transferred time code and a 1 Hz timing signal from the spacecraft. Because only one GRO TTU can be active, this test required coordination with the other instruments when a switch to TTU-B was required. With the GRO utilizing TTU-A, the BATSE test conductor sent command 7184 to configure BATSE to receive data from TTU-A. From this point, the proper spacecraft time and presence of the 1 Hz signal could be verified by examination of the three time words in BATSE data. Each combination of TTU, RIU, CCF, and instrument power is exercised to verify full cross-strapping capability.

TP-212 is the discrete command test procedure and was executed fourth in the succession of BATSE integration tests. Beginning on RIU-A and CCF-A, the RLYNOM command file of 100 discrete commands is executed and proper telemetry verified. Subsequently, four discrete commands are sent to execute the following; start the flight software on CCF-A, load and start the flight software on CCF-A, enable the CCF-A watchdog timer, and then disable the CCF-A watchdog timer. After these commands are properly executed, BATSE is switched to CCF-B, where an identical sequence of commands are processed. As with all of the TP-200 series tests, this cycle is executed once through RIU-A and again through RIU-B.

The final test in the TP-200 series was TP-216, the RIU passive analog measurement test. This procedure also allowed for a cursory check of the BATSE flight heater functionality, as one of the telemetry measurements tested in TP-216 is the return of voltage dividers indicating the status of BATSE heater circuitry. Operating initially through RIU-A on CCF-A, the GRO engineering telemetry measurements for BPM +5 V and +15 V current are verified in several states of BATSE instrument configuration. Parameters 1BPMTMP (temperature of the BPM) and 1CEU0TMP (CEU temperature CCF-A) are verified to have the correct HKG values. BATSE is then switched to CCF-B for a check of 1CEU1TMP. The final temperatures examined are the detector module temperatures reported through GRO telemetry. All temperature measurements from the GRO telemetry are compared to BATSE telemetry for agreement. With heater power enabled, the proper voltage return is verified for the BATSE primary thermal control, makeup, and STS heater circuits. At the completion of these steps, BATSE is switched to operate through RIU-B, and the process is repeated. The second time through the procedure is slightly different because only the redundant thermal control and make-up heaters are visible through RIU-B. BATSE flight heater telemetry is not cross-strapped to either RIU, and the STS heater status is only routed through RIU-A.

Following this test, each of the five sets of BATSE flight heaters were verified. Table 3.92 details the cross-strapping configurations allowed for each heater and the RIU required by BATSE to verify the telemetry status.

Table 3.92. BATSE Flight Heater Circuits, Test Command Sequences, and RIU Required for Telemetry Verification

BATSE Heater Circuit (# of Htrs)	MPS-1	MPS-2	RIU required for TLM
Primary T/C heaters (8)	BATSPHTR	BATSPHTRA	RIU-A
Primary M/U heaters (8)	BATSPMU	BATSPMUHA	RIU-A
Backup T/C heaters (8)	BATSRHTR	BATSRHTRA	RIU-B
Backup M/U heaters (8)	BATSRMUH	BATSRMUHA	RIU-B
BATSE STS (shuttle) heaters (8)			RIU-A

When any of the heater circuits listed in Table 3.92 are powered off, the status voltage reads approximately 0.0 V. When power is applied to the heater circuit but the thermostat is open (heater is not on), the proper telemetry indication is between 2.0 and 2.5 V. The third heater state, when power is applied and the thermostat is closed, returns a voltage of approximately 5.0 V. During this checkout, none of the thermostats were closed because of the ambient temperature in the high bay. Each of the heater circuits returned a status voltage near 2.0 V when powered.

The final test performed as part of the BATSE integration verification sequence was TP-100, the BATSE engineering test. This operation was identical to the numerous iterations of TP-100 which were performed previously. The test, despite its familiarity to the test conductors, was extremely important for several reasons. First, the cables installed on the spacecraft had not been used in 7 months and had been subject to a large amount of handling and manipulation. The existence of a broken wire or an error in the routing of the cables would have been a major problem. Second, four of the detector modules were inverted and transported in the upside-down position with the GSE described previously. The possibility for damage to a module under those circumstances was not negligible. TP-100 proved that the modules had been able to withstand some rather unorthodox handling. Third, a total of 64 connections were required to fully integrate the detector modules to the CEU and BPM. Many of these were made in cramped locations without the full visibility and accessibility one would desire. Interchanging two connections or damage to the connectors would also have been a large problem. TP-100 verified that the modules in the various locations around the spacecraft were connected to the proper CEU and BPM ports, with no damage.

4. Detector Module Mirrored Radiator Damage

On the evening of January 17, 1989, BATSE detector module B1 sustained major damage to the side radiator panel located next to the HVPS. This damage was incurred during the installation of test-only thermal vacuum heaters which are mounted directly onto the surface of the mirrored radiator. These heaters were affixed to the mirrored radiator panel exposed by the MLI blanket to regulate the energy flow from the mirror to the cold wall, thus allowing more control of the detector module thermal environment. The heater was installed initially on the

wrong side of the detector module. When the error was recognized, the heater was removed, and the damage occurred. Despite damaging the module, heater tape was further installed onto six of the eight flight detectors. B0 and B2 remained without the heaters.

Damage to the radiator was evident on 6 of the 24 mirror segments not covered by the detector module MLI flap. On three segments, the mirrored surface was fractured and completely removed from the radiator. Remaining damage consisted of cracks and or shattering of the mirror.

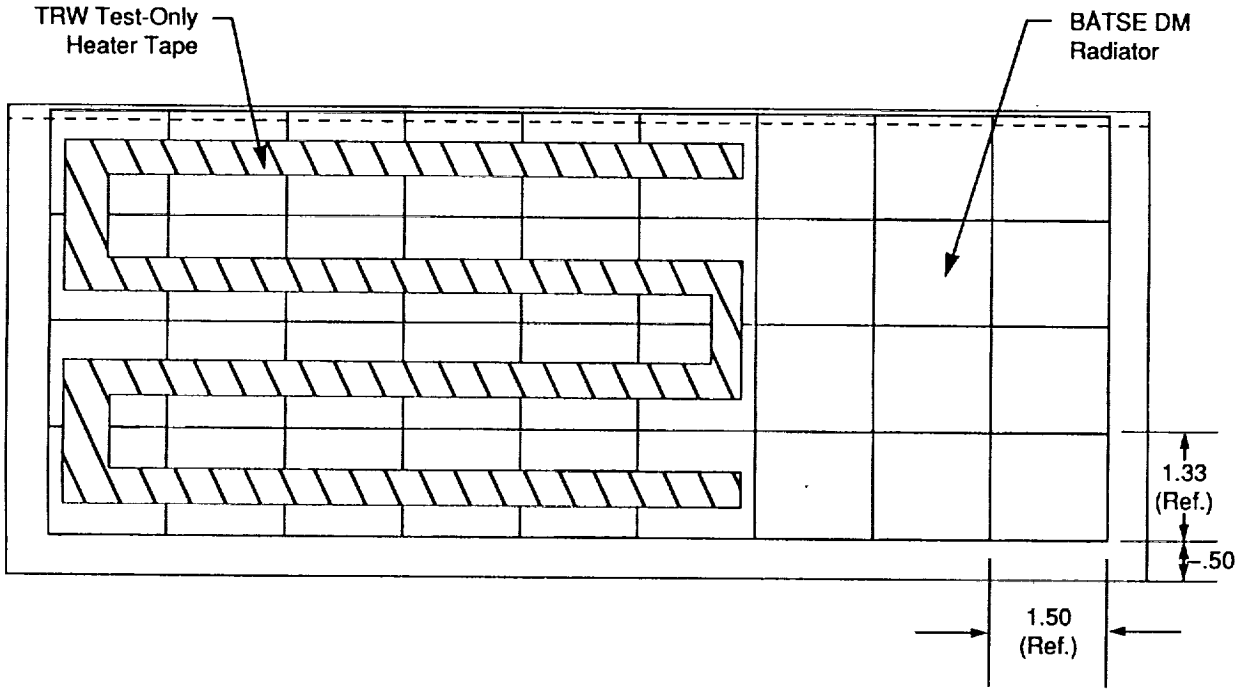

Figure 3.43. BATSE Thermal Radiator Panel with Test-Only Heater Installed.

The heater used was a standard Claiborne heater tape, which is a Kapton-like tape with an acrylic adhesive containing wires. Standard TRW procedure was to remove these heaters by pulling carefully and then cleaning the surface with alcohol to remove any residue.

Although the damage occurred to the non-flight side mirror, because the problem occurred during the removal, it became the concern of the BATSE team that other flight-side mirrors would be damaged later in the program. BATSE was further constrained by the lack of spare mirrors. The mirror panels could not be moved from one side of the detector module to the other because each has a particular handedness. Leaving these heaters on through thermal

vacuum test would possibly make the adhesive more difficult to remove, causing more damage than necessary.

The BATSE structural test article mirrored radiator panel was shipped to TRW to allow the thermal technicians a test-bed for removal of heater tape. After several practice runs on the STA, the heaters were removed from all flight modules. Four mirror segments were damaged during the removal, two on B3, and one each on B4 and B6, bringing the total number of damaged segments to 10. After a few weeks of consideration and planning of the repair, these segments were cleaned, any mirror fragments were removed, and the holes patched with aluminized Kapton tape. Mr. Bruce Monteith, principal thermal engineer of the GRO spacecraft, provided a calculation which showed that the a/e ratio of the mirrored surface was not substantially affected by the presence of the Kapton tape in place of a mirror.

5. Instrument Data Run #1

On January 20, BATSE test conductors began the first full-scale calibration of the Instrument since installation onto the GRO spacecraft. Each of the BATSE TP-series tests were performed, providing baseline values for all aspects of instrument performance. Furthermore, this sequence of events offered the first opportunity to verify the burst trigger and solar flare trigger signals with the other three GRO instruments on-line.

During the first day of testing, TP-110, TP-105, TP-188, and TP-200 were all completed. No anomalies were present during the tests. Having thoroughly exercised the instrument 3 days prior to these tests during the integration verification tests, no anomalies were expected. Chip Meegan and John Horack were the test conductors. On the second day of testing, January 21, BATSE test conductors completed another iteration of TP-110, TP-170, TP-171, and TP-120. The CPD tests provided some interesting results. Table 3.92 contains the count rates from each of the eight CPDs at various +HV command file settings. The +HV values used here were identical to those from the instrument system-level bench testing in November.

Table 3.93. TP-170 CPD Rates at CPDHVn Voltage Settings
BATSE Instrument Data Run #1 -- January 1989

	CPD Count Rate at Various +HV Command File Settings							
	Detector Module							
	B0	B1	B2	B3	B4	B5	B6	B7
CPDHV1	84.1	89.9	113.7	106.3	86.6	100.3	88.8	108.9
CPDHV2	70.7	74.5	92.5	87.1	74.1	83.8	78.3	89.4
CPDHV3	68.1	72.8	87.7	81.7	71.3	78.9	73.8	85.4
CPDHV4	66.9	68.1	84.2	75.9	68.1	75.6	70.9	80.1
CPDHV5	63.3	65.8	78.9	71.2	65.3	69.9	68.3	75.2
CPDHV6	60.5	62.3	74.3	66.6	61.8	66.3	64.6	69.9
CPDHV7	56.3	55.4	66.0	58.2	57.4	60.0	59.3	62.3
CPDHV8	51.5	49.3	57.3	50.2	51.0	50.0	54.2	53.6

Comparison of the data in Table 3.93 with that of the previous test indicates a substantial drop in counting rate for some of the odd-numbered detectors at a given voltage. The results of TP-171 further substantiate this observation. The coincidence count rates determined in TP-171 (see Table 3.94) show a deficiency of nearly 2 counts/second in the odd-numbered detectors when compared with the even-numbered detectors. This deficiency is caused by the spacecraft absorption of incident muons and high energy cosmic ray secondaries, emanating from a distribution which is peaked at the local zenith. Those detector modules on the bottom of the spacecraft (odd numbers) are shielded from the incident flux by the spacecraft mass overhead, and consequently display a lower counting rate.

Table 3.94. Coincidence Counting Rates for BATSE Detector Modules
TP-171 -- Instrument Data Run #1

Detector Module	Coincidence Rate
B0	20.8
B1	18.2
B2	22.9
B3	18.4
B4	21.1
B5	17.9
B6	21.3
B7	18.3

January 23 was the third day of the instrument data run, and BATSE test conductors performed the long calibration, TP-140. As with previous iterations of this test procedure, small Ba 133, Co , Cs 137, and Cd 109 isotopes were used in front of each of the detector modules. Isotope placement was not as easy with each of the modules now on the spacecraft. Four long vertical poles were placed at the corners of the GRO. Attached to each of the poles was an adjustable clamp assembly, similar to the clamps seen in high school chemistry laboratories. The isotopes were placed into the clamp end of the assembly and adjusted for the optimum source location. The intent was to replicate the standard 50.8-cm on-axis location as closely as possible. After the placement of the sources, a measurement was made to determine the actual location with respect to the centers of the LAD and SD. Additionally, an offset angle and distance from the LAD axis were recorded. An offset angle of 0° corresponded to a location directly above the LAD axis. Table 3.95 summarizes the source locations for instrument data run #1.

Table 3.95. Isotope Locations for Instrument Data Run #1

	LAD Distance (cm)	SD Distance (cm)	Offset Angle (°)	Distance to LAD Axis (cm)
B0	50.8	64.1	200	2.54
B1	50.8	58.4	45	10.2
B2	50.8	67.3	240	2.54
B3	50.8	63.5	300	8.89
B4	50.8	71.1	45	2.54
B5	50.8	66.0	0	1.27
B6	50.8	68.6	120	5.1
B7	50.8	64.8	30	2.54

With the isotopes placed in the locations described by Table 3.95, numerous spectra were obtained each with a duration of approximately 32 minutes. Single PMT spectra were obtained from the LADs with the Cs 137 source in place. These one-tube spectra were obtained at nominal + HV and nominal +100 V. Knowledge of the photopeak location and the voltage used for each of these spectra allowed for the calculation of the PMT gain exponents for all LAD phototubes. The gain varies with +HV as voltage to the Nth power. Consequently, the exponent N can be found from the following relation:

$$\log (E1/E2) = N \log(HV1/HV2) \tag{3.3}$$

The gain exponent values shown below are in good agreement with those obtained as early as the individual PMT screening tests described in section III.A.4.

	Gain Exponent for PMT		
	A	B	C
BO	7.1	6.9	5.6
B1	7.0	6.7	5.9
B2	7.1	6.4	6.9
B3	6.4	5.9	7.2
B4	6.3	5.5	6.6
B5	5.9	5.8	6.1
B6	7.2	7.3	7.2
B7	6.3	6.5	5.6

TP-140 also provided a calibration of LED location in HER channel space for each of the allowed command amplitudes. During this portion of the test, the LEDs were powered on and commanded to a particular value. Spectra were obtained, and the location of the LED peak was recorded. This process was repeated for all 16 possible LED amplitudes. Table 3.96 contains the results of this operation.

Table 3.96. HER Channel Location of LED Peak for Associated Amplitudes from TP-140 - Long Calibration, Instrument Data Run #1

	HER Channel Location of LED for Module							
LED Hex Amplitude	B0	B1	B2	B3	B4	B5	B6	B7
3	Off	Off	Off	Off	Off	Off	Off	Off
4	13	27	15	22	21	30	24	23
5	30	62	35	52	47	68	55	50
6	49	83	57	75	70	90	77	72
7	66	97	72	72	85	100	96	87
8	76	102	84	99	97	106	100	97
9	86	107	96	103	101	112	105	101
A	96	112	98	107	105	118	109	105
B	98	117	101	111	109	124	114	109
C	100	122	104	115	112	127	118	112
D	102	127	107	119	116	127	122	115
E	104	127	110	123	120	127	126	118
F	106	127	112	123	123	127	127	122

The instrument data run continued through January 28, 1989. During the remaining time, BATSE test conductors executed TP-180 (three options), TP-190 (two options), TP-188, TP-200, and a check of all BATSE heaters. The other three Instruments successfully received burst and solar flare trigger signals on both primary and redundant lines. All facets of the burst data test and pulsar data tests were successful. The final test of instrument data run #1 was completed at 14:30 on January 28.

6. BATSE Re-Integration Verification Tests

In February 1989, an alert was put forth on a Teledyne T05 relay part number M39016/30/060P with lot-date code #84-29. Instances of internal corrosion had caused failure of T05 relays on several projects, including the CLAES experiment on the UARS satellite. Each of the RIUs on the GRO contained several of these relays. BATSE has a total of 142 similar relays installed on the flight hardware, but with different lot-date codes, and slightly different part numbers. The BPM has 18, with the CEU containing the remaining 124 relays. To date, BATSE has not seen any anomaly related to the failure of a T05 relay internal to the BATSE hardware. Because of the anomaly with these relays, each of the RIUs on GRO were removed and shipped to Fairchild Corporation of Germantown, Maryland, where replacement relays were installed.

Removal of the BATSE RIUs required that all BATSE detector module interfaces to the CEU and BPM be broken so that the panel could be opened. The panel remained opened without RIUs for over 2 weeks and was finally closed on March 6. During this time, BATSE was unable

to test the instrument in any manner. In the meantime, MSFC engineers performed analysis on nine spare relays, and found no verifiable evidence of a problem in these relays. This parts analysis was performed under the direction of Mr. Dennis Ellsworth (EJ-21), BATSE Chief Engineer.

After removal of the flight RIUs, temporary units were installed, the BATSE panel was closed, and all detector module interfaces were re-mated. At that point, another iteration of TP-100 was required to verify that all connections had been made properly and that no damage had occurred during the removal and replacement of the RIUs. TP-100 was begun on March 7, 1989, and concluded the next day. The results of this test, which served as the only functional test prior to the radioactive source survey, are on file in the BATSE library. No anomalies were discovered during the test, and BATSE was declared fully functional again on the evening of March 8.

7. GRO Radioactive Source Survey Test

a. Overview

The first operation performed at the spacecraft level directly related to science was the radioactive source survey test. Five days were required for completion of the test, with each day having a different test configuration and objective. The first 4 days of testing were directed by the BATSE test conductors, with the final day being directed by COMPTEL.

The test was designed to provide data on how the spacecraft mass scatters radiation into the BATSE detector modules. During on-orbit operations, part of the detected flux from a gamma ray burst will be directly incident radiation, and another part will be scattered radiation, primarily from the spacecraft and the atmosphere. Proper deconvolution of the count spectrum into a photon spectrum requires knowledge of the behavior of the detector in that scattering environment. The data from the radioactive source survey, along with Monte Carlo simulations, were used to determine the spacecraft-scattering component of the detector response matrices so that a correct photon spectrum could be generated.

Isotopes of Co 60, Ba 133, and Cs 137 were used during this test. These sources were the same as those used in the BATSE angular response calibration. To limit the region which was illuminated by the source, the isotope was installed into a lead cone. This cone provided collimation to a region 50° in cross-sectional aperture. The lead portion of the cone was wrapped in tin to provide absorption of K-shell x-rays generated in the lead. Figure 3.44 details the construction of the lead cone.

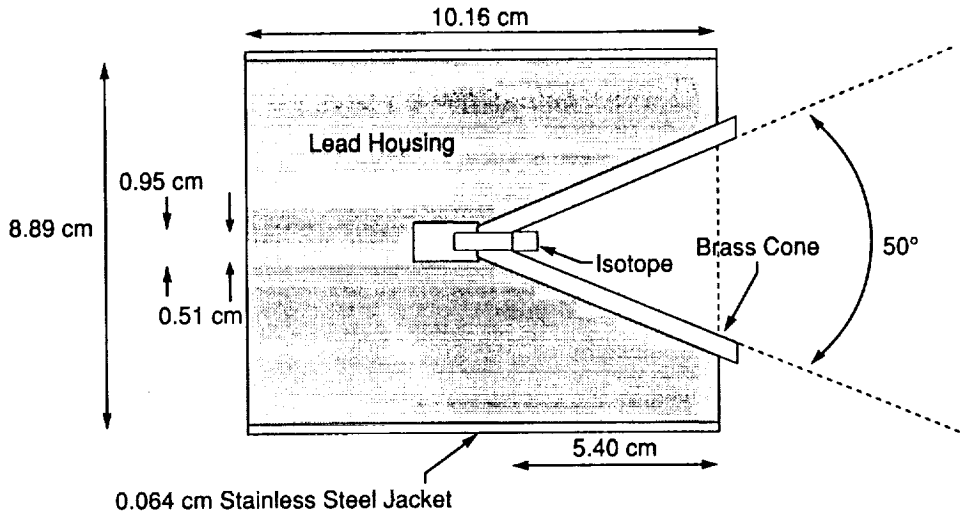

Figure 3.44. GRO Radioactive Source Survey Isotope Collimator and Holder.

Because the test was primarily concerned with gamma rays which scatter into the detectors after hitting the spacecraft, a shield was developed for the BATSE large area detectors to obstruct direct flux from entering the LAD. This cover was fabricated from octagonal pieces of lead, wood, tin, and copper. The shield mounted to the detector module lifting brackets and is schematically shown in Figure 3.45.

The 4 days of BATSE-controlled testing consisted of numerous spectral accumulations from all three isotopes placed at 21 different locations around the GRO. These locations were distributed at points throughout the R7A high-bay on three sides of the spacecraft. The +X, -X, and -Y sides of the GRO were illuminated from many different heights. The +Y side of the GRO was not illuminated because of space constraints, and because of its geometric similarity to the -Y side. In the following sections, each day's events will be detailed, along with precise source locations and testing configurations. Each of the following paragraphs have nearly identical structure so that comparison of related information from different days is easily facilitated.

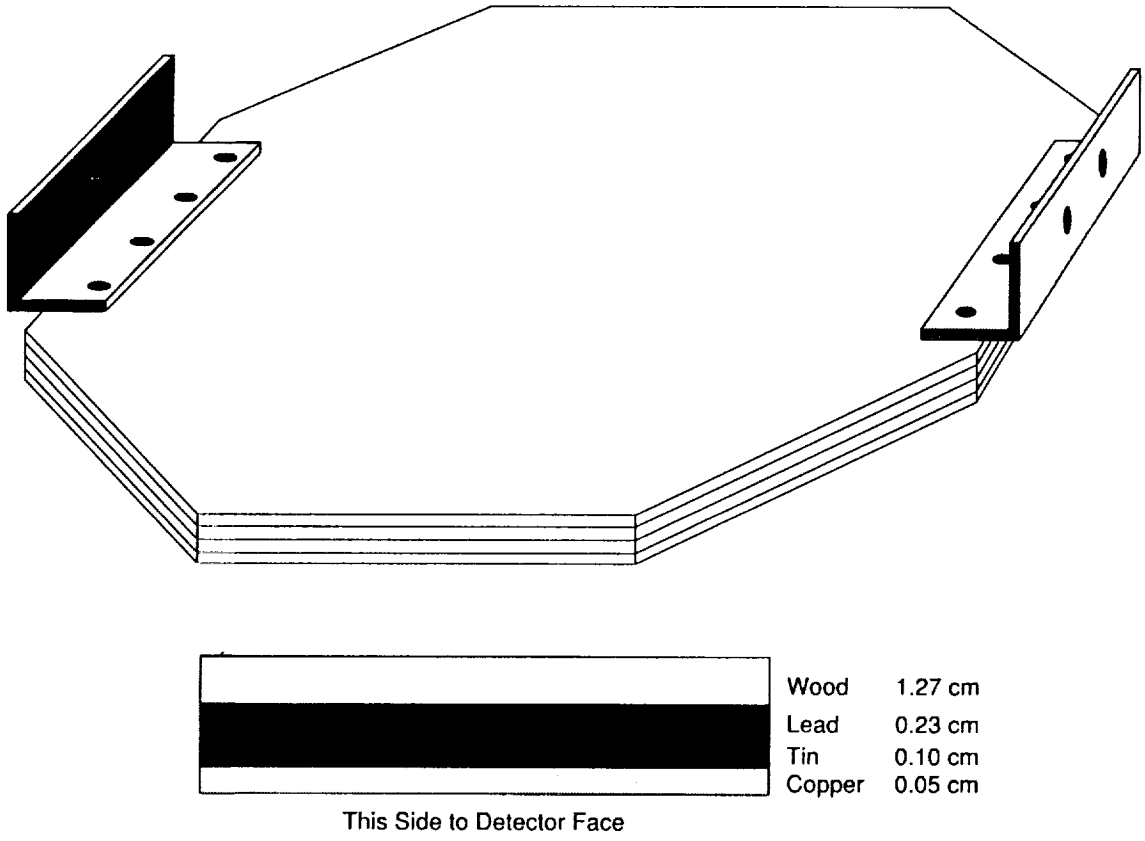

Figure 3.45. BATSE Radioactive Source Survey LAD Shields (one of four).

b. Day #1 Operations

The first day of the source survey was March 9, 1989. The BATSE occulting shields were installed onto B0, B1, B2, and B3. Isotope locations were confined to seven places in the +X hemisphere of the GRO coordinate system. These locations are shown in Figure 3.46.

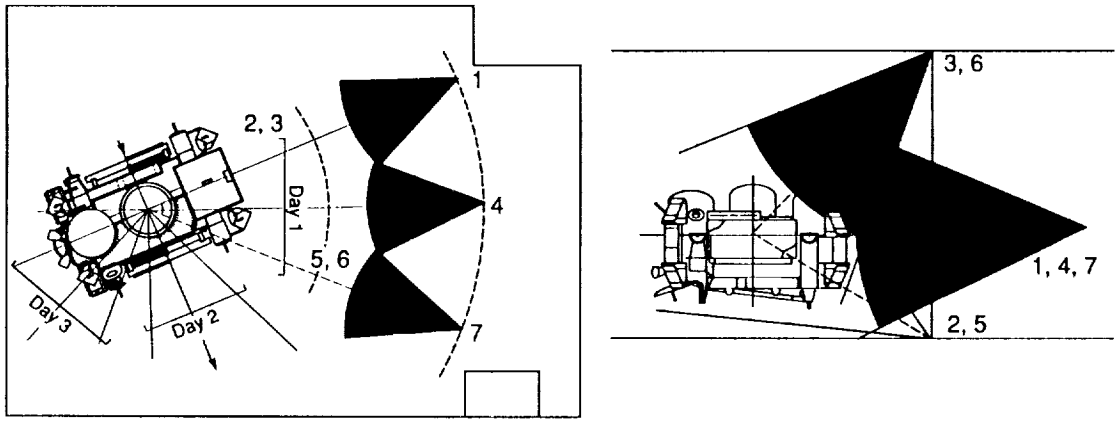

Figure 3.46. Radioactive Source Survey Day #1 Isotope Locations.

Using the GRO star-tracker optical reference fixture, the actual location of these positions could be determined precisely in the GRO coordinate frame. Table 3.97 shows the measured values (in inches) for each of the seven isotope locations on the first day of the source survey.

Table 3.97. Isotope Placement Data in GRO Coordinates, Radioactive Source Survey - Day #1

	GRO Coordinates			Distance to GRO Center (0,0,0)
Location	X	Y	Z	from isotope location
01	+479.4259	+0.2731	-0.0606	479.4260
02	+268.3351	-38.4979	-121.7375	297.1629
03	+274.4610	-40.2353	+286.3014	398.6430
04	+444.9044	-182.0965	-0.0449	480.7277
05	+216.3704	-163.5496	-121.7376	297.2956
06	+220.6061	-168.9993	+278.1844	393.2104
07	+337.8181	-339.3447	-0.0047	478.8277

With the source location at the apex of the cone known to such exact values, the BATSE team could define the approximate extent of the illuminated region by simply finding two other points on the cone. With these three points, the illumination region is uniquely defined. To accomplish this task, the isotope and the cone were placed into the desired position, and the measurements in Table 3.97 were determined. Then, using binoculars and a tape measure, two locations were found where the source region was cut-off by the edge of the cone. Although this method provided a rather crude measurement, it was entirely suitable for the purpose of defining

the approximate region of illumination. These locations were referenced to the GRO's 40,000 pound, orange support structure, and the X-Y coordinates were recorded. The Z coordinate (unless otherwise noted) is the height of Dr. Gerald Fishman's eyes, approximately 178 cm. Because these measurements are rather crude, a full set of photographs was taken from the aspect of the source holder. These photos, available in the BATSE library, will provide the interested reader with a detailed look at the test environment. Figure 3.47 details the measurements from the first day of the radioactive source survey.

Locations #3 and #6 were executed first, as all three sources were cycled through these two places. This was done so that the MGSE which supported these positions could be removed from obstructing the field of view from locations #1, #4, and #7. Following these first two locations, data were taken from the Co 60 source at all remaining locations, followed by the Cs 137 isotope, and finally the Ba 133 isotope. This was done to minimize the required handling and exchange of radioactive material during the procedure.

At each location, an integration of approximately 15 minutes duration was obtained. Background spectra were taken throughout the day, and each spectrum obtained was stored to floppy disk for later analysis. Each of these disks, along with the archive tape, are available for inspection in the BATSE data library.

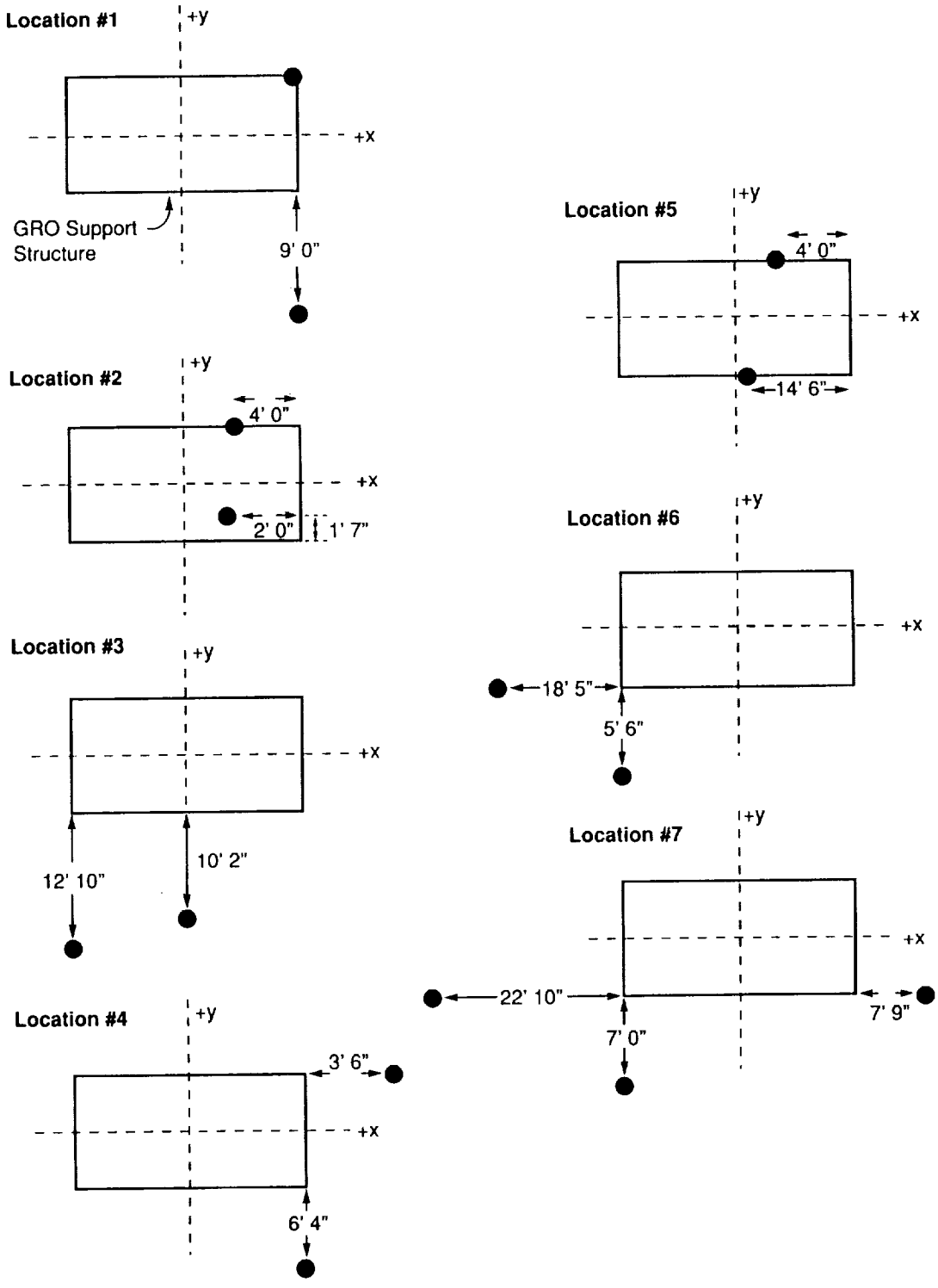

Figure 3.47. Two Points of the Illumination Cone for Each Isotope Location Radioactive Source Survey - Day #1.

c. Day #2 Operations

The second day of the source survey was March 10, 1989. The BATSE occulting shields were installed onto B6, B1, B7, and B3. Isotope locations were confined to seven places in the 479.4259 hemisphere of the GRO coordinate system. These locations are shown in Figure 3.48.

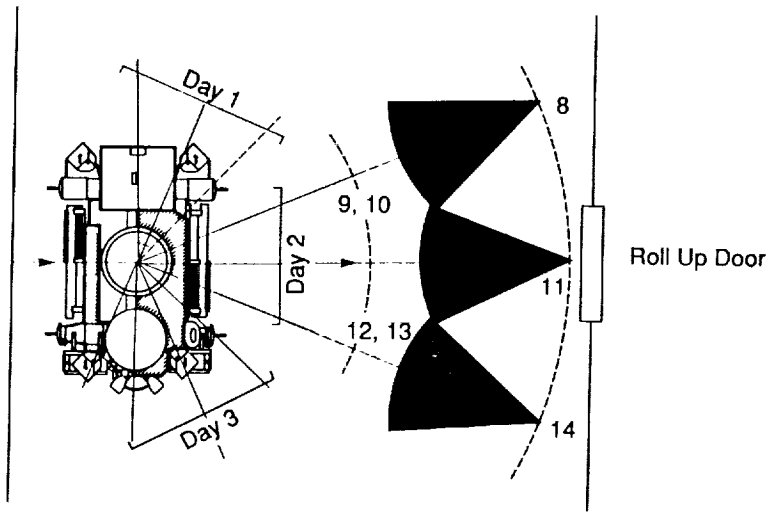

Figure 3.48. Radioactive Source Survey Day #2 Isotope Locations.

Using the GRO star-tracker optical reference fixture, the actual location of these positions could be determined precisely in the GRO coordinate frame. Table 3.98 shows the measured values (in inches) for each of the seven isotope locations on the second day of the source survey.

Table 3.98. Isotope Placement Data in GRO Coordinates, Radioactive Source Survey - Day #2

	GRO Coordinates			Distance to GRO Center (0,0,0)
Location	X	Y	Z	from isotope location
08	+184.5463	-443.6147	-0.2079	480.4700
09	+67.7651	-262.7327	-120.7083	297.2755
10	+71.6892	-270.3140	+277.1849	393.7518
11	-0.2288	-463.3988	-0.0594	463.3998
12	-67.6711	-262.2672	-120.3841	296.7102
13	-66.5457	-266.9500	+281.0001	393.2578
14	-184.4763	-435.5344	+0.6759	472.9928

With the source location at the apex of the cone known to such exact values, the BATSE team could define the approximate extent of the illuminated region by simply finding two other points on the cone. With these three points, the illumination region is uniquely defined. To accomplish this task, the isotope and the cone were placed into the desired position, and the measurements in Table 3.98 were determined. Then, using binoculars and a tape measure, two locations were found where the source region was cut-off by the edge of the cone. Although this method provided a rather crude measurement, it was entirely suitable for the purpose of defining the approximate region of illumination. These locations were referenced to the GRO's 40,000 pound, orange support structure, and the X-Y coordinates were recorded. The Z coordinate (unless otherwise noted) is the height of Dr. Gerald Fishman's eyes, approximately 178 cm. Because these measurements are rather crude, a full set of photographs was taken from the aspect of the source holder. These photos, available in the BATSE library, will provide the interested reader with a detailed look at the test environment. Figure 3.49 details the measurements from the second day of the radioactive source survey.

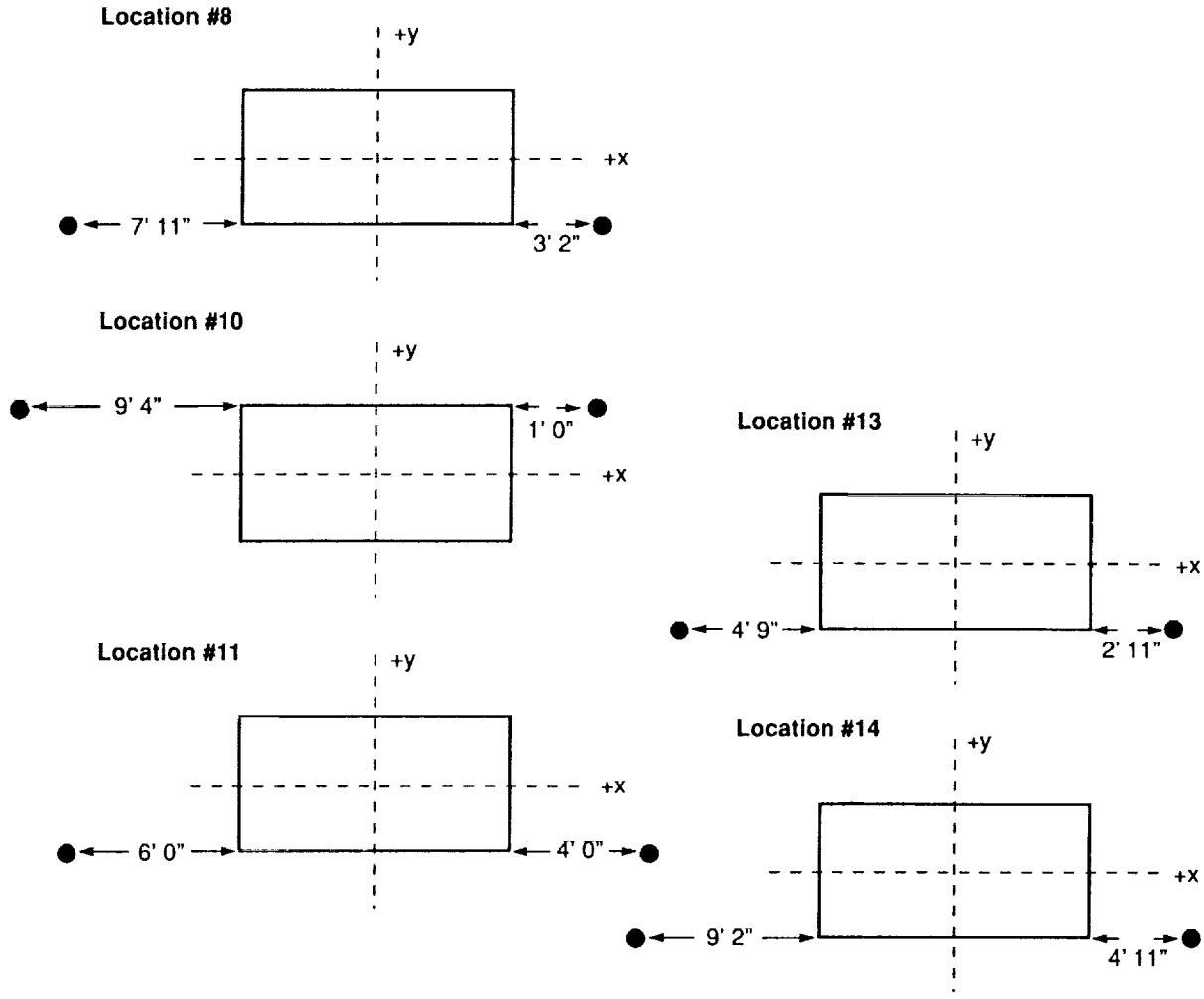

*NOTE: The two floor locations, #9 and #12 are not available.

Figure 3.49. Two Points of the Illumination Cone for Each Isotope Location Radioactive Source Survey - Day #2.

Locations #10 and #13 were executed first, as all three sources were cycled through these two places. This was done so that the MGSE which supported these positions could be removed from obstructing the field of view from locations #8, #11, and #14. Following these first two locations, data were taken from the Co 60 source at all remaining locations, followed by the Cs 137 isotope, and finally the Ba 133 isotope. This was done to minimize the required handling and exchange of radioactive material during the procedure.

At each location, an integration of approximately 15 minutes duration was obtained. Background spectra were taken throughout the day, and each spectrum obtained was stored to floppy disk for later analysis. Each of these disks, along with the archive tape, are available for inspection in the BATSE data library.

d. Day #3 Operations

The third day of the source survey, March 11, 1989, mirrored that of day #1; however, operations were conducted in the -X hemisphere of the GRO coordinate system. The BATSE occulting shields were installed onto B4, B5, B6, and B7. As with the previous 2 days, seven isotope locations were again used for the third day. These locations are shown in Figure 3.50.

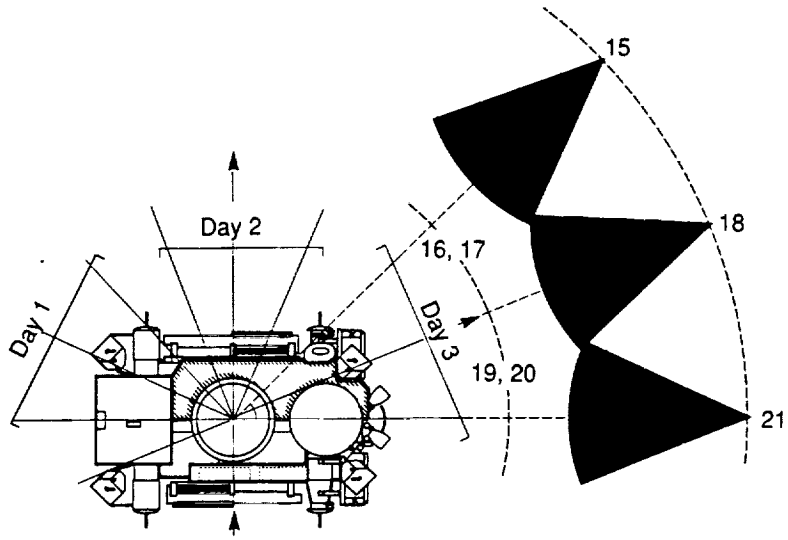

Figure 3.50. Radioactive Source Survey Day #3 Isotope Locations.

Using the GRO star-tracker optical reference fixture, the actual location of these positions could be determined precisely in the GRO coordinate frame. Table 3.99 shows the measured values (in inches) for each of the seven isotope locations on the third day of the source survey.

Table 3.99. Isotope Placement Data in GRO Coordinates, Radioactive Source Survey - Day #3

Location	GRO Coordinates X	Y	Z	Distance to GRO Center (0,0,0) from isotope location
15				479.3481
16				296.7361
17	-211.4691	-162.9682	+272.2252	381.2930
18	-443.8810	-184.3631	+1.9109	480.6493
19	-268.4260	-37.2374	-119.4775	296.4689
20	-263.9705	-36.9679	+272.2419	281.0023
21	-480.4127	+0.3699	-0.0626	480.4128

With the source location at the apex of the cone known to such exact values, the BATSE team could define the approximate extent of the illuminated region by simply finding two other points on the cone. With these three points, the illumination region is uniquely defined. To accomplish this task, the isotope and the cone were placed into the desired position, and the measurements in Table 3.99 were determined. Then, using binoculars and a tape measure, two locations were found where the source region was cut-off by the edge of the cone. Although this method provided a rather crude measurement, it was entirely suitable for the purpose of defining the approximate region of illumination. These locations were referenced to the GRO's 40,000 pound, orange support structure, and the X-Y coordinates were recorded. The Z coordinate (unless otherwise noted) is the height of Dr. Gerald Fishman's eyes, approximately 178 cm. Because these measurements are rather crude, a full set of photographs was taken from the aspect of the source holder. These photos, available in the BATSE library, will provide the interested reader with a detailed look at the test environment. Figure 3.51 details the measurements from the third day of the radioactive source survey.

Locations #17 and #20 were executed first, as all three sources were cycled through these two places. This was done so that the MGSE which supported these positions could be removed from obstructing the field of view from locations #15, #18, and #21. Following these first two locations, data were taken from the Co 60 source at all remaining locations, followed by the Cs 137 isotope, and finally the Ba 133 isotope. This was done to minimize the required handling and exchange of radioactive material during the procedure.

At each location, an integration of approximately 15 minutes duration was obtained. Background spectra were taken throughout the day, and each spectrum obtained was stored to floppy disk for later analysis. Each of these disks, along with the archive tape, are available for inspection in the BATSE data library.

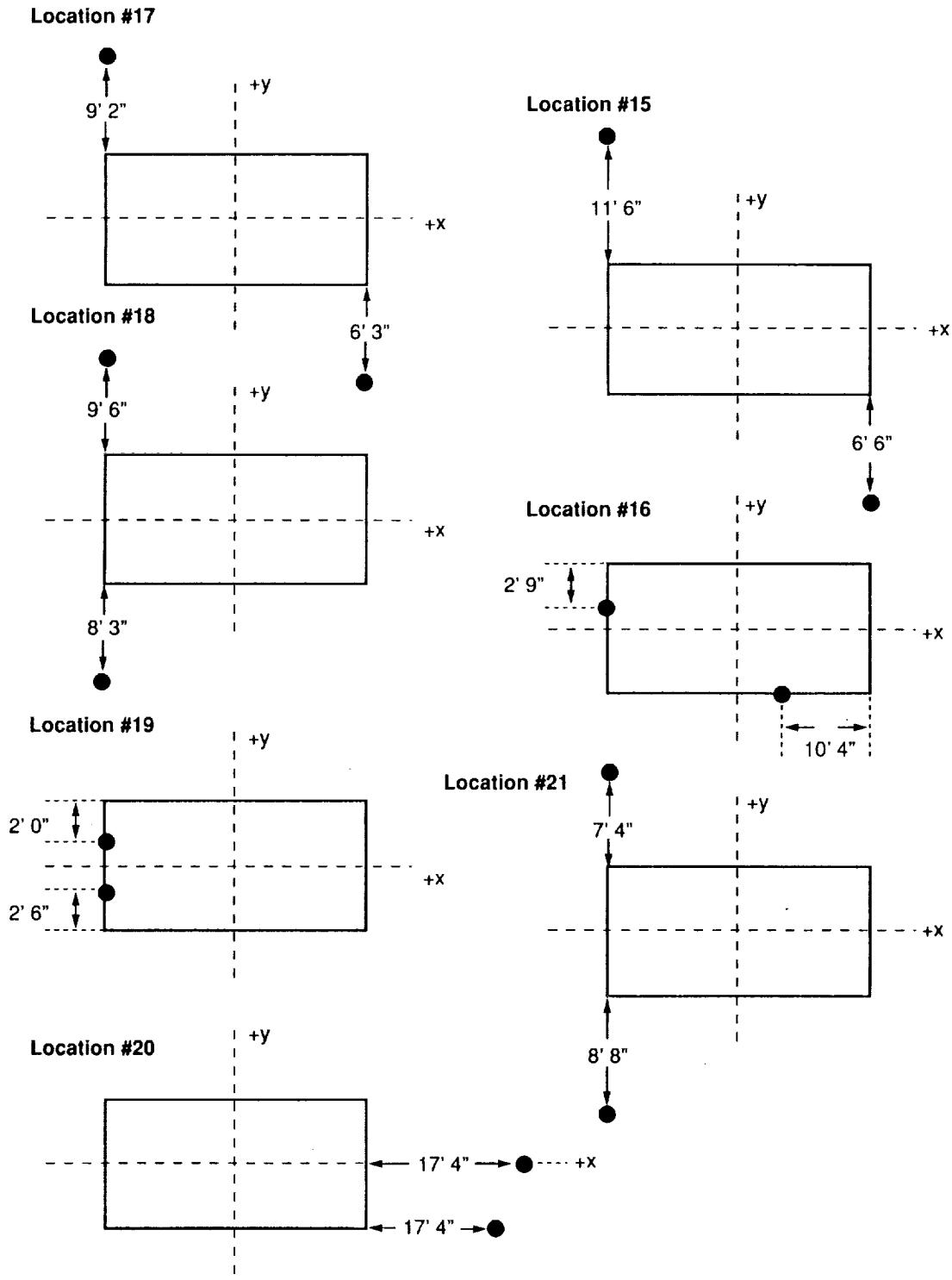

Figure 3.51. Two Points of the Illumination Cone for Each Isotope Location Radioactive Source Survey - Day #3.

e. Day #4 Operations

Day #4 of the radioactive source survey took place on March 13, 1989. The operations performed on this day differed somewhat from those of the previous 3 days. The BATSE occulting shields were removed from the spacecraft so that all detector modules were afforded an unobstructed view of the incident flux. Integrations were obtained from sources at five of the previous locations, #13, #16, #21, #11, and #1. Figure 3.52 shows these locations with respect to the spacecraft.

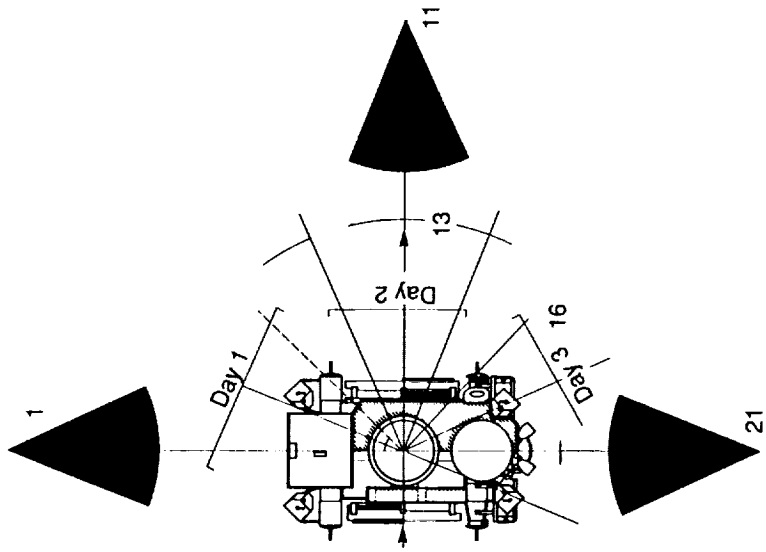

Figure 3.52. Radioactive Source Survey Day #4 Isotope Locations.

In an identical manner, the location of the isotope positions in GRO coordinate space was determined using theodolite stands and the spacecraft's star-tracker optical reference fixture. These five locations were re-measured for this day, in the event that any of the locations had moved a slight amount. Table 3.100 details the results of the source location measurements.

Table 3.100. Isotope Placement Data in GRO Coordinates
Radioactive Source Survey - Day #4

	GRO Coordinates		
Location	X	Y	Z
01	+479.4259	+0.2731	-0.6894
11	+0.7734	-463.9275	-0.5598
13	+274.4610	-40.2353	+286.3014
16	-216.7162	-162.8679	-119.9168
21	-480.4127	+0.3699	-0.0626

With the source location of the apex of the cone known to such exact values, the BATSE team could define the approximate extent of the illuminated region by simply finding two other points on the cone. With these three points, the illumination region is uniquely defined. To accomplish this task, the isotope and the cone were placed into the desired position, and the measurements in Table 3.100 were determined. Then, using binoculars and a tape measure, two locations were found where the source region was cut-off by the edge of the cone. Although this method provided a rather crude measurement, it was entirely suitable for the purpose of defining the approximate region of illumination. These locations were referenced to the GRO's 40,000 pound, orange support structure, and the X-Y coordinates were recorded. The Z coordinate (unless otherwise noted) is the height of Dr. Gerald Fishman's eyes, approximately 178 cm. Because these measurements are rather crude, a full set of photographs was taken from the aspect of the source holder. These photos, available in the BATSE library, will provide the interested reader with a detailed look at the test environment. Figure 3.53 details the measurements from the fourth day of the radioactive source survey.

Location #13 was utilized first during day #4. The Co 60, Ba 133, and Cs 137 sources were cycled through this location, and spectra were obtained from all eight detector modules. Following the three isotope integrations, the Cs 137 source was utilized to trigger a "burst" by suddenly exposing the source to the spacecraft after burst triggering had been enabled. The intensity of the source was modulated by repeatedly opening and then obstructing the aperture with a lead brick. The burst readout was allowed to complete, and the source was left in the exposed configuration for nearly 1 hour. Unfortunately, these data were archived onto an unreadable tape and cannot be recovered.

When the burst readout and exposure were complete, the GSE used to support location #13 was removed to prevent obstruction of the field of view from location #11. The Co 60 source was cycled through the remaining locations, followed by the Cs 137 source and the Ba 133 isotope. Day #4 concluded the BATSE portion of the radioactive source survey.

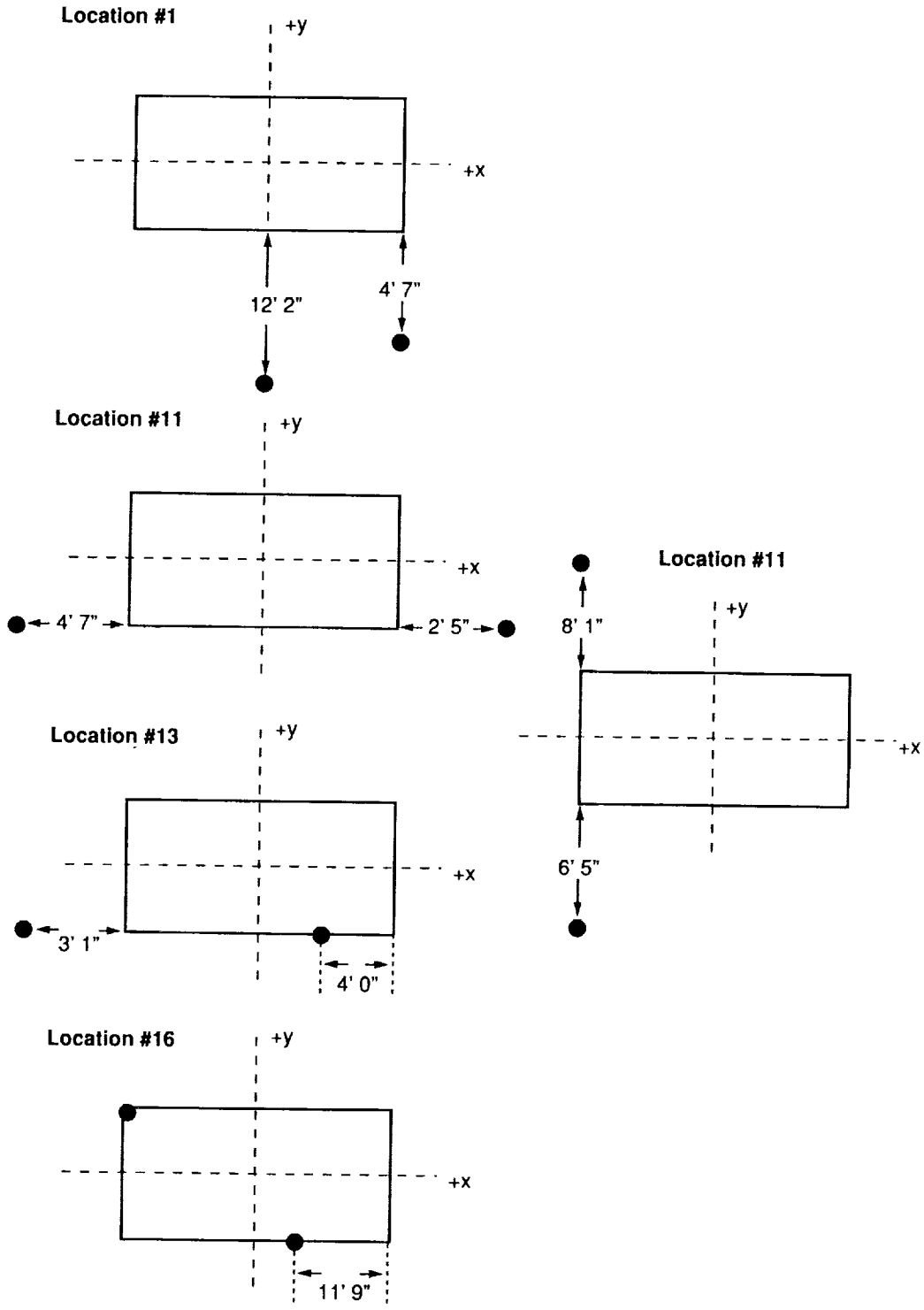

Figure 3.53. Two Points of the Illumination Cone for Each Isotope Location Radioactive Source Survey - Day #4.

f. Day #5 Operations

The final day of the source survey was under the direction of personnel from the COMPTEL Instrument. To obtain an adequate data set, COMPTEL required additional data from different isotope locations than the ones used in the previous 4 days of testing. Several new isotopes were used, including Mn 54 (2 mCi), Na 22 (2 mCi), and Na 24 (1.7 mCi at 11:00 on March 14), which has a half-life of only 15 hours. The diminishing intensity of this isotope was clearly noticeable during the acquisition of data on this day.

The locations of the isotope positions were handled in a different manner than those of the previous 4 days. One location, #13, was repeated using the COMPTEL source holder (described later in this section). In addition, seven new locations were used. Table 3.101 describes these new locations with respect to the GRO coordinate system.

Table 3.101. Radioactive Source Survey Day #5 Isotope Locations

Location #	Azimuth (°)	Elevation (°)	Distance (cm)
22	0.0	10	762
23	0.0	45	762
24	120	10	762
25	120	45	762
26	240	10	762
27	240	45	762
28	0.0	90	762

These measurements are made in a different manner to those from the BATSE locations. Azimuth is measured in the GRO X-Y plane. 0 degrees corresponds to the X-axis, with the angle increasing towards the -Y axis. The elevation is the measured angle out of the X-Y plane, with a positive angle corresponding to a positive Z coordinate. Figure 3.54 shows a view of these locations from a point located on the GRO Z-axis.

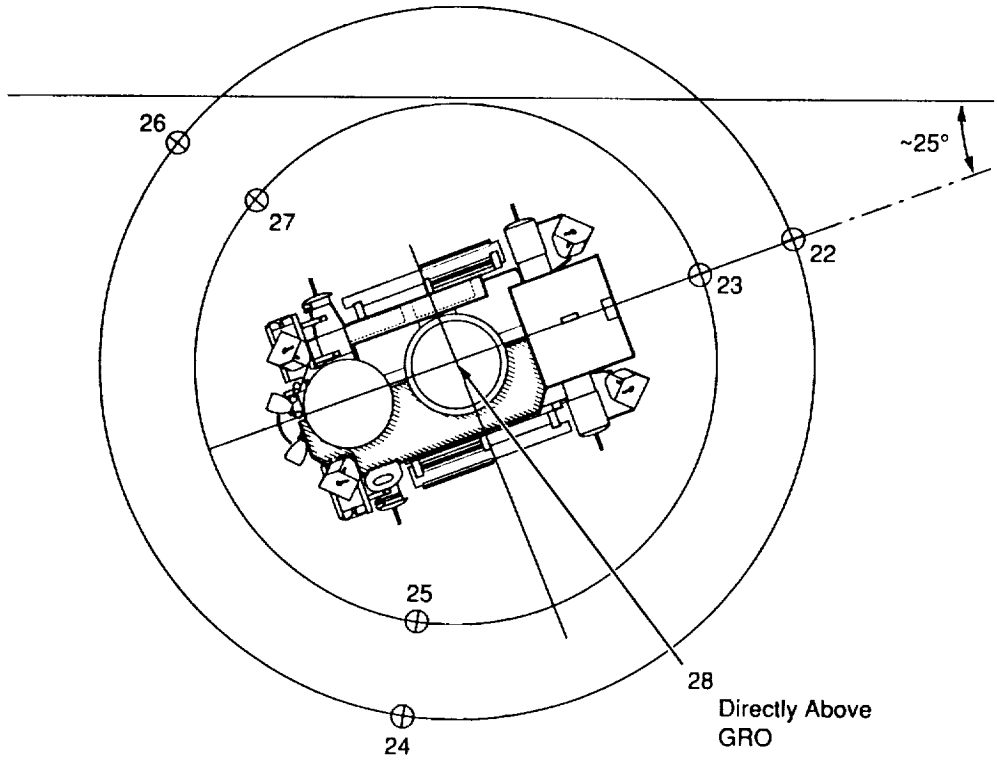

Figure 3.54. Radioactive Source Survey Day #5 Isotope Locations.

COMPTEL's source holder differed from the one which BATSE used on the first four days of the test. Because the BATSE source holder completely enclosed the isotope in lead, a concern arose that a significant amount of back-scattered radiation from the holder would be present in the detector spectra. Consequently, the COMPTEL team developed their own holder. Figure 3.55 schematically shows the construction of this holder.

The holder also serves to collimate the radiation to the standard 50° opening angle used during the previous days of testing. The isotope is mounted in a Teflon plug which slides into an opening at the rear of the fixture. Although the holder was helpful in reducing the amount of back-scattered radiation, it had the drawback of creating a significant amount of 511-keV radiation because of electron-positron pair production from gamma rays interacting in the lead. This 511-keV radiation is prominent in most spectra taken with this holder.

Location #28, directly over the center of the spacecraft, was exercised first, with spectra obtained using Na 24, Na 22, Mn 54, and finally Ba 133. Each isotope remained in place for approximately 20 minutes. The same sequence of isotopes was then cycled through locations #27 and #23, followed by #25 and #22, and #24 and #26. The testing concluded with spectral accumulations of the Cs 137 and Na 22 isotopes at location #13, followed by a background collection. All data obtained on day #5 by the BATSE instrument are available for inspection in the BATSE library. The reader interested in a more detailed account of the proceedings on day #5 should contact COMPTEL team members Roland Deihl at MPI or John Macri at UNH.

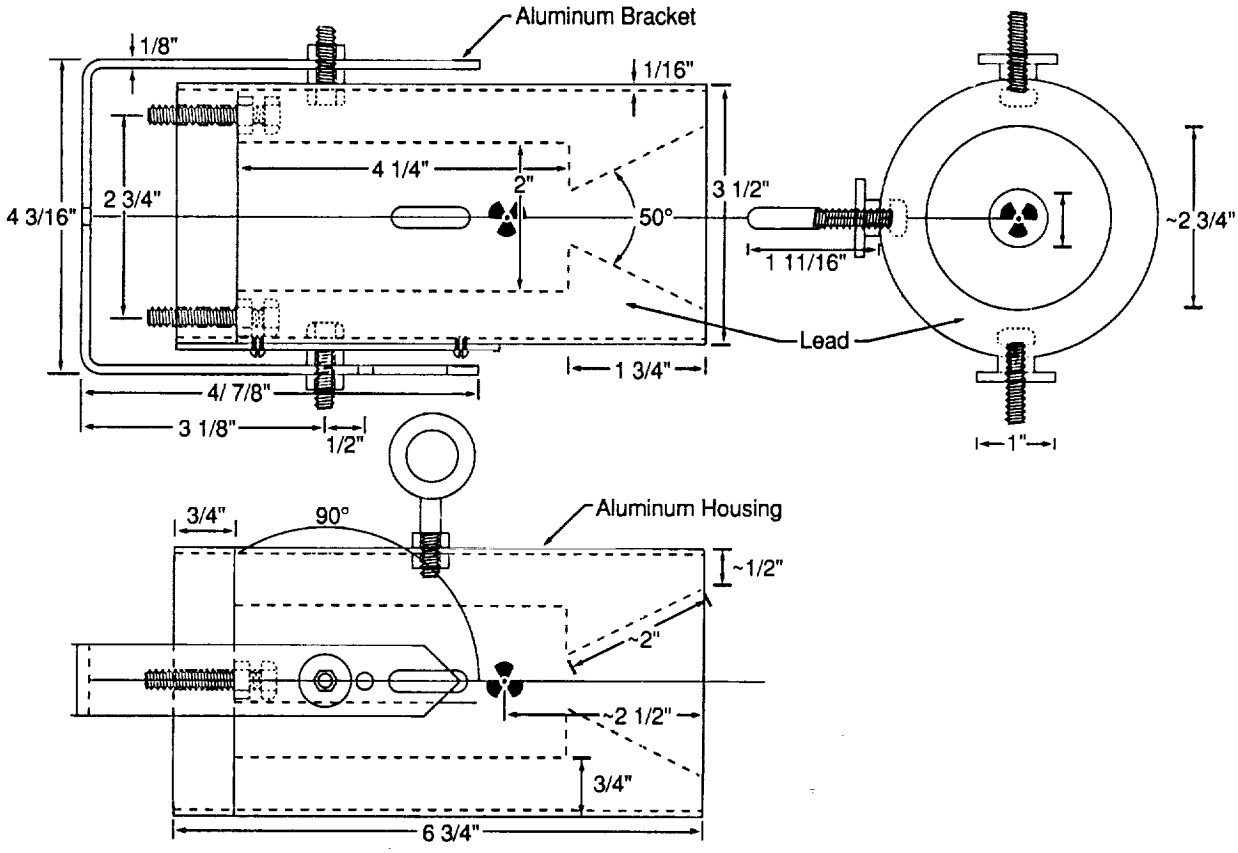

Figure 3.55. Radioactive Source Survey Isotope Holder - Day #5.

8. BATSE Mechanical Preparations for GRO Acoustics Test

a. Installation of Flight RIUs

Upon completion of the radioactive source survey test, the BATSE detector module interfaces were once again broken to facilitate the opening of the BATSE electronics panel. This disconnection took place on March 16, 1989, to allow the newly-repaired flight RIUs to be installed. BATSE received RIU serial numbers 26 and 27 to be used for flight. After a safe-to-mate bench test, the RIUs were declared ready for installation. Reconnection of the BATSE panel was completed on March 27, 1989. Despite BATSE concerns, the standard TP-100 interface verification test was not performed prior to the GRO acoustics test because of schedule constraints. The BATSE instrument entered the test without the verification that all interfaces were properly connected, and without the knowledge that the removal/reinstallation of the two RIUs had no effect on the operation of the hardware.

b. BATSE Mirrored Radiator Repair

On March 22, 1989, the 10 damaged mirror segments on the BATSE detector modules were repaired with small patches of Al-Teflon tape. Wherever possible, only the damaged portions of the segment were removed and the remaining fraction of the mirror saved. For segments which exhibited damage in excess of half the area, the entire segment was removed. In either instance, the interface layer was thoroughly cleaned, and the patch of tape was applied. This operation was done by TRW technician Mel Shier, along with BATSE representatives Scott Storey (ES62) and Bill Horn (CQ12). The test-only heaters which were mounted on the front face of the radiator panels were relocated to the back (inside) portion of each panel.

c. BATSE Thermal Blanket Installation

As described in section III.F.2, the bottom portion of the detector module thermal insulation blanket was placed onto the spacecraft as each module was installed. The upper portion of the thermal blanket remained in storage during all subsequent testing to this point. BATSE representatives Scott Storey (ES62), Bill Horn (CQ12), and Joe Wynn (EL62) performed the blanket installation. The process of blanket installation required 2 full days. All -Z detectors received blankets on March 21, 1989. The +Z MLI blankets were installed the next day.

Table 3.102. BATSE Detector Module to Thermal Blanket Correspondence

Detector Module	Blanket Serial Number
B0	007
B1	012
B2	002
B3	004
B4	008
B5	011
B6	003
B7	006

Two minor anomalies were present during this procedure. The blanket on detector module B2 suffered a small (approximately 1 cm in length) tear near the harness hole in the rear of the blanket. This small tear was patched with a piece of reflective Kapton tape. Second, four of the blankets did not fully cover the velcro attach points on the mirrored radiator panels, leaving a narrow strip of velcro exposed. A modification was implemented to alleviate concern that the velcro would degrade over time because of the space environment and exposure to the Sun. In the four locations where velcro was not covered, a strip of mating (hook or loop) velcro was cut to the same dimensions as the exposed portion. Aluminized Teflon was sewn to the back of this strip, and the unit was fastened to the velcro which was exposed.

Each of the blankets is designed for a particular location on the spacecraft and are not interchangeable. Detector insulation on the -Z portion of the GRO contains white-painted Kapton only to the interface of the GRO -Z tent. Upper (+Z) modules have blankets which are fully painted. Each of these two types of MLI blankets contain two left-handed and two right-handed blankets to expose the proper mirrored radiator panel. The MLI blankets are cut to expose the panel which most nearly faces the -X (away from the Sun) direction on the spacecraft. The upper portion of the BATSE MLI blanket contains an access port so that the LAD evacuation procedure (TPS-46) can be performed when the blanket is installed. During flight, this access port is covered with a patch, approximately 20 cm x 10 cm. These patches were not put into place until the spacecraft was at the Kennedy Space Center.

9. GRO Acoustics Test

The first environmental test performed at the spacecraft level was the GRO acoustics test. This operation was designed to verify the spacecraft's capacity to withstand the noise environment of a launch aboard the space shuttle. On April 6, 1989, the GRO was rotated for the first time into the launch orientation. To accomplish the reconfiguration, the spacecraft is lifted at the -X trunnions and rotated into a vertical position above the +X trunnions. GRO is then lifted off the horizontal support structure and is transported to a vertical support stand.

The spacecraft was moved from TRW Building R7A to the acoustic chamber, where the test was performed on April 7. During the test, the GRO was entirely passive, with no power to the spacecraft or instruments. Acoustic testing only required 1 day to complete and the spacecraft returned to building R7A on April 8. After a few minor reconfiguration tasks were funished, the GRO was moved to the horizontal position on April 10.

10. GRO Confidence Test

Following the last episode of BATSE testing with power to the instrument, many things had happened to the spacecraft. All detector module interfaces had been disconnected, and the BATSE electronics panel had been opened. After the opening of the panel, the temporary RIUs were removed, and the flight RIUs were installed. Upon closing the panel again, all BATSE detector module interfaces were re-mated. The spacecraft was then rotated 90°, transported a kilometer to the acoustics chamber, exposed to the noise environment of launch, and returned to the horizontal position in the R7A high-bay. In light of the high activity level, a "confidence test" was performed prior to the Observatory functional to verify that no problems had occurred during the previous month of operations. During this test, which commenced on April 12, the BATSE test conductor performed the set of test procedures outlined in Table 3.103.

Table 3.103. BATSE Tests Executed During GRO Confidence Testing

- TP-100 — BATSE interface verification test
- TP-200 — BATSE power control function test
- TP-204 — RIU command and telemetry test
- TP-212 — CEU discrete command test
- TP-216 — RIU passive analog test

Each of these procedures had been performed previously; however, under the circumstances of the confidence test, each of them contained particular objectives. TP-100 verified the proper connection of all detector module interfaces to the CEU and BPM. To this point, the panel has not been re-opened. Usually, TP-200 is executed primarily to verify the functionality of the BATSE power control system. In this instance, the test had the additional emphasis of verifying the proper relay status telemetries because all of these values are routed through the two new RIUs. RIU-A and B were subjected to a full check of discrete and serial command capabilities. All passive analog measurements and time-transfer unit functionality were also verified.

The GRO confidence test concluded on April 15, 1989, with a test of the BATSE burst-overwrite capability and with no major anomalies. Test data and results from the GRO confidence test are available for inspection in the BATSE library.

11. GRO Observatory Functional Test #1

a. Overview

As the name might suggest, the Observatory functional test (OFT) was the first instance in the A&T program where the spacecraft was functionally tested as a unit. Prior to this time, spacecraft and instrument testing carried an emphasis on the functionality of one subsystem, or a single aspect of a subsystem. Placed between the acoustics test and the thermal vacuum test, successful completion of the OFT verified the GRO's ability to endure the acoustic environment of launch and indicated the spacecraft's readiness to proceed with the thermal vacuum test.

During the OFT, most operations were run in parallel. BATSE testing coincided with tests of the spacecraft's command and data handler (CADH), attitude control and determination system (ACAD), electrical power distribution system (EPDS), compatibility test-van / POCC testing through the TDRSS satellite, and other instrument activities. Exceptions to the parallel activities were determinations of the spacecraft power-profile and internal electromagnetic compatibility tests.

BATSE testing began on April 21, 1989. The sequence of test procedures executed during the OFT was similar to that of the system-level bench test and integration-verification proceedings. An additional procedure (TP-192) was added to calibrate the BATSE pulsar clock frequency against the spacecraft clock frequency. The BATSE data consistency test (TP-195), and the long calibration (TP-140) were not executed. Table 3.104 lists the procedures performed during the OFT.

Table 3.104. BATSE-OFT #1 Test Procedures

- TP-100 — Engineering test
- TP-105 — Detector module test
- TP-110 — Power-up/aliveness test
- TP-120 — Coincidence test
- TP-125 — Background test
- TP-170 — CPD calibration
- TP-171 — CPD/LAD coincidence run
- TP-180 — Burst data test (three options)
- TP-188 — Burst trigger/solar flare trigger signal test
- TP-190 — Pulsar data test
- TP-192 — Pulsar clock frequency calibration
- TP-200 — Power control functional test
- BATSE thermal control system test

b. New BATSE Tests and Results

TP-192 was added to this sequence to provide a baseline relationship between the frequency of the spacecraft clock and the frequency of the BATSE pulsar clock. The GRO spacecraft clock is driven by a highly stable oscillator in the CADH module, kept inside an "oven" at a stable temperature. The BATSE pulsar clocks (CCF-A and CCF-B) are not as accurate. To properly obtain and analyze pulsar time profiles, an accurate knowledge of the BATSE clock's behavior with respect to "true" time is required. Not surprisingly, the frequency difference in the BATSE clock compared to the spacecraft clock is a function of the temperature. This temperature dependence will be discussed during the thermal vacuum portion of this document.

To perform the test, the BATSE test conductor establishes parameters for a 1-second pulsar accumulation with 1000 scans. During each pulsar data packet which the CEU generates, the spacecraft time of the start and finish of the pulsar accumulation is included. In this particular instance, it is known that the BATSE clock ticked-off precisely 1000 seconds. The ratio of the two elapsed times yields the frequency percent difference.

Because of difficulty with the initial version of the procedure, this operation was performed only on CCF-A, at a temperature of 24 °C. The test showed a frequency percent difference of 6.375×10^{-6}, the positive value indicating that the BATSE clock runs faster than the spacecraft clock. The elapsed time of the accumulation was therefore slightly less than 1000 seconds according to the GRO clock.

c. Data Comparison to Previous Testing

The OFT provided an opportunity for the comparison of data between the instrument data run and the present test. TP-170 and TP-171 provided insight into the behavior of the CPDs over time. Table 3.105 contains the difference in count rate between the OFT and instrument data run for all eight CPDs at the various CPDHVn voltages.

Table 3.105. TP-170 (OFT - Data Run) Rates at CPDHVn Voltage Settings

	CPD Count Rate Difference at Various +HV Command File Settings Detector Module							
	B0	B1	B2	B3	B4	B5	B6	B7
CPDHV1	-9.7	-16.3	-27.1	-12.7	-1.9	7.4	-4.6	-1.0
CPDHV2	-6.3	-9.9	-19.8	-11.1	-1.8	4.9	-3.9	-0.4
CPDHV3	-6.6	-11.0	-18.5	-9.0	-2.5	4.7	-4.3	-1.9
CPDHV4	-7.0	-10.3	-17.0	-7.5	-2.7	4.5	-3.1	-0.7
CPDHV5	-5.3	-9.3	-14.1	-5.6	-2.2	5.7	-3.7	-0.9
CPDHV6	-6.2	-4.7	-13.3	-5.6	-2.5	4.0	-2.2	0.6
CPDHV7	-5.6	-5.9	-11.2	-5.6	xxx	1.4	-3.1	-0.7
CPDHV8	-4.1	-5.1	-8.1	-3.3	-2.4	2.9	-3.5	-0.3

The data in Table 3.105 indicate slightly lower counting rates during the OFT than in the instrument data run. The exception is detector module B5, which shows an increase of a few counts per second. The magnitude of the changes are small enough to be explained by changes in the spacecraft environment and do not indicate any detectable degradation in CPD performance. Detector B7 shows virtually no change in the CPD over the 3-month span. Detector module B2 displayed the largest decrease in the counting rate. However, inspection of the data from the instrument data run shows that this module had the highest rate at that time. The decrease in the rate on this detector brings it into closer agreement with detectors which see a similar environment (e.g., B0). The rate difference in detector B4 at level #7 is not available because of a lost command on the spacecraft, causing the voltage not to be decremented from the previous value.

The data from TP-171 reveal a slight increase in the rejection rate when compared with the rates from the instrument data run. Again, however, these changes are of the order of 3%, and do not indicate any problem with the operation of the detector or the anti-coincidence circuitry. The top-to-bottom anisotropy in the rejection rate is still present, as one would expect. A comparison of the rejection rates from the OFT and the instrument data run is presented in Table 3.106.

Table 3.106. Comparison of CPD Rejection Rates from OFT and Instrument Data Run

Detector Module	Data Run Rate	OFT Rate
B0	20.8	21.7
B1	18.2	19.7
B2	22.9	21.7
B3	18.4	18.5
B4	21.1	22.1
B5	17.9	18.6
B6	21.3	23.2
B7	18.3	19.4

The background collection test, TP-125, offered the ability to compare the LAD and SD performances with previous calibrations and tests. Spectra taken during the OFT indicated no detectable degradation in detector or PMT performance. Although isotopes were not used, examination of the line emission from naturally occurring radioactivity provided the BATSE team with a qualitative comparison of the detector resolutions. All other BATSE test procedures were executed without anomaly and showed no detectable degradation in the performance of the flight hardware when compared to previous test results.

d. GRO Power Profile Test

The power profile test was an Observatory-level check of the EPDS system and a determination of how much power each subsystem was consuming. The data obtained from this test verified that the power production system (i.e., solar arrays and batteries) could generate enough power to operate all spacecraft electronics, with some room to spare. BATSE participated in the test by first powering up the CEU only. This requires approximately 5.0 A at 5 V for a power dissipation of approximately 25 W. Subsequently, the detector modules were powered on one-at-a-time, and a measurement of the +15Vdc BPM current was made with +HV off and then with +HV on. The current monitor used was the GRO engineering telemetry parameter 1BPM0CM. This measurement is internal to BATSE and does not take into account any power dissipated through the step-down transformer. This transformer converts +28 Vdc power from the GRO power-bus into +15 Vdc for the detector modules. Table 3.107 lists the +15 Vdc current at each of the described configurations. To determine the total power dissipation, multiply the +15 Vdc current entry by 15 and add 25 W for the CEU. Computations made with BATSE HKG telemetry yield the same power dissipation at each of the various levels. "All Nominal" indicates that for each of the detector modules powered on, their respective +HV is at nominal levels. Modules which are powered off, of course, have no +HV on. Each module when powered up without +HV requires approximately 0.2 A at +15 Vdc. The apparent inconsistency in the B0 power requirement is an artifact of an offset in the current monitor and not an actual difference in power requirements.

Table 3.107. BATSE Power Dissipation Profile Data Table

Status	+HV Configuration	1BPM0CM (+15 Vdc Current) (Amps)
BO - B7 on	All Nominal	2.46
B0 - B7 on	B7 +HV = 00	2.34
B0 - B6 on	All Nominal	2.15
B0 - B6 on	B6 +HV = 00	2.02
B0 - B5 on	All Nominal	1.79
B0 - B5 on	B5 +HV = 00	1.70
B0 - B4 on	All Nominal	1.51
B0 - B4 on	B4 +HV = 00	1.39
B0 - B3 on	All Nominal	1.19
B0 - B3 on	B3 +HV = 00	1.07
B0 - B2 on	All Nominal	0.84
B0 - B2 on	B2 +HV = 00	0.75
B0 - B1 on	All Nominal	0.56
B0 - B1 on	B1 +HV = 00	0.44
B0 only on	All Nominal	0.24
B0 only on	B0 +HV = 00	0.12

e. GRO Electromagnetic Self-Compatibility Test

A formal EMC/EMI test such as the one performed on BATSE at the system level (see section III.D.3) was not performed on the entire spacecraft. Instead, a self-compatibility test was done. One objective of the test was to measure any conducted transients on the MPS-1 and 2 busses which might be present due to significant load or voltage changes created by instrument operations. A second goal was to define and create the worst-case steady state EMI source for each Instrument. EGRET, for example, fully powered their instrument and initiated their spark chamber to provide a worst-case EMI source. Finally, the test set out to define and create the most sensitive (EMI susceptible) operating condition for each instrument. Once in these modes, the instrument and Observatory test conductors would monitor data for any sign of an EMI effect on the performance of their particular subsystem or instrument.

At the outset of the test, the GRO was operating in the most quiet EMI conditions for the normal pointing mode. Reaction wheels, magnetic torquers, and antenna drivers were all powered off. Each of the four instruments were then powered into the most EMI-sensitive mode. For BATSE, this principally entailed a lowering of the LLDs. Following the establishment of the sensitive configuration, each subsystem of the spacecraft (e.g., RF-antenna transmission, solar array operations, reaction wheel changes, etc.) was individually transitioned into a noisy configuration. The instrument test conductors monitored their data throughout to determine if any ill effects were present. No anomalous effects were found during any of the spacecraft quiet-to-noisy transitions.

The final portion of the test required each instrument to individually transition through the most significant load change possible, while the other instrumenters examined their data for anomalies. The most significant transition for BATSE is to arrive at the full-up configuration from the power-off state. During the BATSE transition, no anomalous effects were reported. Likewise, no other instrument transition was seen to affect the quality of BATSE data. When in the most noisy configuration, the GRO test team made measurements of conducted emissions on the MPS-1 and MPS-2 power bus in the frequency domain of 30 Hz to 50 MHz. The test concluded with no EMI-related anomalies.

12. GRO Thermal Vacuum Test

a. Overview

The GRO thermal vacuum test was the most complex and compreshensive activity performed during the time BATSE was in California. Preparations for this test required nearly 1 year to complete. The GRO was placed into the launch orientation, as it was for the acoustics test, and installed onto the in-plant transporter structure, which had been specially fitted with insulation and cold plates. The spacecraft was then moved to the thermal vacuum facility in TRW building M4, and placed in the chamber. The site of instrument control remained in building R7A, even though the spacecraft had been transferred to a different facility. The test ran exceptionally well throughout the 4-week duration, especially when one considers the size and complexity of the operation.

The test consisted of four complete thermal cycles between the temperatures of 0 °C and 30 °C. The first three cycles were executed without a planned plateau. Once the final temperature measurement reached the target temperature, the next transition was started. The fourth and final cycle included extended plateaus at the hot and cold cases. At these plateaus, a full-functional test of the instrument was performed, and thermal balancing of the spacecraft was executed. BATSE +HV was not powered until 48 hours after a chamber pressure of 5×10^{-5} Torr was reached on July 7, 1989.

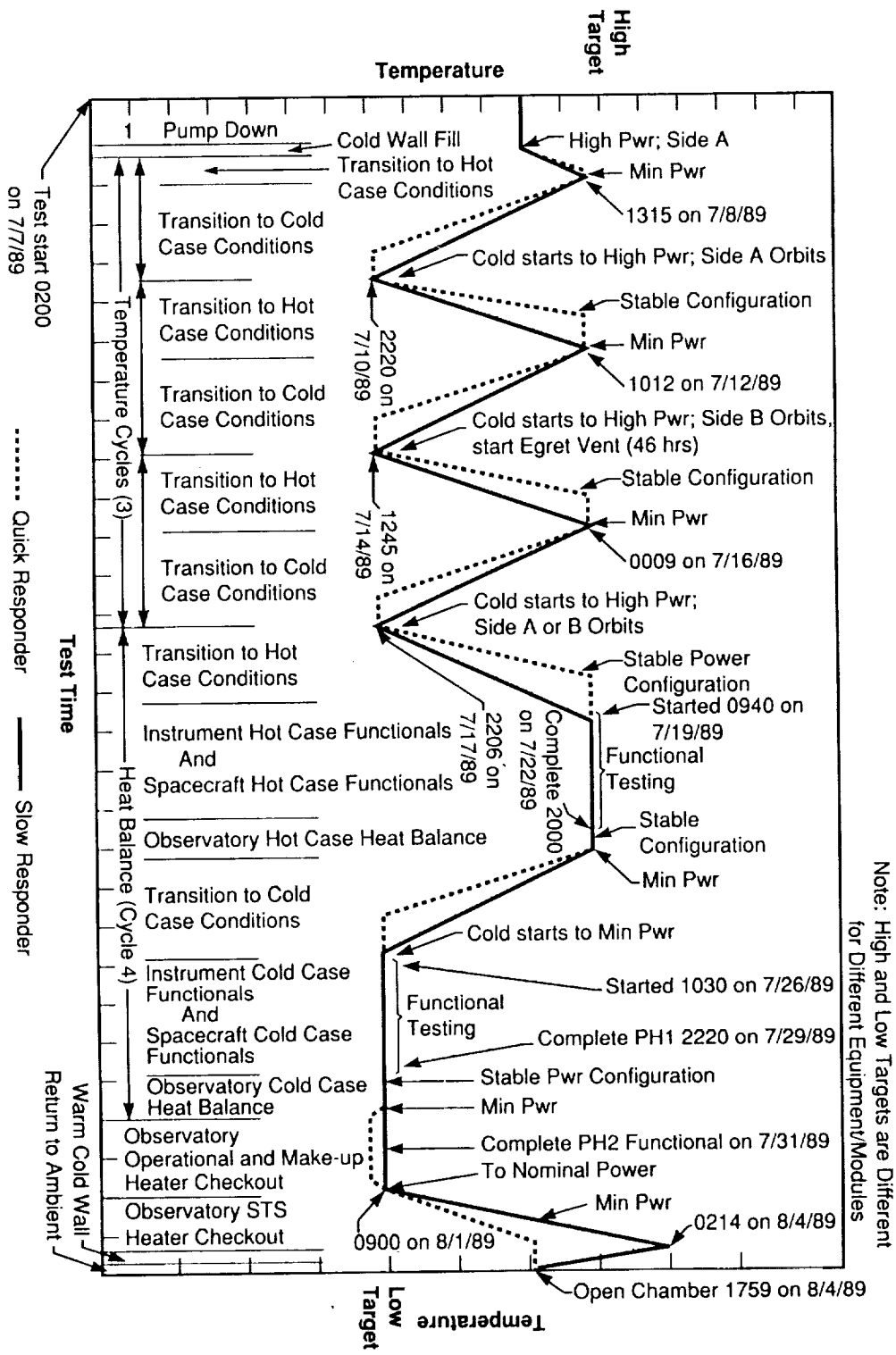

Figure 3.56. GRO Thermal Vacuum Test As-Run Timeline.

b. BATSE Mechanical Preparations and Configuration

Several mechanical operations were required for the BATSE instrument in order to configure it fully for the thermal vacuum test. Test-only heaters had been installed onto the interior portion of the radiator panels prior to the thermal blanket installation. Each detector module received a test-only patch to cover the LAD access port on the thermal blanket. These patches consist of multi-layer insulation, covered with white-painted Kapton on one side. The assembly is attached to the thermal blanket with reflective Kapton tape. Unlike the flight hardware, these test-only patches are not electrically grounded to the detector module structure. MLI closeouts were completed on May 24, 1989.

An additional major change to the configuration of BATSE was the removal of the STS heater in-flight jumper. The BATSE internal STS heater circuit is accessible at connector on the 146 bracket. During flight, a jumper is installed which routes the heater power through the thermostats, thus powering the heaters only when the thermostats are closed. While in the thermal vacuum configuration, however, this jumper was replaced with an STS heater cable which routed the STS heater circuit out of the spacecraft, through the chamber wall, and into a breakout box. The box allowed the thermal test conductor to power these heaters directly, disable them, or to place the heaters under thermostat control. Direct powering of the heaters outside of the range of thermostat closure enabled the spacecraft to more quickly transition from the cold- to hot-case temperature.

c. BATSE/GRO "On-Lid" Functional Test

After the transport of the GRO to the M4 facility, the spacecraft was placed onto the thermal vacuum chamber lid, and all necessary interfaces were mated. Prior to the closing of the chamber, a functional test of the spacecraft was performed to ensure the hardware was ready to begin the testing. BATSE participated fully in this test and was able to execute more testing than was actually planned. This testing marked the first time in which BATSE powered on while the spacecraft was in the vertical orientation.

Table 3.108 lists the testing procedures which were performed as part of the on-lid functional. These procedures were identical to those performed during previous BATSE testing. One additional test was added for the on-lid functional. As part of the GRO thermal vacuum test, a pressure monitor was constantly measuring the pressure internal to the thermal vacuum chamber. In the event of a partial pressure loss, the instruments required an immediate disabling of their +HV. Operation of the +HV in the corona region could cause severe damage to flight hardware. The pressure sensor was integrated to the GRO base-band equipment and would trigger +HV-off commands in the event of a loss of vacuum. The emergency high voltage off system was verified on July 3, 1989. The on-lid functional test was completely successfully with no anomalies. BATSE was declared ready to begin participation in the GRO thermal vacuum test on July 5, 1989.

Table 108. BATSE Test Procedures for GRO On-Lid Functional

- TP-110 — Power-up and aliveness test
- TP-105 — Detector module test
- TP-125 — Background collection procedure
- TP-170 — CPD calibration
- TP-171 — CPD/LAD coincidence test
- TP-180 — Burst data test
- TP-188 — Coordinated BTS/SF signal test
- TP-190 — Pulsar data test
- TP-192 — Pulsar clock calibration
- TP-200 — Power control functional test
- BATSE heater power and cross-strap test
- Emergency + HV off test

d. Thermal Cycle #1

Evacuation of the chamber began early in the morning hours of July 7, 1989. At approximately 9:30 a.m., the chamber pressure had reached a value of 5×10^{-5} Torr. Pressures lower than this value are considered safe for the operation of high voltage. Under previously determined rules of the test, BATSE was allowed to turn on high voltage 48 hours after this value was reached, to allow sufficient time for the outgassing and establishment of vacuum in isolated regions of the BATSE +HV system. Figure 3.57 schematically shows the rise to the first hot-case temperature for thermal cycle #1.

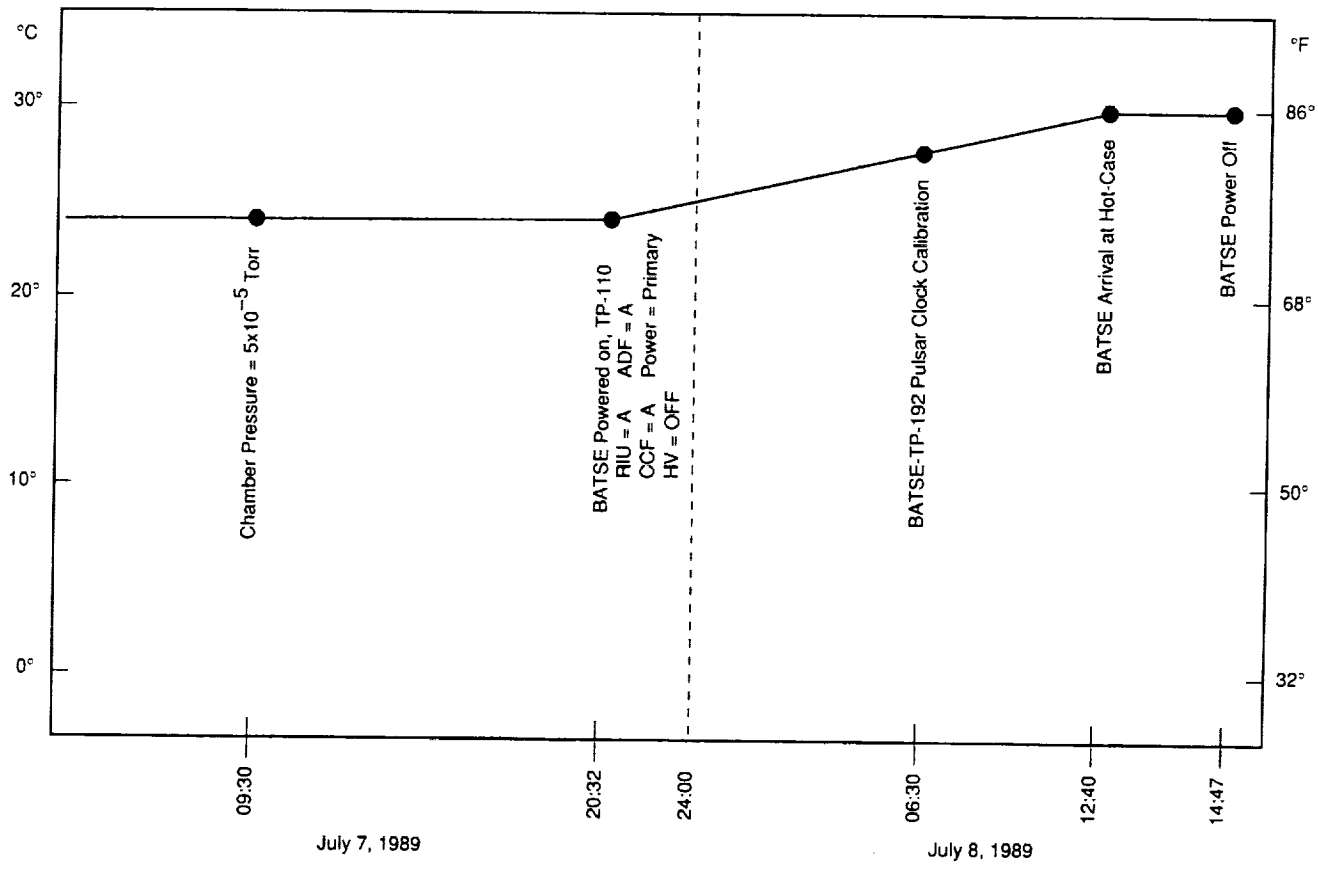

Figure 3.57. GRO T/V Timeline - Rise to Hot-Case Temperature for Thermal Cycle #1.

BATSE was powered up at 20:32 on July 7 to begin the transition to the hot-case temperature for thermal cycle #1. TP-110 was executed, with the change to the procedure to leave the high voltage powered off. The instrument was operated in the primary mode, with RIU-A, CCF-A, and primary power throughout this thermal cycle. As the temperature increased, the first pulsar clock frequency calibration was performed. The eight detector modules reached the hot-case temperature of 30 °C at 12:40 on July 8. Approximately 2 hours later, the remainder of the spacecraft reached the target temperature, and BATSE was powered off for the transition to the cold case.

During each of the cold transitions where BATSE was off, a small "state of health" test (TP-106) was performed once every 8 hours. This test allowed BATSE personnel to verify the operation of the instrument and to collect the multiplexed housekeeping temperature measurements from the detector modules. The procedure is very similar to TP-110, the power-up and aliveness test, but not as comprehensive. Primary thermal control and make-up heater power was enabled during the cold transition. Becasue BATSE was utilizing RIU-A, the status of the redundant heater systems could not be determined at this time. Thermostat closure was monitored by the BATSE team through the GRO engineering telemetry. Table 3.109 lists the times and temperatures of thermostat closure for both primary heater sets.

Table 3.109. BATSE Primary T/C and M/U Heater Thermostat Opening Times and Temperatures, GRO Thermal Vacuum Test - Thermal Cycle #1

Heater and Detector Module	1DMnTEMP (°C)	Time	Date
B0 Primary T/C	1.9	18:15	7-9-89
B1 Primary T/C	2.6	17:05	7-9-89
B2 Primary T/C	0.6	19:57	7-9-89
B3 Primary T/C	5.3	15:12	7-9-89
B4 Primary T/C	0.9	18:15	7-9-89
B5 Primary T/C	2.9	15:43	7-9-89
B6 Primary T/C	0.6	17:51	7-9-89
B7 Primary T/C	1.9	18:05	7-9-89
B0 Primary M/U	-0.8	11:39	7-10-89
B1 Primary M/U	-0.8	23:29	7-9-89
B2 Primary M/U	-1.5	00:44	7-10-89
B3 Primary M/U	-0.5	23:11	7-9-89
B4 Primary M/U	-1.1	00:08	7-10-89
B5 Primary M/U	-0.8	22:52	7-9-89
B6 Primary M/U	-1.5	22:39	7-9-89
B7 Primary M/U	-0.8	00:10	7-10-89

All BATSE detector module primary heater thermostats were verified to be operational. The BATSE CEU and BPM reached the cold case faster than the eight detector modules, arriving at the target temperature on July 9 at 20:40. Once at the cold case, the CEU and BPM were powered, and their temperatures were stabilized until the remainder of the spacecraft was ready for the next phase of the test. The final detector module arrived at the cold case at 04:00 on July 10. At this time, each of the detector modules were powered on; however, the high voltage remained off. Because the BATSE hardware transitioned from hot to cold much faster than the remainder of the GRO, a significant amount of time was available at the cold case during which BATSE tests could be performed while waiting for the rest of the spacecraft to "catch-up" at the cold temperature.

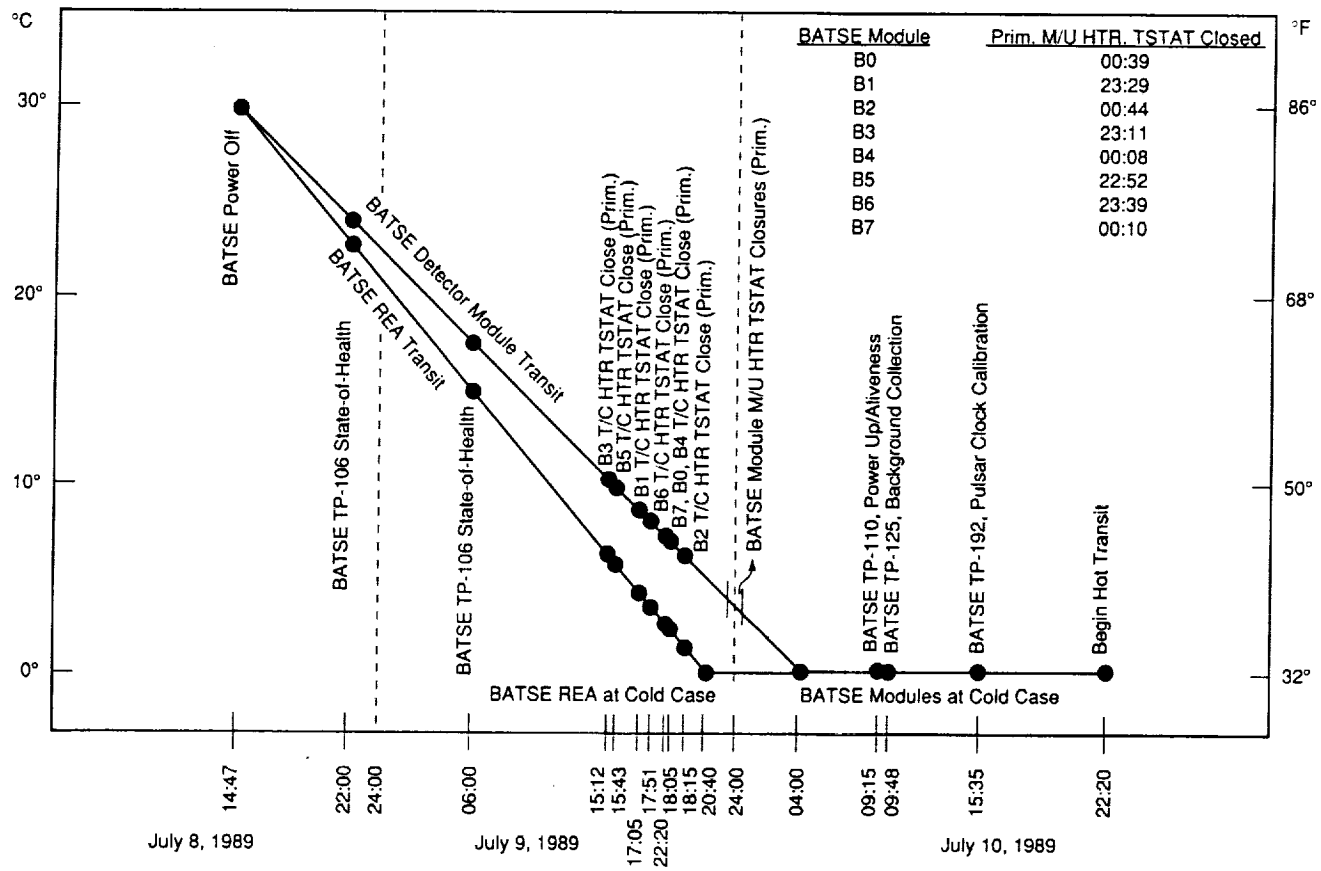

Figure 3.58. GRO T/V Timeline - Transition to Cold Case for Thermal Cycle #1.

Approximately 48 hours after the appropriate chamber pressure was reached, all 40 of the BATSE +HV circuits were powered for the first time in the test. Each of the +HV supplies operated as expected, with no anomalies or evidence of +HV breakdown. Thirty minutes later, a long-duration background spectrum was accumulated from all LADs and SDs. These spectra, which are on file in the BATSE library, show no indication of anomalies or poor performance.

After the spectral accumulations were completed, another iteration of TP-192 was performed on CCF-A. The second hot transition began at 22:20 on July 10, approximately 24 hours after the BATSE hardware arrived at the cold case. For the sake of organization of the test, the first thermal cycle was declared "complete" with the arrival at the cold-case temperature, despite the fact that an entire transition back to the initial temperature had not been reached. In the following pages, the organization will comply with that of the original test. Thermal cycle #1 was completed without any anomalies.

e. Thermal Cycle #2

BATSE remained powered during the transition to the hot-case temperature. Heater power was enabled, and heaters remained on because of the closed state of the thermostats. During the temperature rise, three iterations of the pulsar clock calibration were performed. While executing the second of these tests, BATSE experienced the first anomaly of the test. At 07:15 on the morning of July 11, during the execution of TP-192, detector module B1 CPD exhibited a current-limit condition at 202 μA, indicative of a breakdown in the high voltage system. The CPD rate on this detector was seen to increase over 100-fold in coincidence with the anomalous current reading. Symptoms of this anomaly were identical to the +HV anomaly seen during the BATSE system-level thermal vacuum test. This event occurred after nearly 24 hours of normal +HV operation. The CPD was powered off immediately and remained off for the next 6 days.

As the temperature increased, the BATSE flight heater thermostats were monitored and verified to properly open, removing power from the heater circuits. Table 3.110 contains the time and temperature of thermostat openings.

Table 3.110. BATSE Primary T/C and M/U Heater Thermostat Opening Times and Temperatures, GRO Thermal Vacuum Test - Thermal Cycle #2

Heater and Detector Module	1DMnTEMP (°C)	Time	Date
B0 Primary T/C	5.3	01:48	7-11-89
B1 Primary T/C	2.3	01:20	7-11-89
B2 Primary T/C	7.4	01:52	7-11-89
B3 Primary T/C	2.6	01:19	7-11-89
B4 Primary T/C	5.7	01:33	7-11-89
B5 Primary T/C	5.3	01:26	7-11-89
B6 Primary T/C	5.7	01:29	7-11-89
B7 Primary T/C	4.7	01:21	7-11-89
B0 Primary M/U	1.3	23:54	7-10-89
B1 Primary M/U	0.6	00:05	7-11-89
B2 Primary M/U	1.9	00:04	7-11-89
B3 Primary M/U	0.9	00:04	7-11-89
B4 Primary M/U	1.9	00:13	7-11-89
B5 Primary M/U	1.6	00:07	7-11-89
B6 Primary M/U	1.9	00:05	7-11-89

During this transit, OSSE deployed a Cs 137 isotope outside the thermal vacuum chamber. The source was located to radiate in the -Z direction of the GRO, and directly onto the OSSE detectors. BATSE obtained coincident spectral accumulations, which are on file in the BATSE library. The isotope was exposed for approximately 4 hours, beginning at 15:42 on July 11. Following the removal of the source, a long-duration background exposure was obtained.

BATSE detector modules reached the hot-case temperature at 11:40 on the morning of July 12. Subsequently, the instrument was powered off to allow a more rapid transition to the cold temperature region. Figure 3.59 details the transition to the upper temperature and notes some of the major events during this time period.

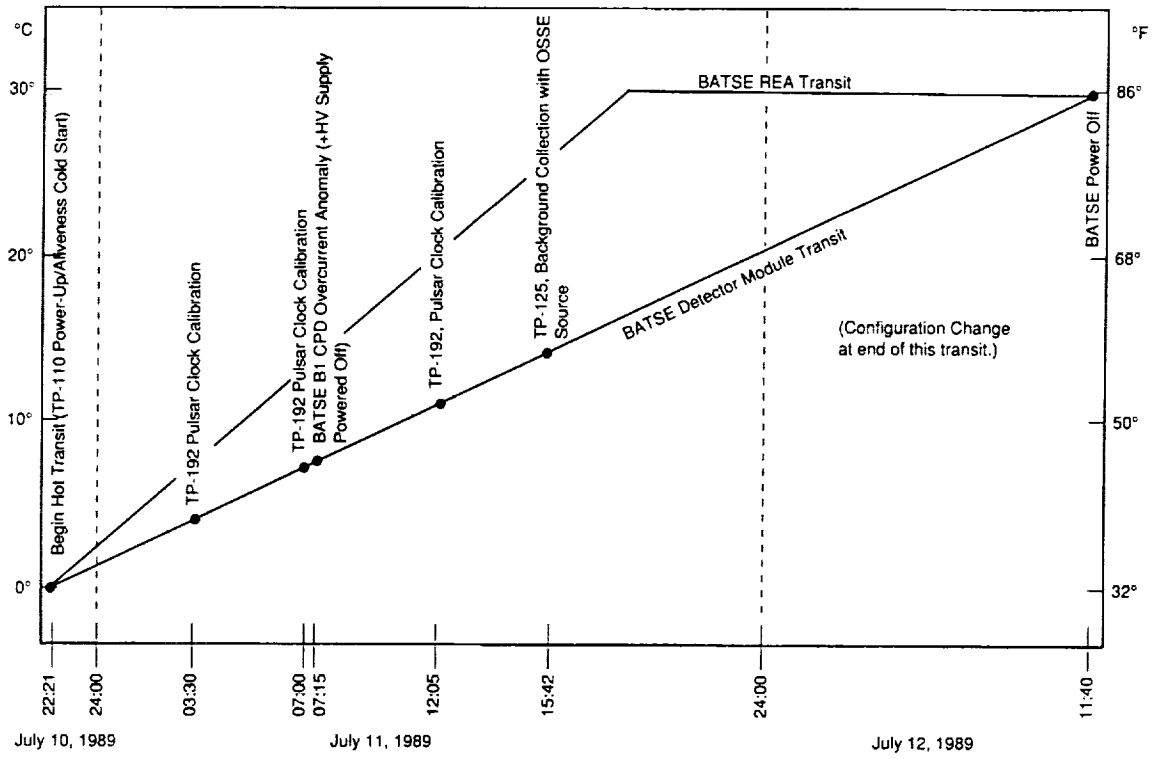

Figure 3.59. GRO T/V Timeline - Transition to Hot Case for Thermal Cycle #2.

The flight hardware was reconfigured for the cold transition of thermal cycle #2. The RIU, CCF, and ADF were all switched to the redundant units, and all BATSE relays were placed into the backup-on configuration. BATSE power remained on the primary side, from the nominal MPS. The switch in the RIU allowed BATSE to monitor the redundant set of thermal control and make-up heater circuits so that thermostat closure could be verified.

Four state-of-health tests were performed during this cold transit, each of which were approximately 8 hours apart. The first of these tests was executed at 18:00 on July 12. All data from these tests indicated that BATSE was operating normally, with the exception of the CPD on B1, which was not tested at these times.

Near the end of the cold transition, the BATSE flight heater thermostats began to close. Each pair of thermostats on the BATSE detector modules were verified functional. Table 3.111 shows the times and temperatures of thermostat closure.

Table 3.111. BATSE Redundant T/C and M/U Heater Thermostat Closure Times and Temperatures

Heater and Detector Module	1DMnTEMP (°C)	Time	Date
B0 Redundant T/C	1.2	15:10	7-13-89
B1 Redundant T/C	3.6	11:19	7-13-89
B2 Redundant T/C	0.6	15:10	7-13-89
B3 Redundant T/C	5.0	10:35	7-13-89
B4 Redundant T/C	0.9	15:10	7-13-89
B5 Redundant T/C	4.0	10:28	7-13-89
B6 Redundant T/C	1.3	12:44	7-13-89
B7 Redundant T/C	1.9	12:13	7-13-89
B0 Redundant M/U	-0.1	18:15	7-13-89
B1 Redundant M/U	-0.8	18:40	7-13-89
B2 Redundant M/U	-0.8	18:40	7-13-89
B3 Redundant M/U	-0.8	18:44	7-13-89
B4 Redundant M/U	-0.5	18:49	7-13-89
B5 Redundant M/U	-1.1	18:15	7-13-89
B6 Redundant M/U	-0.8	18:43	7-13-89
B7 Redundant M/U	-0.8	18:43	7-13-89

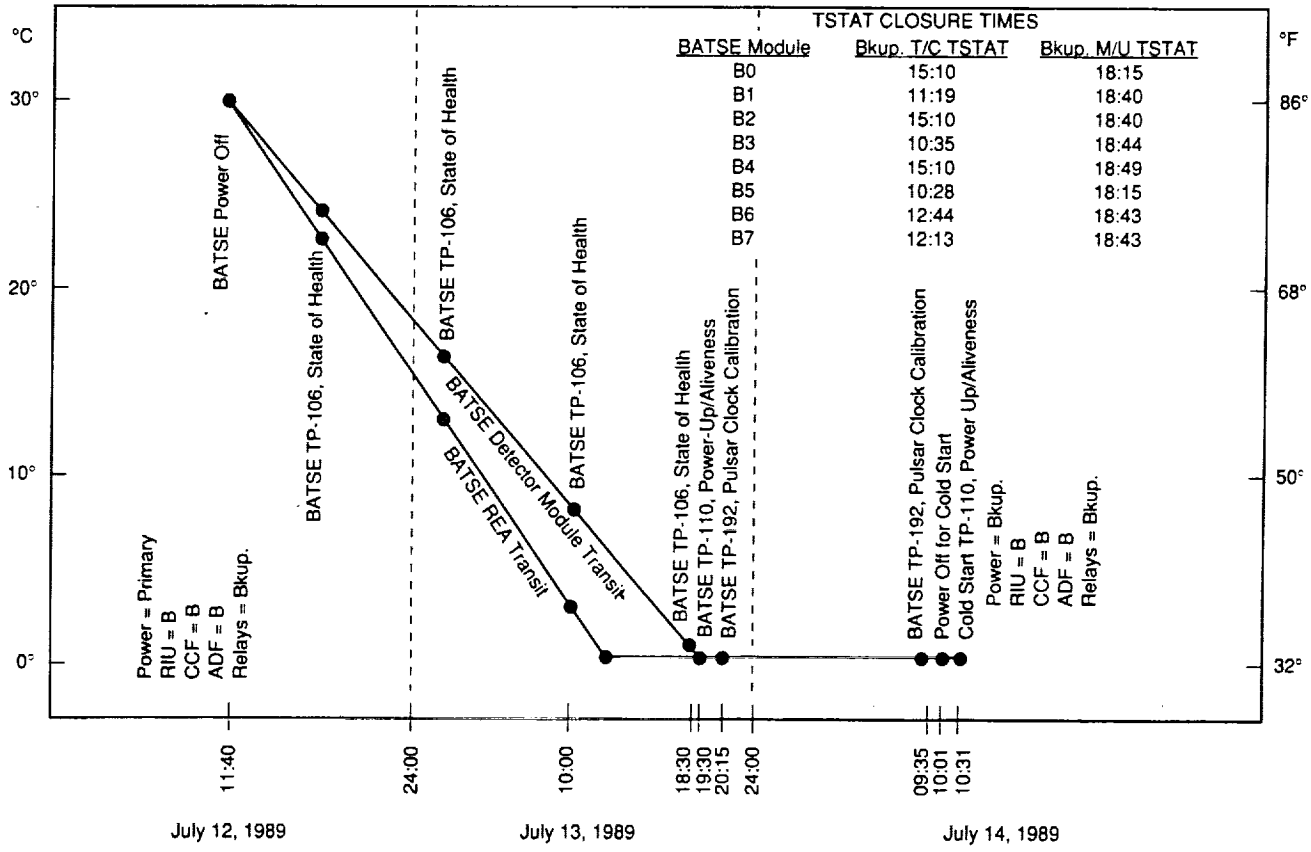

Figure 3.60. GRO T/V Timeline - Transition to Cold Case for Thermal Cycle #2.

Arriving at the cold case faster than the remainder of the spacecraft allowed the BATSE test conductors to perform numerous procedures at temperatures near 0 °C. A BATSE cold-start was performed at 19:30, using TP-110, the power-up and aliveness test procedure. The first two pulsar clock frequency calibrations on CCF-B were also performed during the wait. At 10:00 on the norming of July 14, BATSE was powered down, marking the ened of the second thermal cycle.

f. Thermal Cycle #3

The third thermal cycle began with a cold-start exercise, following approximately 30 minutes of power off while at 0 °C. BATSE remained in the B-side configuration, and switched from primary power to backup power. Each of the redundant thermal control and make-up heater thermostats were verified to open properly and disable their respective heaters. The transition to the hot case was rather unremarkable, with five iterations of the pulsar clock frequency calibration taking place. During this transition, the spacecraft had been switched over to TTU-B. The BATSE test team did not realize this switch until after four iterations of TP-192. In these four tests, the data appeared to show an error in clock frequency 10 times the expected error. Afterward, it was realized that BATSE was looking for time updates from TTU-A, not TTU-B, causing the results of TP-192 to be meaningless. Switching BATSE over to TTU-B corrected the problem. Figure 3.61 shows this transition to the hot case.

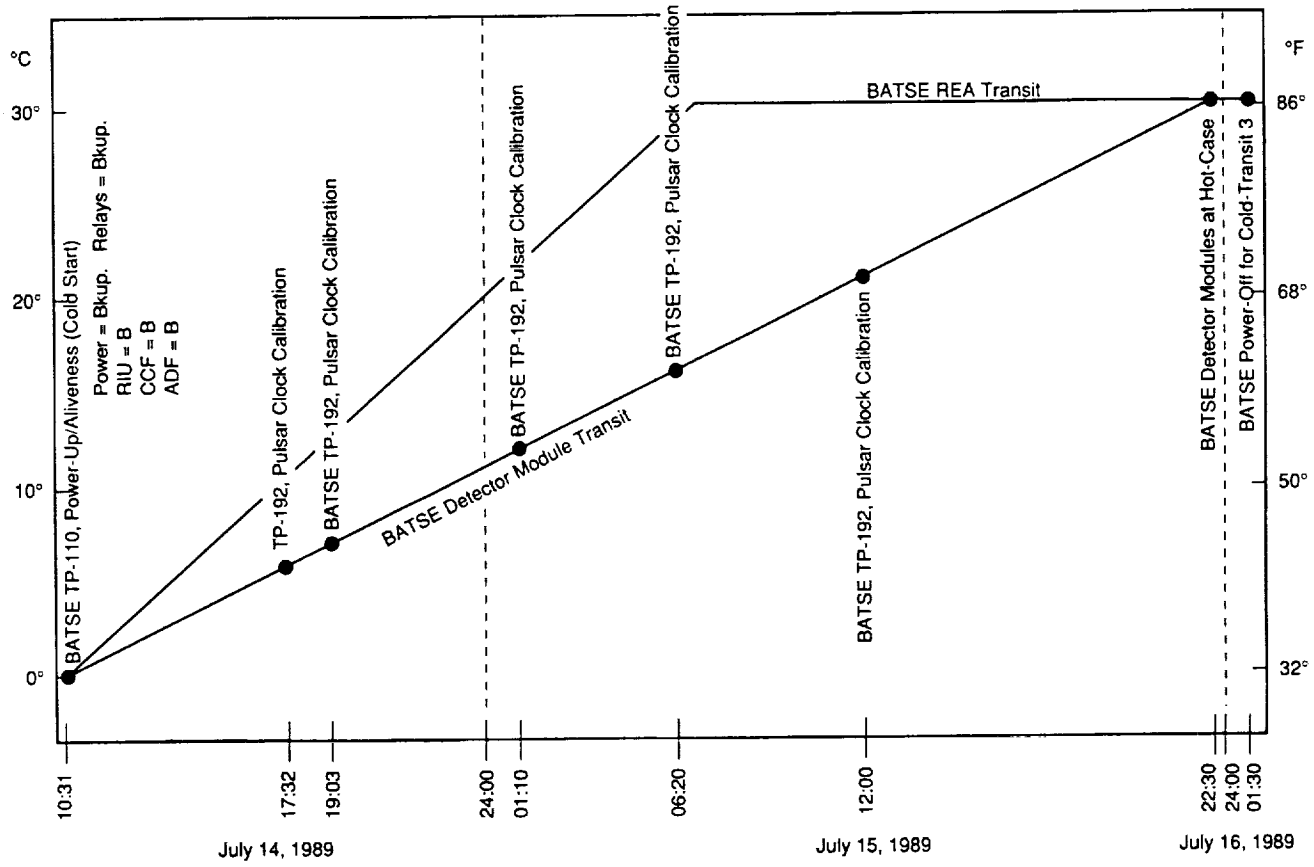

Figure 3.61. GRO T/V Timeline - Transition to Hot Case for Thermal Cycle #3.

BATSE arrived at the hot-case target temperature of 30 °C by 00:00 of July 16. One and one-half hours later, the instrument was powered off for the transition to the cold case. During this transition, BATSE was switched back over to RIU-A. During the test, the GRO test team greatly desired to keep all instruments and subsystems in roughly the same configuration to avoid confusion, and to allow for easy verification that all cross-strapping configurations were exercised. In the previous transitions, several spacecraft primary heater circuits, only visible to RIU-A on their particular subsystem, were not verified. Consequently, each subsystem was asked to return to the A-side RIU. BATSE remained on CCF-B and ADF-B internally.

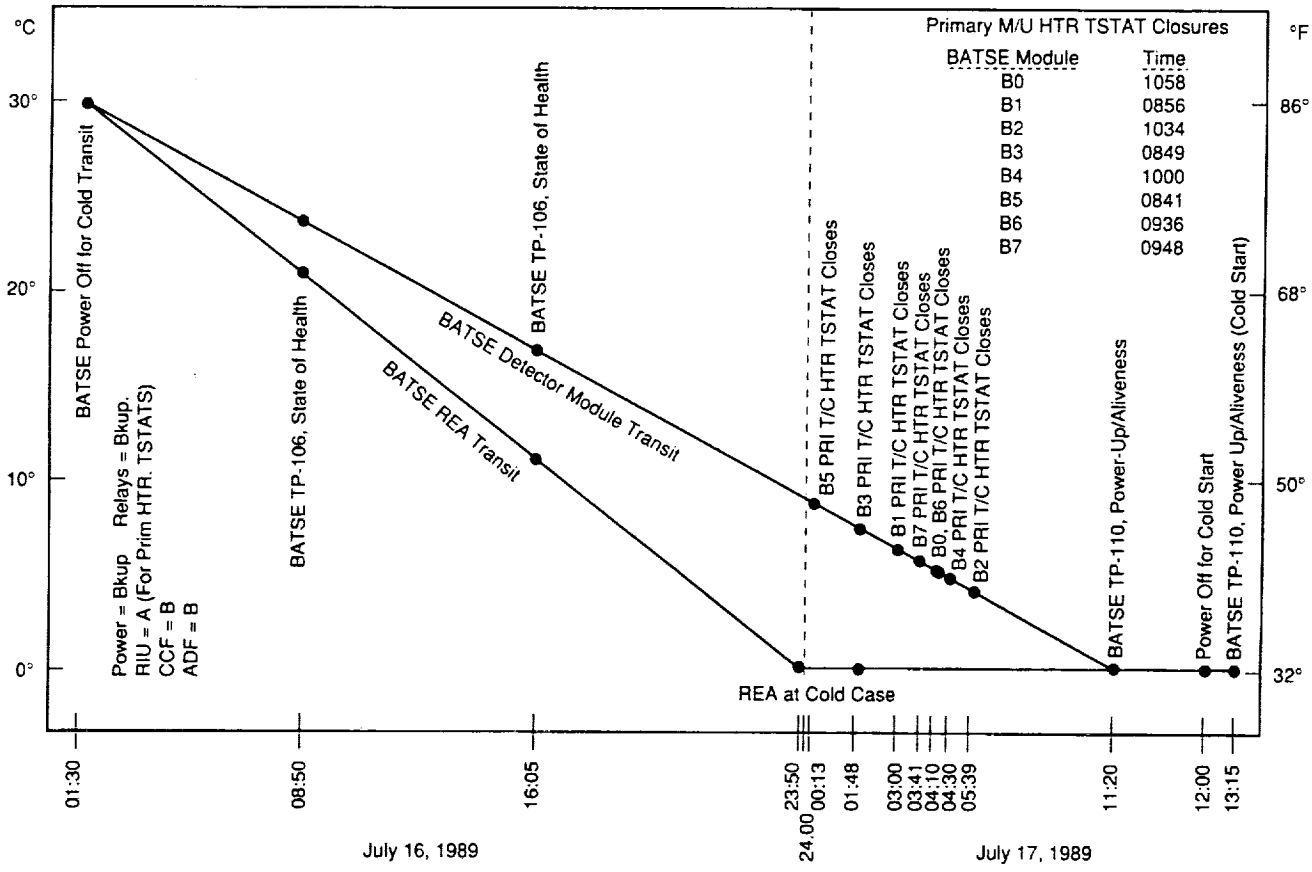

Figure 3.62. GRO T/V Timeline - Transition to Cold Case for Thermal Cycle #3.

During the cold transition, BATSE was powered twice to perform the state-of-health test and to obtain multiplexed housekeeping temperature values from the detector modules. These tests proceeded without anomaly. Shortly after midnight, early in the morning of July 17, the BATSE primary thermal control heater thermostats began to close. The temperature readings of the closures are within 1 °C of the previous temperatures. All thermal control heaters had been powered by 05:30. Subsequently, the primary make-up heater thermostats began to close as the temperature dropped further. All eight of the make-up heater circuits were powered by thermostat closure between 08:41 and 10:58 on the morning of July 17. Figure 3.62 details the transition from hot to cold during the third thermal cycle.

After all detector modules had arrived at the cold case, they were powered on to help stabilize the temperature. The CEU and BPM had been powered on several hours earlier after they transitioned to their desired temperatures. A successful power on was executed using TP-110, the power-up and aliveness test, at 11:20 a.m. At noon, BATSE was again powered off in preparation for a cold-start test, marking the end of thermal cycle #3.

g. Thermal Cycle #4

Thermal cycle #4 began at 13:30 on July 17, as BATSE performed a cold-start test. BATSE was operated on primary power, RIU-A, and ADF-A. CCF-B was utilized, creating the first RIU to CCF cross-strap configuration. A cold-start test was repeated at 20:30 prior to the initiation of the hot transition. Four iterations of the pulsar clock frequency calibration were performed, each yielding nominal results.

Detector module B1 CPD was repowered at 08:40 on July 18 for the first time in 6 days. No sign of +HV breakdown was apparent immediately after power up, and the CPD operated normally throughout the remainder of the test.

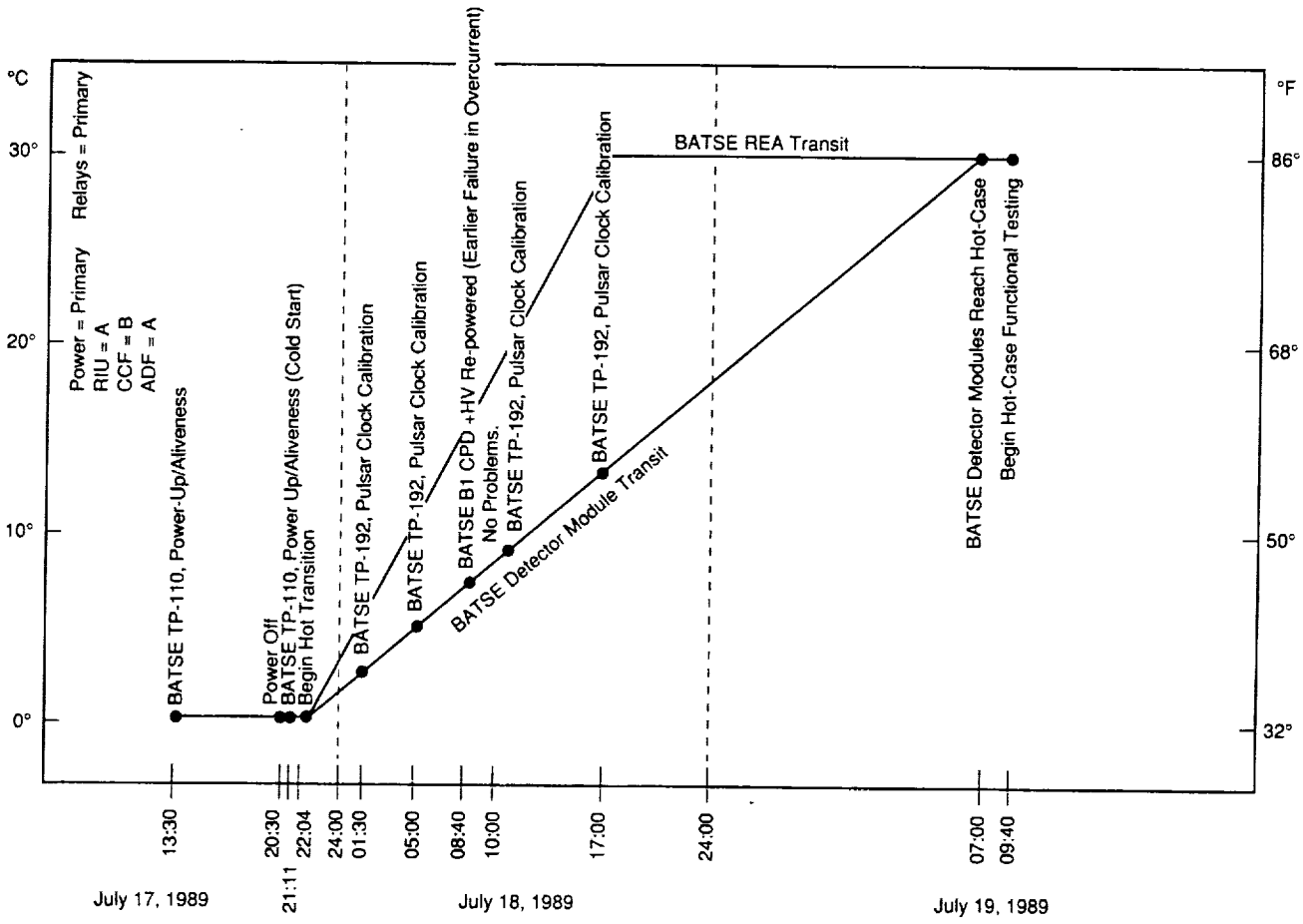

Figure 3.63. GRO T/V Timeline - Transition to Hot Case for Thermal Cycle #4.

The hot transition of thermal cycle #4 was completed at 07:00 on the morning of July 19, when BATSE detector modules arrived at the target temperature of 30 °C. BATSE was declared ready for the start of hot-case functional testing at 09:00 that morning.

Functional testing at 30 °C mirrored the tests performed during the BATSE portions of the Observatory functional test. An additional cross-strapping test was added to provide a record of operations in a wide variety of configurations. This test was orchestrated in coordination with the other instruments and spacecraft subsystems. Table 3.112 lists all tests that were performed during the hot-plateau period.

Table 3.112. BATSE Hot-Case Functional Test Sequence - GRO Thermal Vacuum Test

- TP-110 — Power-up and aliveness test
- GRO cross-strap testing
- TP-125 — Background collections (with and without OSSE source)
- TP-192 — Pulsar clock calibration
- TP-200 — Power control function test
- TP-188 — Coordinated BTS/SF trigger signal test
- TP-105 — Detector module test
- TP-170 — CPD calibration
- TP-171 — CPD/LAD coincidence run
- TP-192 — Pulsar clock calibration
- TP-190 — Pulsar data test (options 1 and 2)
- TP-180 — Burst data test (options 1, 2, and 3)
- TP-125 — Background collection (at various LLD settings)
- TP-190 — Pulsar data test (option 2 re-run)
- TP-120 — Coincidence/EXFLAGS test

The cross-strapping test was the only new procedure placed into the sequence of tests and was executed at the outset of the functional testing. BATSE switched over to CCF-A for this operation and executed one iteration of TP-106, the state-of-health test, for each of the spacecraft configurations contained in Table 3.113. Those configurations not shown in the table were exercised somewhere else throughout the course of the GRO thermal vacuum test.

Table 3.113. BATSE Cross-Strapping Test Configurations at Hot Case

BATSE RIU	Time	Power Bus	MPS	CADH Unit
A	10:47	Primary	1	A-Side
B	11:50	Primary	1	A-Side
B	12:13	Primary	2	A-Side
B	12:37	Primary	2	B-Side
B	13:10	Redundant	2	B-Side
A	13:28	Redundant	2	B-Side
A	13:47	Redundant	2	A-Side
A	14:10	Primary	1	A-Side

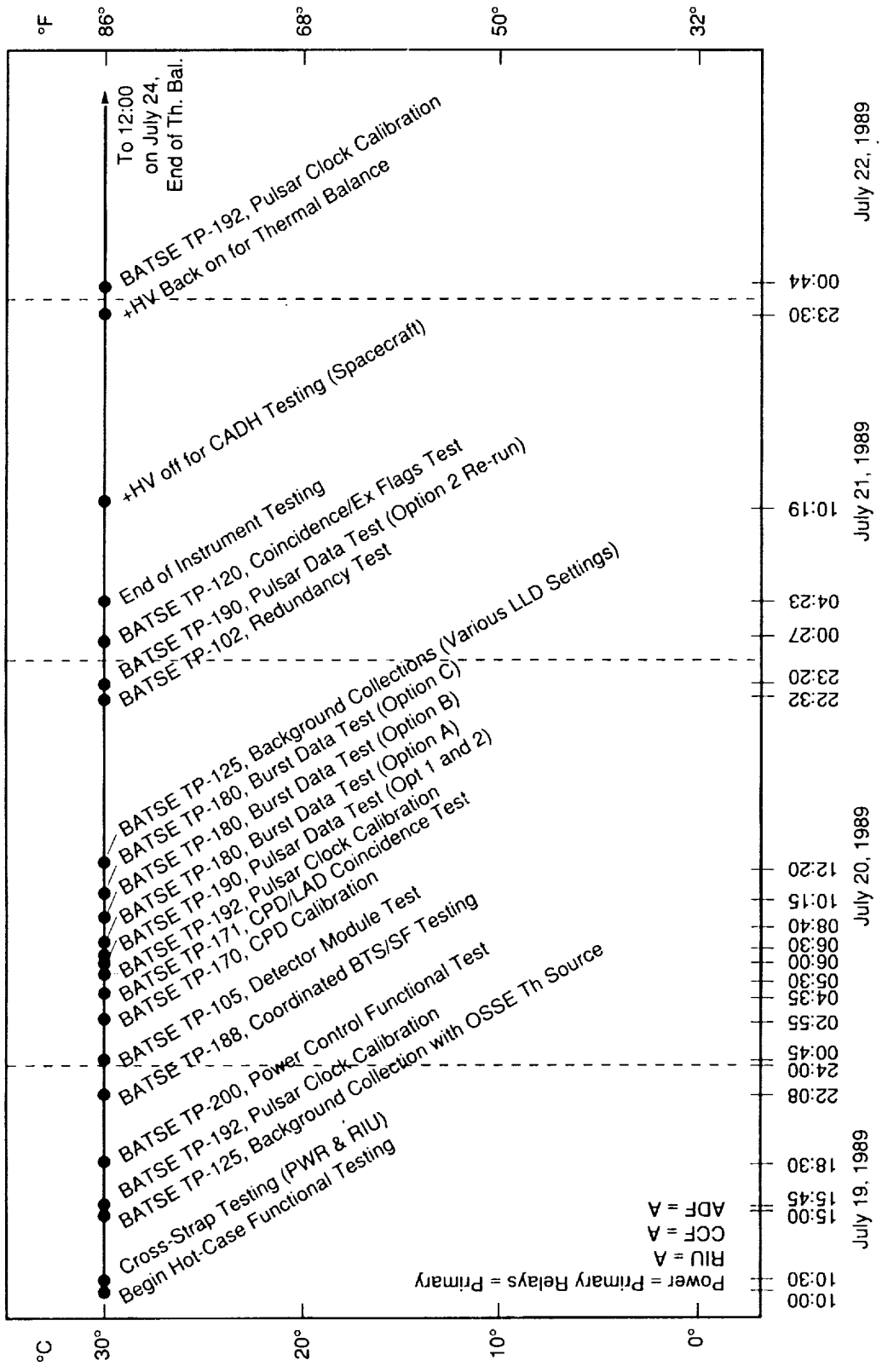

Figure 3.64. GRO T/V Timeline - Hot-Plateau and Functional Tests - Thermal Cycle #4.

The first nominal BATSE test procedure was started at 15:00 on July 19. Through a previous agreement among the four instruments, the first portion of the OSSE was provided with a 3-hour period in which to deploy their Th 228 source outside the T/V chamber and illuminate their detectors inside. This time period was placed as close as possible to the beginning of the functional test time to give each instrument team the maximum amount of uninterrupted testing time. During the OSSE source exposure, numerous spectra were accumulated and are on file in the BATSE library.

When planning the sequence of events for this test, the resident instrument representatives blocked out the next 2 hours for base-level functional testing for each instrument. For BATSE, this meant an execution of TP-200, the power control function test. At the same time, each of the other instruments were executing similar tests of power switching, redundancy, mode changes, and other fundamental operations tests.

The final coordinated test slot was allocated to the burst trigger and solar flare trigger signal test. Under the direction of the BATSE test conductor, burst trigger signals were sent to the other three instruments from ADF-A and ADF-B. The solar flare trigger signal to OSSE was tested, as was the solar flare trigger signal route to COMPTEL via the OBC. All of these tests were successful, and each of the instruments continued individual testing following the completion of coordinated exercises.

BATSE test conductors proceeded with the normal sequence of functional testing, starting with TP-105, the detector module test. During this test, each bit of the 40 +HV supplies were tested. Detector module B1 CPD, which had exhibited a failure of the +HV system, was verified to have eight operational command bits. All subsequent tests were concluded with no major anomalies or hardware problems. The results obtained from each of the procedures are on file in the BATSE data library. Hot-case functional testing concluded at 04:25 on July 21, 1989.

The next major section of the plateau was devoted to functional testing of the spacecraft. Each of the subsystems (e.g., CADH, EPDS, propulsion, ACAD) was fully exercised and verified operational. During this time, the instruments were unable to accomplish successful tests because of telemetry interruptions, power switching, and spacecraft reconfiguring. No BATSE tests were planned during this time because of the interference of spacecraft operations. The BATSE test conductors monitored the performance of the instrument, archived data, and obtained spectral accumulations over a wide range of LLD settings. BATSE thermal engineers used this time to obtain characteristics of the thermal properties of the hardware to help stabilize the temperature, in preparation for the subsequent thermal balance exercise.

Thermal balance testing of the GRO was performed between 00:00 and 08:00 on July 24. Because most of the subsystems had stabilized during the spacecraft testing, this operation proceeded more smoothly than anticipated. Four hours after the completion of the thermal balance, the transition to the cold-case temperature commenced.

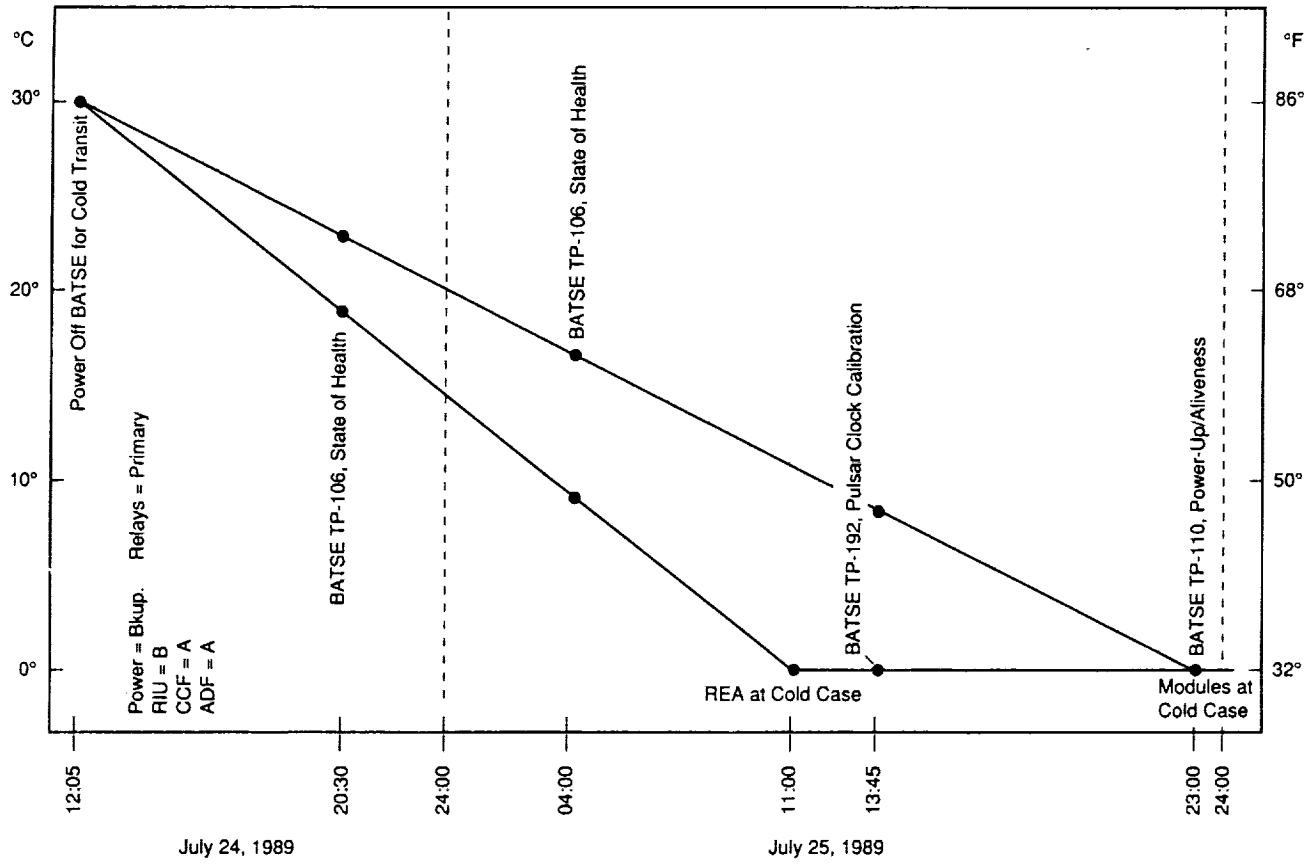

Figure 3.65. GRO T/V Timeline - Transition to Cold Case for Thermal Cycle #4.

The BATSE hardware was reconfigured for the transition to the cold case. The instrument was operated through RIU-B, utilizing CCF-A and ADF-A. This configuration exercised the remaining RIU to CCF cross-strap configuration. Power remained off during the transition, except for the normal iterations of TP-106, the state-of-health test, which was performed every 8 hours. At 11:00 on July 25, the CEU and BPM arrived at the cold-case temperatures and were powered on using the redundant power bus. At the time of power-up, the BATSE test conductor changed the instrument configuration again, this time utilizing CCF-B and ADF-B. TP-192, the pulsar clock frequency calibration, was performed shortly thereafter.

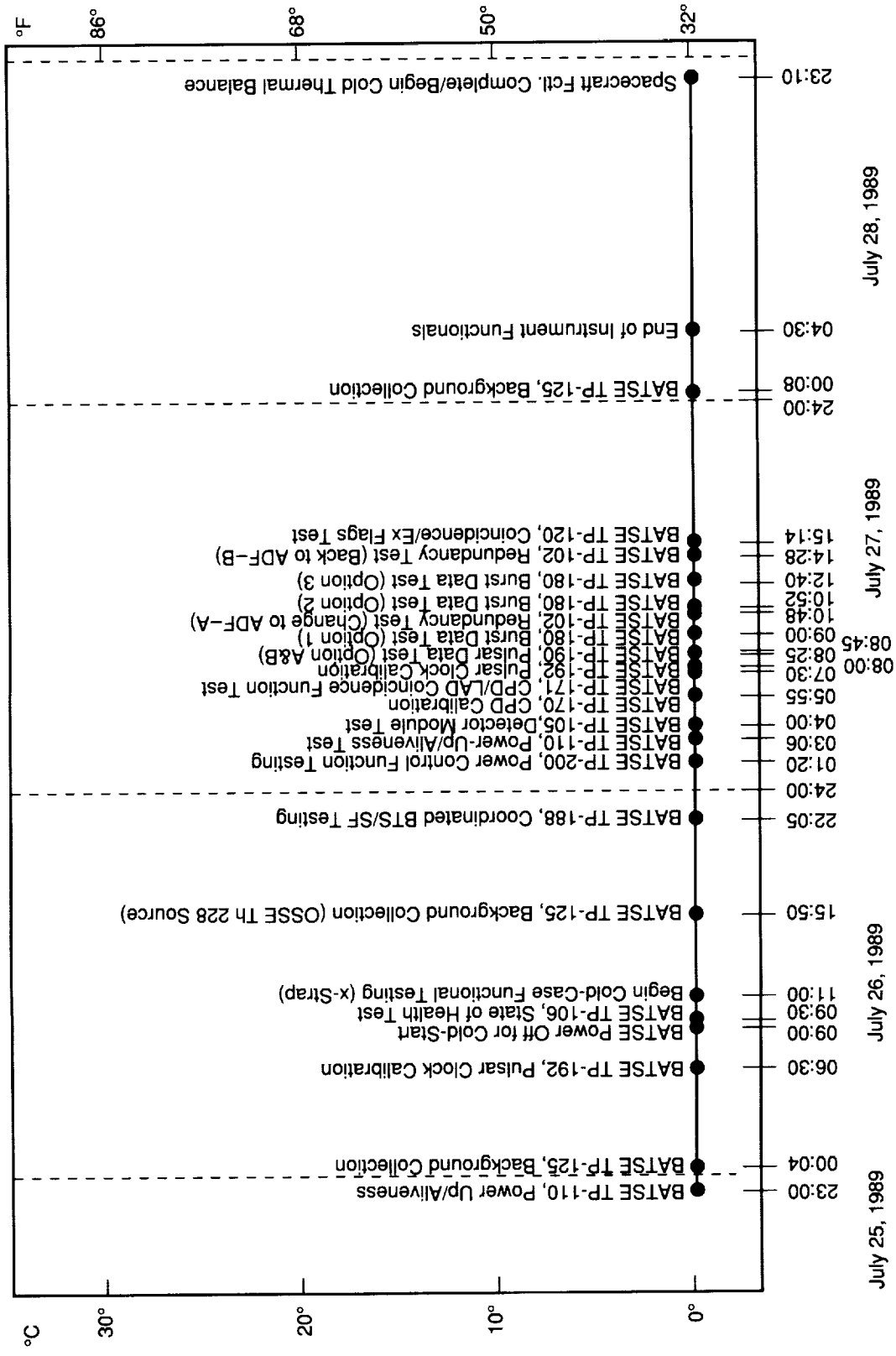

Figure 3.66. GRO T/V Timeline – Cold–Plateau and Functional Tests – Thermal Cycle #4.

Detector modules reached their target temperatures by 23:00 on July 25. Again, BATSE hardware arrived at the cold case more rapidly than the remainder of the spacecraft, affording the test conductors some time to perform testing. Shortly after midnight, TP-125 was performed, collecting spectra at a variety of LLD settings. These spectra were taken for comparison with the hot-case spectra at a variety of LLD settings. Background acquisitions lasted nearly 6 hours, after which a pulsar clock frequency calibration was performed. This testing period ended at 09:30 on July 26, when the hardware was powered off in preparation for the cold-start demonstration.

The structure of the cold-plateau test time was identical to that of the previous hot-case plateau. The initial portion of the testing was reserved for GRO cross-strapping tests involving the instruments. For each of the configurations desired, one iteration of TP-106 was performed. Table 3.114 details the cross-strapping configurations utilized during the cold-plateau testing. At the completion of the cross-strapping tests, the BATSE hardware remained on RIU-B, CCF-B, ADF-B, and redundant power. The BATSE relays were configured to their backup-on positions.

Table 3.114. BATSE Cross-Strapping Test Configurations at Cold Case

BATSE RIU	Time	Power Bus	MPS	CADH Unit
A	12:50	Primary	1	A-Side
B	13:00	Primary	1	A-Side
B	13:20	Primary	2	A-Side
B	13:50	Primary	2	B-Side
B	14:06	Redundant	2	B-Side
A	14:20	Redundant	2	B-Side
A	14:55	Redundant	2	A-Side
B	15:15	Redundant	1	A-Side

Following the cross-strapping exercise, OSSE again deployed their Th 228 isotope. As with the previous plateau, BATSE obtained spectral accumulations through the TP-125 procedure. The Th 228 isotope was present for a period of approximately 4 hours, starting at 17:15 on July 26.

The final coordinated test period was allocated for the performance of the burst trigger and solar flare trigger signal tests. TP-188 was performed under the direction of the BATSE test conductor, and successfully exercised the burst trigger signals to each of the other three instruments. In addition, the solar flare signal to OSSE and the solar flare signal to COMPTEL through the OBC were also successfully exercised.

Independent instrument testing began at 01:30 on the morning of July 27. BATSE test conductors performed TP-200, TP-110, and TP-105. During the detector module test, all command bits of each +HV supply were verified to be fully operational, including the eight bits of the B1 CPD. Although the +HV system on this detector suffered an earlier anomaly, the system was verified to be fully operational at the hot and cold temperature regions.

Iterations of TP-170, TP-171, TP-180, TP-190, TP-120, and TP-125 completed the BATSE functional test at the cold-plateau. The results of these tests were in close agreement with the results from the previous functional testing sequence. Each of these tests and all associated data reside in the BATSE library for inspection. Instrument functional testing was compelted at 04:30 on the morning of July 28.

During the next 60 hours, spacecraft functional testing and thermal balance testing were performed. BATSE remained in a monitoring mode throughout the time period, with the exception of an iteration of the pulsar clock calibration test on the morning of July 29. After completion of the thermal balance portion of the testing, the spacecraft remained in the cold case while several low temperature thermostats and STS heater thermostats were verified to be operational. In many cases, this required the transition of a particular box or subsystem to a temperature below that of the original cold-case target. The STS heaters were powered externally throughout the test and were used as an energy source to drive the temperature of the detector modules. A verification of the operation of the STS heater thermostats is discussed in the next section. All verifiable GRO thermostas (approximately 600 in number) were shown to be operational by the time, this portion of the test was completed. The rise to ambient temperature began at 09:00 on August 1, 1989.

Two anomalies were noticed during the cold-plateau following functional testing. Early in the morning of July 30, several of the +HV supplies for the CPDs exhibited an oscillatory current measurement through the BATSE housekeeping data. The oscillation magnitude was approximately 6 μA about the nominal value. The current oscillation was not accompanied by a fluctuation in either the counting rate voltage. This behavior went away during the rise to ambient temperature. Because the high voltage power supplies are constructed to regulate the load of the 12.7 cm PMTs, the regulation of the smaller 5.08-cm PMTs becomes more difficult, especially at the cold case. If this behavior replicates itself on-orbit, there is no impact to operations or to the quality of science data. An instrument anomaly report was generated and closed with the action to use "as-is."

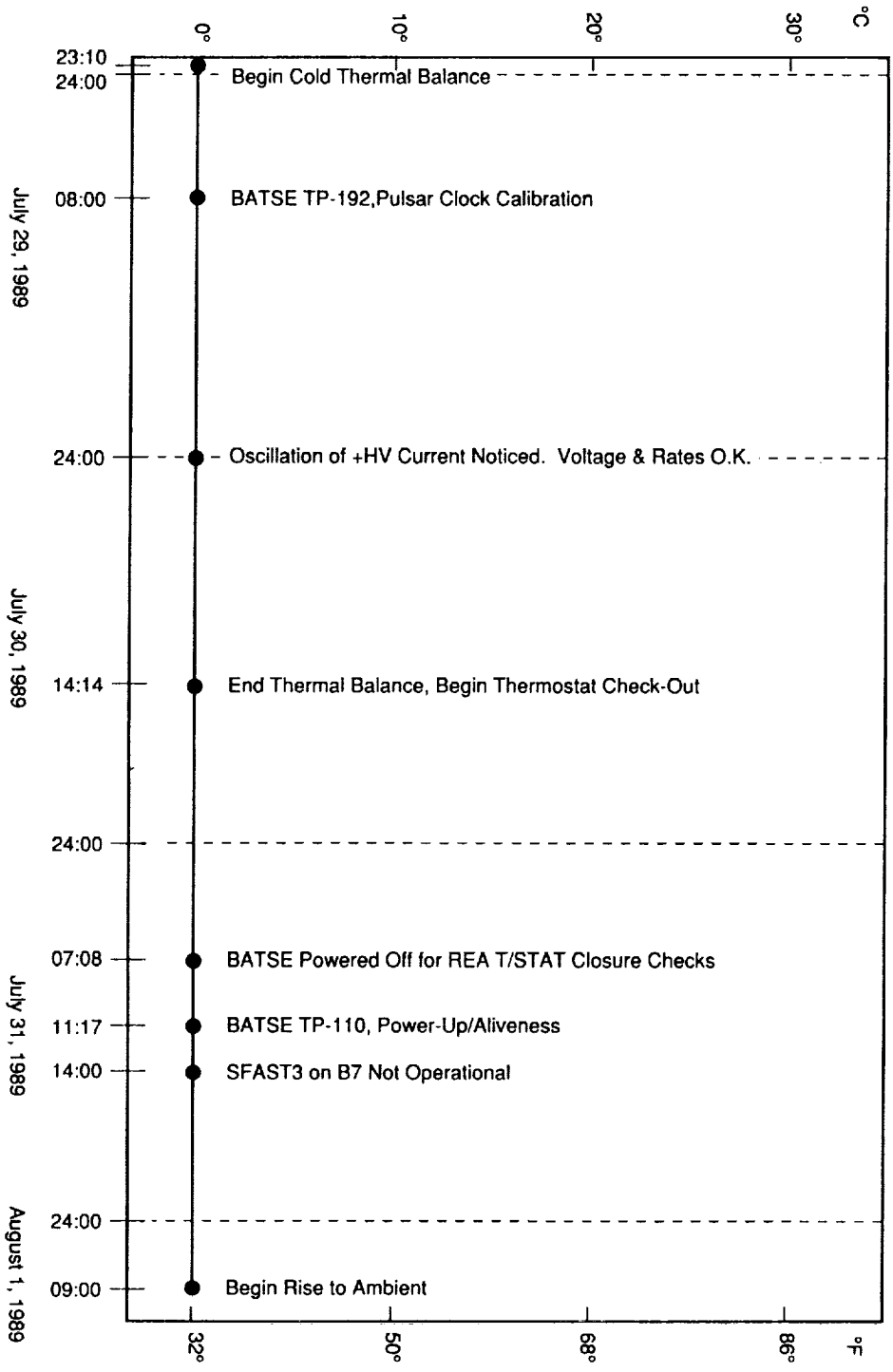

Figure 3.67. GRO T/V Timeline - Cold Thermal Balance and Thermostat Tests - Thermal Cycle #4.

The second anomaly was a repeat of a problem seen in the BATSE system-level thermal vacuum test at MSFC. The SFAST3 discriminator on detector module B7 displayed a non-integral behavior. This was first noticed at 14:00 on July 31. To this point, the discriminator had functioned flawlessly throughout the four thermal cycles. The characteristics of the SFAST3 behavior were identical to those described in section III.D.4 of this document. The BATSE team was aware that this problem resided in the CEU, and presented this anomaly in a pre-test meeting as something to watch for during the test. The response to this problem was identical to the response given during the MSFC test. Because there is little impact to mission operations, or to the quality of science data, the BATSE team decided to live with the problem if it appears during on-orbit operations.

h. Rise to Ambient Temperature

The final temperature transition began at 12:30 on August 1, 1989. As mentioned in the previous paragraph, the STS heaters had been used to this point as an energy source to drive the temperature of the detector modules. In this configuration, the heaters are powered directly from the outside, and operation of the thermostats cannot be examined. At the final transition, the STS heaters were reconfigured to apply power through the thermostats. Because the Instrument was at the cold case, all thermostats were closed. Consequently, the exact turn-on temperature of these heaters could not be determined; however, it was obvious that all thermostats had closed. During the temperature rise, the turn-off points were monitored. After all of the thermostats had opened, the STS heaters were again configured for external power directly to the heater elements. Table 3.115 contains information relevant to the opening of the eight flight STS heater thermostats.

Table 3.115. BATSE STS Heater Thermostat Opening Times and Temperatures GRO Thermal Vacuum Test

Heater and Detector Module	1DMnTEMP (°C)	Time	Date
B0 STS Heater	4.7	13:42	8-1-89
B1 STS Heater	6.4	15:24	8-1-89
B2 STS Heater	6.7	13:22	8-1-89
B3 STS Heater	6.4	15:20	8-1-89
B4 STS Heater	4.7	13:37	8-1-89
B5 STS Heater	6.4	15:38	8-1-89
B6 STS Heater	5.7	13:35	8-1-89
B7 STS Heater	6.7	15:22	8-1-89

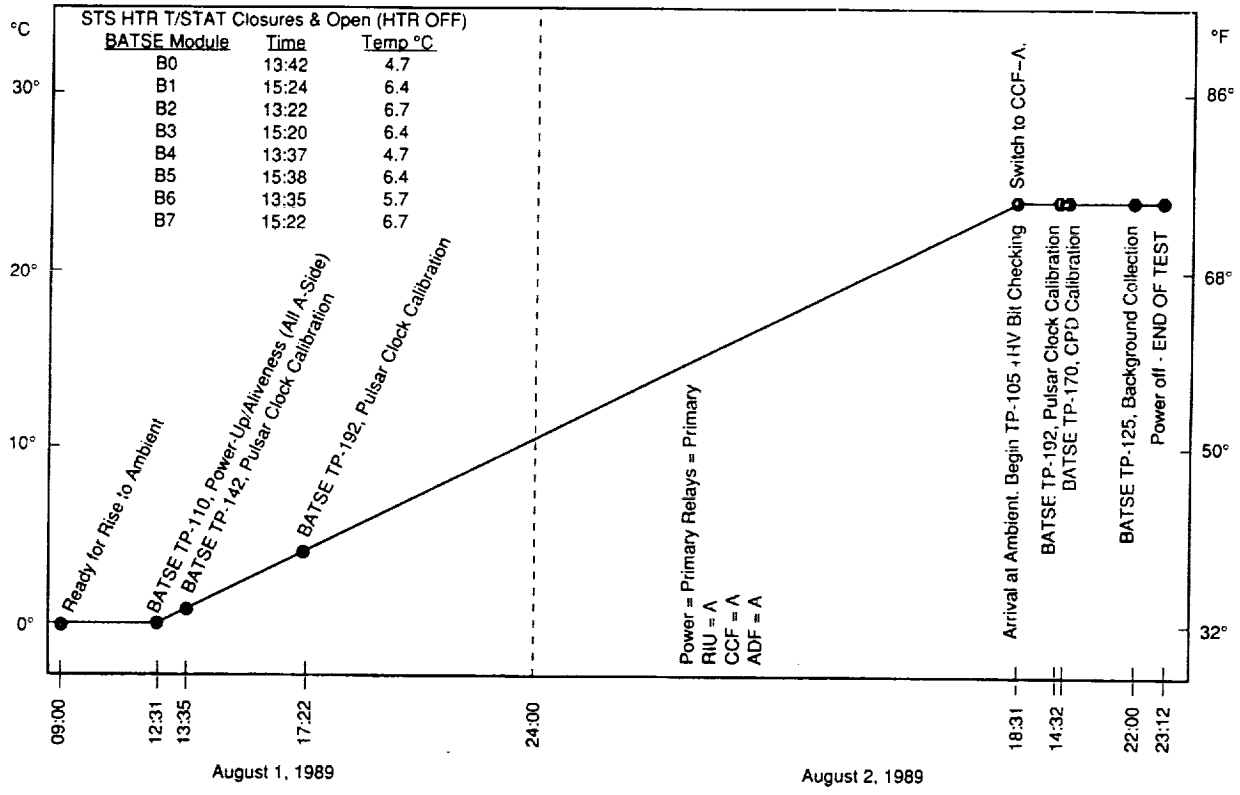

Figure 3.68. GRO T/V Timeline - Rise to Ambient, Thermal Cycle #4.

During the temperature transition, two iterations of the pulsar clock frequency calibration were performed. These were the final tests prior to arrival at ambient temperature (23 °C). The transition lasted approximately 30 hours, concluding on August 2 at 18:30. Once the target temperature had been reached, nearly 5 hours were allowed to stabilize the temperature and bring

the spacecraft into equilibrium. During this time, the BATSE test conductors performed the +HV command bit check from TP-105. This was a critical test in assessing the validity of the repairs performed on the BATSE +HV supplies after the initial system-level thermal vacuum testing. The test verified that each command bit of the 40 high voltage supplies operated successfully throughout the duration of the test. This includes the command bits on CPD B1, where an early instance of high voltage breakdown had occurred.

The final tests performed under vacuum conditions were iterations of TP-192, TP-170, and TP-125. These procedures were executed successfully, and their results are on file in the BATSE data library.

i. Summaries

(1) Cross-Strapping and Run Times

During the thermal vacuum test, considerable attention was paid to the configuration of the instrument and to testing in as many different modes as possible. The four items of primary concern to BATSE were the RIU, the CCF, the ADF, and instrument power. Exercising the cross-strapping capabilities and distributing the run-time evenly for these functions were two principal motivations during the test. Table 3.116 indicates the approximate run time on each of these components.

Table 3.116. Approximate Run Time of BATSE Components in GRO Thermal Vacuum Test

• Instrument Power (CEU and modules)	21 days	14 hours	24 minutes
Primary Power	11 days	22 hours	53 minutes
Redundant Power	9 days	15 hours	31 minutes
• Instrument High Voltage (B1 CPD is less because of power-off time)	15 days	13 hours	33 minutes
• RIU-A	12 days	8 hours	50 minutes*
• RIU-B	9 days	5 hours	34 minutes*
• CCF-A	10 days	10 hours	18 minutes
• CCF-B	11 days	4 hours	6 minutes
• ADF-A	11 days	20 hours	21 minutes
• ADF-B	9 days	17 hours	53 minutes

*This time reflects only the duration in which the instrument was powered through the particular RIU. The RIU remains active (i.e., powered on) even when BATSE is powered off.

The data in Table 3.116 were constructed from the BATSE thermal vacuum test instrument notebook. Each of the numbers in the table is accurate to within 5% of the true power-on time. Distribution of power-on time between redundant components is nearly 50% for each unit. The RIU remains "active," or powered on despite the fact that the BATSE hardware may be on or off. The times listed for the RIUs represent only the times when BATSE was powered on. For each of the RIUs, their actual power-on time was substantially longer. At any given time during the entire T/V test, one of the two units was active. Table 3.117 displays the as-run configuration of the BATSE instrument for each portion of the thermal vacuum test.

Table 3.117. BATSE As-Run Instrument Configuration-GRO Thermal Vacuum Test

T-V Phase	Power	RIU	CCF	ADF	Relays	Flt. Htrs.	STS Htrs.	+HV
TC #1 - Rise	A	A	A	A	Primary	Prmy - EN Red - OFF	External	OFF
TC #1 - Sink	A	A	A	A	Primary	Prmy - EN Red - OFF	External	OFF
TC #2 - Rise	A	A	A	A	Primary	Prmy - EN Red - OFF	External	ON
TC #2 - Sink	A	B	B	B	Backup	Prmy - OFF Red - EN	External	ON
TC #3 - Rise	B	B	B	B	Backup	Prmy - OFF Red - EN	External	ON
TC #3 - Sink	B	A	B	B	Backup	Prmy - EN Red - OFF	External	ON
TC #4 - Rise	A	A	B	A	Primary	Prmy - OFF Red - OFF	External	ON
Hot Fctl.	A/B	A/B	A	A	Primary	Prmy - OFF Red - OFF	External	ON
TC #4 - Sink	B	B	A	A	Primary	Prmy - OFF Red - OFF	External	ON
Cold Fctl.	A/B	A/B	B	B	Backup	Prmy - OFF Red - OFF	External	ON
Heater Check	B	A/B	A	B	Primary	Prmy - OFF Red - OFF	External	ON
STS Htr. Check	A	A	B	A	Primary	Prmy - OFF Red - EN	AESE	ON
Rise to Amb.	A	A	B	A	Primary	Prmy - EN Red - OFF	External	ON
Ambient Test	A	A	A	A	Primary	Prmy - OFF Red - OFF	External	ON

(2) Pulsar Clock Frequency Calibration

The GRO thermal vacuum test provided an opportunity to quantitatively determine the behavior of the BATSE pulsar clocks with respect to the spacecraft clock as a function of temperature. Measurements of the frequency fractional difference between the clocks were obtained at numerous temperatures between -5 °C and 45 °C.

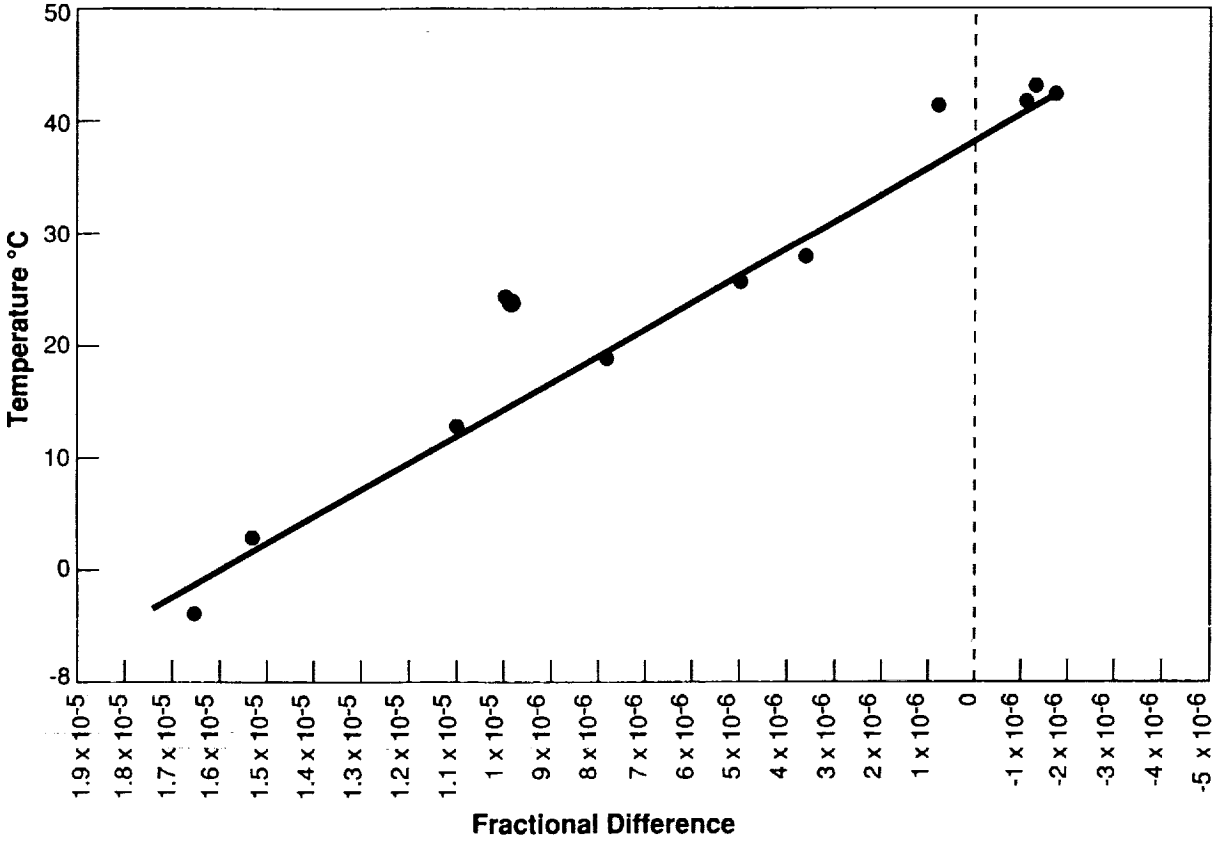

Figure 3.69. BATSE CCF-A Pulsar Clock Calibration
Frequency Fractional Difference vs. Temperature.

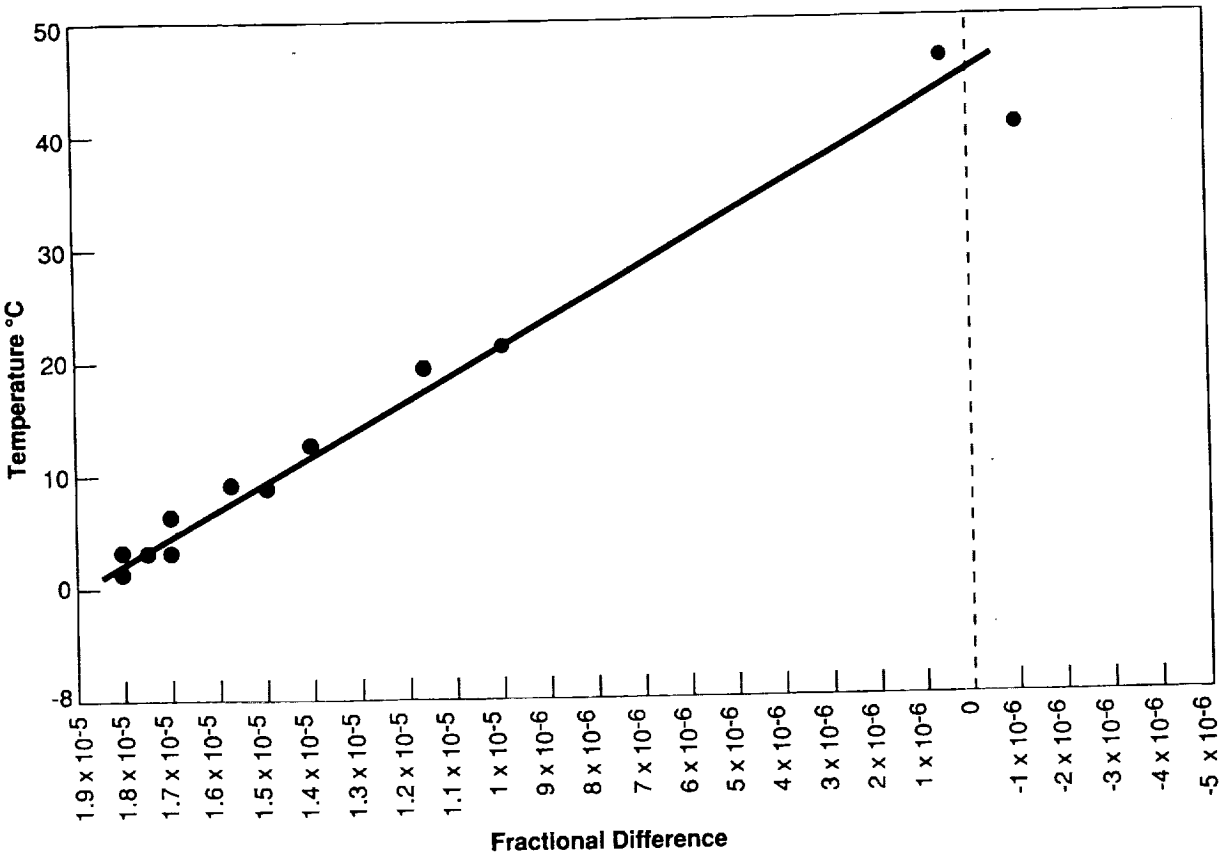

Figure 3.70. BATSE CCF-B Pulsar Clock Calibration
Frequency Fractional Difference vs. Temperature.

The two figures in this section display the correlation in a visual manner. The fractional difference in clock rates is nearly a linear function of the temperature. The slope of this linear relation is virtually the same for both of the CCF board clocks, with an offset of approximately 7 °C between them. At a given temperature, the CCF-A clock runs slightly slower than the CCF-B clock. CCF-A operates at the same rate as the spacecraft clock near a temperature of 37 °C. For CCF-B, this condition occurs at a slightly higher temperature, near 45 °C.

(3) Anomalies

(a) Detector Module B4 Odd-Even Effect

During the fourth thermal cycle, the HER spectrum obtained from detector module B4 displayed an anomaly in the uppermost portion of the spectrum. The anomaly is characterized by the appearance of an alternating excess and depletion of counts in successive compressed-gain channels of the uppermost quadrant. The number of counts in a given channel thus appears to depend on whether the channel is an odd- or even-numbered channel. An "average" background, drawn through these odd-even data points, results in a smooth, continuous, normal background level in this quadrant. Because this appears only in the uppermost quadrant of the HER spectrum, the source of the anomaly is known to reside inside the CEU and is most likely a differential non-linearity in the sorting of MQT pulses from the detector. All spectral gain compression is done after the signals leave the detector module. Figure 3.71 shows a spectrum from the thermal vacuum test displaying the odd-even effect.

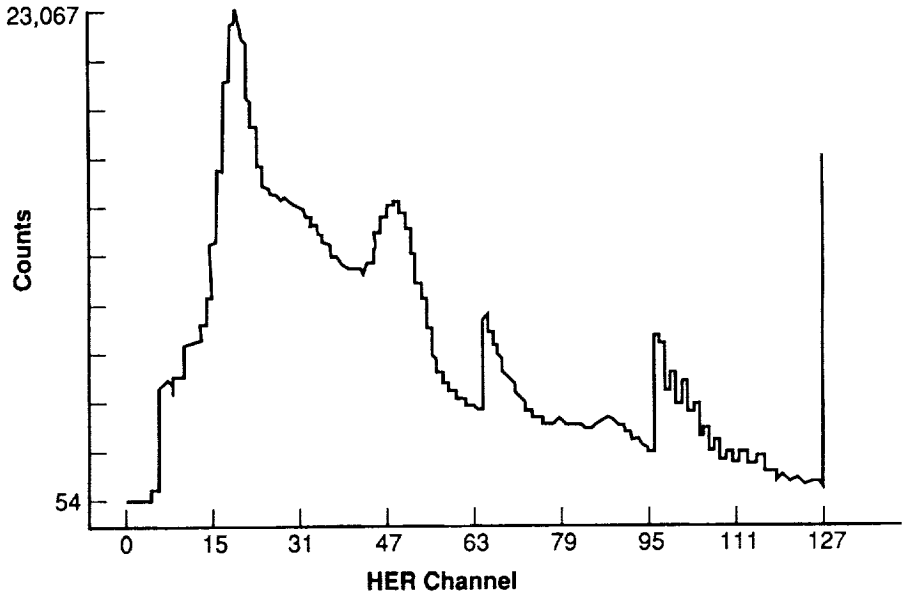

Figure 3.71. BATSE B4 HER Spectrum Displaying Odd-Even Effect.

This behavior was noticed prior to the GRO thermal vacuum test and was identified at the pre-test review as a possible occurrence. The BATSE team has done a large amount of investigation into the problem and determined several constraints. First, no counts are being lost from the HER integration. A comparison of background spectra closely spaced in time indicates that the counting rate is the same with and without the odd-even effect. At most, counts are being shifted one channel to the left or to the right. Second, no other BATSE detector (LAD or SD) has displayed this problem. Even on detector module B4, this anomaly cannot be initiated on command. Third, the amount by which these counts are displaced (one or two channels) is less than the intrinsic resolution of the detector. During normal operations and data analysis, adjacent channels in this region will most likely be summed together, effectively eliminating the anomaly and causing minimal impact to science operations. The BATSE team has decided that this anomaly is of no impact or constraint to flight.

(b) Detector B1 CPD Overcurrent Anomaly

In light of the difficulties seen during the BATSE system-level thermal vacuum test, the BATSE team waited for 72 hours at vacuum prior to powering the +HV supplies on the flight hardware. As mentioned previously in this section, all 40 +HV supplies were powered without incident. After nearly 24 hours of continuous operations under vacuum conditions, the CPD on detector module B1 tripped into overcurrent protection as a result of +HV breakdown. This occurred at 07:30 of July 11. Under direction from Dr. G. J. Fishman, BATSE Principal Investigator, the CPD was immediately powered off, and remained that way until 09:30 on July 18. After re-establishing power, the CPD continued to operate normally throughout the remainder of the test. A total time exceeding 8 days of operation in vacuum conditions was logged without incident. The apparent source of the anomaly was an outgassing problem at a connector or remote +HV circuit location. To previent a similar occurrence on-orbit, the BATSE team will wait for a period exceeding 5 days at vacuum prior to powering this +HV supply.

(c) Detector Module B7 SFAST3 Anomaly

The problem seen previously with the SFAST3 discriminator on B7 appeared again during the cold soak of the GRO thermal vacuum test. The discriminator returned to normal operations during the warming transition, near a temperature of 4 °C. As discussed in section III.D.4 this problem was isolated to the receiving circuitry at the CEU, on port #7, where module B7 is connected. This anomaly is characterized by a loss of the integral nature of the SFAST3 discriminator. Counts can appear in this discriminator; however, they are less than those of the SFAST4 channel above. The non-integral nature can be explained by a partial failure of the discriminator over the 2.048-second integration time in which it counts. The amount of information lost because of this failure is small because of the integral discriminators above and below in energy (SFAST4 and SFAST2). In 1988, the BATSE team decided that this anomaly was of minimal impact to science operations. The re-appearance of the SFAST3 problem in this test did not change the BATSE team's position.

(d) CPD +HV Current Oscillation

During the cold-case soak, the +HV currents on several of the BATSE CPDs displayed a slow oscillatory behavior. The oscillation was approximately 6 μA in magnitude about the nominal value. This problem went away during the temperature rise to ambient conditions. During the time when the anomaly is present, the voltages associated with the changing currents are well regulated. The counting rate on the associated CPDs are also remarkably steady. The regulation circuits on the HVPS cards are designed for the load of the 12.7-cm PMTs of the LAD and SD. Under these circumstances, the regulation of a 5.08-cm PMT is more difficult because of the different load presented by the smaller tube. The steady counting rate shows that the oscillation has no impact on the science operations of BATSE. The voltage is also well regulated during these times. Consequently, the BATSE team has taken the position that this condition is not one which impacts operations of BATSE, and it will not be remedied.

(e) Separation of B6 Thermal Blanket

During the GRO thermal vacuum test, the thermal blanket on detector module B6 suffered a partial separation of the aluminized Teflon front face from the Kapton surface underneath. This was caused by the pressure from trapped air under the aluminized Teflon surface exerting an outward force on the blanket. This blanket was present during the thermal vacuum test at MSFC; however, no sign of delamination was present then. The B6 blanket was repaired by removing the delaminated portion of the aluminized Teflon. This represented approximately two-thirds of the total area and was limited to the upper portion of the blanket. Following the removal, residual bonding material was cleansed from the Kapton with successive applications of tolulene and isopropyl alcohol. Next, a grounding strap was fashioned, threaded through the blanket, and applied to the inner VDA side of a new aluminized Teflon patch. Approximately 19 cm^2 of 0.005" aluminum tape and 2 oz of eccobond conductive epoxy were used to fasten this grounding strap. A measure of the resistance between the VDA and the end of the ground strap yielded a measurement less than 5 Ohms. Following the ground-strap application, successive rows of 2.54 cm width transfer tape were applied directly on to the Kapton portion of the blanket from which the delamination occurred. The aluminized Teflon patch was fastened to the blanket with this transfer tape, and approximately 15 small stitches were applied to the perimeter of the blanket to hold this layer in place.

Photographs of this repair operation were taken and are on file in the BATSE data library. The operation was performed with the thermal blanket removed from the spacecraft. Upon installation, the new ground strap was fastened to the detector module structure. The repair was performed by John Horack and Mr. Steve Holcombe, TRW's prime thermal technician on the GRO. When the GRO arrived at the Kennedy Space Center, the other seven detector module blankets received some re-work to prevent debonding of the aluminized Teflon once the GRO was on-orbit. This operation is described in section III.G.2.

13. GRO Propulsion System Pressurization Test

Following removal of the GRO from the thermal vacuum chamber, the spacecraft was taken to the acoustics test facility for a flight-pressurization test of the propulsion system. BATSE did not require any special preparations or configurations for this test. However, following the completion of the test on August 28, 1989, the propulsion system was loaded with a radioactive tracer gas containing 40 mCi of the isotope Krypton 85. The tracer gas would aid in the determination of any leaks which might be present in the propulsion system following the thermal vacuum test. Krypton 85 is a gamma ray emitting isotope, with a line emission at 514 keV and a 10.74 year half-life. Bremsstrahlung radiation produced in the interaction between beta particles and the fuel tanks added significantly to the amount of detected radiation. Consequently, all BATSE spectra taken between August 28 and September 6 display varying amounts of Kr 85 emission in the background. The propulsion system was repeatedly flushed and back-filled to remove the tracer gas. The removal of the gas required many iterations of this process. Any reader interested in utilizing BATSE data taken from these times should be cautioned of the contamination in the background spectra from the propulsion system. Data obtained after September 6 contain virtually no trace of the Kr 85 emission.

14. BATSE SFAST3 and SFAST4 Energy Threshold Calibration

The two SD discriminators SFAST3 and SFAST4 are located above the energy range of the SD MQT, and consequently cannot be subjected to a direct measurement of their energy threshold. section II.F of this document describes the various discriminators and their relationships to the BATSE data types. The energy threshold of these discriminators is an important piece of information for the understanding of BATSE data. Consequently, a measurement of these thresholds was made during the period following the GRO thermal vacuum test.

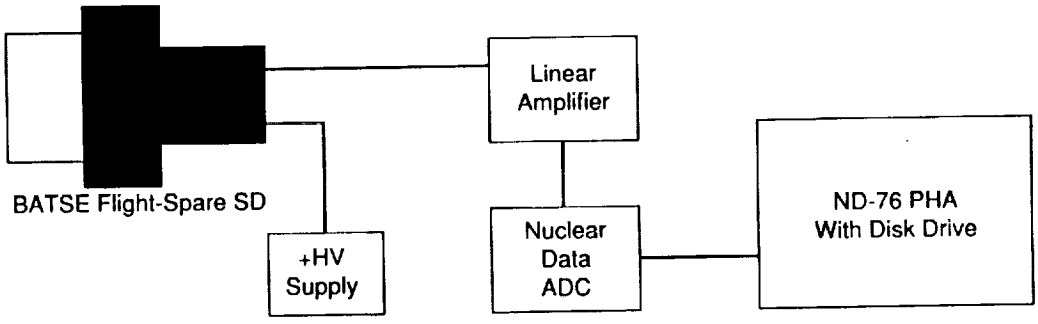

Figure 3.72. BATSE SFAST3 and SFAST4 Threshold Measurement - Test Configuration.

A BATSE SD flight spare was connected to a controllable +HV supply and a linear amplifier as shown in Figure 3.72. The output of the linear amplifier was sent to an analog-to-digital converter, which served as the input to a Nuclear Data pulse height analyzer. The channel-to-energy correlation was determined using a Co 60 isotope and a Th 228 isotope with known emission lines. After this relation was known, the linear amplifier multiplication factor was reduced to extend the spectrum to approximately 50 MeV in energy. The channel-to-energy correlation of the new spectrum was found by multiplication of the old value by the amount of reduction in gain at the linear amplifier. A 60,000-second background integration was obtained with the flight spare in the same orientation as the SDs on the GRO. One spectrum was obtained for the upper detectors and one for the lower detectors.

With the flight detectors set at 4X gain, a measurement of the SFAST3 and SFAST4 rates were obtained. These rates were subsequently multipled by 60,000 to determine the number of counts in each discriminator over this time period. After these numbers were obtained, the flight spare spectrum was examined. The threshold of the SFAST discriminators is found by determining the channel where the total number of counts above that energy matches the calculated numbers from the flight detectors. Once that channel is found in the spectrum, the channel-to-energy conversion yields the energy. The results for each of the eight flight SDs are presented in Table 3.118.

Table 3.118. BATSE SFAST3 and SFAST4 Measured Energy Thresholds in MeV

Detector Module	SFAST3 Energy (MeV)	SFAST4 Energy (MeV)
B0	8.02	12.35
B1	8.29	13.34
B2	7.79	11.70
B3	8.16	12.94
B4	7.79	11.98
B5	8.74	14.11
B6	7.97	12.91
B7	8.79	14.11

Examination of Table 3.118 reveals a disparity between the upper (+Z, even numbers) and lower detectors (-Z, odd numbers). Each of the upper detectors show a lower energy threshold than the lower SDs. This is a direct result of the difference in counting rate above and below the spacecraft. Those detectors on the top see a larger incident rate than those on the bottom. Although two separate flight spare spectra were obtained, it is extremely difficult to replicate the shielding environment produced by the GRO, and seen by the flight SDs on the bottom of the spacecraft. The rates of the -Z SDs are low compared to that of the flight spare spectrum taken in the same orientation. This low rate produces a higher channel number in the calibration spectrum, and consequently a higher computed energy for the SFAST threshold.

15. Instrument Data Run #2

The first testing of BATSE flight hardware to follow the GRO thermal vacuum test was accomplished during the second instrument data run. Strictly speaking, this operation was both a verification of functionality following the T/V test, and an opportunity to obtain calibration data from the Instrument. Beginning on September 12, 1989, BATSE was fully exercised, through the standard series of tests provided in Table 3.119. The instrument data run was executed in two portions, with a center time interval devoted to POCC testing, CTV/TDRSS testing, and CADH exercises. The second portion of the instrument data run was used for tests requiring radioactive isotopes. By the time of part two, the amount of Kr 85 in the propulsion system had been reduced to a level below the instruments' detectability. For the first portion of the testing, the test conductors were John Horack and Pat Lestrade.

Table 3.119. BATSE Testing Sequence for Instrument Data Run #2

- TP-200 -- Power control functional
- TP-110 -- Power-up and aliveness test
- TP-105 -- Detector module test
- TP-170 -- CPD calibration
- TP-171 -- CPD/LAD coincidence run
- TP-192 -- Pulsar clock frequency calibration
- TP-190 -- Pulsar data test (two options)
- TP-180 -- Burst data test (three options)
- BATSE special pulsar data type collections
- TP-125 -- Background collection procedure
- BATSE LAD and SD PMT balance and gain setting procedure
- TP-140 -- Long calibration
- TP-140A -- BATSE high counting rate measurement test

In addition to the previously performed operations, two new tests were added, and a PMT balance operation was exercised. Several spacecraft activities were performed in parallel with these tests, including POCC end-to-end test #2, during which BATSE remained powered through the night.

TP-200 was performed first to verify that all BATSE interfaces were healthy following the GRO thermal vacuum test. All BATSE interfaces and power controls were verified to be fully functional. Following a power-up and aliveness test, TP-105 was performed on the BATSE hardware. This test was important for several reasons. TP-105 offered the first comprehensive check of the detector modules following the environmental test program. The test also included a thorough

check of all +HV supply command bits. Through this test, each of the 40 +HV supplies on the instrument were verified to be fully operational and capable of normal functioning while subjected to vacuum conditions.

TP-170 was the next test performed during the data run. In the customary manner for this test, measurements of the CPD rates were obtained at a number of voltage settings. These results are presented in Table 3.120. Comparison of the odd-numbered (-Z detectors) CPD rates at the higher voltage settings with data obtained previously shows a marked disparity. As the voltage is decreased (CPDHVn increases), the computed rates fall into agreement with previous results. This indicates that most of the excess rate is at low energy. The increase in the counting rate for instrument data run #2 is a direct result of the Kr 85 gas contained in the propulsion system, located on the bottom of the spacecraft. The computed rates in the CPD on B0, B2, B4, and B6 are all in reasonable agreement with previous results. CPDHV8 rates are not available because of a problem with the IGSE at the time of testing. Data obtained in this exercise are on file in the BATSE library.

Table 3.120. TP-170 CPD Rates at CPDHVn Voltage Settings
Instrument Data Run #2 -- September 1989

	CPD Count Rate at Various +HV Command File Settings							
	Detector Module							
	B0	B1	B2	B3	B4	B5	B6	B7
CPDHV1	79.5	121.7	97.3	169.3	84.5	113.0	92.5	107.5
CPDHV2	66.5	76.4	76.3	90.3	70.6	85.8	75.0	84.2
CPDHV3	62.9	69.8	72.1	78.9	66.0	81.7	71.9	79.1
CPDHV4	60.5	64.7	67.3	70.1	64.5	75.3	68.3	73.2
CPDHV5	58.1	58.7	64.3	63.8	61.1	71.1	65.5	70.1
CPDHV6	55.2	55.1	60.5	60.2	59.0	66.9	62.0	65.1
CPDHV7	50.5	48.8	54.0	52.9	53.1	58.4	55.9	56.7
CPDHV8	--Not Available--							

The coincidence counting rate, obtained in TP-171, is in close agreement with previous values obtained during the first data run and the OFT. Table 3.121 displays the coincident rate computed for each of the eight detector modules. The modules again display the familiar top-to-bottom anisotropy in the rejection rate, indicative of the incident rate difference on the top of the spacecraft compared to the bottom for higher energies.

Table 3.121. Detector Module Coincidence Counting Rate from TP-171
BATSE Instrument Data Run #2 -- September 1989

Detector Module	Coincidence Rate
B0	20.52
B1	17.01
B2	20.66
B3	17.55
B4	20.89
B5	17.80
B6	21.06
B7	17.62

The next procedure the BATSE team performed was TP-192, the pulsar clock frequency calibration. This test was performed only on CCF-A, and yielded a frequency fractional difference of 5.75×10^{-6}. This result is entirely consistent with the values obtained from the GRO thermal vacuum test for a temperature near 25 °C. CCF-B was not tested during this operation.

Following the pulsar clock frequency calibration, TP-180 and TP-190 were performed. TP-180, the burst data test, was executed in all three possible configurations with no anomalies. Likewise, the pulsar data test was performed without difficulties in both of its possible configurations. Pulsar data testing continued with the production of each of the BATSE pulsar data types. TP-190 has the disadvantage that it only produces one form of pulsar data from each board, namely, PSRFULA and PSRFULB. For the test of mission operations and data analysis software, the BATSE team required a thorough set of each pulsar data type. During this test, each of the pulsar data types were generated using both A and B boards. The LED was utilized for these operations at a frequency of 100 Hz and various amplitudes. Consequently, the energy channel into which the LED fell was variable. Furthermore, each of the data types exercised a different detector module configuration and location in the pulsar parameter table. Table 3.122 contains the various configurations in which these data were obtained.

Table 3.122. BATSE Configurations for Pulsar Data Accumulations
Instrument Data Run #2

Data Type	Detector Modules	PSR No.	NSCANS	EBASE	LED Rate (Hz)
PSRFULA	B3, B5	1	1000	0	100
PSRFULB	B0	2	500	0	100
PSRSELA	B7	3	500	12	100
PSRSELB	B2	4	500	10	100
PSRSUMA	B1, B6	5	500	0	100
PSRSUMB	B4	6	500	0	100
PSR16A	B0, B4, B7	7	500	0	100
PSR16B	B2, B4, B5, B6	1	500	0	100

These data were archived onto tape and are available for inspection in the BATSE data library. For the testing of mission operations and data analysis software, these data were made into a daily data set for analysis in the MOPS environment.

The first portion of the instrument data run concluded on September 19, 1989, with long-duration background integrations utilizing TP-125. For this test, the burst trigger thresholds (T1, T2, and T3) were lowered to 4.25, 3.75, and 3.5 σ, respectively, so that EXFLAGS could be obtained at a later date. Integrations of 65-minute duration were obtained with the SDs at 4X and 1X gain. These spectra are on file in the BATSE library. From these data, BATSE was able to verify that the level of Kr 85 in the propulsion system had diminished substantially and that it no longer constituted a significant portion of the detected background radiation.

Instrument data run testing resumed on October 6, 1989. In the preceding time period, BATSE participated in the second GRO-POCC end-to-end test. The instrument was powered to provide flight-like data (including gamma ray burst and solar flare event simulations) for the POCC to process. BATSE operations in Huntsville were tested through the receipt and manipulation of the data from PACOR. No BATSE flight hardware tests or calibrations were performed.

The second portion of the data run commenced with a comprehensive PMT balance and gain adjust. A 5 μCi isotope of Cs 137 was placed at a distance of 76.2 cm in front of the LAD on-axis, and each of the PMTs were adjusted according to the desired location of the 662-keV photopeak. The LADs were balanced to provide a dispersion of 5 keV/linear channel. The SD voltages were established at three different dispersions: 1 keV/linear channel (4X gain), 4 keV/linear channel (1X gain), and 10 keV/linear channel (0.4X gain). Table 3.123 contains the final PMT settings for each of the desired gains.

Table 3.123. BATSE +HV Values Following PMT Balance - October 1989 Instrument Data Run #2

	High Voltage Setting for Desired Gain					
Detector Module	PMT-A	PMT-B	PMT-C	SD 4X	SD 1X	SD 0.4X
B0	1506	1506	1580	1559	1260	1110
B1	1655	1640	1648	1612	1295	1138
B2	1551	1527	1581	1543	1260	1122
B3	1609	1609	1593	1455	1181	1051
B4	1618	1649	1684	1511	1228	1079
B5	1672	1641	1674	1410	1150	1012
B6	1481	1387	1414	1512	1233	1083
B7	1684	1653	1711	1630	1323	1157

Following the completion of the PMT balance and gain setting operation, 5-minute integrations were performed, accumulating spectra from all detectors. These spectra are on file in the BATSE library and are available for inspection.

The next operation requiring the use of radioactive isotopes was TP-140, the long calibration. Bob Wilson and Geoff Pendleton replaced Pat Lestrade for these tests, which required three test conductors. The geometrical arrangement of the isotopes used in this operation is identical to that of the first instrument data run and is fully described in section III.F.5. With each isotope in place, a 32-minute integration is obtained and stored to disk. Single PMT spectra were again obtained with Cs 137 isotopes deployed in front of each detector module. Integrations were obtained in this configuration while the +HV was set to values of nominal, and nominal +100 V. The gain exponents were then calculated according to equation (3.3). Table 3.124 contains the results from that calculation.

Table 3.124. BATSE LAD PMT Gain Exponents Determined from TP-140 Long Calibration - Instrument Data Run #2

	Gain Exponent for PMT		
Detector Module	A	B	C
B0	6.7	6.2	5.6
B1	5.7	6.1	6.1
B2	6.4	7.0	6.0
B3	5.8	7.1	6.8
B4	4.6	5.9	5.8
B5	5.2	5.8	5.5
B6	6.9	6.8	6.8
B7	5.3	6.0	5.4

Comparison of these values with those in section III.F.5 from the first instrument data run shows a difference in gain exponents for some PMTs that is larger than one might expect. The voltage changes required to establish new gains were not especially large, or unpredictable, indicating that the PMT behavior over time is rather stable. All other indications of PMT behavior, especially the derived spectra, show well-behaved PMTs. The reason for the discrepancy in the two measurements is not well understood; however, the difference in the measured gain exponent is not indicative of a problem with the PMTs. For the initial version of mission operations and data analysis software, the averages of the two measurements are used.

TP-140 again provided a mapping of the LED peak location in HER channel space for each of the 16 possible command values. The locations of the LED were expected to change slightly following the rebalancing operation; and, in fact, several LEDs displayed a shift of one or two channels. Table 3.125 contains the results of this mapping.

Table 3.125. HER Channel Location of LED Peak for Associated Amplitudes from TP-140 -- Long Calibration, Instrument Data Run #2

	HER Channel Location of LED for Module							
LED Hex Amplitude	B0	B1	B2	B3	B4	B5	B6	B7
3	Off	Off	Off	Off	Off	Off	Off	Off
4	13	27	15	22	20	29.5	24	23
5	30	63	34	51	45	67	55	49
6	49	83	56.5	74	68.5	89	77	71
7	66	97	72	91	83	100	94	86
8	75.5	102	84	98	96	105	100	96
9	85	108	95	103	100	111.5	104	100
A	95.5	112.5	98	107	103	118	109	104
B	98	117.5	101	111	107	123	113	107
C	100	122	104	115	110.5	127	117.5	111
D	102	125	107	119	114	127	122	114
E	104	126	109	123	118	127	125	117
F	106	126	112	123	121	127	126	121

A new test procedure was performed during the second instrument data run. TP-140A was performed to obtain measurements of the hardware performance during conditions of a high incident counting rate. The test results allowed the BATSE team to better ascertain the dead time in various branches of BATSE data, and to determine behavior such as the amount of gain shift caused by a high counting rate. The results of the data analysis from these and other similar operations are presented in the BATSE calibration summary document.

The GRO spacecraft was moved to the center of the R7A high-bay, allowing for a minimum of 3.7 meters of floor space in front of each module. For each of the detector modules, three locations were identified on the floor of the high-bay. These locations were established so that the placement of an isotope above these floor spots would yield a horizontal distance of 0.9, 1.8, and 3.7 meters to the center of the LAD. Each module location was unique, and the detector modules were tested individually.

During this test, the CEU was commanded to an alternate data output schedule, involving HER, SHER, and PSRFULA. The PSRFULA packets contained pulsar data with a folding period of 10 ms and included only the detector module under test. The LED was powered on at a rate of 1 kHz, with an amplitude sufficiently high that the peak equivalent energy exceeded 662 keV. The corresponding MER/PSR energy channels were recorded, and rates from the four FASTn discriminators were obtained. After turning off the LED, these measurements were repeated.

A small (1 μCi) isotope of Co 60 was then fastened to the support stand in front of the module under test at the standard TP-140 distance. The LED on-off operation described in the preceding paragraph was then repeated. Subsequent repetitions of this process were executed with a 5 mCi Cs 137 isotope placed at the 3.7, 1.8, and 0.9 meter distances marked on the floor. The final operation on the detector module was to obtain CPD counting rates as a function of +HV values, similar to what is done in TP-170. In this case, however, the Co 60 isotope is in place, and the Cs 137 isotope is located at the 0.9-meter distance.

This process was repeated for each of the detector modules, and the various dead times were calculated. Data acquisition for TP-140A took place on October 9-10, 1989, with Bob Wilson, Geoff Pendleton, and John Horack performing the procedure.

16. Final Optical Alignment Measurements and Results

Section III.B.1.c describes the internal portion of the BATSE optical alignment procedure, TPS-28. The data derived from this test are the pointing vectors of the LADs in a coordinate system referenced onto the optical cube. The measurements taken at TRW built upon these data, eventually allowing one to calculate the pointing vectors in the coordinate space of the GRO. After each of the modules were installed onto the spacecraft, measurements of the position of the optical alignment cubes were made several times. These measurements determined the location of the cube-face normal vectors in the GRO coordinate frame. For a perfectly constructed cube, these vectors are simply the basis vectors of the system in which the TPS-28 data are described. However, each of the optical fixtures' front-to-back relationship was not identical. Consequently, measurements of the cube orientation with respect to the rear flat were required. After this relationship was found, the LAD pointing vectors could be fully described in the GRO coordinate space. Table 3.126 contains the final calculated results of the eight LAD pointing vectors in the GRO coordinate (X,Y,Z) space. These vectors contain compensation factors for the relaxation of the spacecraft outside of the 1-g environment in which the measurements were made.

Table 3.126. Final Normalized LAD Pointing Vectors in GRO Coordinates

Detector Module	X	Y	Z
B0	0.57852	0.57475	0.57878
B1	0.57683	0.57690	-0.57831
B2	0.57686	-0.57803	0.57715
B3	0.57726	-0.57603	-0.57875
B4	-0.57775	0.57524	0.57906
B5	-0.57669	0.57947	-0.57589
B6	-0.57597	-0.57645	0.5796
B7	-0.57701	-0.57772	-0.57732

For all eight Detector Modules, the "ideal" vector components would have absolute values equal to $1/\sqrt{3}$, or 0.57735. The dot-product of the measured pointing vector with the "ideal" pointing vector is a scalar measure of the pointing error. The angle which one obtains is the half-angle of a cone generated by rotating the true pointing vector about the ideal pointing vector. The results of this operation are given in Table 3.127.

Table 3.127. BATSE Pointing Vector Offset Angles from "Ideal" Direction

Detector Module	Angular Offset (arc min)
B0	11.0
B1	4.1
B2	3.0
B3	6.6
B4	9.4
B5	9.1
B6	9.6
B7	1.7

BATSE has an absolute pointing error requirement of 1° with a pointing knowledge requirement of 0.1°. For this last set of November 1989 measurements, all BATSE detector modules meet these requirements. TRW has stated their measurement accuracy to be 20 arc seconds relative to the GRO star-trackers. The data in the tables above, however, have a larger uncertainty, estimated to be approximately 1.5 arc minutes. The larger uncertainty is primarily attributable to the method of determining the internal pointing vector, described in section III.B.1.c.

17. Observatory Functional Test #2

The final Observatory functional test at TRW began on October 30, 1989. No configuration changes had been made to the BATSE flight hardware between the previous instrument data run and this functional test. This was the final full-scale test of the BATSE hardware prior to shipment of the spacecraft to KSC. The results of these tests remained with the flight hardware until launch, at which time they were filed into the BATSE data library. Because these tests produced nominal results, nearly identical to those of previous tests, only a brief mention of each test will be included here. Those readers interested in a more in-depth look at this data are encouraged to look at the results contained in the BATSE data library.

TP-105, the detector module test, was performed after a normal power-on sequence during the morning of October 30. Each of the detector module functions were checked and verified, including the functionality of each of the +HV command bits for all 40 supplies. Each module was declared fully functional following the completion of TP-105.

All options of TP-180, the burst data test, and TP-190, the pulsar data test, were executed without anomaly. All cross-strapping configurations of the burst trigger and solar flare trigger signals were exercised in coordination with the other three instruments. TP-170 and TP-171 were performed, and each yielded results consistent with previous tests. TP-200, the power control functional test, was performed without anomaly, and each of the BATSE flight heater circuits were verified. Cross-strapping of heater and instrument power was also exercised. TP-192, the pulsar clock frequency calibration, was performed on CCF-A, yielding a frequency fractional difference of 6.35×10^{-6}. All internal cross-strapping capabilities were performed, including ADF, CCF, and relay cross-strapping. The BATSE portion of the Observatory functional test concluded on November 2, 1989, with the accumulation of a 100-minute background integrations using TP-125. The results of all testing were successful.

18. GRO Pre-Shipment Abbreviated Functional

The final testing performed on the BATSE instrument in California was done during the pre-shipment abbreviated functional. These tests began on December 6, 1989, and lasted only 2 days. During this shortened period of testing, the BATSE team established simple functionality of the instrument without testing in great detail. Table 3.128 lists the tests performed during this operation.

Table 3.128. BATSE Tests Performed During GRO Pre-Shipment Abbreviated Functional

- BATSE flight heater power and cross-strapping tests
- TP-200 — Power control functional test
- TP-110 — Power-up and aliveness test
- TP-180 — Burst data test
- TP-190 — Pulsar data test
- TP-125 — Background collection
- BATSE instrument power cross-strapping tests

The pre-shipment testing took place in two phases. The first portion of the test was done to verify fundamental operations of the instrument, including relay functionality, heater functionality, and cross-strapping configurations. A comprehensive heater power and cross-strapping test, in addition to TP-200, verified these fundamental functions. The second portion of the testing involved verification of the second-level operations of BATSE, including module +HV, CEU data operations, and collection of spectra. To accomplish these objectives, TP-110, TP-180, and TP-190 were performed. The final testing performed in California concluded on the afternoon of December 7, with a collection of background spectra using TP-125. Following these tests, all of the instrument ground support equipment was packed, and BATSE was ready for shipment to the Kennedy Space Center. Table 3.129 contains the power-on time for all activities at TRW.

Table 3.129. BATSE Powered Operations Total Time at TRW

	BATSE Power On Time
Non Thermal Vacuum	600 hours
Thermal Vacuum	518 hours
Total at TRW	1,118 hours
Total to date	2,154 hours

19. Observatory Shipment to KSC

Preparations for shipping the Gamma Ray Observatory were made throughout the entire month of January 1990. The GRO was placed into a specially-made shipping container for the journey to the launch site. The shipping container possessed a complete environmental control system to regulate the temperature and humidity of the spacecraft environment during transit. On the evening of February 7, 1989, the GRO was transported in the shipping container a few miles north of the TRW facility to the Los Angeles International Airport. At the airport, the spacecraft was loaded onto an Air Force C5 military transport plane. The trailer on which the spacecraft was taken to the airport

was also placed on the plane, along with numerous crates of spacecraft GSE. On the evening of February 8, 1990, the spacecraft left Los Angeles on the C5 for an overnight flight to the Kennedy Space Center. The C5 aircraft landed at KSC's Shuttle Landing Facility in the early morning hours of February 9.

G. BATSE Testing at the Kennedy Space Center

1. KSC Observatory Functional #1

Nearly 1 month was required to prepare the GRO for testing in the Payload Hazardous Servicing Facility (PHSF) at the Kennedy Space Center. GRO was the first spacecraft to utilize this facility. Following transport from the Shuttle Landing Facility, the spacecraft was removed from the shipping container, placed onto the support structure, and mechanical reconfiguring began. The Observatory was finally ready for full-scale testing on March 2, 1990, when the first OFT at KSC commenced.

BATSE testing was quite extensive during this period. Table 3.130 lists those tests performed during the first OFT at KSC.

Table 3.130. BATSE Testing Sequence for First KSC Observatory Functional Test

- TP-100 — Engineering and interface verification test
- TP-200 — Power control functional test
- TP-110 — Power-up and aliveness test
- TP-125 —Background collection procedure
- TP-188 —Coordinated burst and solar flare trigger signal test
- TP-190 — Pulsar data test (options A and B)
- BATSE flight heater power and cross-strapping verification
- OBC South Atlantic anomaly sequence verification
- TP-105 — Detector module test
- Power cross-strapping tests
- TP-170 — CPD calibration
- TP-171 — CPD/LAD coincidence tests
- TP-180 — Burst data test (option A)
- TP-192 — Pulsar clock frequency calibration (both CCFs)
- TP-180 — Burst data test (options B and C)
- TP-125 — Background collection procedure with filament sources
- GRO power profile testing

This sequence of testing required four extended shifts to complete, ending on March 9, 1990. TP-100 was performed first to verify that no damage had occurred to the BATSE hardware during transit. This procedure would have found any broken wire, separated interfaces. cross-talk on command lines, or anomalous detector module operations if these were present. No anomalies were discovered furing TP-100. All command bits of the 40 +HV supplies were functional, and all functions of the BATSE hardware were verified at the engineering level.

TP-200 was performed immediately after the engineering test to verify full control of all power relays and related functions. In addition, relay status indications of GRO engineering telemetry were checked through both RIUs. This test uncovered a previously unseen anomaly in the GRO engineering telemetry. During TP-200, the BATSE test conductor cycles power to each of the CEU boards, and also powers them through both relay configurations. Engineering telemetry from BATSE and the spacecraft is verified for all four possible relay configurations. During the check of STTE/SHER memory boards (42A30936), the GRO telemetry failed to report the proper state of the board when it was in the primary-off configuration. BATSE telemetry simultaneously verified the proper state of the board. The BATSE telemetry measures the current flowing through the power relay to determine the status, while the GRO engineering telemetry has a separate relay circuit in the CEU to perform a measurement of the board status. Three attempts were made to put the GRO measurement into the proper status, and all failed. All other GRO telemetry indicators functioned normally, including those for the other STTE/SHER board. The GRO indicator failed only when the STTE/SHER board was in the primary-off state. The other three states are correctly reported by the spacecraft sensor circuit. The behavior of this status indication is identical through both of the RIUs, indicating that the problem is in the sensor itself, and not in the telemetry or transmission of the sensor information. The cause of the anomaly is an open-failure, or a poor contact in the GRO primary status indication relay. This relay is not the one which supplies power to the board and in no way affects the performance of the hardware. To prevent any further possible damage to the relay circuit or to BATSE hardware, the power relays to this board were not cycled during any further testing prior to launch.

The formal verification of the OBC South Atlantic Anomaly (SAA) sequence was a new addition to the Observatory functional test. In previous end-to-end tests, the spacecraft was operated with a simulated ephemeris, and these commands were executed by the OBC as part of a normal "orbit." During the times of passage through the SAA, BATSE requires that the +HV on the instrument be turned off to prevent damage from the high level of charged particles in this portion of the orbit. The cycling of the +HV is handled by an automatic sequence stored in the OBC and is activated at the predicted times of entry and exit from the SAA. Upon entry to the SAA, the OBC powers off the +HV and disables burst triggering. This operation requires two serial commands; however, the sequence contains four commands to account for either CCF being operational. When the SAA is exited, the +HV is repowered, and burst triggering is again enabled. This test was performed without anomaly.

All of the BATSE flight heaters were powered in each of the possible configurations without anomaly, and the full complement of instrument cross-strapping configurations were successfully

exercised. Each of the subsequent BATSE procedures were executed without anomaly. Results from these tests remained at the Kennedy Space Center until the launch of the GRO. After this time, all test results were placed into the BATSE data library for reference.

2. BATSE Detector Module Thermal Blanket Retaining Stitch Application

The separation of the aluminized Teflon layer from the B6 thermal blanket during the GRO thermal vacuum test was described in section III.F.12.i(3)(e). This separation occurred because of residual trapped air behind this layer exerted an outward force on the Teflon when the blanket was placed in vacuum conditions. To prevent this type of failure on the other detector module blankets, an application of retaining stitches was made to the other seven thermal blankets. These blankets were modified in situ on the spacecraft.

Each of the detector modules received five stitches. One stitch was placed at each of the bottom corners of the Teflon layer, one at the upper corner, and the remaining two along the curved upper portion of the Teflon. Each stitch was located approximately 2 cm from the perimeter of the aluminized Teflon layer. The knot which secured each of these stitches received a bead of epoxy to prevent it from working loose. After the epoxy had dried, any remaining thread was trimmed away from the stitch area. This work was performed during the first week of March 1990, by TRW thermal technician Steve Holcombe and BATSE representative John Horack. It required 2 days to complete. A full set of photographs were taken of each module before and after the modifications were effected.

3. Instrument Special Checks

The next sequence of powered activity at KSC was performed on March 12, 1990. This test, the instrument special checks test, allowed the four experimenters to use radioactive isotopes in testing the flight hardware. Because the normal GRO functional test did not provide for the use of isotopes, a special test had to be constructed. OSSE was the primary user of isotopes during this time. The OSSE team made use of Th 228, Co 60, and Cs 137 isotopes of 200 μCi activity during this period. BATSE was placed into a passive, data-collecting mode, and TP-125 was performed during these times. The primary BATSE operation during the instrument special checks involved the creation of an artificial gamma ray burst using OSSE's Cs 137 isotope.

OSSE's source was located 366 cm in front of the GRO on the spacecraft's X-axis. The isotope was mounted in a collimator with a 45° opening angle and effectively illuminated BATSE detector modules B0-B3. The isotope was occulted, and the instrument was allowed to recompute the new background level. After the background had been recalculated, burst triggering was enabled. The isotope was then rapidly exposed to the spacecraft and its intensity modulated by placing a lead plate in the path of the radiation at various frequencies. BATSE triggered a gamma ray burst event, as expected, and data were archived. This data set was used in the test of data analysis and mission operations software at MSFC. Data from this test are available for inspection in the BATSE data library.

4. End-to-End Test #3

The first major end-to-end test with the spacecraft at KSC began on March 26, 1990. Test conductors at KSC primarily served as test monitors and as backup in the event of an anomaly. Instrument operations were controlled from Marshall Space Flight Center and by BATSE personnel at Goddard Space Flight Center. Instrument power was applied using commands supplied by the flight operations team at GSFC.

ETE #3 lasted approximately 36 hours and provided the BATSE teams at MSFC and GSFC the opportunity to test the instrument with the POCC in the link, in a similar fashion to the BATSE on-orbit activation sequence. A normal power-up procedure was executed during the first three TDRSS passes. During the fourth pass, spectra were obtained from the detectors and from each individual phototube. Pass #5 allowed for a small calibration of the LLD. A triggered burst event was planned for pass #6, and burst triggering threshold tests were performed during the seventh TDRSS contact. The remaining contacts were used for pulsar operations and for updating the output schedule onboard the instrument. During these times, the test crew at KSC continually monitored the instrument operations and archived all data to tape through the BATSE IGSE. Additional non-instrument tests were performed, such as the updating of limits files at the POCC. All data acquired during these operations are available for inspection in the BATSE data library.

A major anomaly was confirmed by the BATSE team at KSC. During the instrument special checks, a possible problem with a PMT on B5 was noted but was not confirmed because of the operational sequence of events. During this end-to-end test, extremely high rates were seen from the LAD on B5 shortly after the +HV was turned on. A sequential removal of power from PMT-A, -B, and finally -C failed to remove the rates until the final PMT was turned off, indicating a possible connection with PMT-C. Each PMT was then powered up in sequence again without further anomaly. Cycling of the +HV appeared to "fix" the anomaly. These tubes operated normally for the remaining 36 hours of the test.

5. B5 Troubleshooting Test #1

After confirmation of the anomaly described above, a troubleshooting test was carefully designed to further characterize and understand the improper behavior seen on detector module B5. The first of these tests was performed on April 20, 1990. To begin the test, all eight detector modules were powered on with all +HV off. Previous testing had indicated a possible connection between the anomalous behavior and PMT-C on B5. Consequently, this PMT alone was powered into its nominal configuration in an attempt to isolate the anomaly. After nearly 2 minutes of normal operations, the anomaly was verified. The current on the PMT immediately jumped to 203 μA, then returned to a near normal value of 120.6 μA. Rates in the first three FAST discriminators from the LAD were each in excess of 4,000 counts per second. During the time of the anomaly, rates and HKG parameters were stored to disk and printed out.

Approximately 15 minutes after the appearance of the high rate, the PMT returned to a normal operating condition. This result was completely unexpected. After 45 minutes of nominal operations, the BATSE test conductor performed several steps to attempt a recreation of the difficulty. It was thought that raising the +HV would place the PMT into a more susceptible mode, especially if the anomaly was related to the charging of foreign material inside the PMT. Three increments of 100 V were applied to PMT-C. At each level, the PMT was allowed to operate for 15 minutes, a sufficient time to allow the anomaly to appear. At each of the three levels, the PMT operated normally. Following the increments of +HV, six, 100-V decrements were applied, starting at the nominal voltage value. Again, the PMT was allowed to operate for several minutes at each level. No anomalies were discovered.

With attempts to recreate the problem proving unsuccessful, the PMT was powered off for 40 minutes. It was believed that powering off the PMT for a period of time might allow for the anomalous condition to re-establish itself when the PMT was powered again. PMT-C was repowered at the end of the 40-minute period with no anomalies. After 20 minutes of normal operation, the tube was turned off, and remained off for 1 hour. A 1-hour power-off time was also insufficient to cause the high rates to appear when the PMT was turned back on.

Several operations were performed after the 1-hour time period failed to recreate the anomaly. With PMT-C powered off, several operations were performed on PMT-A and -B to determine their combined performance in the event that PMT-C was lost. The gains of the tubes were adjusted to provide a total dispersion of 5 keV/channel in the LAD. This required voltages of 1,825 and 1,794 V for PMT-A and -B, respectively. Resolution measurements obtained from two PMT spectra indicate a FWHM resolution of approximately 30%-35% at 80 keV, somewhat higher than the average 28% seen on the other LADs. This procedure required 4 hours to complete, during which time PMT-C remained off.

The final portion of the test was a repowering of PMT-C after this extended power-off time. Despite a 4-hour rest, the anomaly was not found to be present after 30 minutes of operation when the PMT was repowered.

This first troubleshooting test verified a connection between the anomaly and PMT-C. Furthermore, the data from this test indicated that the anomaly with PMT-C could be removed by either cycling the +HV or by allowing it to "burn itself out." Last, the minimum time required for the PMT to be off before the anomaly would re-appear was found to be between 4 and 14 hours. Therefore, entry and exit from the SAA would not be long enough to incite the problem.

6. B5 Troubleshooting Test #2

The results from the first troubleshooting exercise provided some answers to questions regarding the anomaly but also raised more questions which required answers. This second test was performed on March 11, 1990, in conjunction with the GRO modified functional test. To begin the test, the CEU and detector modules were powered, and +HV remained off. This configuration duplicated that of the previous test. PMT-C on B5 was subsequently powered to its nominal operating voltage, where it performed normally for 4.25 minutes. At this time, the previously seen anomaly manifested itself through a tremendous jump in the counting rate and a full-scale reading of the current measurement. Aside from the somewhat longer period of nominal operation, this behavior was in keeping with previous occurrences of the anomaly.

After the anomalous behavior was present, the test procedure called for several operations to be performed. The first was to place the HKG multiplexer onto the PMT-C voltage and to dwell on this reading. As expected, the voltage was well regulated during the time of the anomaly, indicating that the HVPS was performing normally. Second, the +HV was lowered in decrements of 200 V until the anomaly went away or the minimum voltage was reached. The first drop of 200 V removed the anomalous condition. After operating at nominal 200 V for 2 minutes, the voltage was again lowered with no evidence of the anomaly. This sequence was repeated until the minimum voltage was obtained. No indication of a problem was present at any of these levels.

When the PMT had operated at the minimum voltage for 10 minutes without incident, the nominal voltage setting was re-established. Immediately, the anomaly was present again in the PMT. This result was in direct contrast to previous testing, which had demonstrated that once the anomaly was removed, it could not be re-established unless the PMT was powered off for a period of time exceeding 10 hours.

Also during previous tests, the anomaly was seen to clear itself up after approximately 10 minutes of operation. Because of this behavior, it was decided to let the anomaly ride itself out again. However, after nearly 40 minutes of operation, the anomaly was still present. This result was a second major difference from previous testing. Following a caucus with parties at MSFC, the high voltage was raised 100 V. Three minutes of operation at this higher voltage cleared up the anomaly. Subsequent increments of 100 V were applied to the PMT, each producing normal operations. PMT-C operated at the final value of 2,000 V for approximately 20 minutes without incident. After incrementing the +HV, the tube was commanded back to its nominal value where it performed without incident for the remainder of the day.

In light of these results, the BATSE team began preparation for a removal and changeout of PMT-C on detector module B5. Several additional tests were performed during this period, including TP-188, TP-125, a check of heater power and cross-strapping, instrument power cross-strapping, and the BATSE portion of the GRO power profile test.

7. BATSE PMT Changeout and Retest

PMT-C on detector module B5 (#112402-17) was removed from the spacecraft on June 4, 1990, and replaced with a flight spare using BATSE-ES-62-TP-305. Mechanical test conductor Joe Ozbolt of MSFC performed the operation with the assistance of Bob Austin, Jerry Fishman, Fred Berry, and John Horack. Quality assurance from MSFC was represented by Bill Horn. Extensive preparation was required before this delicate operation could be performed. Testing of the BATSE protoflight module was done to determine the best-qualified replacement PMT. PMT-A from this module (#112306-13) was eventually selected because of its superior performance characteristics. The phototube had been operated under vacuum conditions on two previous occasions during protoflight thermal vacuum tests at MSFC. A day-run of the PMT removal procedure was performed on the protoflight module at MSFC to evaluate possible hazards or difficulties which were not foreseen during the writing of the test procedure.

The procedure required one, 8-hour shift to completge. After the replacement PMT was installed, an electrical verification test was performed on the PMT, using TP-105. This included identification of the proper +HV and signal connections, in addition to PMT balancing and performance measurements. Performance of the replacement PMT was completely normal. The thermal blanket for detector module B5 was re-installed on June 5, 1990. The results of this test are in the BATSE library and are available for inspection.

8. End-to-End Test #4

The changeout of PMT-C on B5 was fortunate to precede the fourth end-to-end test. ETE #4 provided 84 continuous hours of BATSE operation, during which any problems with the new PMT would be easily identified. During the test, BATSE personnel at KSC were primarily assigned the task of monitoring the instrument, while personnel at GSFC and MSFC initiated testing actions. During the first day, an automatic PMT balance operation was performed using commands stored in the OBC. The second day was devoted to the creation of solar flares for use by the COMPTEL instrument, so that their OBC processors could be verified. The first sequence of commands sent from the FOT to BATSE contained an improper LED value, causing the solar flare test to fail. The BATSE test conductor reconfigured the instrument at KSC; however, he inadvertently placed detector module B0 into coincidence mode. This operational error was not noticed until the same test conductor arrived back at work the next day. On the third day, source occultation simulations were performed. The LEDs in several detectors were cycled on and off in half-orbit periods to simulate the emersion and immersion of a source from behind the limb of the Earth. These data were subsequently used to test BATSE mission operations software at MSFC.

The end-to-end test was completed at 11:00 p.m. on the evening of June 9. During the entire 84 hours of operation, the replacement PMT operated flawlessly. No instrument anomalies were identified during the test.

9. End-to-End Test #5 / Observatory Functional Test

During July 1990, two operations were performed involving the BATSE flight hardware, ETE #5 and a brief Observatory functional test. The end-to-end test began on July 20 with BATSE being powered up by command from the POCC at the Goddard Space Flight Center. The role of the KSC test conductors was to again serve as monitors of the proceedings and to command the instrument in the event of an emergency. However, shortly into the test, the BATSE IGSE suffered a catastrophic failure of a device-driver card in the ground computer. This had no effect on the BATSE flight hardware; however, the KSC test team no longer had visibility into the configuration of the spacecraft. BATSE was powered off until repairs to the IGSE could be completed. The system was repaired by Scott Storey of ES62 in time for the final 8-hour segment of the brief end-to-end test. During this final segment, however, difficulties in the ground system at the POCC and MSFC made the test less than completely successful. The spacecraft performed flawlessly during this test; however, most of the equipment around it did not perform as well. ETE #5 ended on the afternoon of July 21, 1990.

A brief Observatory functional test was performed after ETE #5. During this test, BATSE test conductors focused in on obtaining spectroscopy detector data from a variety of gain settings. Using TP-125, long-duration spectra were obtained from each of the SDs at gain settings of 2X (2.0 keV/channel uncompressed), 1X (4 keV/channel uncompressed), 0.4X (10 keV/channel uncompressed), and at the lowest possible gain settings for each of the SDs, 1,000 V. These data were all background spectra and were used in the determination of the functional form of the channel-to-energy relation for the spectroscopy detectors. No other BATSE testing was performed as a part of the functional test.

10. End-to-End Test #6

The sixth end-to-end test was considerably more successful than ETE #5. Beginning on August 15, 1990, the test spanned a 36-hour period in which additional POCC, CMS, and BATSE-MSFC functions were tested using the spacecraft. BATSE was powered on by the crew at KSC, who performed routine monitoring of the instrument throughout the entire 36-hour period. The BATSE team at MSFC successfully loaded pulsar parameters, output schedules, and other instrument data to the spacecraft through the TDRSS network. South Atlantic Anomaly operations were verified functional, and the burst trigger signal was tested in the end-to-end environment.

11. GRO Modified Functional Test

As with previous functional test opportunities, the BATSE team utilized this power-on session to acquire data which was needed back at MSFC for particular test or calibration operations. During this modified functional test, which started on September 6, 1990, the BATSE team obtained long-duration spectra from the LADs and SDs to further help the determination of the functional form of the channel-to-energy calibration. Spectra were obtained +HV values of nominal, nominal +2 steps, and nominal -2 steps for each of the eight large area detectors. Similar settings were used for the SD at 2X (2.0 keV/channel uncompressed) gain. Each of these spectra were 2.6 hours in duration and are on file in the BATSE library for inspection.

12. Second GRO Modified Functional Test

Another modified functional test was performed in October 1990. The BATSE team again generated "custom" data from the instrument to supplement mission operations, data analysis, and calibration efforts underway at MSFC. The first of these tests occurred on October 22, 1990. BATSE utilized the OSSE Cs 137 isotope in generating a simulated gamma ray burst event. In an analogous fashion to the one described in section III.G.3 the isotope was shielded from the spacecraft, while the instrument computed the background level and had its burst trigger enabled. Following completion of these items, the source was rapidly exposed and modulated, causing the instrument to trigger a burst. Unlike the previous test, where the isotope was located on the +X end of the GRO, the Cs 137 isotope was now located in the GRO X-Z plane, 305 cm from the rear of the spacecraft and 46 cm off of the floor. Consequently, detectors B5 and B7 were the most brightly illuminated during the exposure of the isotope.

Additional nominal, nominal +2 steps, and nominal -2 steps spectra were obtained from each of the LADs and SDs (at 2X gain). Unlike the previous spectral accumulations, these spectra were obtained with four Coleman lantern filaments in front of each of the detector modules. These filaments contain nitrates of thorium, and consequently are slightly radioactive. Emission lines are easily visible from these filaments at 80 keV and 2.614 MeV, among others. These spectra provided enhanced knowledge of energies in channel space for the calibration of the functional form of the energy-to-channel relation. Two full days of testing were required to obtain all the data with lantern filaments and several background spectra.

13. End-to-End Test #7

The seventh and final planned end-to-end test involving the GRO instruments began on October 30, 1990. BATSE was powered by the crew at KSC, who subsequently monitored various facets of instrument performance. One particular aspect of BATSE performance was the presence of several packets in which a data byte appeared to have been dropped out, and all remaining data bytes were shifted to the left by one location. This behavior was noticed at MSFC in the inspection of ETE #6 data and was subsequently traced back as far as the GRO thermal vacuum test. These events are nearly impossible to detect in real time using the BATSE IGSE system because of the infrequent

nature of the events and the lack of suitable "trapping" software in the IGSE system. Consequently, several parameters were placed into the BATSE instrument memory that would appear in the data stream during one of these events, making it easily identifiable to the MOPS software user at MSFC. The byte-drop anomaly is discussed in detail in the next section of this document.

End-to-end #7, like previous tests, demonstrated the ability of the Flight Operations Team at GSFC to control the spacecraft, and allowed personnel at MSFC to run the BATSE hardware, uploading parameters, data, and output schedules through the GRO-TDRSS network. Burst and solar flare events were manufactured during this test, and all spacecraft OBC functions such as SAA entry and exit were verified. ETE #7 was the most successful end-to-end test to date. This operation was concluded at midnight on the morning of November 3.

14. BATSE/RIU Byte-Drop Anomaly

a. Overview

The byte-drop anomaly experienced by BATSE during testing at TRW and KSC is characterized by a data packet which has been corrupted so that one byte (8 bits) of data is missing from the telemetry stream and the remaining data have shifted one location upward in the packet. Each time the event occurs, it is the lower byte of a 16-bit word which is lost. This is a constraint to possible failure scenarios inside the hardware. Additionally, no events have been present in which more or less than eight bits are lost. The final byte of the packet is populated with the contents of the BATSE memory from outside the region in which the packet is constructed. These 16 bits are always written into the BATSE shift register, but under normal circumstances, are overwritten by the start of the next packet and never make it into the telemetry stream. The anomaly was first noticed during inspection of ETE #6 data. At that time, previous data were examined, and the anomaly was found in BATSE data as early as the GRO thermal vacuum test in July 1989.

After the discovery of these events, special attention was paid to their presence in ETE #7. The data from ETE #7 provided a rather alarming result. Prior to that test, the rate of occurrence for these anomalies was approximately one per 24-hour period. During ETE #7, 17 events were found in a 72-hour period, a substantial increase. Consequently, the BATSE team became involved in a thorough investigation and troubleshooting effort to characterize and explain the anomaly.

b. Troubleshooting Investigations

The first investigative test was performed on November 9, 1990. An examination of the events to this point had uncovered an association of event occurrences with operation on RIU-A. One event from ETE #7 occurred within 3 seconds of a switch to RIU-B; however, it is believed to be from a time when BATSE was utilizing RIU-A. Of nearly 300,000 packets of data from the GRO thermal vacuum test, ETE #4, and ETE #6, each of the byte-drop anomaly events occurred on RIU-A.

Both BATSE CCF units were found to be operating during the time of at least one event. For this first test, BATSE was operated through RIU-B to investigate the existence of the anomaly in this configuration. Over 11,600 packets were generated on November 9, with no RIU-B events.

A second investigative test was performed on November 12, in the same manner as the preceding operation. BATSE was operated on CCF-B this time, and RIU-B was still utilized. A total of 10,571 packets were generated during the second test, with no byte-drop occurrences.

The first two investigative tests failed to produce an event on RIU-B. One possible explanation for this was that the BATSE instrument required an extended period of operational time prior to the onset of these difficulties. To this point, no byte-drop event had been seen in BATSE data unless the instrument had been powered for 24 hours previous to the first event. Consequently, a 32-hour test was performed, starting on November 19, 1990. This test had three main purposes. First, the test was to determine the rate at which these events occur. Second, ETE #7 had demonstrated a substantial increase in the rate of events. This test was performed to determine if that rate was continuing to increase. Third, a correlation between event rate and spacecraft activity was sought. BATSE operated through RIU-A to provide a known configuration in which these events had occurred. Software patches were placed into the GROCC computer to trap these anomalous packets in real time. However, after generating 52,319 packets, no events were found, and the test was concluded.

A second long-duration test was performed starting on November 27, 1990. During this operation, the spacecraft was configured as closely as possible to the ETE #7 configuration in an attempt to reproduce the byte-drop anomaly. A total of 51,696 packets were generated during this long-duration test without a replication of the byte-drop anomaly.

With no additional events in-hand, a final sequence of tests were planned in coordination with the final Observatory Functional Test (see section III.G.15). Starting on December 4, BATSE would be powered each day in the course of functional testing, and would monitor the data for byte-drop events. During the final three days of testing, December 12-14, BATSE would remain in a power-on configuration to obtain a long-duration test. During this time, the POCC also came on-line, along with the other instruments, and ETE #7A was performed. This test therefore replicated the conditions of ETE #7 in which the problem was seen. Finally, during this extended testing time, four byte-drop events were produced. This brought the total number of events seen to 32. Table 3.131 lists these events.

Table 3.131. BATSE Byte-Drop Anomaly Events in Ground Testing

Date	TJD	Spacecraft Time	RIU	CCF
7-11-89	7718	6,404.65	A	A
7-11-89	7718	28,944.93	A	A
7-12-89	7719	29,218.34	A	A
7-19-89	7726	35,663.13	A	B
7-21-89	7728	16,629.58	A	A
7-23-89	7730	48,036.83	A	A
7-23-89	7730	80,012.21	A	A
7-24-89	7731	6,049.71	A	A
6-8-90	8050	7,707.xx	A	A
8-16-90	8119	68,041.xx	A	A
8-17-90	8120	80,617.xx	A	A
10-31-90	8195	34,039.94	A	A
10-31-90	8195	45,144.19	A	A
10-31-90	8195	53,642.96	A	A
10-31-90	8195	55,330.94	A	A
10-31-90	8195	83,597.44	A	A
11-1-90	8196	27,083.90	A	A
11-1-90	8196	27,774.08	A	A
11-1-90	8196	29,176.96	A	A
11-1-90	8196	30,049.41	A	A
11-1-90	8196	74,005.63	A	A
11-2-90	8197	16,029.82	A	A
11-2-90	8197	17,023.10	A	A
11-2-90	8197	25,292.93	A	A
11-2-90	8197	25,804.93	A	A
11-2-90	8197	29,550.93	A	A
11-2-90	8197	78,112.90	A	A
11-2-90	8197	84,258.94	A*	A
12-11-90	8236	75,600.14	A	A
12-13-90	8238	84,152.06	A	A
12-14-90	8239	43,537.15	A	A
12-15-90	8240	71,321.74	A	A

*Event occurred within 3 seconds of a switch to RIU-B. The timing of events in the sequence is not well understood at this time, but is believed to be RIU-A.

c. Background and Possible Causes

It is currently presumed that the problem lies in the request for telemetry to BATSE. For each spacecraft packet which is generated, the GRO central unit computer issues 910 requests to BATSE for eight bits of data. The BATSE data are read from a 16-bit shift register, so two requests are required to clean the register of data. The BATSE microprocessor (SBP 9900) is served by a dual J-K flip-flop with an interrupt (I1) for every other telemetry request so that the 16-bit register can be provided with new data. The circuitry used in the GRO interface is schematically shown in Figure 3.73.

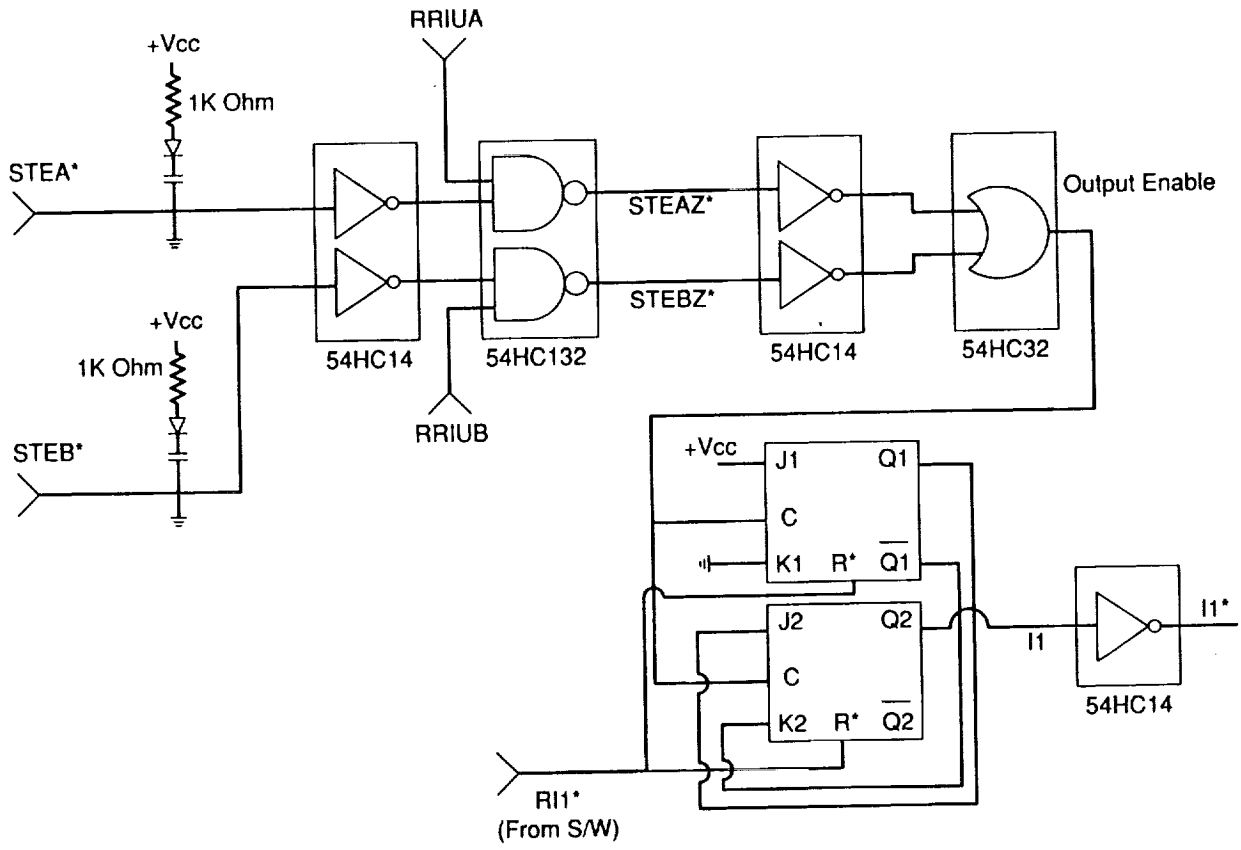

Figure 3.73. BATSE/GRO Interface Circuitry Schematic (One of Two).

The first 16 bits of the packet are written into the shift register after an interrupt by the GRO major frame synchronization pulse (I7). The next 455 interrupts cause the BATSE computer to write each subsequent 16-bit word into the register. Consequently, a total of 456 16-bit words are written to the shift register, of which 455 are placed into the data stream by the spacecraft. The final 16-bit

word is from outside the region in which the BATSE packet is constructed, and under normal circumstances is overwritten at the major frame synchronization when BATSE receives the I7 interrupt. The loss of eight bits in the BATSE packet, coupled with a shifting of the remaining data upward in the packet, causes half of these final 16 bits to enter the BATSE data stream at the final location in the BATSE packet. When the BATSE memory is filled with a known value at this location, the byte-drop anomaly is easily identified by the presence of this data value in the final location of the BATSE packet.

The BATSE team pursued an extensive investigation into possible causes of the anomaly which would fit all the observed data. The simplest cause of the byte-drop anomaly is an additional spurious data request from the RIU-A to the BATSE instrument. This additional request would trick the BATSE electronics into thinking that eight bits of data had been read from the register, and would cause I1 to be serviced prior to a complete read from the 16-bit register, overwriting half the data contained therein. This additional request is most likely not noise related, because of the appropriate noise rejection designed into the circuit. A "jitter" on the RIU active signal (see Figure 3.73) would also cause an additional input at the J-K flip-flop, yielding an overwrite of eight bits in the 16-bit register.

Most of the BATSE team's effort centered on possible causes internal to the BATSE instrument which would yield the byte-drop anomaly. The only scenario which the team was able to devise to fit all of the observed boundary conditions was a reset of the second flip-flop, without resetting the first. The flight software is handling all interrupts to the microprocessor properly, and the interrupt is being cleared normally by resetting the J-K flip-flop. This can be determined through examination of data during the anomalous condition. However, if only the second flip-flop is reset by the software, the next request for telemetry will cause another interrupt at the output of the two J-Ks. In this scenario, the software services the proper number of interrupts, a lower byte is always lost, and all other constraints are realized. However, this sequence of events is extremely unlikely. Both of the J-K resets are tied together, making it extremely difficult to reset one without the other. Second, this problem would have to be present in both BATSE CCF interface circuits, and happen only during the time BATSE is using RIU-A.

d. Conclusions

At this point, the precise cause of the byte-drop anomaly has not been determined. With the data available, the BATSE team believes that RIU-A is serving BATSE with an additional spurious data request, causing the flight software in the instrument to write data into the 16-bit register early, overwriting the lower eight bits, which never get into the telemetry stream. A hardware/software interface problem inside the BATSE CEU is unlikely, for the reasons mentioned in section III.G.14.c but cannot be definitively ruled out. Noise on the RIU active signal is also a possible cause of the anomaly.

Despite the belief that the problem is located inside RIU-A, no scenario exists which might explain the observations. The BATSE team made several requests for a detailed look at the

operations of the RIU as early as October 1990; however, no detailed investigation similar to the one done on the internal BATSE hardware was performed on the RIU. BATSE personnel were not knowledgeable enough about the RIU to perform such an exercise.

Operationally, this is an extremely minor problem. Testing demonstrated that the rate of occurrence was not worsening, and at the present rate, only one packet in a 24-hour period would exhibit the anomaly. In most instances, the entire packet can be reconstructed, with the exception of the data byte which was lost. The impact to science operations is nearly zero. Although the cause of the anomaly is not understood, the BATSE team decided to accept the performance "as-is," and fly in the current configuration. In the event of a severe degradation, RIU-B has demonstrated freedom from these events and can serve as a backup.

15. Final BATSE/GRO Functional Test

The final full-scale functional test of the BATSE hardware prior to launch began on December 4, 1990. All facets of the instrument's performance and behavior were tested. Dr. G. J. Fishman, John Horack, and Michelle Flickinger of the BATSE team performed these operations. The results of these tests provided the "baseline" performance prior to launch of the Gamma Ray Observatory. Full cross-strapping capability was verified, as was the proper functioning of all BATSE flight heaters. Table 3.132 details all procedures performed during this test in chronological order.

Table 3.132. BATSE Tests Performed During Final Instrument Functional Test at KSC

- TP-110 — Power-up/aliveness test
- TP-105 — Detector module testm
- TP-170 — CPD calibration
- TP-171 — CPD/LAD coincidence run
- TP-125 — Background collection
- TP-180 — Burst data test (options 1 and 2)
- TP-125 — Background collection with OSSE Th 228 isotope deployed
- TP-190 — Pulsar data test (options 1 and 2)
- TP-125 — Background collection with OSSE Cs 137 isotope deployed
- TP-192 — Pulsar clock calibration (CCF-B)
- TP-192 — Pulsar clock calibration (CCF-A)
- TP-180 — Burst data test (option 3)
- BATSE flight heater power and cross-strapping tests
- BATSE special radioactive source data collection test #1 (energy-channel data)
- BATSE PMT balance and gain adjustments
- BATSE special radioactive source data collection test #2 (LLD data)
- BATSE LED to HER channel mapping

Most of the functional testing performed during this time period was done with BATSE operating through RIU-B. This configuration was used to obtain the maximum amount of time on the instrument using RIU-B to gain confidence that this RIU was free of the byte-drop anomaly. No byte-drop events were found during B-side testing.

After a normal power-up on the morning of December 4, testing began with an execution of TP-105, the detector module test. During this test, each of the command bits of all 40 +HV supplies were tested and verified to be fully functional. All detector module functions, including the LEDs, LLDs, and housekeeping measurements, were also examined. No anomalies were present during the detector module test.

TP-170, the CPD calibration, was the next test performed in the sequence. During this test, each of the CPDs are operated at eight different voltages. While at each of the voltages, the counting rate is determined so that a plot of rate vs. +HV can be constructed. Because the CPD has no pulse height analyzer, this method is used to determine the approximate location of the CPD threshold in energy space. The results of this test are presented in Table 3.133.

Table 3.133. TP-170 CPD Rates at CPDHVn Voltage Settings
KSC Final Functional Test -- December 1990

	CPD Count Rate at Various +HV Command File Settings Detector Module							
	B0	B1	B2	B3	B4	B5	B6	B7
CPDHV1	48.4	49.8	51.6	54.9	56.3	61.0	57.9	64.0
CPDHV2	44.3	44.0	45.6	46.8	50.4	50.9	52.0	53.5
CPDHV3	42.8	42.3	45.1	45.0	48.5	49.3	50.1	51.4
CPDHV4	43.8	40.5	43.8	43.4	46.9	47.4	48.3	48.7
CPDHV5	42.2	39.3	42.5	41.1	45.2	45.6	46.1	46.2
CPDHV6	40.1	38.3	40.4	41.2	43.7	43.6	45.3	44.9
CPDHV7	39.1	36.4	39.2	37.5	41.6	38.7	41.8	40.5
CPDHV8	36.5	33.0	36.1	34.1	38.8	35.2	39.4	36.1

TP-170 determined that all CPDs were functioning normally and were operating at or near the desired energy range. A determination of the location of the CPD threshold will be made again during the on-orbit activation phase of the GRO mission.

TP-171 was performed immediately following the CPD calibration to determine the rate at which the PDs were rejecting events from the LAD. Three spectra were obtained from each of the large area detectors, one with the CPD on and in coincidence mode, and the other two in the anti-coincidence mode with the CPD on and off. The appropriate regions of the two anti-coincidence spectra were subtracted and compared with the same energy region of the spectrum taken in the

coincidence mode. If the CPD rejection circuitry is operating normally, the number of counts in the coincidence spectrum should approximately equal the difference in counts from the two spectra in the anti-coincidence mode. The results of this test are presented in Table 3.134.

Table 3.134. CPD Rejection and Coincidence Counting Rates - TP-171
KSC Final Functional Test -- December 1990

Detector Module	Coincidence Rate	Rejection Rate
B0	21.4	22.0
B1	18.2	19.3
B2	20.6	20.8
B3	18.5	18.6
B4	21.0	22.3
B5	18.1	18.8
B6	21.8	22.6
B7	18.2	18.4

The data in Table 3.134 show excellent agreement with previous testing results. The coincidence rate and the rejection rate from all detectors are approximately equal, as expected. In addition, the top-to-bottom anisotropy in the rejection rate seen in all previous tests is again easily visible. TP-171 verified that all coincidence/anti-coincidence circuitry was fully operational and that each of the eight CPDs were properly rejecting events as expected.

During several portions of the final functional test, the OSSE team required the use of a radioactive isotope to aid in the testing of their instrument. Three different isotopes were used, Th 228, Co 60, and Cs 137. The location of these isotopes was confined to the +X region of the GRO, near the OSSE instrument, and therefore were only viewed to a significant extent by detector modules B0-B3. Despite the limited viewing, the BATSE team performed iterations of TP-125, the background collection procedure, during these times. All spectra were stored to disk and also printed to hard-copy. These data reside in the BATSE library and are available for inspection.

TP-190 and TP-180 were also performed during the times in which OSSE was deploying isotopes for calibration. The pulsar data test, TP-190, verified the proper execution of both PSR-A and PSR-B memory boards. No anomalies were found during the pulsar data test. The burst data test successfully exercised all BATSE burst data types. During the third option of TP-180, which immediately followed a switch from CCF-B to CCF-A, the burst readout schedule was severely out of order and contained data types which were not expected. A memory dump indicated that the locations of the burst output schedule were corrupted. The CEU executed these corrupted instructions properly and produced the anomalous output. After identification of the anomaly, the burst readout was aborted, and serial command 712E was sent to re-initialize all parameters. A second dump of the memory was done to verify the correction, and a normal burst and data readout

were executed. Two additional burst readouts have been performed since this functional test, as a part of the BATSE VPF/LC-39 1-hour test rehearsals. Neither of them have shown any anomalous behavior.

The pulsar clock frequency calibration (TP-192) was performed on both CCF-A and CCF-B to determine final values for the relationship between the BATSE pulsar clock and the GRO spacecraft clock. The results of these tests are summarized in Table 3.135.

Table 3.135. BATSE Pulsar Clock Frequency Calibration Results -- TP-192
KSC Final Functional Test -- December 1990

BATSE CCF	Temp. (°C)	Frequency Fractional Difference
A	23	6.51×10^{-6}
B	23	8.42×10^{-6}

A complete examination and verification of the BATSE flight heaters was performed. Both sets of thermal control and make-up heaters were verified to be operational using either MPS as the power source. All telemetry indications through the GRO engineering data were verified. Both of the BATSE RIUs properly returned the status of their respective heater circuits in both power-on and power-off states. The thermostats for these heaters obviously were not tested because of the inability to lower the temperature of the spacecraft environment.

The first special radioactive source test was performed to obtain a final data set for the determination of the energy to channel functional form. Dr. Patrick Lestrade requested a similar data set to those previously generated, however this time utilizing radioactive isotopes instead of Coleman Lantern filaments or background. Small (~1 μCi) isotope sets of Cs 137, Ba 133, and Co 60 were cycled in front of each of the eight LADs, with the exception of B4, which was inaccessible. These isotopes were placed as closely as possible to the standard 75-cm distance used during TP-140, the long calibration. With one isotope in place before seven of the modules, 13-minute integrations were obtained with the SD at 2X gain, and the LADs at nominal, nominal +2 steps, and nominal -2 steps. Thus a total of three spectral accumulations were made for each module with each isotope. These spectral accumulations were repeated with no source present in front of the detector module. This data collection exercise went very smoothly, with no instrument anomalies. The data obtained from this operation are on file in the BATSE library and are available for inspection.

After completion of the spectral accumulations, the BATSE team performed a final balance and gain determination for all PMTs on the instrument. With Cs 137 isotopes deployed in front of each of the modules, the 662-keV emission line was used to balance the gains from the three LAD PMTs and to establish voltage settings for the various SD gains. The results of this operation are contained in Table 3.136.

Table 3.136. Final Flight Voltages for PMTs on BATSE at Various Gain Settings
KSC Final Functional -- December 1990

	Detector Module							
	B0	B1	B2	B3	B4	B5	B6	B7
PMT-A	1530	1691	1606	1656	1660	1727	1520	1747
PMT-B	1534	1680	1585	1655	1669	1677	1434	1708
PMT-C	1612	1700	1640	1644	1723	1835	1450	1769
SD-0.4X	1126	1150	1134	1063	1098	1031	1094	1173
SD-1X	1276	1313	1269	1201	1245	1171	1245	1337
SD-2X	1405	1445	1394	1315	1366	1283	1370	1469
SD-4X	1570	1617	1547	1468	1535	1430	1528	1642

The voltages displayed in Table 3.136 will be the initial values used on-orbit for the LAD and the SD. The CPD voltages were not adjusted during this time because of the satisfactory performance of these components during TP-170, CPD calibration. During the initial phase of on-orbit operations, the CPDs will be commanded to their nominal values and adjusted as necessary.

The second radioactive source test was performed to determine the behavior of the spectroscopy detector spectrum in the region of the LLD, especially at low levels. A large amount of scientific information is contained near the low-end of the SD spectrum, a noteworthy example being that of cyclotron absorption lines in the spectra of some gamma ray bursts. To glean the largest amount of scientific results obtainable from the data, it is desirable to know in precise detail the effect of the LLD on counts in the neighboring region of the spectrum. This procedure was therefore developed to obtain a mapping of the LLD over the spectrum so that its behavior could be precisely determined.

Spectra were obtained at the 1X and 4X gain settings. While at 1X, a Ba 133 isotope was placed in front of each of the detector modules. The LLD was then set to amplitudes of 10, 12, 14, 16, 18, 1A, and 1C. At each of these levels, 6.5-minute integrations were obtained and stored to disk. These configurations were repeated with no isotopes present so that background spectra could be obtained. At the 4X level, a similar set of Ba 133 spectra were obtained; however, the LLD was set to levels of 10, 20, 40, 48, 50, 58, 60, 68, 70, and 80. No background spectra were acquired at the 4X gain setting. These data are on file in the BATSE library and are available for inspection.

The final test performed as part of the last functional test was a mapping of the LED into HER channel space for all possible LED settings. Each LED was commanded to a particular value, and a short HER spectrum was accumulated. From that spectrum, the channel number of the LED peak was determined and recorded. The spectra were printed and stored to disk for future reference. A summary of each LED peak location is provided in Table 3.137. Comparison of these data with those from Table 3.125 shows that the performance of the LED has not degraded in any of the detector

modules. The change in peak location is due to the fact that the PMTs were rebalanced, and nominal gain settings were re-established, slightly adjusting the peak location in energy space.

Table 3.137. HER Channel Location of LED Peak for Associated Amplitudes
KSC Final Functional Test -- December 1990

LED Hex Amplitude	HER Channel Location of LED for Module							
	B0	B1	B2	B3	B4	B5	B6	B7
1	Off	Off	Off	Off	Off	Off	Off	Off
2	Off	Off	Off	Off	Off	Off	Off	Off
3	Off	Off	Off	Off	Off	Off	Off	Off
4	14	29	15	23	21.5	29.5	25	24
5	31.5	65	35	53	47.5	67	58	52
6	52	86	58	75.5	71	89	79	73.5
7	68.5	98.5	73	93	86.5	100	96	89
8	78.5	104	84.5	99.5	97	106	101	97.5
9	89	109	96	104	101	112	106	101.5
A	96	114.5	99	108	105	118	110.5	105
B	99	120	101.5	112	109	124	115	109
C	101	124.5	104.5	116.5	113	127	119.5	112.5
D	103.5	125	107	120.5	117	127	124	116
E	105.5	126	110	123	120.5	127	126	119.5
F	108	126	112.5	123	124.5	127	126	123

Functional testing of the BATSE instrument was completed on December 14, 1990, at the end of the long-duration ETE #7A. This test was not the final power-on opportunity for the instrument. Subsequent BATSE testing after this functional test prior to launch of the GRO consists of two, 1-hour tests. The first of these tests is performed in the Vertical Processing Facility, and the second is performed while BATSE is inside the orbiter payload bay on launch pad 39B. Both tests are identical and consist of TP-110, followed by TP-190, and concluding with TP-180. During these tests, all A-side flight heaters are tested and verified. The burst readout from TP-180 is aborted after 1 hour. The burst trigger signal to the other three instruments is exercised as a part of TP-180. These tests are not designed to extensively test BATSE in great detail, rather to verify fundamental functionality during the pre-launch phase of the program.

H. BATSE Total Test and Calibration Time

During the entire test phase of BATSE, a detailed testing log was kept with the hardware which included times of power-on, power-off, critical tests, anomalies, etc. From this log, the total number of hours BATSE has operated prior to launch was calculated. The results of these tabulations are presented below.

o BATSE Testing at MSFC

Non Thermal Vacuum	416 hours
Thermal Vacuum	620 hours
Total MSFC Test Time:	1,036 hours

o BATSE Testing at TRW

Non Thermal Vacuum	600 hours
Thermal Vacuum	518 hours
Total TRW Test Time:	1,118 hours

o BATSE Testing at KSC

Before PMT Change in PHSF	92 hours
After PMT Change in PHSF	490 hours
VPF Instrument Test	1 hour
LC-39 Instrument Test	1 hour
Total KSC Test Time:	584 hours

o Total BATSE Test Time 2,738 hours

The times presented here are accurate to within ±5%. All BATSE configurations are included in these times, of which detector module operation and +HV operation is a subset. From examination of the testing log, one can estimate that the modules are operated a minimum of 90% of the time when the CEU is powered, and the +HV is operated nearly 80% of that time. This estimation yields a minimum figure of 1,970 hours of +HV operation, and 2,640 hours of module operation. The cross-strapping configurations have only been calculated for thermal vacuum testing; however, as a rule-of-thumb, most testing was approximately two-thirds on primary components, and one-third on backup systems.

APPENDIX A - LIST OF ACRONYMS

ADC	Analog to Digital Converter
ADF	Analog Data Function
BATSE	Burst and Transient Source Experiment
BTS	Burst Trigger Signal
CCF	CEU Control Function
CEU	Central Electronics Unit
COMPTEL	Compton Telescope
CONT	Continuous Data
CPD	Charged Particle Detector
DPU	Central Processor Unit
CSA/BLR	Charge Sensitive Amplifier/Baseline Restorer
DC	Direct Current
DCH	Discriminator, Continuous, and High Energy Resolution
DEU	Detector Electronics Unit
DISC	Discriminator Data
DM	Detector Module
EGRET	Energetic Gamma Ray Experiment Telescope
EMC	Electromagnetic Compatibility
EMI	Electromagnetic Interference
FIFO	First In First Out
FWHM	Full-Width-at-Half-Maximum
GRO	Gamma Ray Observatory
GRSE	Gamma Ray Spectrometer Experiment
GSE	Ground Support Equipment
HER	High Energy Resolution
HERB	High Energy Resolution - Burst
HKG	Housekeeping
HV	High Voltage
HVPU	High Voltage Power Unit
Hz	Cycles per Second (Hertz)
ICD	Interface Control Document
IFJ	In-Flight Jimper
keV	Thousand Electron Volts
KSC	Kennedy Space Center
LAD	Large Area Detector
LED	Light Emitting Diode
LLD	Lower Level Discriminator
MER	Medium Energy Resolution
MHz	Million Cycleds per Second
MLI	Multi-layer Insulation

MQT	Charge-to-Time Converter
MSFC	Marshall Space Flight Center
M/U	Make-Up (Heaters)
NaI	Sodium-Iodide
NASA	National Aeronautics and Space Administration
OSSE	Oriented Scintillation Spectrometer Experiment
PCF	Power Control Function
PDR	Preliminary Design Review
PHA	Pulse Height Analyzer
PMT	Photomultiplier Tube
PSR	Pulsar Data
RAM	Random Access Memory
ROM	Read-Only Memory
RIU	Remote Interface Unit
SAA	South Atlantic Anomaly
SD	Spectroscopy Detector
SDF	Science Data Function
SHER	Spectroscopy High Energy Resolution
SHERB	Spectroscopy High Energy Resolution - Burst
SLCC	Standard Load Center Converter
STS	Space Transportation System (Shuttle)
STTE	Spectroscopy Time-Tagged Event Data
T/C	Thermal Control (Heaters)
TP	Test Procedure
TPS	Test Preparation Sheet
TRW	GRO Prime Contractor
TTE	Time-Tagged Event Data
TTS	Time-to-Spill Data
TTU	Time Transfer Unit
UCSD	University of California - San Diego
VDC	Volts Direct Current

APPENDIX B - VACUUM HISTORIES

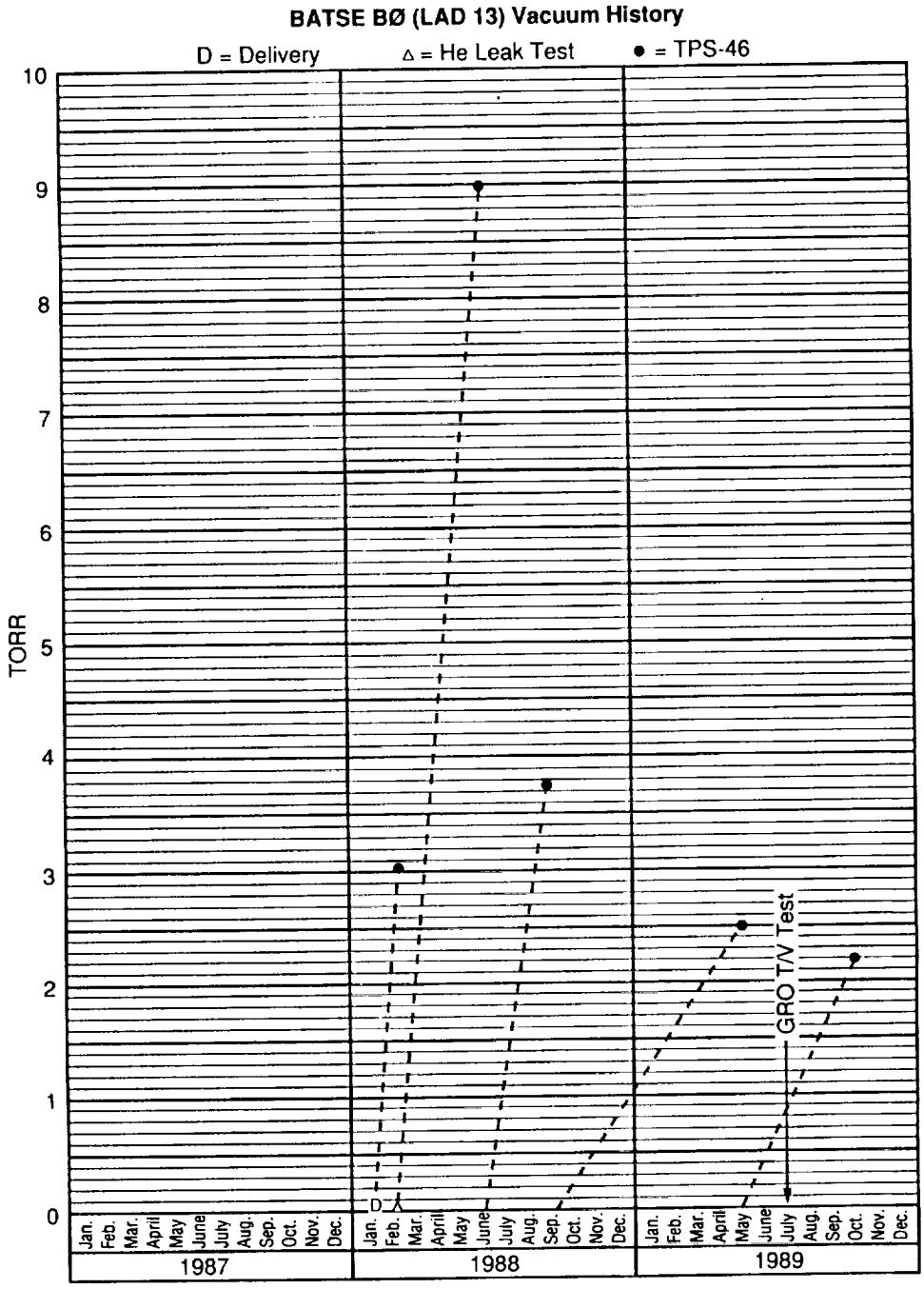

PRECEDING PAGE BLANK NOT FILMED

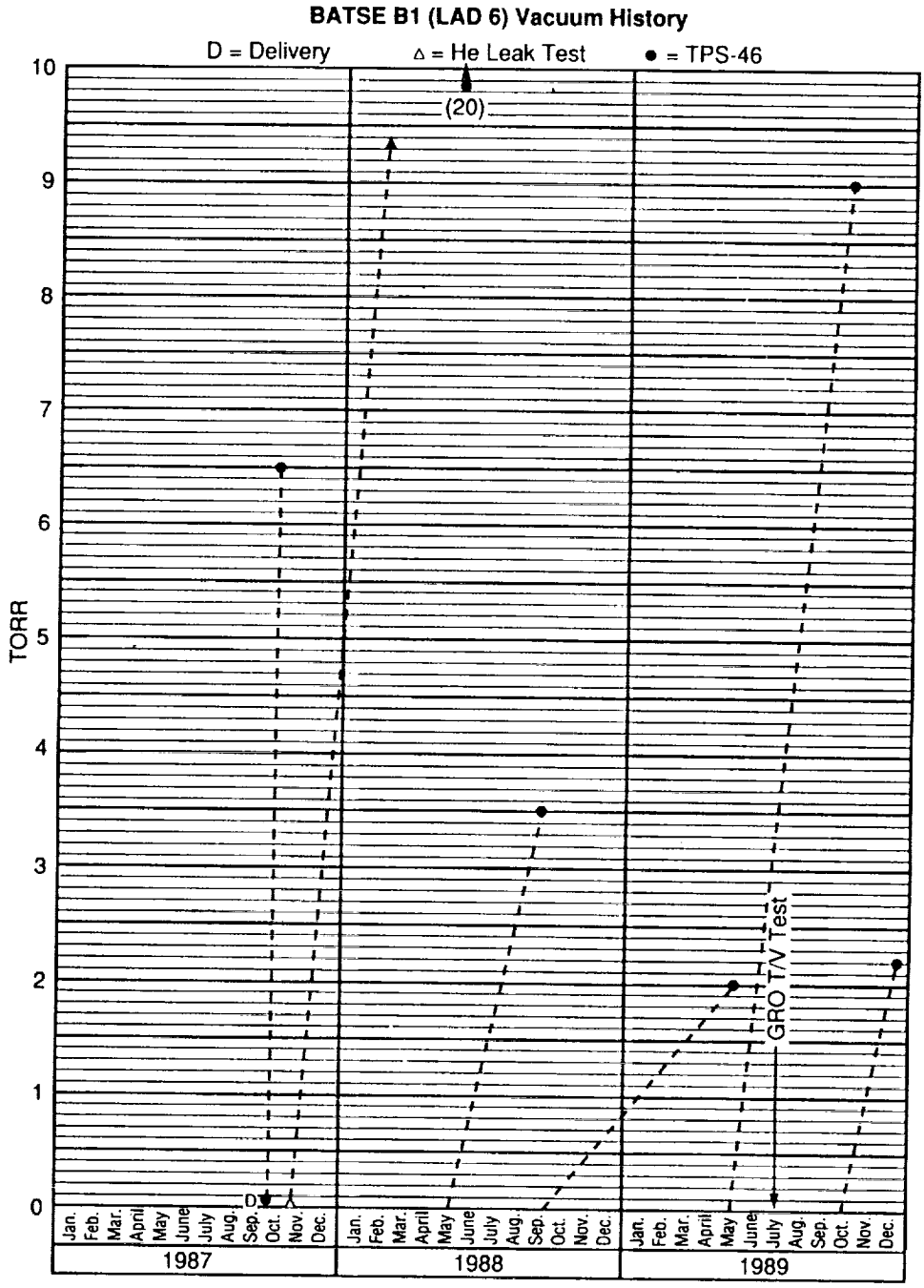
BATSE B1 (LAD 6) Vacuum History
D = Delivery
Δ = He Leak Test
● = TPS-46
(20)
TORR
10
9
8
7
6
5
4
3
2
1
0
D
GRO T/V Test
Jan. Feb. Mar. April May June July Aug. Sep. Oct. Nov. Dec.
1987
1988
1989

BATSE B2 (LAD 7) Vacuum History

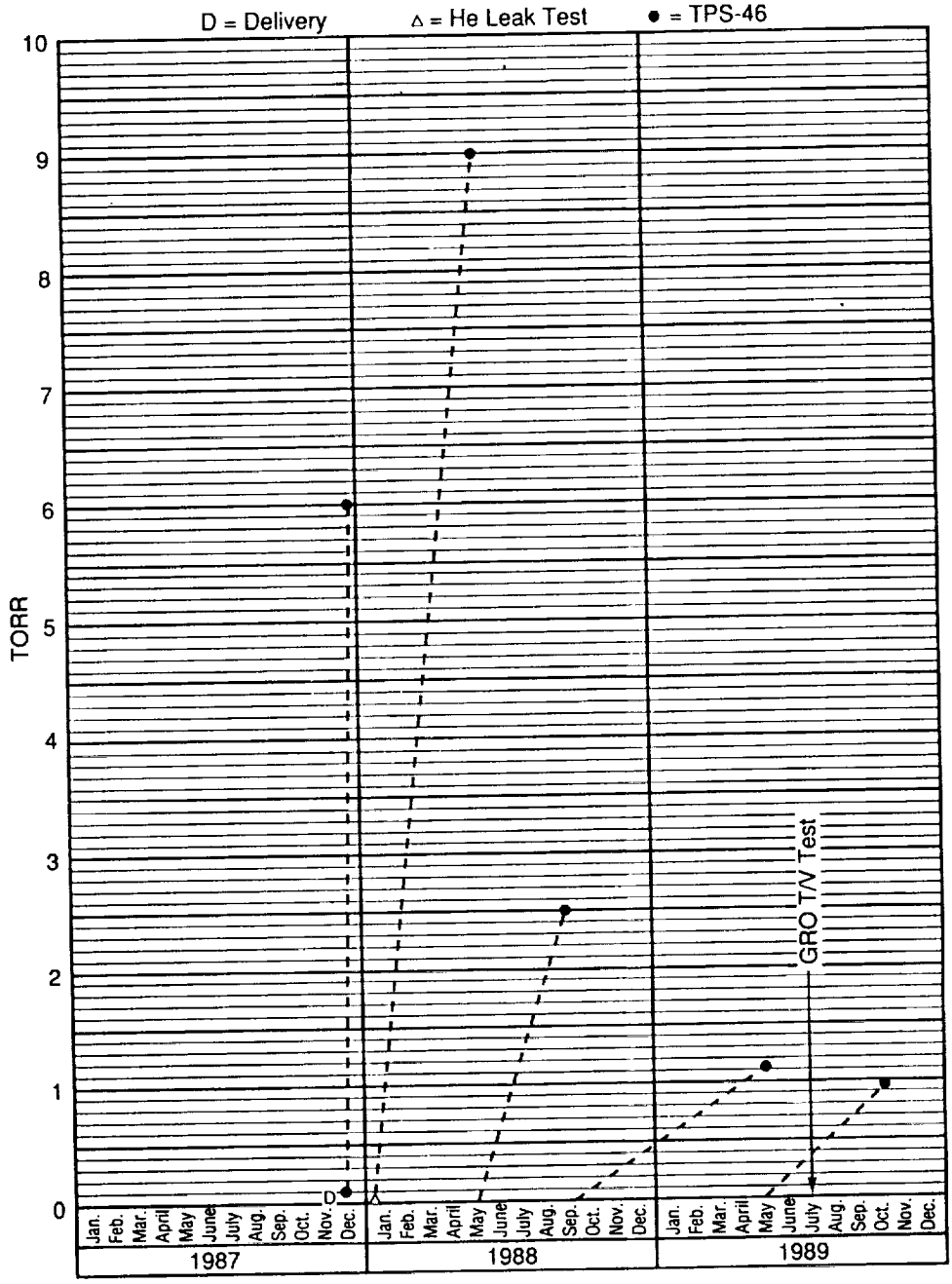

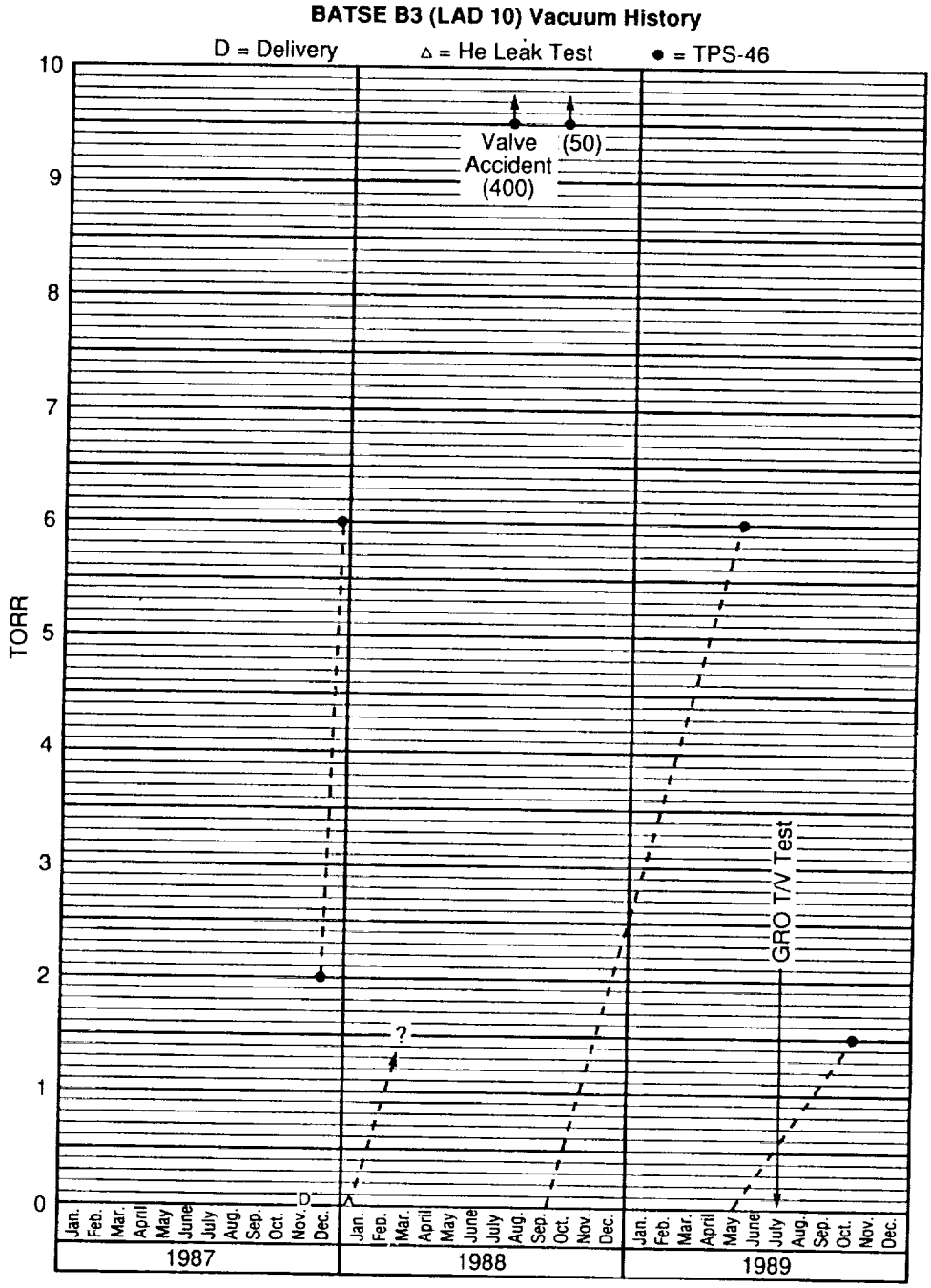
BATSE B3 (LAD 10) Vacuum History
D = Delivery
△ = He Leak Test
● = TPS-46
TORR
10
9
8
7
6
5
4
3
2
1
0
Valve Accident (400)
(50)
GRO T/V Test
?
D
Jan. Feb. Mar. April May June July Aug. Sep. Oct. Nov. Dec.
1987
1988
1989

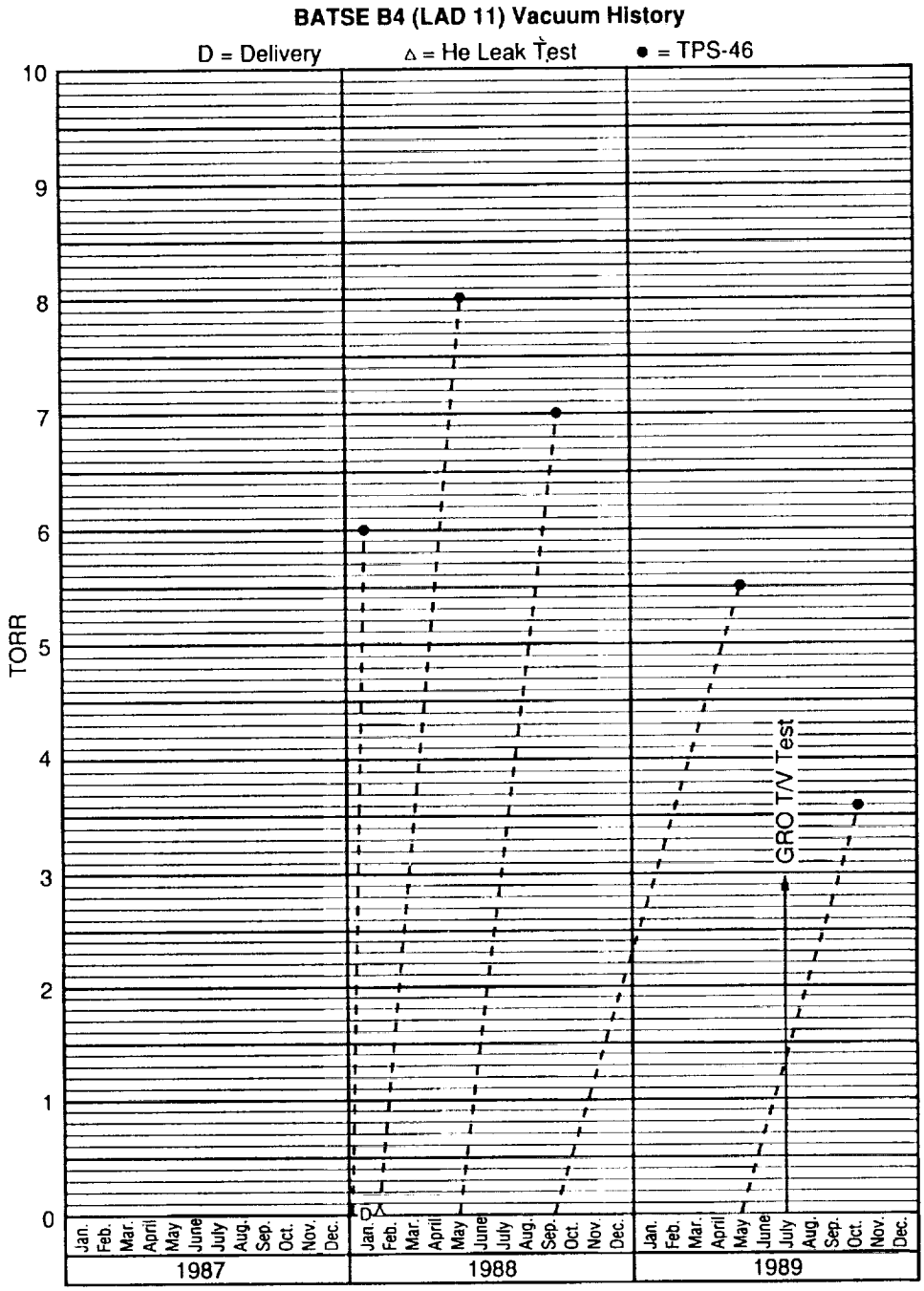
BATSE B4 (LAD 11) Vacuum History
D = Delivery
Δ = He Leak Test
• = TPS-46
TORR
10
9
8
7
6
5
4
3
2
1
0
GRO T/V Test
D
Jan.
Feb.
Mar.
April
May
June
July
Aug.
Sep.
Oct.
Nov.
Dec.
1987
1988
1989

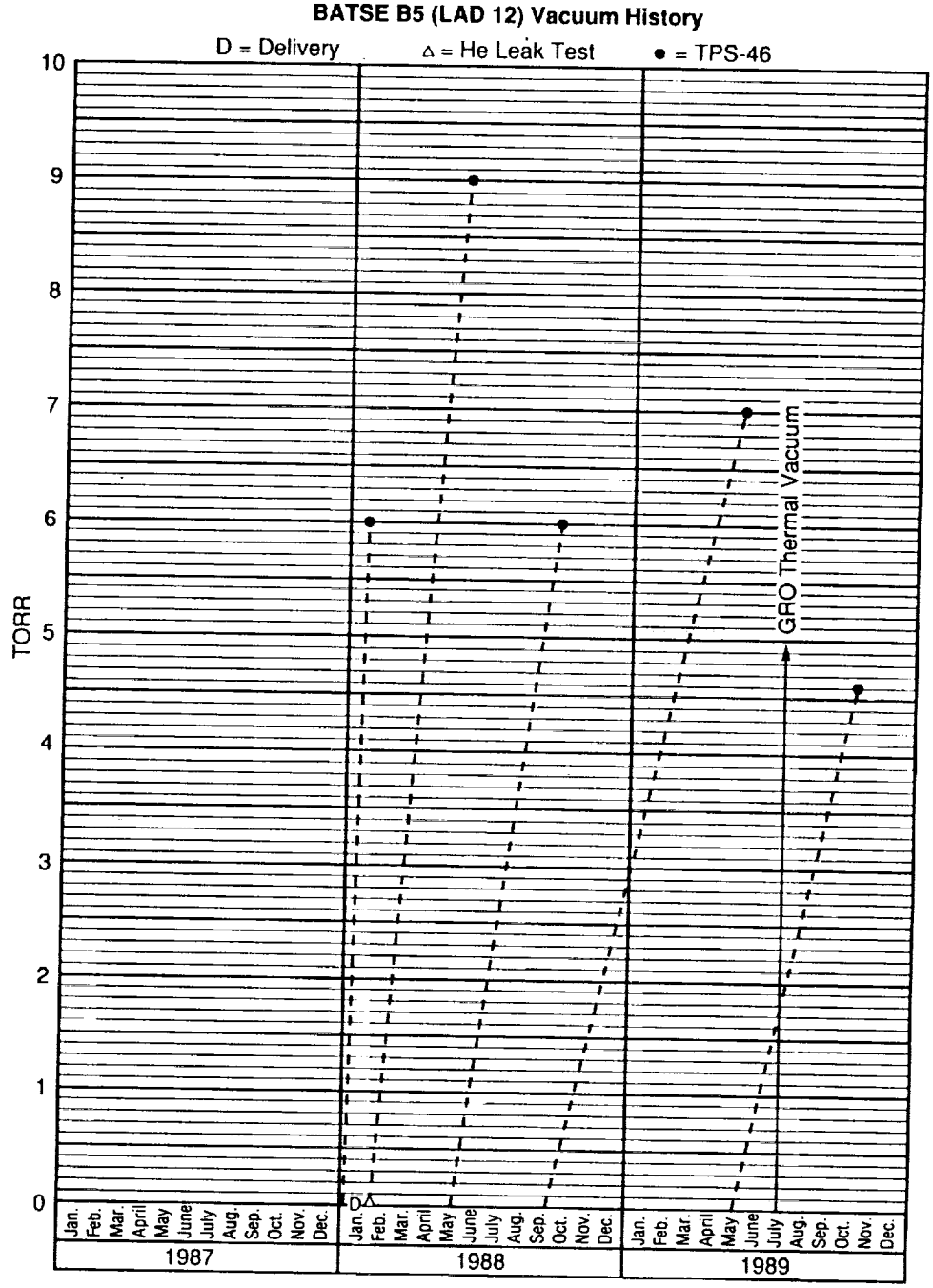
BATSE B5 (LAD 12) Vacuum History
D = Delivery
Δ = He Leak Test
● = TPS-46
TORR
10
9
8
7
6
5
4
3
2
1
0
GRO Thermal Vacuum
D
Jan. Feb. Mar. April May June July Aug. Sep. Oct. Nov. Dec.
1987
1988
1989

BATSE B6 (LAD 15) Vacuum History

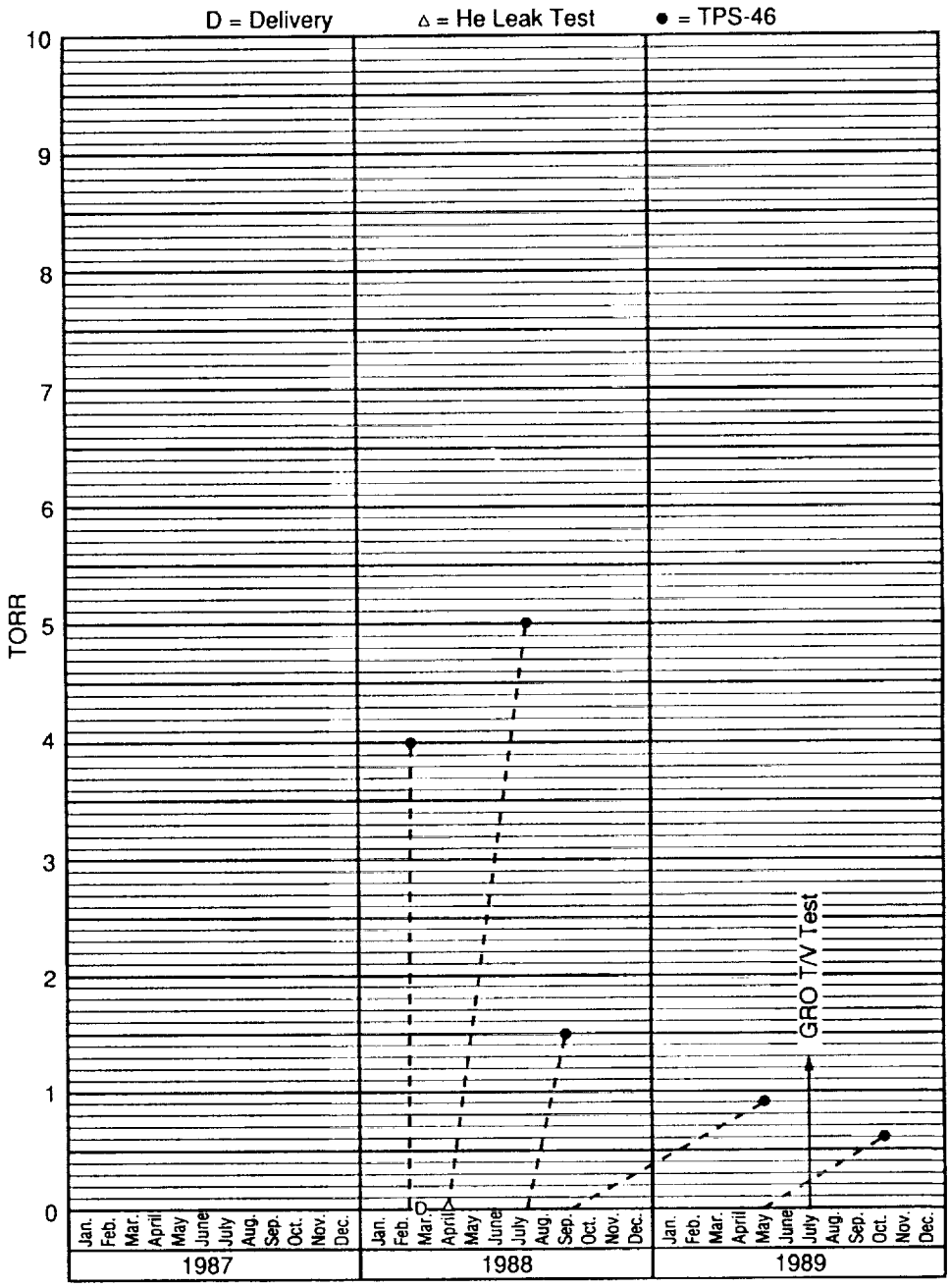

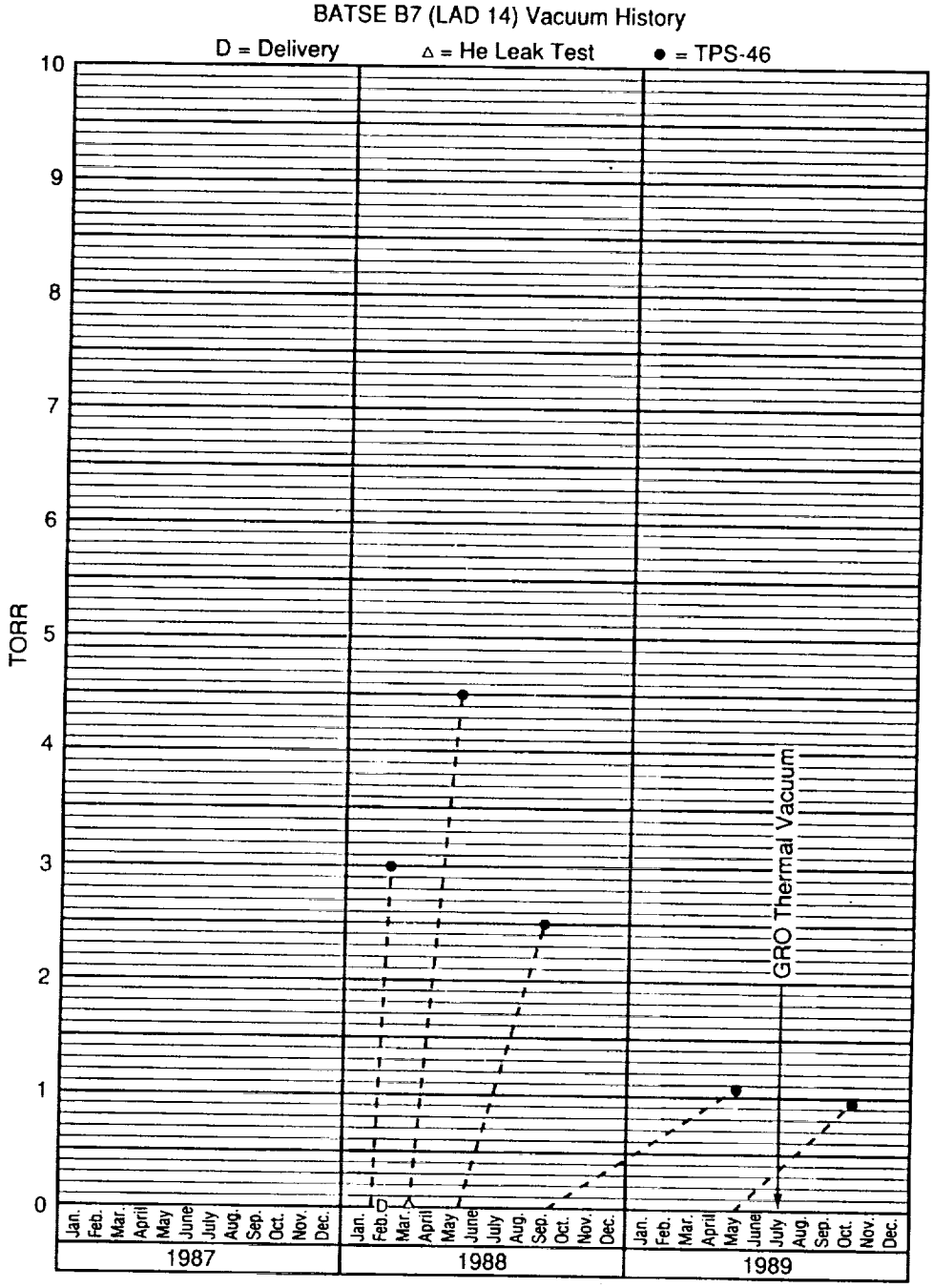
BATSE B7 (LAD 14) Vacuum History
D = Delivery
△ = He Leak Test
● = TPS-46
TORR
10
9
8
7
6
5
4
3
2
1
0
GRO Thermal Vacuum
D
△
Jan. Feb. Mar. April May June July Aug. Sep. Oct. Nov. Dec.
1987
1988
1989

REPORT DOCUMENTATION PAGE

Form Approved
OMB No. 0704-0188

1. AGENCY USE ONLY (Leave blank)	2. REPORT DATE	3. REPORT TYPE AND DATES COVERED
	September 1991	Reference Publication

4. TITLE AND SUBTITLE

Development of the Burst and Transient Source Experiment (BATSE)

5. FUNDING NUMBERS

6. AUTHOR(S)

J. M. Horack

7. PERFORMING ORGANIZATION NAME(S) AND ADDRESS(ES)

George C. Marshall Space Flight Center
Marshall Space Flight Center, AL 35812

8. PERFORMING ORGANIZATION REPORT NUMBER

M-668

9. SPONSORING/MONITORING AGENCY NAME(S) AND ADDRESS(ES)

National Aeronautics and Space Administration
Washington, D.C. 20546

10. SPONSORING/MONITORING AGENCY REPORT NUMBER

NASA RP-1268

11. SUPPLEMENTARY NOTES

Prepared by Space Science Laboratory, Science & Engineering Directorate.

12a. DISTRIBUTION/AVAILABILITY STATEMENT

Unclassified—Unlimited

Subject Category: 89

12b. DISTRIBUTION CODE

13. ABSTRACT (Maximum 200 words)

BATSE, one of four instruments on the Gamma Ray Observatory, consists of eight identical detector modules mounted on the corners of the spacecraft. Developed at the Marshall Space Flight Center, BATSE is the most sensitive gamma ray burst detector flown to date. Details of the assembly and test phase of the flight hardware development are presented here. Results and descriptions of calibrations performed at Marshall Space Flight Center, Alabama, TRW in Redondo Beach, California, and Kennedy Space Center, Florida are documented extensively. With the presentation of each calibration result, the reader is provided with the means to access raw calibration data for further review or analysis.

14. SUBJECT TERMS

Gamma Rays, Gamma Ray Bursts, High Energy Astrophysics, Gamma Ray Observatory

15. NUMBER OF PAGES

324

16. PRICE CODE

A14

17. SECURITY CLASSIFICATION OF REPORT	18. SECURITY CLASSIFICATION OF THIS PAGE	19. SECURITY CLASSIFICATION OF ABSTRACT	20. LIMITATION OF ABSTRACT
Unclassified	Unclassified	Unclassified	